

**Bangor University**

## **DOCTOR OF PHILOSOPHY**

### **Characterisation and analysis of sperm whale clicks**

Goold, John Charles

*Award date:*  
1998

*Awarding institution:*  
University of Wales, Bangor

[Link to publication](#)

#### **General rights**

Copyright and moral rights for the publications made accessible in the public portal are retained by the authors and/or other copyright owners and it is a condition of accessing publications that users recognise and abide by the legal requirements associated with these rights.

- Users may download and print one copy of any publication from the public portal for the purpose of private study or research.
- You may not further distribute the material or use it for any profit-making activity or commercial gain
- You may freely distribute the URL identifying the publication in the public portal ?

#### **Take down policy**

If you believe that this document breaches copyright please contact us providing details, and we will remove access to the work immediately and investigate your claim.

# Characterisation and Analysis of Sperm Whale Clicks

Dissertation for the degree of

Doctor of Philosophy - 1998

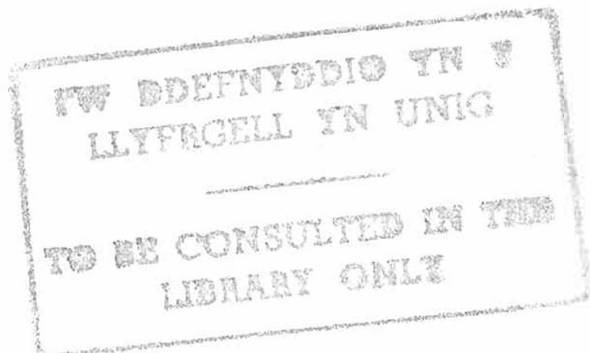
**John Charles Goold**

University of Wales Bangor

School of Ocean Sciences

Menai Bridge

Anglesey. LL59 5EY.



## ACKNOWLEDGMENTS

I would like to thank all those persons both directly and indirectly involved with this project. First, my thanks go to Dr Sarah Jones for her supervision and Dr Jonathan Gordon (Oxford University & International Fund for Animal Welfare) for his advice and the provision of sperm whale recordings. I am also grateful to Jonathan Gordon and the International fund for Animal Welfare for providing me with opportunities to participate in the study of sperm whales off the Azores, and to collect original data.

Thanks are also expressed to Dr Jim Bennell for much assistance and advice throughout this project, and also specifically for his assistance in the design of the sound velocity experiment in Chapter 3. In relation to the aforementioned section, thanks are also due to David Gill for construction of the pressure cell assembly and Stuart Lowe for initial calibrations and measurements using the cell. Thanks are also given to Chris Spurrier of the London Natural History Museum, and the Institute of Zoology, for assisting me to obtaining spermaceti oil and other samples from a beached sperm whale carcass. Thanks also go to Paula Jenkins of the Natural History Museum, for granting access to the scientific collection of cetacean specimens, for further study of sperm whale anatomy.

During the course of this project a number of persons have assisted my studies and I gratefully acknowledge the help of all. Particular thanks go to Captains Bob Slater and Bob Moore, and Dr Alec Simpson, of the Orkney Island Harbour Authority; Harry Ross and Bob Reid of the Scottish Veterinary College; Ed Harland of Defence Research Agency Portland; David Goodson of Loughborough University, and lastly Professor Malcolm Clarke.

Finally, large debts of gratitude are owed to my father, Ralph Goold, for his financial support which made this project possible, but most of all to Lynda, for her steadfast support throughout.

## Abstract

Regular clicks of diving sperm whales *Physeter macrocephalus* were recorded in deep oceanic water off the Azores, and subsequently sampled to computer disk for analysis. A total of 8540 clicks were marked and analysed. Simple temporal analysis of inter-click intervals revealed mean click rates for male sperm whales of  $1.1713 \text{ s}^{-1}$ , and for female sperm whales of  $1.9455 \text{ s}^{-1}$ . Fourier analysis showed distinctive peaks in the spectra of bull male sperm whale clicks at approximately 400 Hz and 2 kHz, which were stable over extended periods of up to 20 minutes. The clicks of smaller female sperm whales showed similar spectral peaks, shifted to approximately 1.2 kHz and 3 kHz, but which were less pronounced and less stable with time than the male peaks. All clicks contained broadband components up to at least 15 kHz. The previously reported multiple pulsed structure of sperm whale clicks is confirmed, and waveform filtering shows the structure to emerge only above certain threshold frequencies, approximating to estimated air sac dimensions in the sperm whale head. It is considered that the function of sperm whale clicks is echolocation.

Sound velocity was measured in samples of spermaceti oil from the spermaceti sac of a 15.6 m male sperm whale *Physeter macrocephalus* under varying temperature and pressure regimes. Measured sound velocities were in the range  $1390$  to  $1530 \text{ ms}^{-1}$  between the limits  $22^\circ\text{C}$  to  $38^\circ\text{C}$  and  $0$  to  $9.1 \text{ MPa}$ . Sound velocity was later measured in castor oil, spermaceti oil from the melon of the dwarf sperm whale *Kogia simus*, and a final sample of the original *Physeter* spermaceti oil. Measured sound velocities in castor oil were in the range  $1490$  to  $1560 \text{ ms}^{-1}$  between the limits  $6^\circ\text{C}$  to  $40^\circ\text{C}$  and  $0$  to  $9.1 \text{ MPa}$ . Measured sound velocities in *Kogia* melon core spermaceti oil were in the range  $1395$  to  $1670 \text{ ms}^{-1}$  between the limits  $9^\circ\text{C}$  to  $38^\circ\text{C}$  and  $0$  to  $9.1 \text{ MPa}$ . Measured sound velocities in *Kogia* melon peripheral spermaceti oil were in the range  $1430$  to  $1510 \text{ ms}^{-1}$  between the limits  $7^\circ\text{C}$  to  $38^\circ\text{C}$  and  $0$  to  $9.1 \text{ MPa}$ . Measured sound velocities in the final *Physeter* spermaceti oil sample were in the range  $1420$  to  $1520 \text{ ms}^{-1}$  between the limits  $12^\circ\text{C}$  to  $38^\circ\text{C}$  and  $0$  to  $9.1 \text{ MPa}$ . In all cases, sound velocity increased linearly with increasing pressure, but decreasing non-linearly with increasing temperature.

Waveform autocorrelation and *cepstrum* analysis techniques were used to measure intra-pulse intervals from sequences of male and female sperm whale clicks. Autocorrelation was generally successful provided that click signals were bandpass filtered, to reveal the high frequency pulsed structure, prior to analysis. *Cepstrum* analysis revealed that sperm whale click spectra contain ripples with periods equal to the reciprocal of the intra-pulse interval, in line with theoretical expectations. *Cepstrum* analysis was successfully used to assess intra-pulse intervals, the resulting data having less scatter than autocorrelation results. Neither autocorrelation or *cepstrum* analysis were sufficiently robust methods for making spot measurements of intra-pulse intervals from individual clicks, but realistic trends were obtained by analysing clicks over individual sequences of 6 minutes. With both autocorrelation and *cepstrum* analysis, a 50 point moving average was applied to the resulting data to visualise the trends in intra-pulse interval with time. Overall *cepstrum* analysis produced results with less scatter than autocorrelation analysis, and reasonable estimates of sperm whale body lengths were extrapolated from the data.

## Symbols & Abbreviations

ASCII	-	American Standard Code for Information Interchange
c	-	Sound Velocity
$C_{\Delta t}$	-	Correlation Coefficient at Time Shift $\Delta t$
DC	-	Direct Current
D	-	Diameter
FFT	-	Fast Fourier Transform
FIR	-	Finite Impulse Response
IPI	-	Intra-Pulse Interval
k	-	Degrees of Freedom of Chi-Squared Distribution
L	-	Sperm Whale Body Length
m	-	Metres
MPa	-	Mega-Pascals
ms	-	Milliseconds
n	-	Positive Integer
NL	-	Isotropic Noise Spectral Density
P	-	Pressure
Pa	-	Pascals
ppt	-	Parts per Thousand
psi	-	Pounds per Square Inch
r	-	Range
rms	-	Root-Mean-Square
s	-	Seconds



S	-	Spermaceti Sac Length
STFT	-	Short-Time Fourier Transform
t	-	Time
T	-	Temperature
V	-	Volts
$X_t$	-	Sample Value of Original Signal at Time t
$Y_t$	-	Sample Value of Replica Signal at Time t
$\chi^2$	-	Chi-Squared
$\Gamma$	-	Gamma
$\lambda$	-	Wavelength (Lambda)

# Contents

<b><u>Chapter 1</u></b>		Page
<b>The Sperm Whale Head</b>		1
<b><u>Chapter 2</u></b>		
<b>Time and Frequency Domain Characteristics of Sperm Whale Clicks</b>		
2.1	Introduction .....	13
2.2	Methods .....	17
2.2.1	Field Data Collection .....	17
2.2.2	Laboratory Data Acquisition .....	22
2.2.3	Data Analysis .....	24
2.2.3(i)	Click Rates .....	24
2.2.3(ii)	Frequency Domain Analysis .....	25
2.2.3(iii)	Time Domain Analysis .....	27
2.2.3(iv)	Time/Frequency Analysis .....	28
2.3	Results .....	29
2.3(i)	Click Rates .....	29
2.3(ii)	Frequency Domain Analysis .....	36
2.3(iii)	Time Domain Analysis .....	49
2.3(iv)	Time/Frequency Analysis .....	54
2.4	Discussion .....	54

## **Chapter 3**

### **Sound Velocity Measurements in Spermaceti Oil Under the combined influences of Temperature and Pressure**

3.1	Introduction .....	71
	Section 3A - 1994 Measurements : Sound Velocity in Spermaceti Oil from <i>Physeter macrocephalus</i>	
3A.1	Methods .....	73
3A.1.1	Spermaceti Oil Sampling .....	73
3A.1.2	Velocity Measurement Apparatus .....	75
3A.1.3	Pressure Cell Calibrations .....	81
3A.1.4	Oil Velocity Measurements .....	87
3A.2	Results .....	90
	Section 3B - 1996 Measurements : Sound Velocity in Castor Oil, Spermaceti Oil from <i>Kogia simus</i> and Spermaceti Oil from <i>Physeter macrocephalus</i>	
3B.1	Introduction & Methods .....	95
3B.2	Results .....	102
3B.2.1	Castor Oil .....	102
3B.2.2	<i>Kogia simus</i> Spermaceti Oil .....	106
3B.2.3	<i>Physeter macrocephalus</i> Spermaceti Oil .....	115
3B.3	Discussion .....	119

## **Chapter 4**

### **Measurement of Sperm Whale Click Intra-Pulse Intervals**

4.1	Introduction .....	128
4.2	Concepts and Methods .....	129
4.2.1	IPI Measurement using Waveform Autocorrelation .....	129
4.2.2	IPI Measurement using Rippled Magnitude Spectra .....	132
4.2.3	<i>Cepstrum</i> Methods .....	144
4.2.4	Generating Windows .....	146
4.3	Results .....	153
4.3.1	Autocorrelation Analysis Results .....	153
4.3.2	<i>Cepstrum</i> Analysis Results .....	161
4.4	Discussion and Conclusions .....	166

## **Chapter 5**

<b>Overview and Conclusions</b>	168
---------------------------------	-----

<b>References</b> .....	173
-------------------------	-----

<b>Appendix 1</b>	Frequency & Polar Response of AQ-4 Hydrophone Element ....	182
<b>Appendix 2</b>	Specifications of Nagra and Sony Tape Recorders .....	185
<b>Appendix 3</b>	PASCAL Programme to Create Waterfall Spectra Display .....	190
<b>Appendix 4</b>	PASCAL Programme to Generate FIR Coefficients .....	206
<b>Appendix 5</b>	Regression Data for 1994 Sound Velocity Measurements .....	211
<b>Appendix 6</b>	Regression Data for 1996 Sound Velocity Measurements .....	217
<b>Appendix 7</b>	PASCAL Programme to perform Waveform Autocorrelation ...	224

## List of Figures

Figure 1.1	Dolphin Head and Nasal Sac Morphology .....	3
Figure 1.2	Female Sperm Whale Skull .....	5
Figure 1.3	Male Sperm Whale Skull & Bony Nares .....	6
Figure 1.4	Anatomy of Sperm Whale Head .....	8
Figure 1.5	Longitudinal Section of Spermaceti Sac .....	10
Figure 1.6	Sections of Nasofrontal Sac Nodules .....	11
Figure 2.1	Example of Female Sperm Whale Click .....	15
Figure 2.2	Calibration Curves for Benthos AQ-4 Hydrophone .....	19
Figure 2.3	Typical Sperm Whale Clicks .....	26
Figure 2.4	Click Rates of Male Sperm Whales .....	30-32
Figure 2.5	Click Rates of Female Sperm Whales .....	33-34
Figure 2.6	Waterfall Spectra of Male Sperm Whale Clicks .....	37-39
Figure 2.7	Normalised Spectra of Male Sperm Whale Clicks .....	40-42
Figure 2.8	Waterfall Spectra of Female Sperm Whale Clicks .....	44-45
Figure 2.9	Normalised Spectra of Female Sperm Whale Clicks .....	46-47
Figure 2.10	Male Click Waveforms, Bandpass Filtered .....	50
Figure 2.11	Female Click Waveforms, Bandpass Filtered .....	53
Figure 2.12	Short-Time Fourier Transform of Male Click .....	55
Figure 2.13	$\frac{1}{3}$ Octave Spectral Density in SW1 Clicks, minutes 0-3 .....	62
Figure 2.14	$\frac{1}{3}$ Octave Spectral Density in SW2 Clicks, minutes 0-3 .....	63
Figure 2.15	$\frac{1}{3}$ Octave Spectral Density in SW3 Clicks, minutes 0-3 .....	64
Figure 2.16	$\frac{1}{3}$ Octave Spectral Density in SW1 Clicks, minutes 9-12 .....	66
Figure 2.17	$\frac{1}{3}$ Octave Spectral Density in SW2 Clicks, minutes 9-12 .....	67
Figure 2.18	$\frac{1}{3}$ Octave Spectral Density in SW3 Clicks, minutes 9-12 .....	68
Figure 3A.1	Sampling Location of Spermaceti Oil .....	74
Figure 3A.2	Schematic of Pressure Cell Assembly .....	77
Figure 3A.3	Schematic of Active Transducer Mounting .....	78
Figure 3A.4	Schematic of Passive Transducer Mounting .....	80
Figure 3A.5	Schematic of Oedometer Apparatus .....	83
Figure 3A.6	Image of Waveform Trace on Oscilloscope Screen .....	85
Figure 3A.7	Cell End Correction Time, Calibration Plots .....	86
Figure 3A.8	Measured & Standard Sound Velocity in Distilled Water .....	88
Figure 3A.9	Sound Velocity in <i>Physeter</i> Spermaceti Oil .....	92
Figure 3B.1	Schematic of Passive Transducer Mounting .....	96
Figure 3B.2	Image of Waveform Trace on Oscilloscope Screen .....	98
Figure 3B.3	Calibration Curves for Velocimeter Cell .....	100
Figure 3B.4	Sound Velocity in Castor Oil .....	104
Figure 3B.5	Schematic of Sagittal Section through <i>Kogia</i> Head .....	107
Figure 3B.6	Sound Velocity in <i>Kogia</i> Spermaceti Oil .....	111-112
Figure 3B.7	<i>Kogia</i> Core & Peripheral Spermaceti Sound Velocity .....	113
Figure 3B.8	Predictive <i>Kogia</i> Spermaceti Sound Velocity Curves .....	116
Figure 3B.9	Sound Velocity in Homogenised <i>Physeter</i> Spermaceti Oil .....	118
Figure 3B.10	Predictive <i>Physeter</i> Spermaceti Sound Velocity Curves .....	124

Figure 4.1	Illustration of Waveform Autocorrelation .....	130
Figure 4.2	Waveform and Spectrum of Unit Impulse Signal .....	133
Figure 4.3	Waveform & Spectrum of Two Unit Impulse Signal .....	135
Figure 4.4	Waveform & Spectrum of Artificial Sperm Whale Click .....	137
Figure 4.5	Waveform & Spectrum of Male Sperm Whale Click .....	138
Figure 4.6	Waveform & Spectrum of Female Sperm Whale Click .....	139
Figure 4.7	<i>Cepstrum</i> of Two Unit Impulse Signal .....	141
Figure 4.8	Waveform & Spectrum of Three Unit Impulse Signal .....	142
Figure 4.9	Waveform & Spectrum of Decayed 3 Unit Impulse Signal .....	143
Figure 4.10	<i>Cepstrum</i> of Artificial Sperm Whale Click .....	145
Figure 4.11	<i>Cepstrum</i> of Male Sperm Whale Click .....	147
Figure 4.12	Windows for Modulating Click Waveforms .....	150
Figure 4.13	Effect of Windowing on Spectrum Ripples .....	151-152
Figure 4.14	Raw IPI Trends from Autocorrelation Analysis .....	154
Figure 4.15	Smoothed IPI Trends from Autocorrelation, SW2 .....	155
Figure 4.16	Smoothed IPI Trends from Autocorrelation, SW3 .....	156
Figure 4.17	Smoothed IPI Trends from Autocorrelation, SW6 .....	157
Figure 4.18	Smoothed IPI Trends from Autocorrelation, SW9 .....	158
Figure 4.19	Raw IPI Trends from <i>Cepstrum</i> Analysis .....	162
Figure 4.20	Smoothed IPI Trends from <i>Cepstrum</i> Analysis .....	163

## List of Tables

Table 2.1	General Information on Click Sequences .....	23
Table 2.2	Mean Equilibrium Click Rates .....	35
Table 3A.1	Sound Velocity in <i>Physeter</i> Spermaceti Oil .....	91
Table 3B.1	Sound Velocity in Castor Oil .....	103
Table 3B.2	Sound Velocity in <i>Kogia</i> Spermaceti Oil .....	109-110
Table 3B.3	Sound Velocity in Homogenised <i>Physeter</i> Spermaceti Oil .....	117
Table 4.1	Mean IPI Values for SW2, SW3, SW6 and SW9 .....	165

## **Chapter 1**

### **The Sperm Whale Head**

The head of the sperm whale is a structure of evolutionary extreme among the odontocetes (toothed whales & dolphins). The members of the cetacean sub-order odontocete are virtually all capable of emitting pulsed sounds, or “clicks” as they have generally become known. Over evolutionary time there seems to have evolved a generalised homology between the nasal structures of odontocetes, particularly evident in the dolphin species (Cranford et al, 1996). Although the precise method by which odontocetes produce clicks has eluded numerous workers over past decades, it seems likely that click production is the result of a mechano-pneumatic action in the nasal structures (Norris et al 1971, Hollien et al 1976, Ridgeway et al 1980, Amundin & Anderson 1983, Ridgeway & Carder 1988, Au 1993). Sound production has been variously attributed to the larynx (Purves & Pilleri, 1973), the nasal plugs (Evans & Prescott, 1962) but perhaps most significantly to the complex of structures that occur around the so called “monkey lips”. The monkey lips are, as the name suggests, a tough lip like structure resembling the simian muzzle which almost certainly regulates the passage of air through the nasal airways. Cranford et al (1996) demonstrated in x-ray CT scans, magnetic resonance scans and cryosections of 40 odontocete specimens, encompassing 19 species including the Physeteridae (sperm whales), that the monkey lips are a common structure - and probably common to all odontocete species. In addition these workers describe in detail the air passages and monkey lips of

several odontocete species, and also the associated lipid sacs (bursae) that form part of the lip structure [Fig 1.1]. They propose that click production in the dolphin head is the result of mechanical impact of tissue projections in the airway against the posterior end of the lipid melon. The melon conducts the energy of this mechanical impact as sound waves to the surface of the head and couples it to the surrounding seawater, which is of reasonably matched acoustic impedance to the melon lipid. The mechanical impact mechanism is proposed to occur in the gaseous medium of the nasal airways, where fluid friction on the movement of the impacting tissue projection prior to impact is minimal. The mechanical events are further proposed to be driven by compressed air in the nasal airways, and the air release regulated by the monkey lips. In essence the lips act as a tightly occluding valve that allow the build up of pressure in the nares. At the desired instant this pressure is released dorsally through the monkey lips into the vestibular sac, and during it's passage past the complex drives the impacting tissue structure to produce the sharp transient click typical to dolphins.

It is interesting to note that Cranford and his colleagues point to the fact that in dolphin species there are two pairs of monkey lips and associated bursae on the left and right side of the spiracular cavity, and that these structures tend to be considerably asymmetric, from one pair to the other, in both size and lateral position. It is hypothesised by the aforementioned workers that this asymmetry is used by dolphins to create the relatively broadband clicks that such species produce. Porpoises have paired monkey lips similar to the dolphins but which are much more symmetrical in size and position. This symmetry is implicated in the relatively narrow band clicks that porpoises produce. The fact that sperm whales have only a single pair of monkey lips is noted at this point and will be addressed in later discussions.

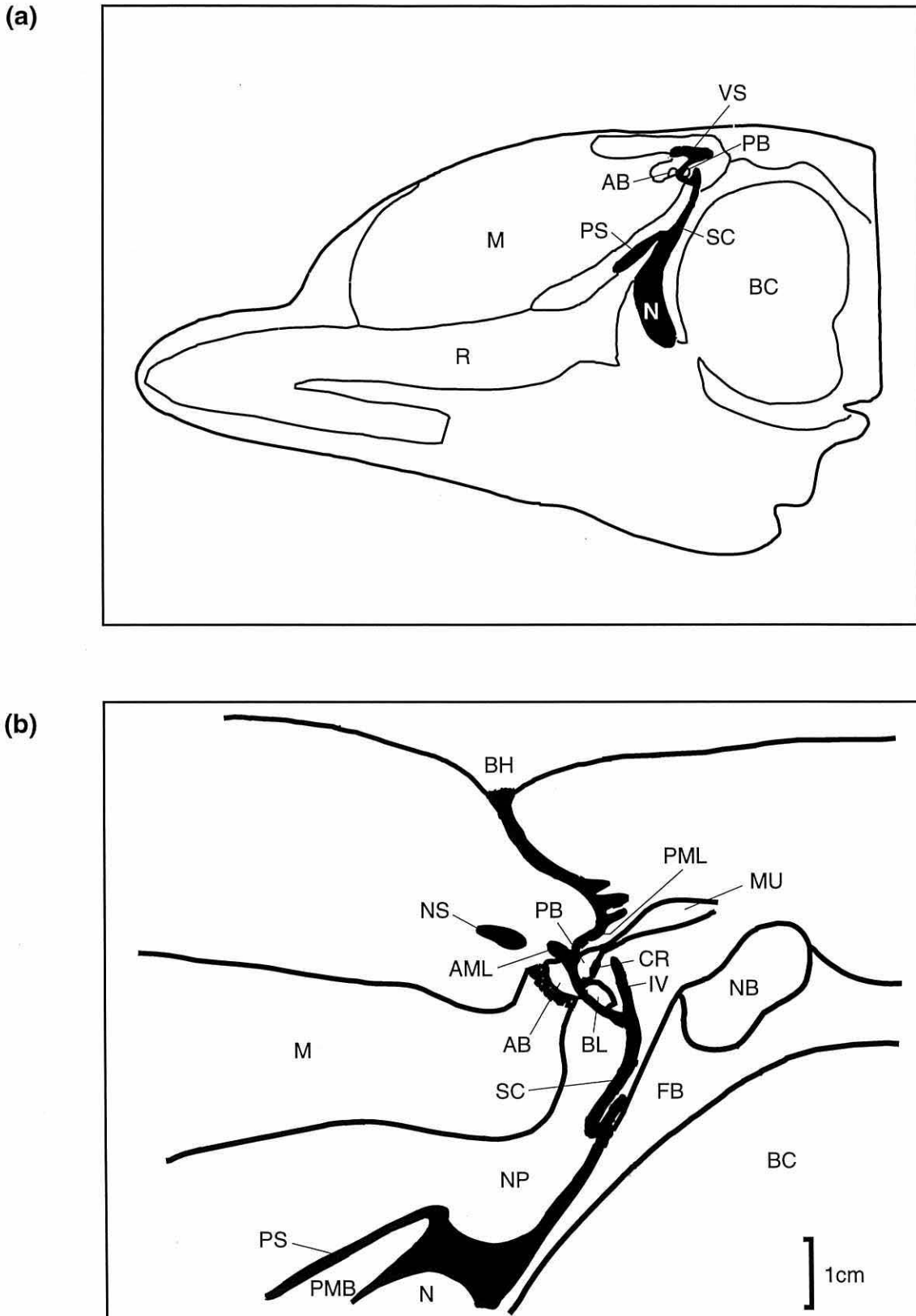


**Figure 1.1** Dolphin head and nasal sac morphology (a) sagittal section schematic of *Tursiops* head and (b) detailed schematic of nasal complex; both redrawn from Cranford et al (1996). AB anterior bursa, AML anterior ridge of monkey lip, BC brain cavity, BH blowhole, BL blowhole ligament, CR bursal cartilage, FB frontal bone, IV inferior vestibule, M melon, MU intrinsic muscle of nasofrontal sac, N bony naris, NB nasal bone, NP nasal plug, NS anterior nasofrontal sac, PB posterior dorsal bursa, PMB premaxillary bone, PML posterior ridge of monkey lip, PS premaxillary sac, R rostrum, SC spiracular cavity, VS vestibular sac.

Although homology exists in the nasal structures of the odontocete head, these structures are greatly distorted in the sperm whales (Physeteridae) when compared to the dolphin case. The gross morphology of the bony structures of the head of the sperm whale *Physeter macrocephalus* [Fig 1.2] are similar in overall appearance to the dolphin structure, with a long narrow rostrum and mandible anterior to the main skull. In sperm whales the mandible (lower jaw) is lined on either side with peg like teeth, whereas teeth tend to be absent in the upper jaw - except in mature animals where vestigial teeth may sometimes erupt in the upper jaw. The remainder of the facial bones are to the rear of the skull forming the brain case, ear bullae, muscle anchorage and articulation points for the jaw. However the rear skull formation of the sperm whale is a distinctly cup shaped structure, often described as a forward facing "amphitheatre" - the dolphin skull does not exhibit this extreme forward curvature. Near the base of the amphitheatre skull of the sperm whale are two bony penetrations, which are the left and right bony nares respectively [Fig 1.3]. It is notable that the left bony nares is considerably wider than the right bony nares, and together suggest very much an asymmetric function. From exterior observation of the living animals it is clear that the gross head shapes of sperm whales and dolphins are considerably different. Whereas dolphin heads viewed from the side have a generally fusiform shape with a narrow beak like rostrum and a bulbous but streamlined melon posterior to it, the sperm whale head viewed from the side appears almost square. There is no narrowing of the fleshy tissue to the front of the head, at least in side view, and the lower jaw of an adult animal appears dwarfed by the overall bulk of the head. In addition the anterior tip of the jaw terminates up to a metre behind the front of the upper head tissue.

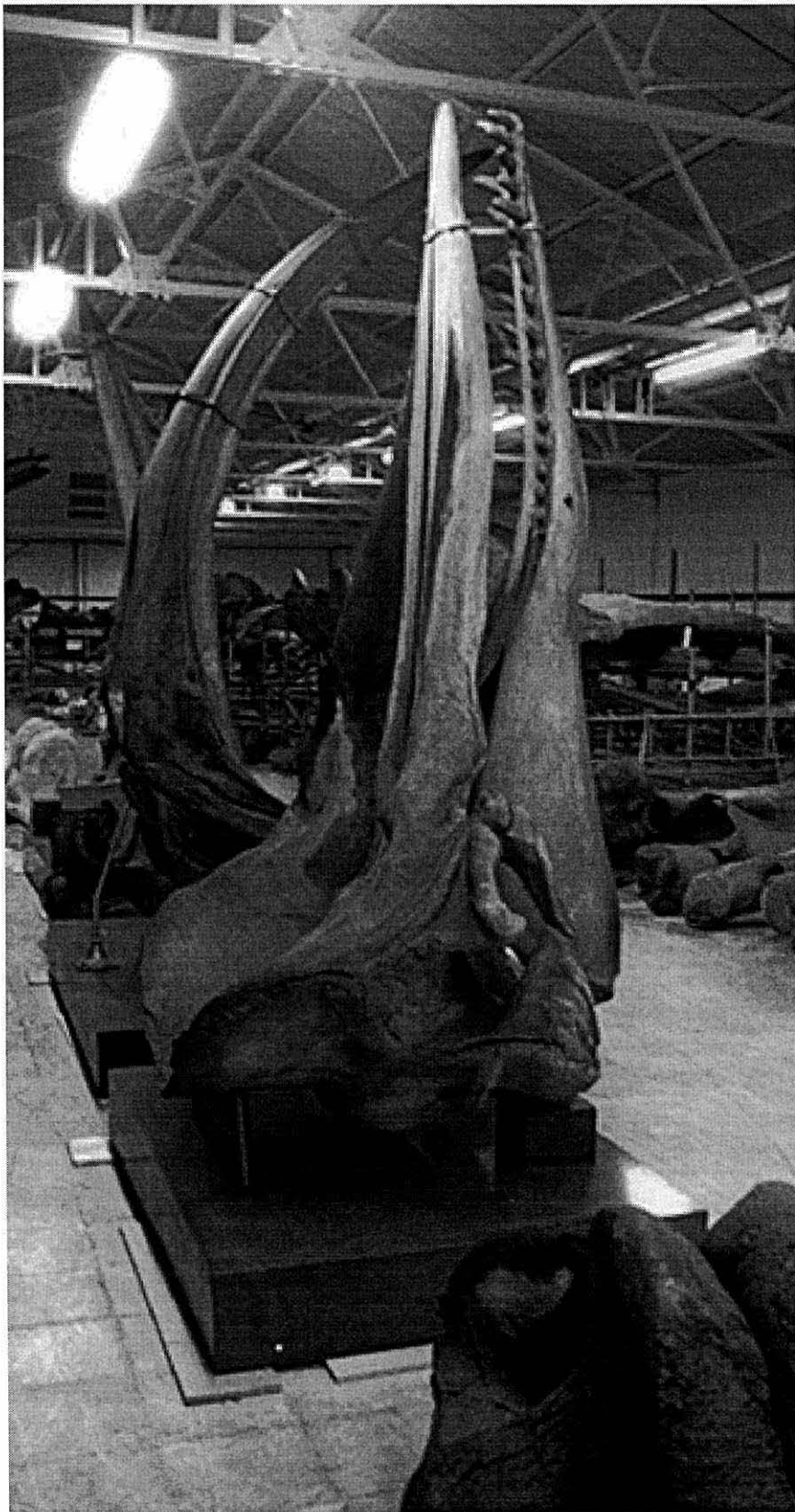


**Figure 1.2** Skull of female sperm whale from the scientific collection of the Natural History Museum, London. Specimen is mounted upright but the gross morphology with ampitheatre skull, long narrow rostrum (upper jaw) and long narrow mandible (lower jaw) is clear.

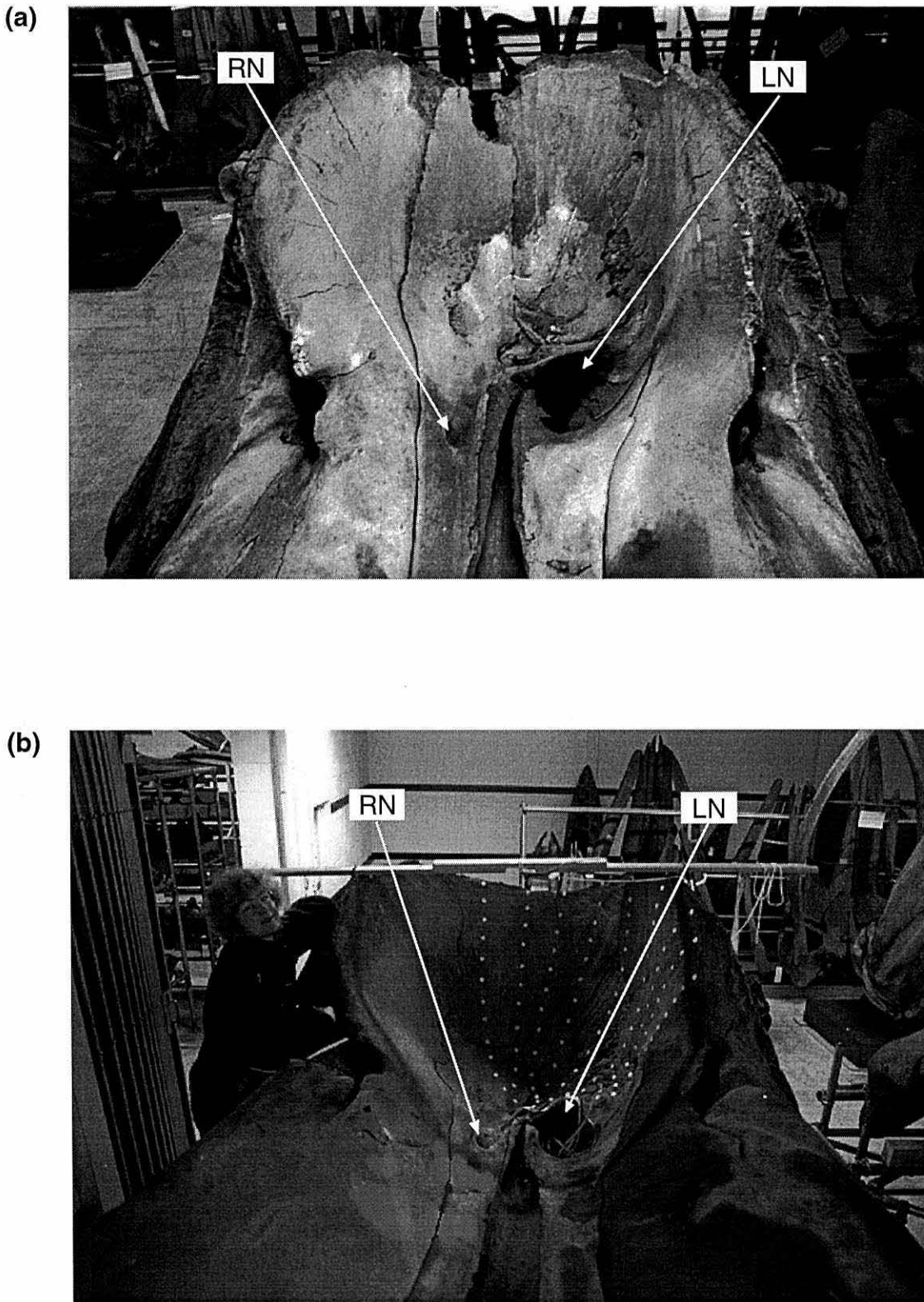


**Figure 1.3** Two examples (a) and (b) of male sperm whale skulls viewed from end of rostrum to the anterior face of the amphitheatre. In each photograph the left bony nares and right bony nares are indicated by LN and RN respectively.

Internally the sperm whale head is a complex 3-dimensional structure of oil sacs, air passages and connective tissue. The entire soft tissue head space is dominated by a huge lipid filled structure called the spermaceti organ. To give a simplified description, this “organ” is a long lozenge shaped pair of oil sacs that sit one above the other atop the long narrow rostrum which runs the entire length of the head from the cusp of the amphitheatre skull to a point overlapping the anterior end of the rostrum [Fig 1.4]. The spermaceti organ accounts for almost the entire soft tissue bulk of the sperm whale head and in an adult male the oil sacs may contain over 2,000 litres of spermaceti oil, for which the animal was highly prized by the whalers of the 19<sup>th</sup> and early 20<sup>th</sup> century. The spermaceti organ is not really an organ in the true sense of the word, but rather a complex of oil sacs and associated air sacs and tissue structures. The term spermaceti organ has become rather engrained in the popular literature, but in this dissertation the entire structure will be referred to as the “spermaceti complex”. The upper of the two main oil sacs is termed the “spermaceti sac” and is composed of a matrix of spongy tissue containing pure spermaceti oil along its length. If a section of this tissue is dissected out of a dead animal it may be squeezed much like a washing up sponge and spermaceti oil will exude from it; this tissue will hereafter be referred to as “spermaceti tissue”. The lower of the two sacs is termed the “junk”, a name from the old whaling days as it was of somewhat lower commercial value than the spermaceti sac. The junk is composed of alternating blocks of spermaceti tissue and connective tissue along its length. Sandwiched between the spermaceti sac and the junk, running the long axis of the head, is a broad flattened tube which is the right nasal passage. This tube terminates at it's posterior end in the nasofrontal sac and at it's anterior end in a single pair of monkey lips on the posterior wall of the distal sac. These monkey lips have been variously described, and generally the structure that they form is termed the *museau de*

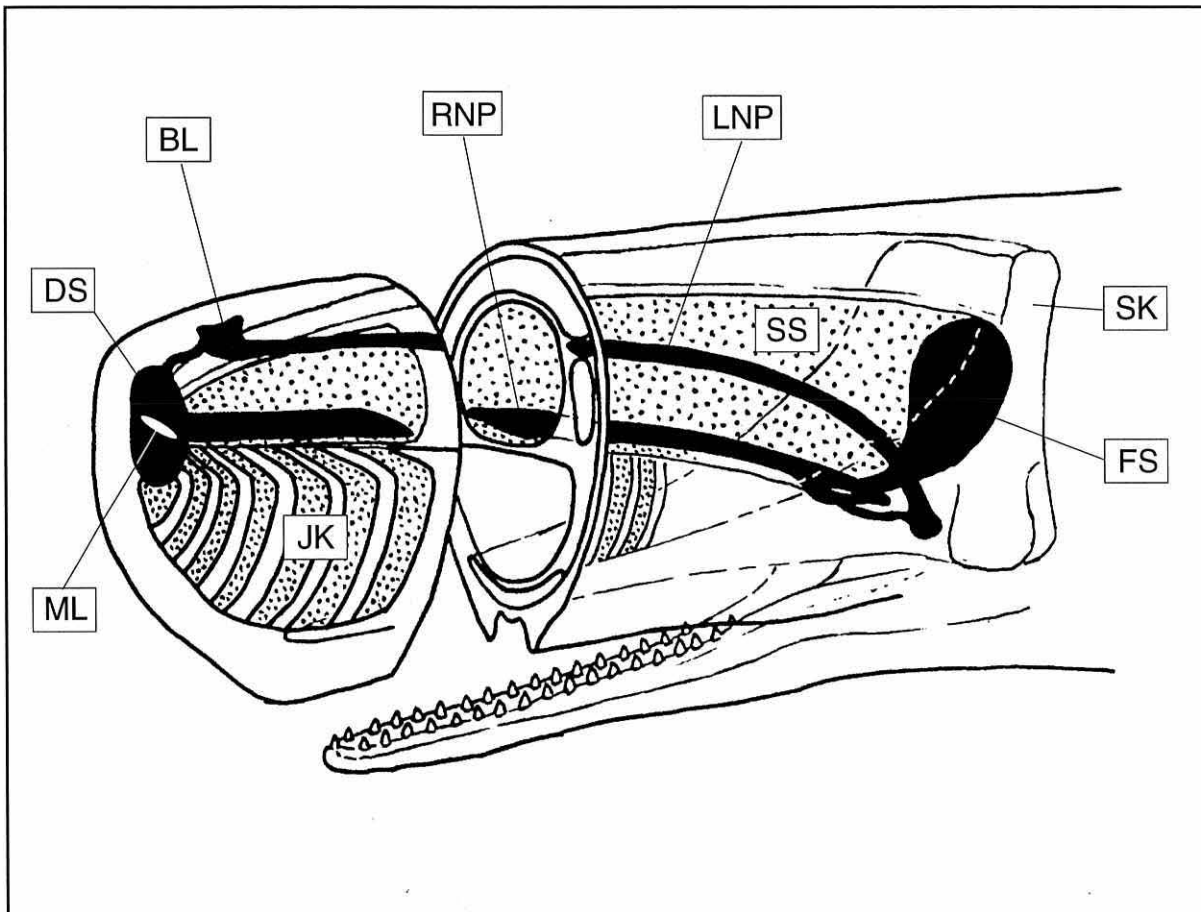
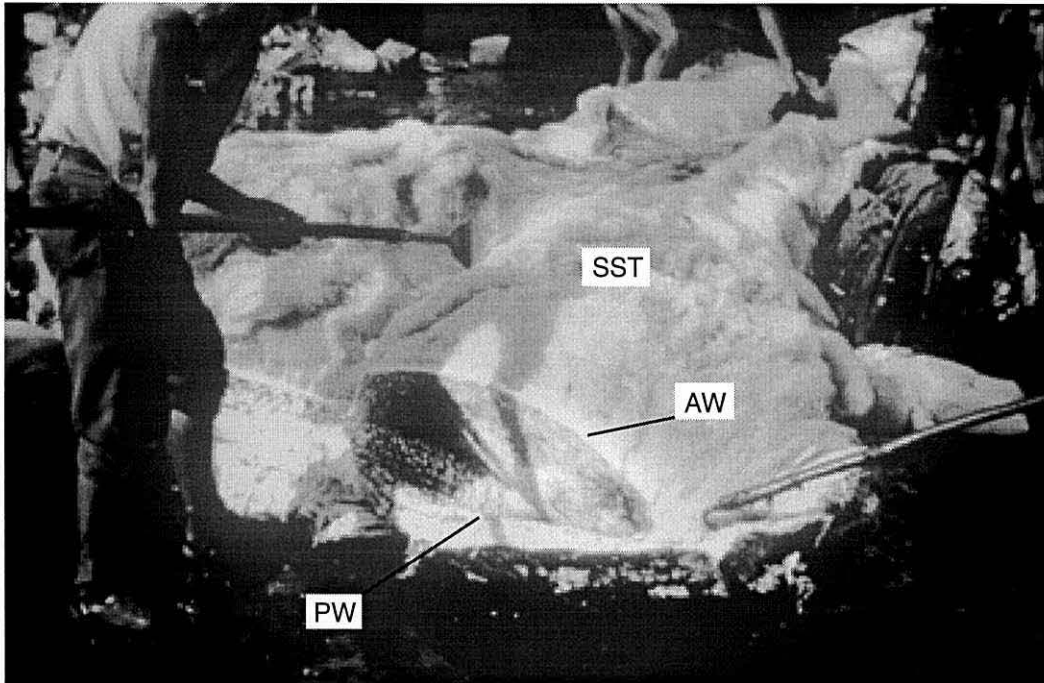


**Figure 1.4** Anatomy of the sperm whale head, drawn after Clarke 1979 copyright 1979 Scientific American Inc, all rights reserved. ML monkey lips, DS distal sac, BL blowhole, RNP right nasal passage, LNP left nasal passage, SK skull, FS nasofrontal sac, SS spermaceti sac (stippled), JK junk.

*singe* or monkey muzzle. This is clearly the same structure that Cranford et al (1996) find homologous throughout the odontocete sub-order and term monkey lips; the structure in the sperm whale head will therefore be called monkey lips hereafter. Just anterior to the monkey lips is the distal sac (synonymous with the vestibular sac of dolphins) which takes the form of a flattened dish shaped air cavity. A small air passage runs dorsally from the distal sac to a chamber just below the blow hole that connects with the left nasal passage. The left nasal passage is a direct pathway for respiration from the blow hole to the lungs, and runs dorsoventrally from the blowhole around the left side of the spermaceti complex and down through the left bony nares of the skull into the lungs. A small air passage diverges from the left bony naris and connects with the nasofrontal sac. The nasofrontal sac is a broad, flattened air space covering an area at the cusp of the amphitheatre skull. This sac is essentially a thin, concave air bladder stuck to the anterior face of the bony amphitheatre skull. The inner posterior surface of the nasofrontal sac is covered with liquid filled nodules [Figs 1.5 & 1.6] and it is thought that this arrangement helps to support the anterior face of the sac under high hydrostatic pressure and maintain a filigree of air in the spaces between the nodules. A slit in the anterior face of the nasofrontal sac opens into the posterior end of the broad flattened right nasal passage previously described.

It is clear from the above description and Figure 1.4 that the air sacs and passages in the sperm whale head form a cyclic system. The hypothesis most generally favoured is that click production in the sperm whale head is produced by pneumatic action on the monkey lips, similar to the mechanism of dolphin click production. Norris & Harvey (1972) described the anatomy of the sperm whale head and the hypothesis of click production at the monkey lips. Essentially it is thought that air pressure is built up in the broad tube of the

(a)



(b)

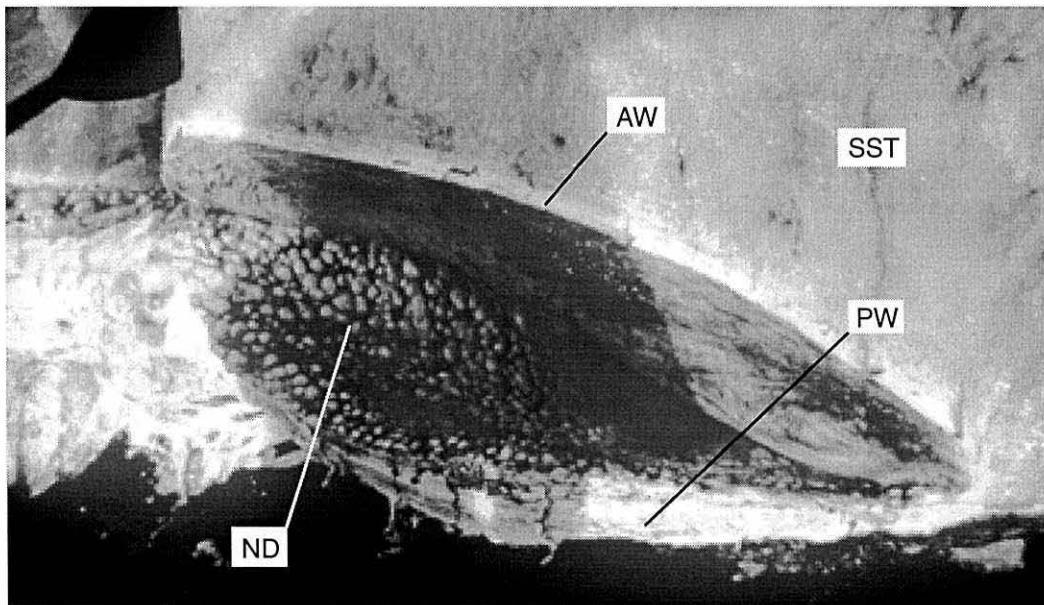
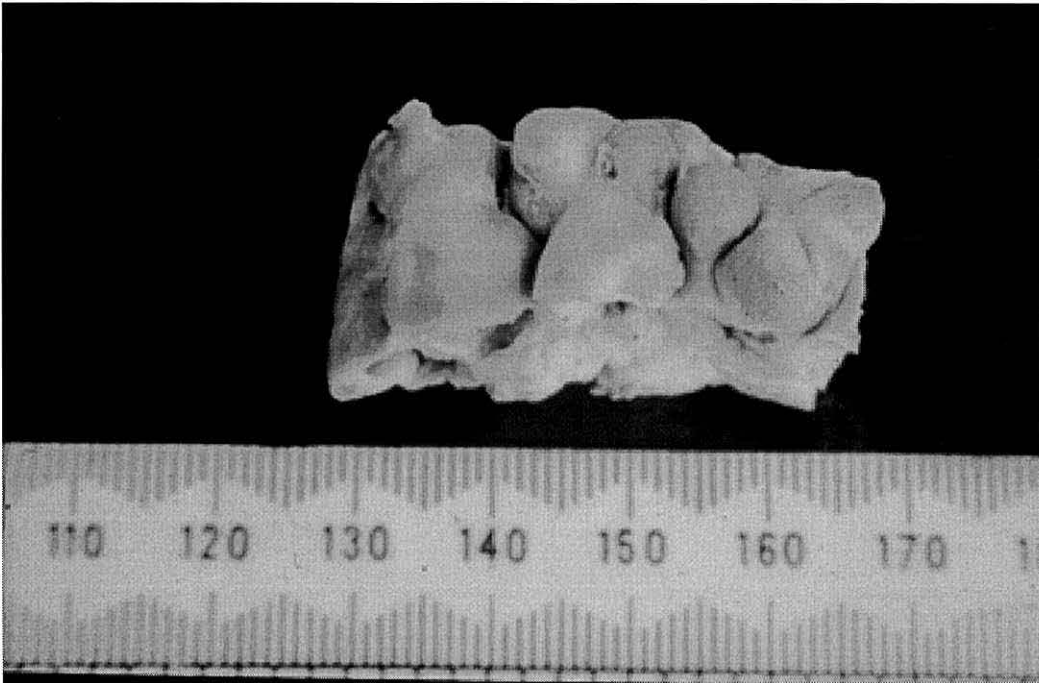


**Figure 1.5** Photographs of (a) unusual longitudinal dissection of spermaceti sac during whaling operations, revealing the nasofrontal sac; AW anterior wall of nasofrontal, PW posterior wall of nasofrontal sac, SST spermaceti sac tissue. Picture (b) shows a close up view of the nasofrontal sac and fluid filled nodules, ND. Photographs courtesy of Malcolm Clarke.

(a)



(b)

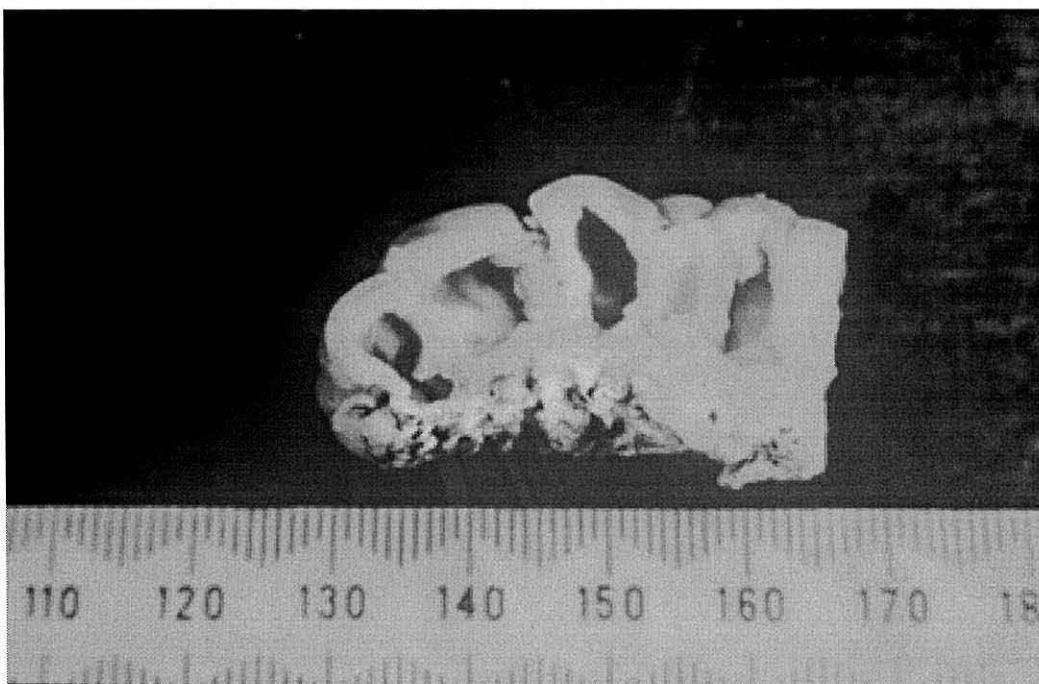


**Figure 1.6** Small nodular section of tissue taken from posterior wall of nasofrontal sac of a 10 m female sperm whale killed off Durban in 1972. In (a) the nodular surface is clearly visible and in (b) the cavities normally filled with fluid can be seen; ruler scale is in mm. Tissue section courtesy of Malcolm Clarke.

right nasal passage, perhaps through peristaltic action of the smooth muscle which lines its length, and high pressure air released in impulsive bursts through the monkey lips into the distal sac. Although no “hammer & anvil” structure in the monkey-lip/distal-sac complex has been adequately described in the sperm whale literature, such detailed anatomical observation is difficult and it is possible that a similar mechanism may occur to couple mechano-pneumatic energy forwards into the surrounding seawater through the tissues of the front of the head. If a release of compressed air into the distal sac indeed occurs, the system of airways would enable recycling of the air for further use in click production. Such air recycling would seem to be a pre-requisite for a pneumatically driven sonar system of an animal that may spend over an hour submerged and produce several thousand clicks during the course of a dive.

At this point it is necessary to describe the general features of sperm whale clicks, and these are addressed in the next chapter. The acoustic structure of sperm whale clicks, however, seems inextricable bound to head anatomy and discussion of this will be raised later. The aim of this dissertation is to examine the temporal and frequency characteristics of sperm whale clicks in some detail and to discuss their possible utility to both the animal and also to human observers who may study them in the open ocean. In addition the sound velocity characteristics of spermaceti oil are examined with a view towards its functional significance in sound transmission within the sperm whale head, and again the significance of its variability to human observation which attempts to study sperm whales in the wild through passive acoustics.

## **Chapter 2**

### **Time and Frequency Domain Characteristics** **of Sperm Whale Clicks**

#### **2.1 Introduction**

During the course of the last four decades acoustic emissions from sperm whales have generated much interest. Sperm whale sounds were first recorded in the 1950's and later identified (Worthington & Schevill, 1957). These workers reported that sperm whales produce loud, impulsive clicks at various repetition rates; an observation that has since been confirmed by several workers (Backus & Schevill, 1966; Bunsel & Dziedzic, 1967; Norris & Harvey, 1972; Gordon, 1987; Weilgart & Whitehead, 1988). A variety of sounds have been attributed to sperm whales (see Gordon, 1987 & Weilgart, 1990 for a review). Sperm whales are prodigious divers and frequently undertake vertical excursions in excess of 500 metres in search of food, primarily deep sea squid (Clarke et al, 1993). Dives of even greater vertical extent, in excess of 2,000 metres, have also been reported (Lockyer, 1977; Watkins et al, 1993). While undertaking these dives, which may last up to 90 minutes, animals invariably produce a monotonous series of clicks with repetition rates between 0.5 - 2 s<sup>-1</sup>. It is generally assumed that the primary function of these sounds is echolocation, and at intervals during the dive click rates increase markedly leading to very "faint" but rapid bursts of clicks with repetition rates of up to 200 s<sup>-1</sup> (Gordon, 1987). Such rapid bursts

sound similar to the final echolocation runs of dolphins (Au, 1993) and bats (Suga, 1990), and it is assumed that these also represent final echolocation runs as sperm whales close on their prey. These rapid bursts are commonly referred to as “creaks” in the sperm whale literature, and the use of this term will be continued in this dissertation.

The regular clicks are broad-band transient signals with a duration of some 10 - 20 ms depending upon the size of the animal producing them. Watkins (1977) noted click energy ranging from below 100 Hz to well in excess of 20 kHz, with major emphases in the 2 - 6 kHz range. Other workers report dominant frequencies of 5 kHz (Backus & Schevill, 1966), 1 kHz (Bunsel & Dziedzic, 1967), 2 - 8 kHz (Levenson, 1974) & 2 kHz (Weilgart & Whitehead 1988). Levenson (1974) calculated a mean broadband (250 Hz - 16 kHz) off axis source level for sperm whale clicks of 171 dB re 1 $\mu$ Pa @ 1m. Individual clicks within creaks have received little attention in the literature and their presence is merely noted in this study, which concentrates exclusively on the so called “regular clicks”.

One striking feature of sperm whale clicks, noted by Backus & Schevill (1966), is that they consist of a series of regularly spaced pulses with decaying amplitude. An example of such a click, recorded from a diving female sperm whale off the Azores, is shown in Figure 2.1. In a classic paper Norris & Harvey (1972) attributed this pulsed structure to multiple reflection of an initial sound pulse between the nasofrontal and distal air sacs within the head of the sperm whale. These air cavities are proposed to act as sound reflectors due to the large difference in acoustic impedance between air and spermaceti oil, even under the elevated pressures encountered at 2,000 metres depth. A meshwork of rounded fluid filled nodules cover the posterior wall of the nasofrontal sac and may help to maintain air spaces

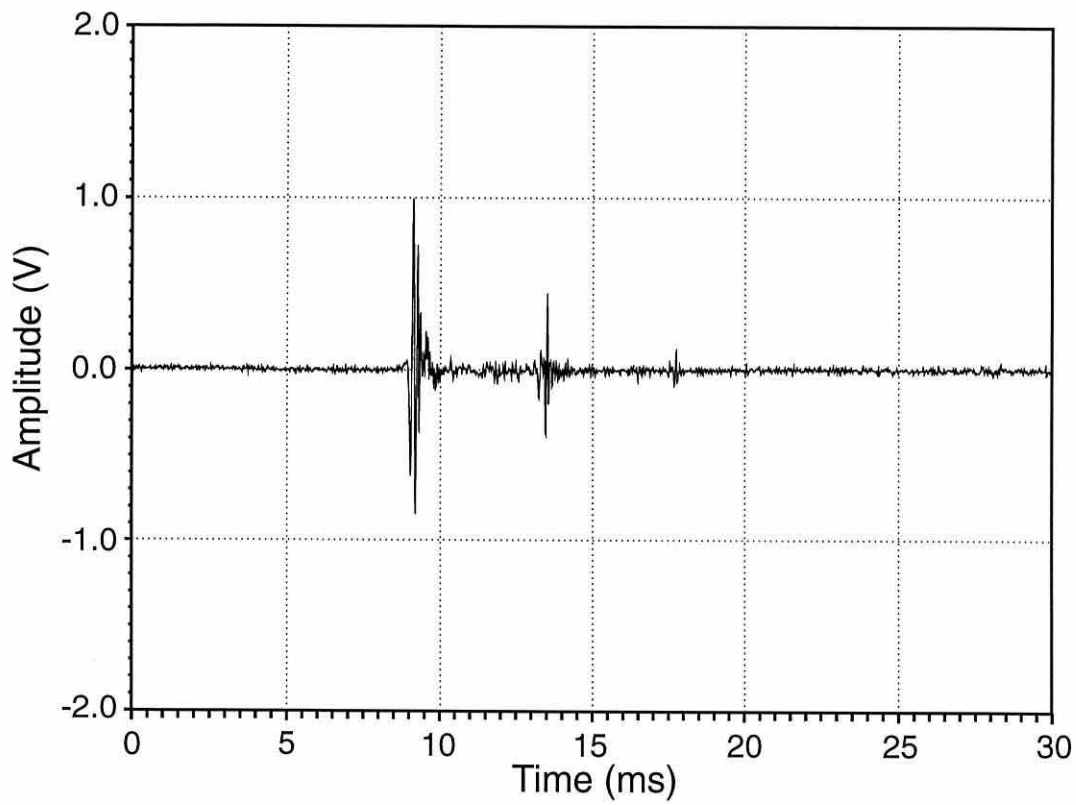


**Figure 2.1** Example click from a diving female sperm whale showing regularly spaced pulses with decaying amplitude.

in the regions surrounding each nodular apex by supporting the anterior face of the sac at high pressures [Figs 1.5 & 1.6]. A similar nodular covering has not been described for the distal sac, but if the click production event is the result of a forward release of high pressure air through the monkey lips into the distal sac it may be expected that this event in itself would inflate the distal sac sufficiently for it to present a temporary acoustic boundary, capable of sound reflection for at least the duration of the click. If sound is produced at the front of the sperm whale head by pneumatic action on the monkey lips, multiple reflections within the head may be an inevitable consequence of a section of the expanding wavefront channelling through the oils of the spermaceti sac between the two air spaces.

If the above described hypothesis of pulsed click generation is correct, it follows that the time delay between successive pulses within a click should be a function of the distance separating the frontal and distal air sacs and the velocity of sound through the intervening medium. In other words the time delay between pulses is directly proportional to the length of the spermaceti sac. The spermaceti sac length is itself a function of the total body length and hence it should be possible to estimate body length from click intra-pulse intervals and a knowledge of sound velocity in spermaceti oil. A few studies since have suggested this to be the case (Alder-Fenchel, 1980; Mohl et al, 1981; Gordon, 1991; Mohl & Amundin in Amundin 1991), and an empirical relationship to relate the intra-pulse interval (IPI) to the spermaceti sac length, and hence body length, of individual animals is quoted in Gordon (1991).

Since Norris & Harvey's (1972) paper, several workers have studied sperm whales in their deep ocean environment, often employing hydrophones and recording equipment for the

purposes of tracking and acoustic studies (Watkins, 1977; Gordon, 1987; Weilgart & Whitehead, 1988; Whitehead & Weilgart, 1990). Passive acoustic monitoring has great potential for the study of cetacean populations in the open sea. Sperm whale clicks propagate well in oceanic water and are easily received at several kilometres range using a hydrophone or array of hydrophones (Gordon, 1987). With the appropriate array geometry, bearing and range to source animals can be calculated. With towed arrays of hydrophones the potential exists to count sperm whale numbers along given transects of ocean (effectively a whale census). A methodology for passive acoustic censusing has already been developed for sperm whales (Hiby & Hammond, 1989), although it has not yet been applied on the scale of ocean basins. While the methodology exists to count sperm whales in the open sea by purely acoustic means, further analysis of the fine structure of the vocalisations may yield additional information. Enhanced processing of sperm whale click structure may enable automated measurement of intra-pulse intervals during surveys, and in turn body lengths of individual animals may be extrapolated. Such information would be useful in evaluating sperm whale population structure in terms of animal size.

## **2.2 Methods**

### **2.2.1 Field Data Collection**

Between 1987 and 1993 the International Fund for Animal Welfare (IFAW) sponsored benign research into the behaviour and ecology of sperm whales in the waters around the Azores, a group of nine North Atlantic islands situated between latitudes 36° 50'N - 39°

50°N and longitudes 31° 30'W - 24° 50'W. Regular clicks of diving sperm whales were recorded from the IFAW research vessel *Song of the Whale*, a 14 metre Ketch, through the field seasons 1987 to 1993. Stereo recordings were made on magnetic tape through towed hydrophones and selected recordings of sperm whale clicks were later taken for analysis at the School of Ocean Sciences, University of Wales Bangor.

The hydrophone assembly used to receive sperm whale sounds consisted of two Benthos AQ-4 transducers, each with separate pre-amplifiers and integral 200 Hz high pass filters, mounted 20 metres apart along the axis of the tow line in a plastic tube filled with castor oil for close impedance matching to seawater. The assembly was towed on 100 metres of strengthened cable behind the vessel. When under sail the array geometry was simply 2 elements 100 metres and 120 metres aft, when stationary the hydrophone assembly and tow cable sank thereby resulting in a geometry of elements 100 metres and 120 metres directly below the vessel. During the field seasons 1987 - 1990 the signals were recorded on a Nagra IV-SJ reel to reel tape machine, from 1991 onwards signals were recorded on Digital Audio Tape (DAT) using a Sony TCD-D10 ProII DAT recorder. According to manufacturers specification [Appendix 1] the frequency response of Benthos AQ-4 elements is flat, -201 dB re 1V/μPa ±1.5 dB (from 200 Hz to 15 kHz) and flat ±3 dB (from 15 kHz to 30 kHz). A similar hydrophone assembly using similar component parts, i.e. a Benthos AQ-4 element and miniaturised transistor pre-amplifier, were calibrated at the Loughborough University of Technology in a test tank against a precise reference transducer. The voltage response curve is shown in Figure 2.2 and indicates that the system output is -172 dB re 1V/μPa ±1.5 dB between 4 kHz and 25 kHz. Calibration was performed broadside to the AQ-4 element, but manufacturers data [Appendix 1] indicates

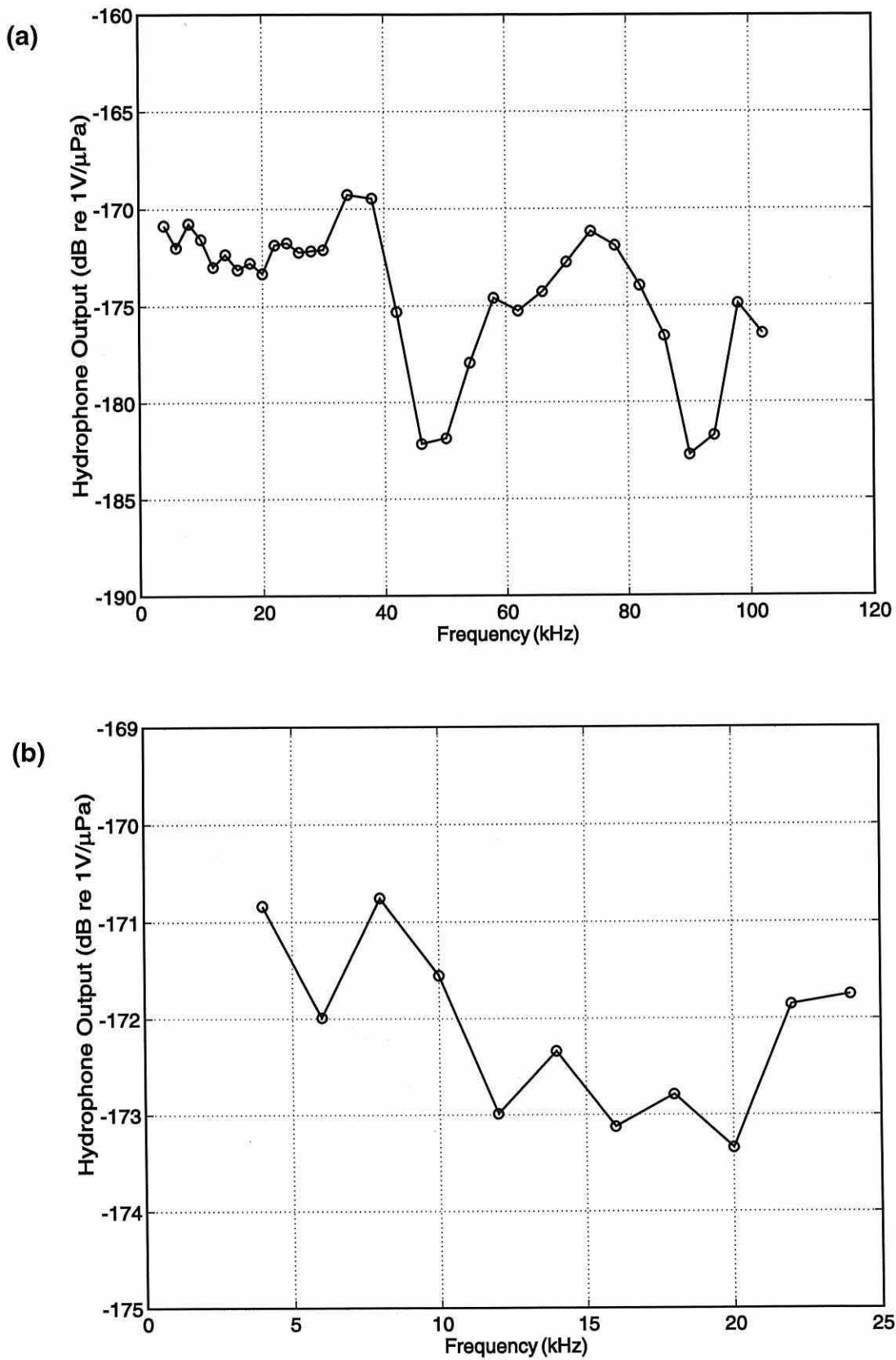


**Figure 2.2** Calibration curves for benthos AQ4 hydrophone element with miniaturised transistor preamplifier in line, (a) shows full frequency range tested and (b) shows frequency range pertaining to sperm whale recordings.

that the element is essentially omnidirectional at frequencies up to at least 20 kHz so the response in Figure 2.2(b) can be assumed at any aspect. Although calibration could not be performed at frequencies below 4 kHz due to tank reverberation, it is assumed that the frequency response will remain flat  $\pm 1.5$  dB re 1V/ $\mu$ Pa down to at least 200 Hz. The response of the hydrophone system used to record sperm whales will therefore be considered flat  $\pm 1.5$  dB between 200 Hz and 25 kHz. The response of the Nagra IV-SJ recorder with an equalised tape is flat  $\pm 1$  dB re 1V from 25 Hz up to 35 kHz at maximum tape speed according to manufacturers specifications [Appendix 2], although recordings were generally made at half speed where the response is specified as flat  $\pm 1$  dB re 1V up to 20 kHz. The frequency response of the Nagra was not measured independently and the equalisation status of the reel-reel tapes during field recording is unknown. As the Nagra specifications give no indication of the likely error for unequalised tapes the frequency response for the Nagra recording system can only be considered as flat  $\pm 1$  dB from 25 Hz to 20 kHz; however from the good quality recordings obtained it seems unlikely to be greatly in excess of this figure. According to manufacturers specifications the Sony DAT recorder frequency response is flat  $\pm 1$  dB re 1V from 20 Hz to 22 kHz [Appendix 2], and this is again assumed to apply to sperm whale recordings on this medium. Low pass filters in the DAT line input sharply attenuate any signal at frequencies higher than 22 kHz to minimise the risk of aliasing; sampling frequency of the DAT recorder is 48 kHz. As error tolerances accumulate through the recording system the click recordings made in the field can not be expected to have a frequency response better than  $\pm 2.5$  dB in any instance. In addition the original field recordings were copied onto second generation DAT via analog channels, hence compounding the final frequency response error to not better than  $\pm 3.5$  dB.

Typically, during daylight encounters with sperm whales off the Azores, the survey vessel *Song of the Whale* was positioned some 300 metres behind a target whale, or as close as possible without causing disturbance to the animal, and maintained this position until the whale “fluked up” and commenced its dive. The action of fluking up usually signifies the beginning of a feeding dive, where the whale brings its tail flukes clear of the water as it assumes a near vertical, head downwards posture and descends beneath the surface. Once a target whale was submerged, a continuous stereo recording was made of its clicks through the hydrophone array, ideally with the vessel holding station and allowing the hydrophones to descend as far as possible from the surface. Deep hydrophones maximise the time delay between the reception of a click at the elements and reception of a “ghost click” after the sound has been reflected back down onto the elements from the ocean surface - which acts as an almost perfect sound reflector. Typically the hydrophone array would take some 3-5 minutes to settle into a vertical position once the vessel had come to a halt and since whales rarely began clicking until 2 - 3 minutes into their dives the array always had time to make sufficient descent for direct path click waveforms to be separate from ghost click waveforms on recordings. From 1990 onwards a Furuno paper trace depth sounder was installed on the boat and was used on occasion to measure the descent rate of target animals. Immediately after a whale fluked up, a characteristic patch of disturbed surface water, known as the “slick” or “footprint” was visible and conveniently marked the point of the whales' submergence. On occasion the vessel was moved quickly onto the slick and the echo sounder activated to yield one strong echo from the target whale. The echo returning from the whale was traced on a moving roll of paper, calibrated vertically in fathoms (1 fathom = 1.8288 metres) and horizontally in minutes. The depth sounder operated to a maximum depth of 900 metres, although it was generally only possible to track the descent of sperm

whales over the first half of this range. Sperm whale descent rates were typically about  $1.6 \text{ ms}^{-1}$  (100 m/min), and whales began clicking some 2 to 3 minutes after fluking up. All clicks recorded through the hydrophone array were therefore being received from behind the whales during the early dive stages. Although the voltage response of a similar hydrophone assembly to the one used during the sperm whale recordings has latterly been obtained, the voltage through-put of the composite field recording system was never calibrated, and a transient crew composition on *Song of the Whale* usually meant that recorder gain settings were not noted. Absolute sound pressure level at the hydrophone elements cannot therefore be extrapolated, and as the depth sounder traces were not well documented or matched with recordings, source levels of sperm whale clicks cannot be estimated. Even if this data had been recorded, the sensing position of the hydrophone was never placed directly ahead of the diving animal so the on-axis peak source level and power spectrum could not actually be measured.

### **2.2.2 Laboratory Data Acquisition**

High quality recordings of sperm whale clicks were selected from the field data, and copied from the master tapes (either analog or digital) onto a second generation of Digital Audio Tape. The selection criteria for click sequences were (i) single, or very few, whale vocalisations making it possible to follow with confidence the clicks of a particular individual over extended time periods and (ii) click sequences with high signal to noise ratio. A total of nine individual click sequences were chosen for analysis and are detailed in Table 2.1. Tape recordings of click sequences were sampled from the analogue output of

Click Sequence Code	Whale Sex	Sequence Duration (minutes)	Total Number of Clicks
SW1	♂	20.7	1,056
SW2	♂	20.1	1,125
SW3	♂	11.0	655
SW4	♂	14.0	775
SW5	♂	13.9	975
SW6	♀	10.8	1,032
SW7	♀	11.1	664
SW8	♀	7.4	547
SW9	♀	15.0	1,711

**Table 2.1** General information on the nine sperm whale click sequences selected for analysis.

the DAT recorder onto computer hard disk using a Cambridge Electronic Design (CED) 1401 laboratory interface. The click sequence recordings were sampled in long continuous sections of 3 minutes duration at a sampling frequency of 62.5 kHz (sample interval 16 $\mu$ s). Such a high sampling rate comfortably oversampled the maximum frequency reproducible by the DAT medium. Sampling in continuous 3 minute sections was the longest sampling period possible given the software and disk space available, and was useful for continuity when examining precise time intervals between clicks in long sequences.

### **2.2.3 Data Analysis**

Analysis of the sampled waveform data was performed using CED SPIKE2 software V4.70. This software enabled the display and manipulation of long sections of waveform data, and output of analysis results to ASCII data files on disk. Important features of the package were power spectrum analysis and digital filtering using FIR filter coefficients designed by the user. The features of sperm whale clicks studied were (i) rates of clicking, (ii) frequency domain characteristics of clicks, (iii) time domain characteristics of clicks & (iv) combined time-frequency characteristics of clicks.

#### **2.2.3(i) Click Rates**

For each animal the click sequence was viewed sequentially and the onset of each click marked by inspection with the waveform channel cursor. Click onset times were stored

sequentially to an ASCII file and used to calculate the intervals between successive clicks by simple subtraction; click rates were calculated as reciprocal values of these intervals. Time intervals between clicks of greater than 4 s were taken as intervals between sub-sequences of clicks, i.e. a whale may stop clicking briefly and then resume clicking at a rate approximately equal to that at which it stopped. Intervals between clicks of greater than 4 s were not included in the reciprocal calculation of inter-click intervals.

### **2.2.3(ii) Frequency domain analysis**

Each click, marked by previous inspection, was transformed to the frequency domain in the form of a power spectrum. Stored click onset times were used as reference points for the analysis of short waveform segments (i.e. individual clicks). The SPIKE2 analysis package employed a 2048 point Fast Fourier Transform (FFT) on 32.768 ms of waveform data, beginning at a point approximately 8 ms preceding each click onset, thus encompassing all significant components of the click. Figure 2.3 shows example time domain views of male and female sperm whale clicks extracted for FFT analysis. As the click waveforms were not significantly truncated, no windowing of waveform data was performed prior to analysis. The FFT routine employed a radix-2 method across  $2^n$  data points, producing  $n/2+1$  power magnitude estimates and  $n/2-1$  phase estimates. Thus, with a sampling frequency of 62.5 kHz, a 2048 point FFT produced 1025 magnitude estimates, each with a frequency resolution of approximately 30.5 Hz. Magnitude estimates were stored to 11 decimal places in ASCII files, phase estimates were discarded. The power magnitude data, held in serial access ASCII files, was subsequently converted to random access format for ease of access

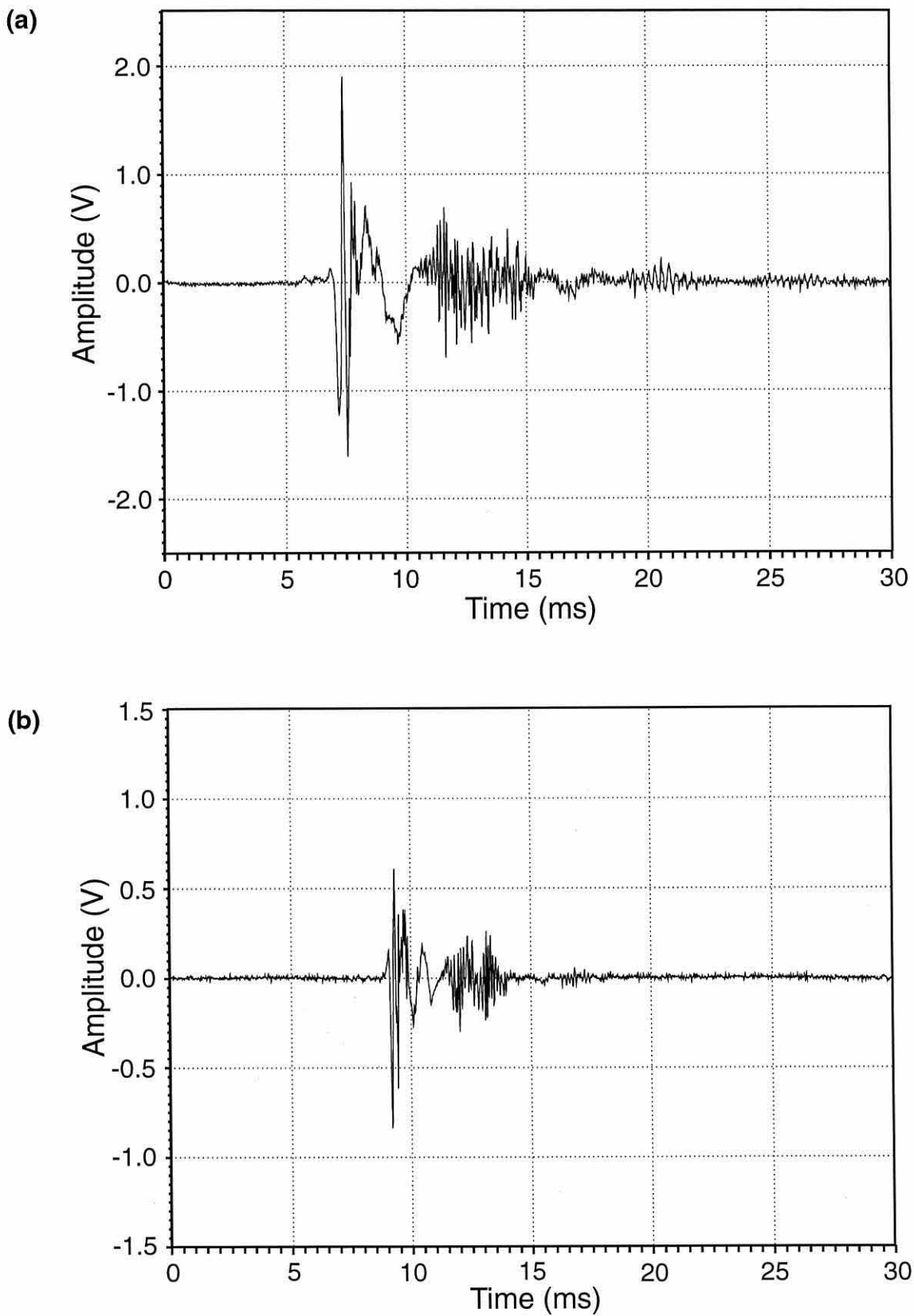


**Figure 2.3** Typical sperm whale clicks recorded during first few minutes of feeding dives: (a) click from large bull male, (b) click from smaller female.

and compression of data. A computer program was then written in Turbo Pascal V6 [Appendix 3] to display the power magnitude data in the form of a 3D cascade of power-frequency graphs along a time axis. To display all the spectral data in this manner would have required a very large number of plots, so the bulk of data was reduced by averaging to enable display of entire click sequences on single plots. Each power-frequency slice of the cascade was normalised and successive blocks of 10 spectral slices averaged to a single slice. These data were then displayed as cascade plots for each click sequence showing an overview of the spectral distribution of energy through the full duration of the respective click sequences.

### **2.2.3(iii) Time domain analysis**

Time domain characteristics of sperm whale clicks were investigated by selective filtering of the original click sequence wavedata files to pass only the components in selected frequency bands. Digital FIR filters were used, filter coefficients being generated using the Kaiser design parameters [Appendix 4], with emphasis placed on sharp passband-stopband transition and low sidelobe ripple levels (Lynn & Fuerst, 1992). Typically filters were generated with passband-stopband transition widths of  $3^\circ$  ( $\pi/30$  radians), with stopband attenuation more than 50 dB re 1 waveform-unit down on the passband. Maximum magnitude of sidelobe ripples was -38 dB re 1 waveform-unit down from the passband. Once a suitable filter was designed the coefficient values were stored as an ASCII data file in the form of a symmetrical impulse response. This file was then used by the SPIKE2 software to filter the waveform data file by digital convolution (Lynn & Fuerst, 1992). As

an odd number of filter coefficients was always used (usually  $n_{\text{coeff}}=251$ ), and filtering began  $(n_{\text{coeff}}/2)+1$  points into the wavedata file, the filtering process exhibited zero phase shift.

### **2.2.3(iv) Time/Frequency analysis**

Selected sections of clicks were subjected to time/frequency analysis using a Short-Time Fourier Transform in order to investigate changes in the levels and distribution of spectral energy within individual clicks as a function of time. The technique employed a sliding FFT window that was short in comparison to the waveform section of interest (i.e. the whale click). The window was stepped through the wavedata sequentially from start to finish, calculating the power spectrum for each frame. A 256 point (approximately 4 ms) window was used, the right hand edge beginning at a point immediately preceding the click onset, so as to begin on a “blank” section of background noise wavedata. STFT analysis was performed across a total of 18 ms of the whale click, advancing in steps of 0.32 ms. For each step the 256 wavedata points in the analysis window were modulated with a raised cosine function (the only tapering window available within SPIKE2), then transformed to a power spectrum with a 256 point FFT. After each FFT operation the SPIKE2 software made automatic compensation for a 3/8 power loss in the spectra, caused by cosine windowing of the source wavedata. The resulting power magnitude data and time shift values were stored and presented in a 3-D cascading waterfall display similar to the sequential click spectra.

## **2.3 Results**

### **2.3(i) Click rates**

Figure 2.4 shows click rates of the male sperm whales SW1 - SW5. Figure 2.5 shows click rates of the female sperm whales SW6 - SW9. Each plot shows click rates as reciprocal values of inter-click intervals against the time since the first click. The time lag between a whale fluking up and the first click was usually only 2 - 3 minutes, so the time axes could, as a crude approximation, be considered as the time during the dive cycle. The figures show that click rates generally begin between 0.5 and 1 click s<sup>-1</sup> and increase gradually over the first 2 - 4 minutes, whereupon click rates tend to oscillate around an equilibrium level. The click rate plot of SW7 [Fig 2.5(b)] is unusual in that it shows click rate to increase across an extended period. Interestingly the amplitude of oscillations in click rate are generally greater in the female sequences than in the male sequences, evident by virtue of all plots scaled to the same axes. During the male sequences [Figs 2.4(a) - (e)] sharp increases in click rate can be seen every few minutes, the majority of these immediately precede creaks. If creaks signify final feeding events, as an animal homes in on its prey, such click rate increases might be expected in the closing stages before a creak.

Mean equilibrium click rates have been calculated for each sequence using the data from 4 minutes onwards in each case, results are shown in Table 2.2. The large bull males SW1-SW4 have the slowest click rates and the females SW6 - SW9 the highest. Interestingly SW5 was judged (from its' IPI) to be a male smaller than a bull, but larger than the females,

Fig 2.4(a)

SW1

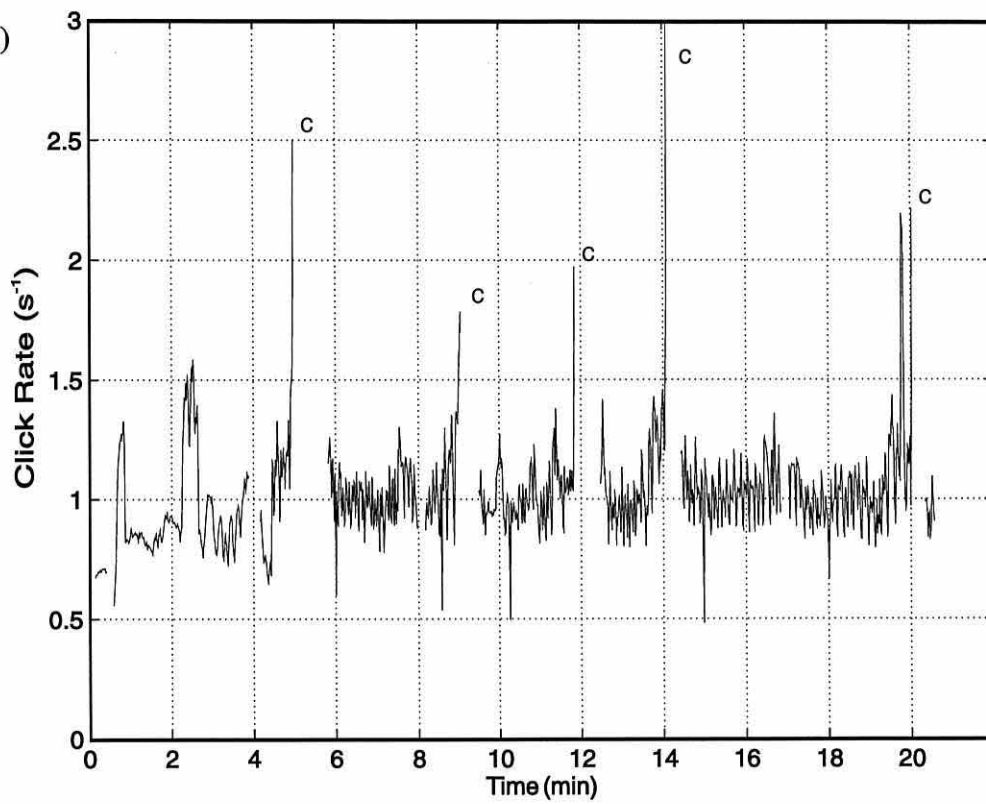
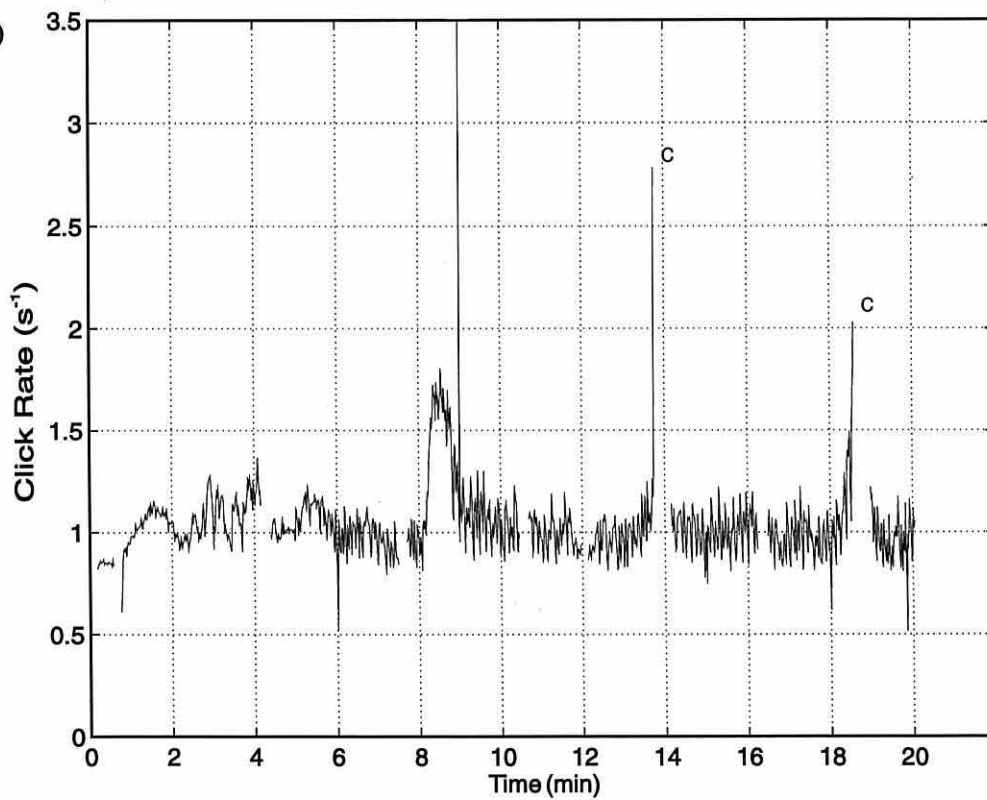
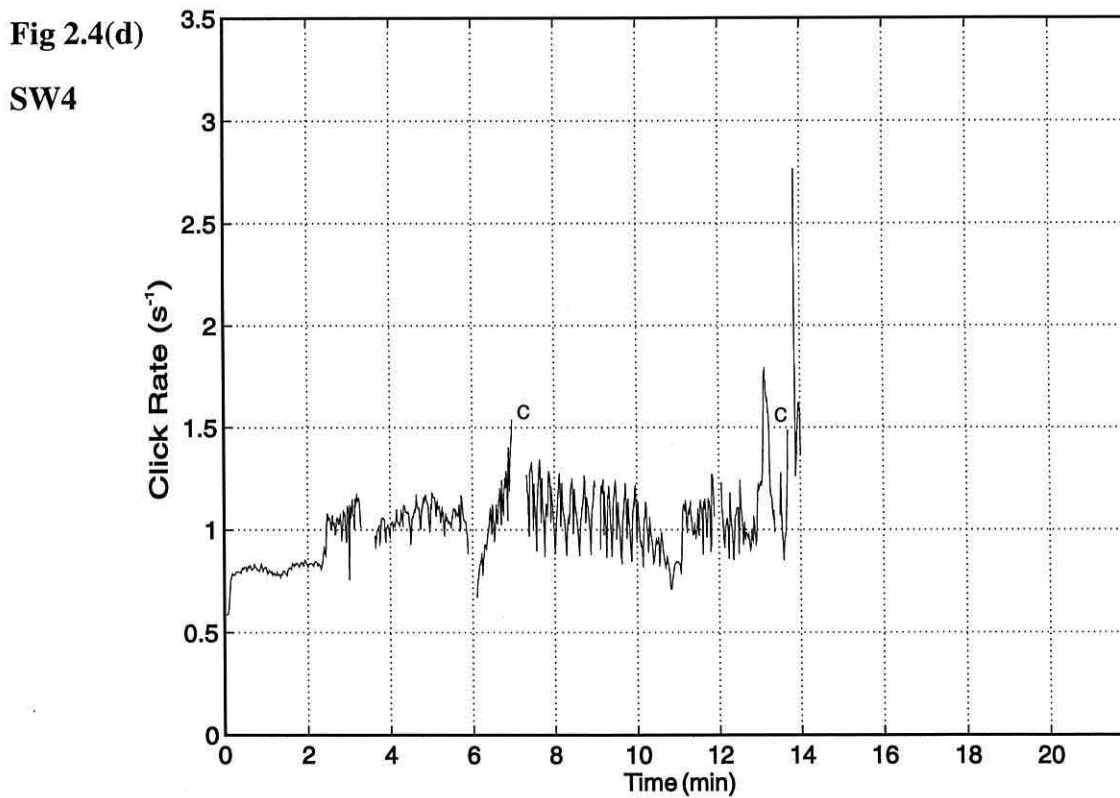
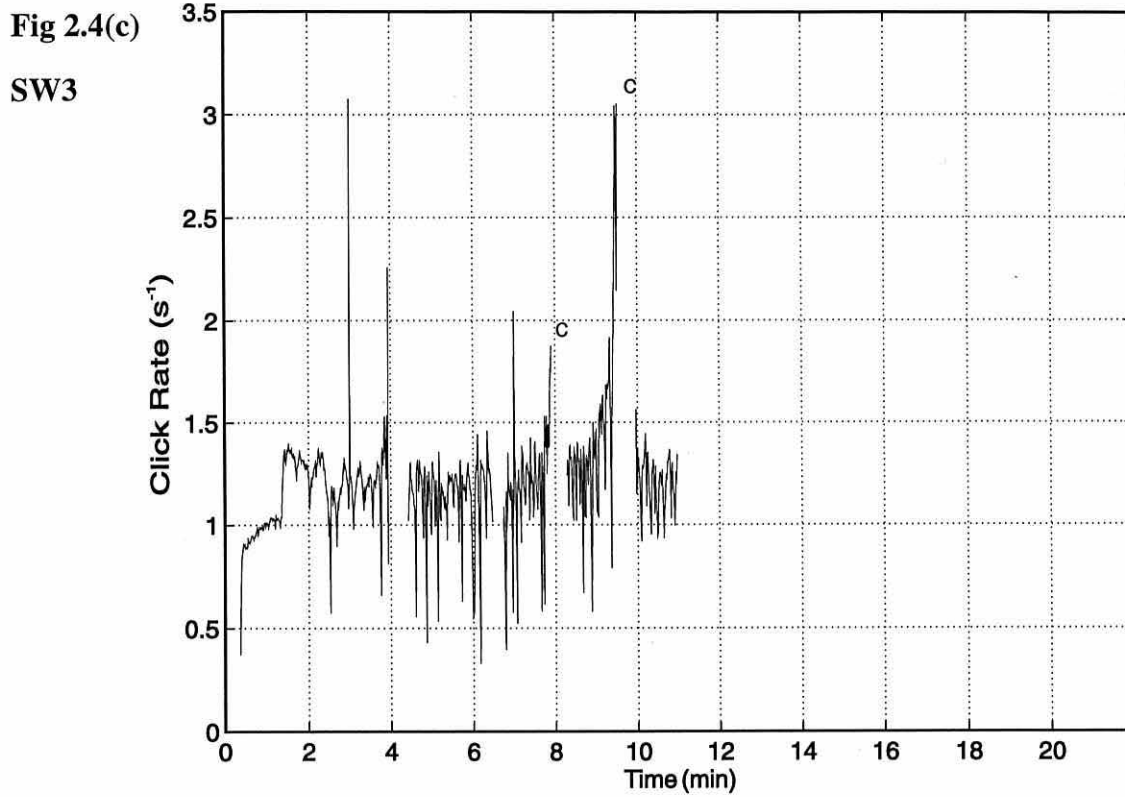


Fig 2.4(b)

SW2



**Figure 2.4** Click rate plots from feeding dives of male sperm whales (a) SW1 and (b) SW2. Occurrence of creaks indicated by "c".



**Figure 2.4** Click rate plots from feeding dives of male sperm whales (c) SW3 and (d) SW4. Occurrence of creaks indicated by "c".

Fig 2.4(e)

SW5

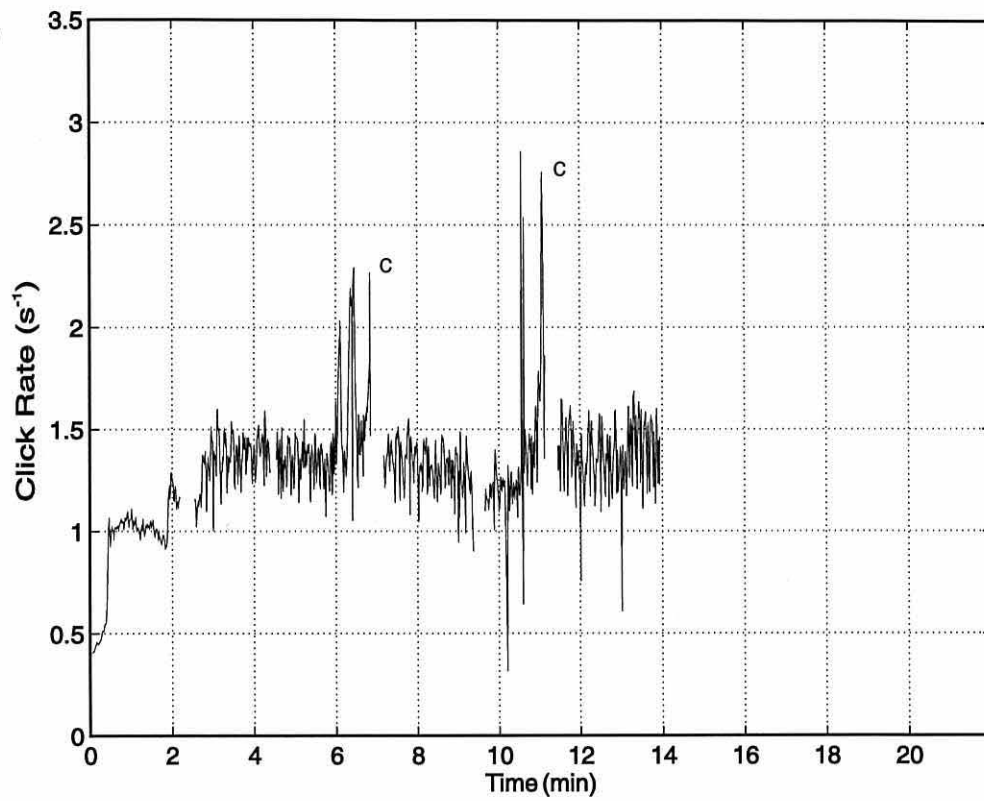


**Figure 2.4** Click rate plot from feeding dive of male sperm whale (e) SW5. Occurrence of creaks indicated by "c".

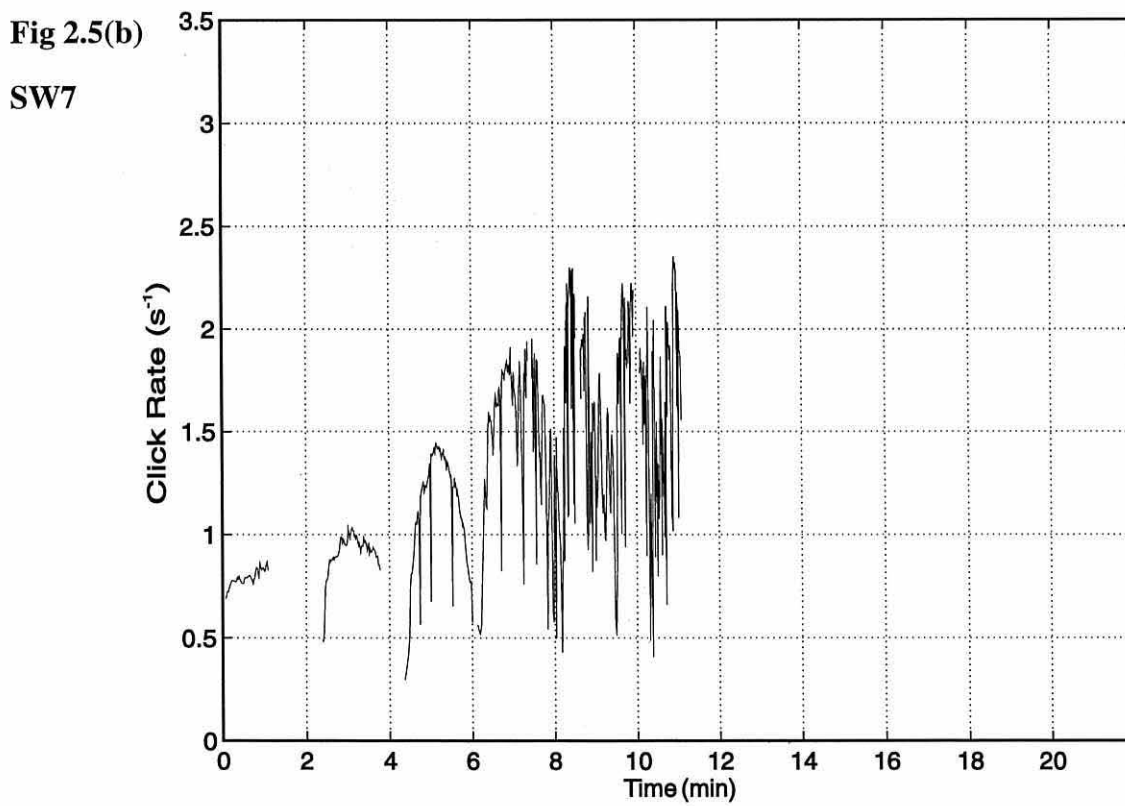
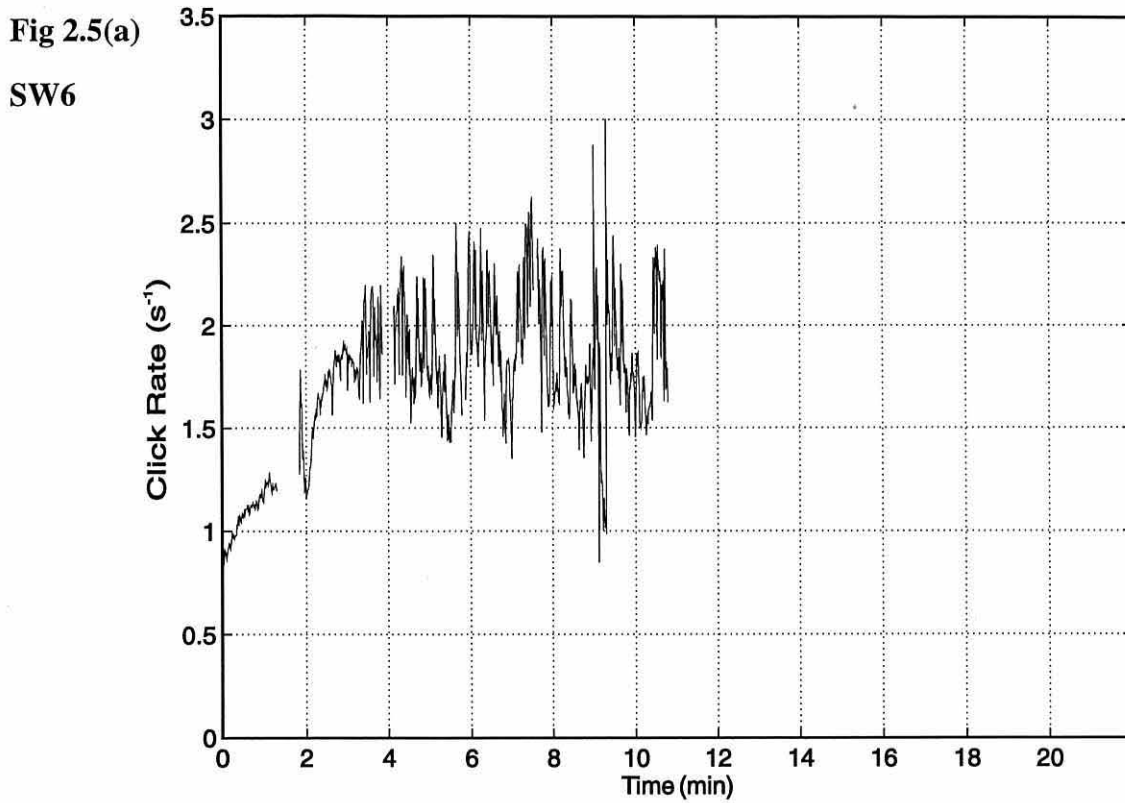


Figure 2.5 Click rate plots from feeding dives of female sperm whales (a) SW6 and (b) SW7

Fig 2.5(c)

SW8

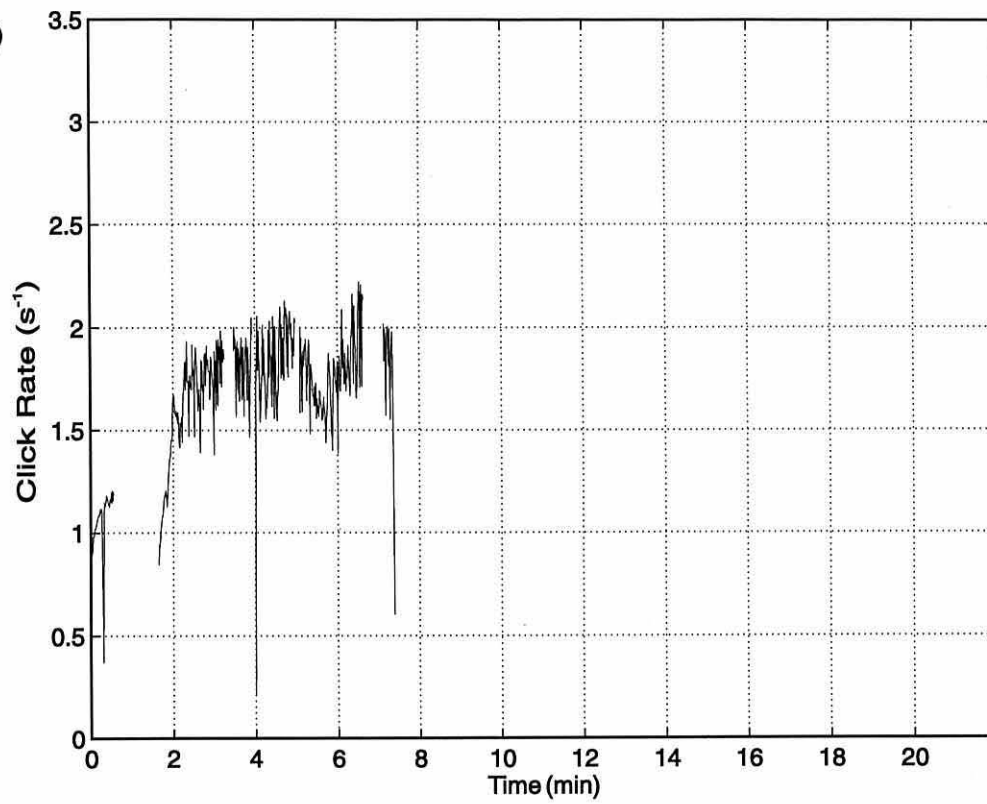
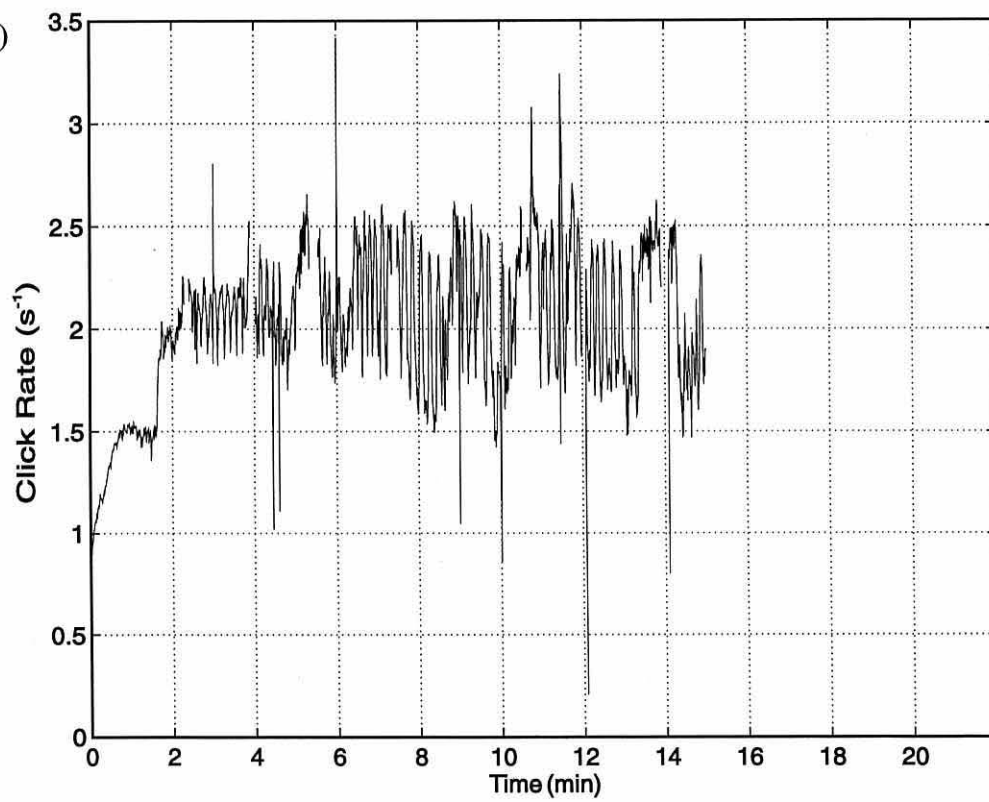


Fig 2.5(d)

SW9

**Figure 2.5** Click rate plots from feeding dives of female sperm whales (c) SW8 and (d) SW9

<b>Click Sequence Code</b>	<b>Mean Equilibrium Click Rate (s<sup>-1</sup>)</b>	<b>Lower Confidence Limit (s<sup>-1</sup>)</b>	<b>Upper Confidence Limit (s<sup>-1</sup>)</b>
<b>SW1</b>	<b>1.0706</b>	<b>1.0554</b>	<b>1.0858</b>
<b>SW2</b>	<b>1.0691</b>	<b>1.0548</b>	<b>1.0835</b>
<b>SW3</b>	<b>1.2943</b>	<b>1.2591</b>	<b>1.3295</b>
<b>SW4</b>	<b>1.0944</b>	<b>1.0790</b>	<b>1.1099</b>
<b>SW5</b>	<b>1.4044</b>	<b>1.3865</b>	<b>1.4223</b>
<b>SW6</b>	<b>1.9205</b>	<b>1.8991</b>	<b>1.9419</b>
<b>SW7</b>	<b>1.5235</b>	<b>1.4860</b>	<b>1.5611</b>
<b>SW8</b>	<b>1.8270</b>	<b>1.8076</b>	<b>1.8464</b>
<b>SW9</b>	<b>2.1543</b>	<b>2.1372</b>	<b>2.1714</b>

**Table 2.2** Mean equilibrium click rate for each of the nine sperm whale click sequences selected for analysis, with lower and upper confidence limits.

and its' mean click rate lies between the other two sets. The confidence limits in Table 2.2 indicate that the mean click rates of SW1, SW2 & SW4 are all similar at the 95% level, SW3 is significantly greater than all three & SW5 is greater still. The mean click rates of SW6 - SW9 cover a broader range but retain tight confidence limits individually. All the mean click rates of females are significantly different from each other at the 95% level, but are all significantly greater than the males. Pooling the male and female click rate data into two separate samples a one way analysis of variance shows that male and female click rates are significantly different with a probability value of 0 and an F value of 8162. Using the pooled data the overall mean click rate for males is  $1.1713 \text{ s}^{-1}$  (standard error  $0.0048 \text{ s}^{-1}$ ) and for females is  $1.9455 \text{ s}^{-1}$  (standard error  $0.0075 \text{ s}^{-1}$ ).

### **2.3(ii) Frequency domain analysis**

Figure 2.6 shows waterfall spectral plots for the first 120 clicks of the large bull males SW1 - SW5, displayed as cascading time series of power spectra. Each graph in a cascade is the power magnitude spectrum of a single click, with time increasing from front to back along the cascade axis. Although all frequencies in the range 0 - 22 kHz were captured, only those components in the 0 - 16 kHz range are displayed, as virtually all the power is represented in this band. The cascade plots of male sperm whale click spectra reveal prominent peaks at approximately 400 Hz and 2 kHz, these peaks have a tendency to dominate the spectrum during the early stages of the dive, although there are exceptions such as the first few clicks of SW1 [Fig 2.6(a)] which can be seen to contain substantial levels of higher frequency energy up to 10 kHz. Another general feature evident in the male click spectra cascades is

Fig 2.6(a)

SW1

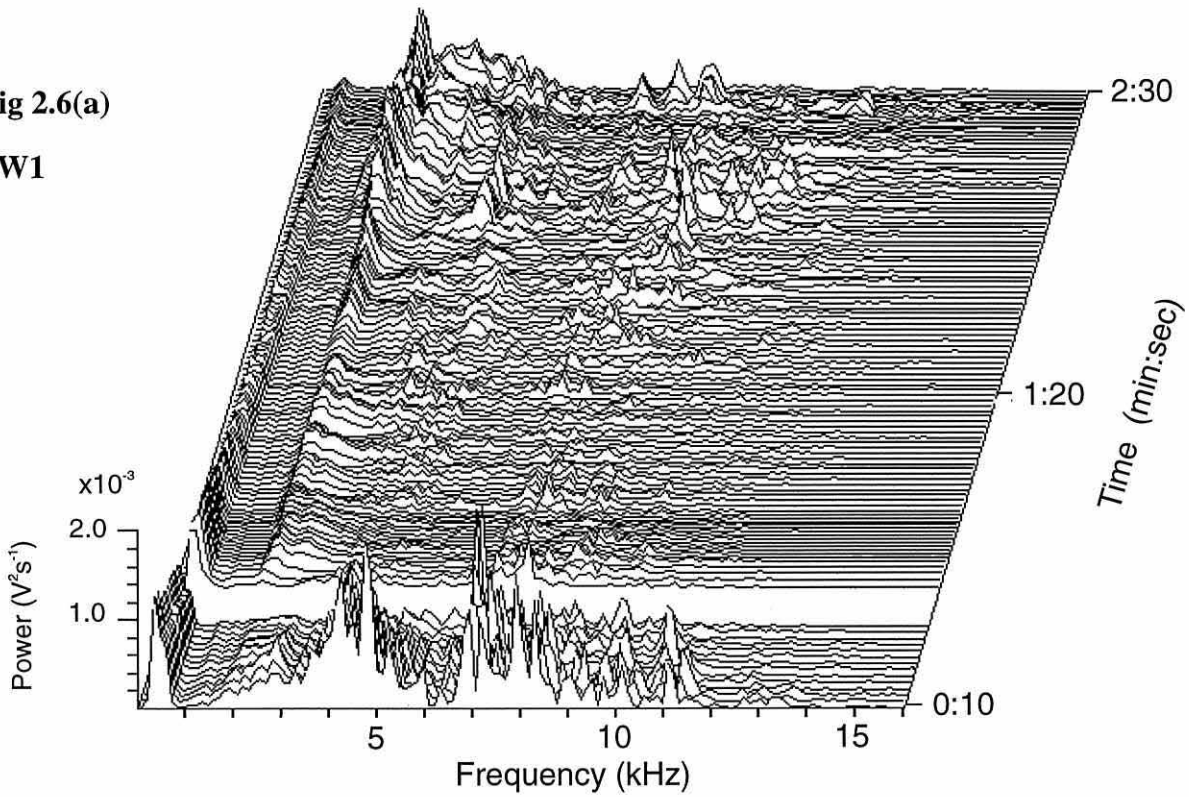
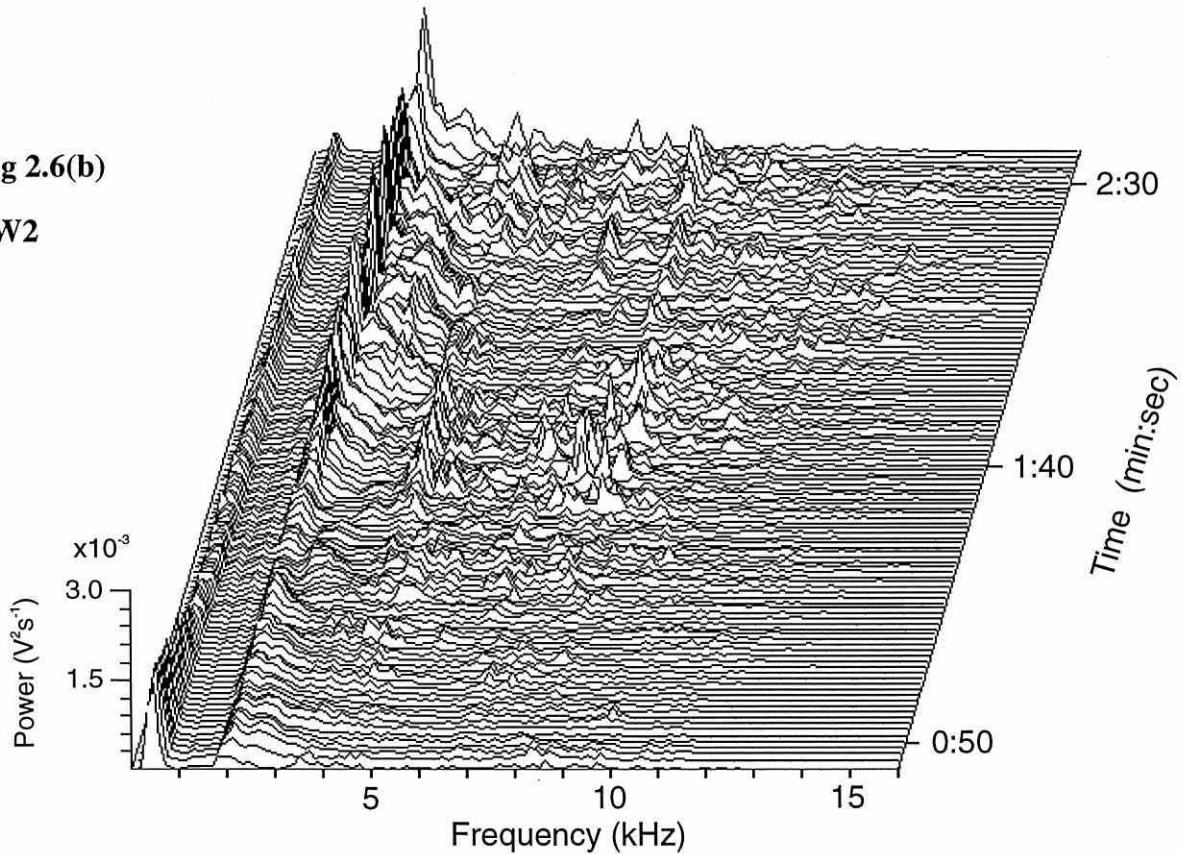


Fig 2.6(b)

SW2



**Figure 2.6** Waterfall displays of sequential click spectra, showing power magnitude data over approximately the first 120 clicks from male click sequences (a) SW1 and (b) SW2. Cascade axes show time elapsed since the first click of the respective sequences.

Fig 2.6(c)

SW3

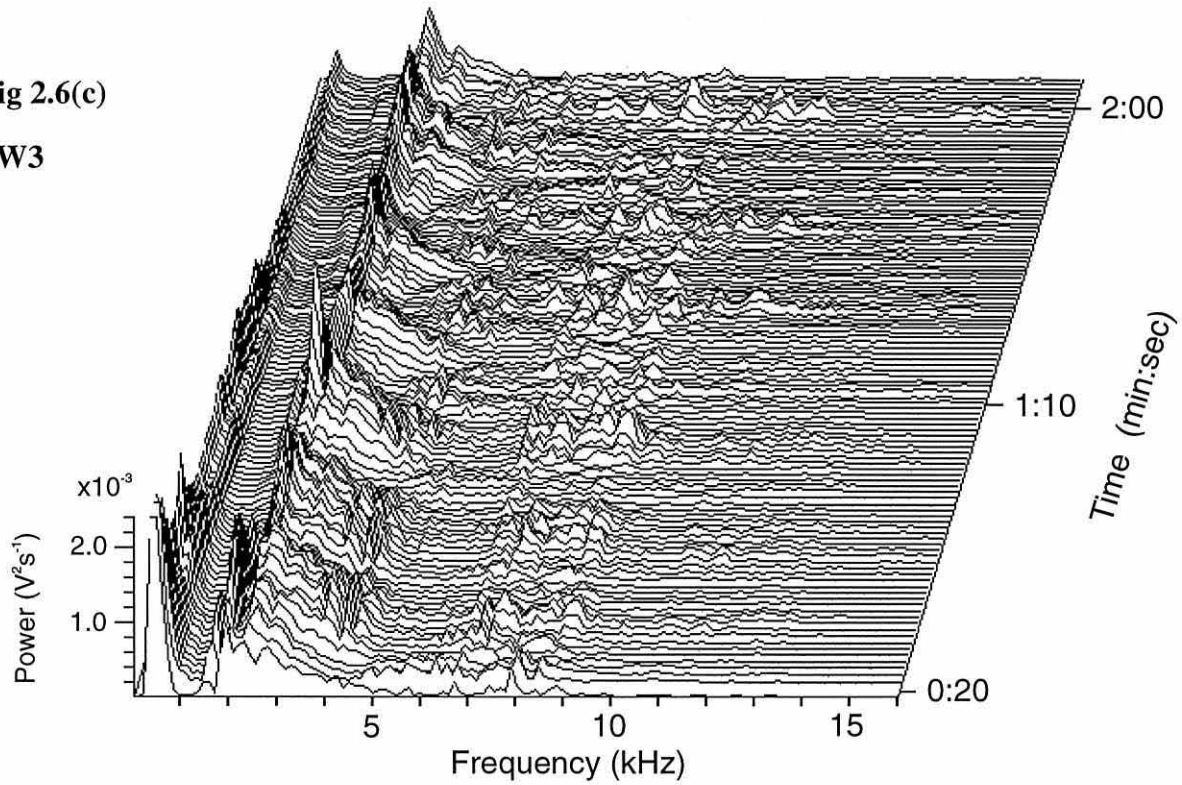
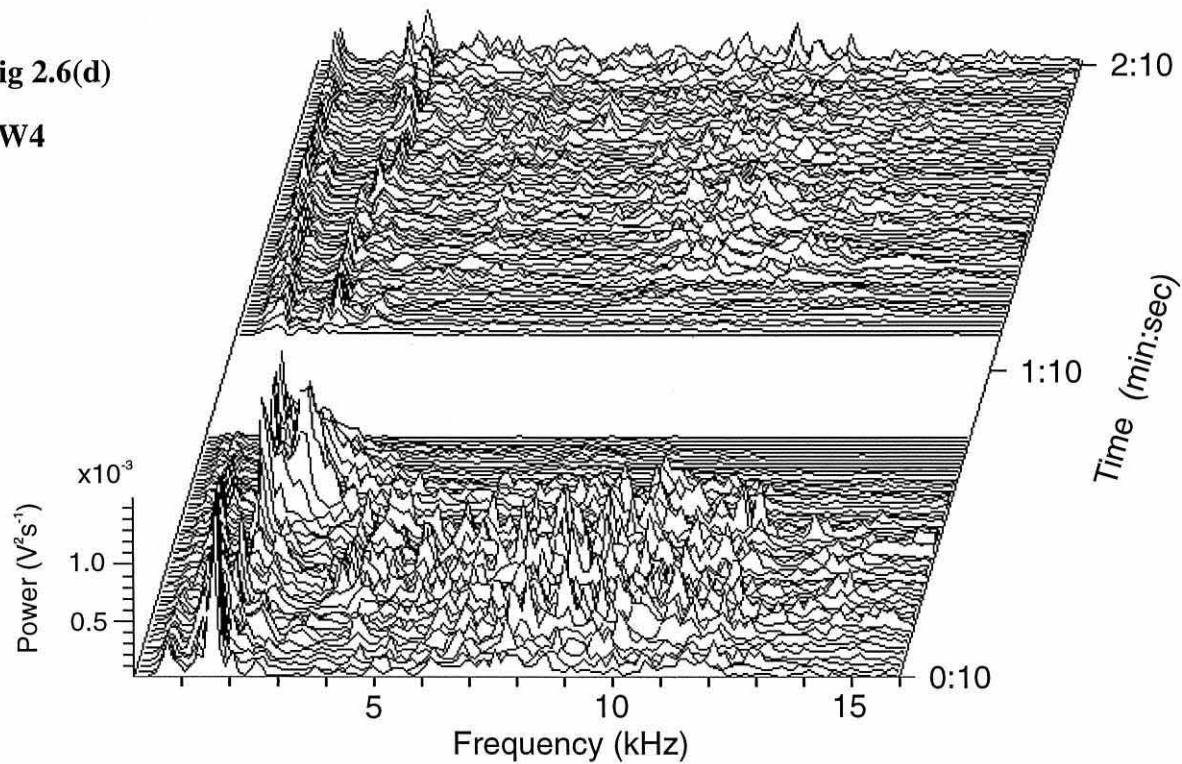


Fig 2.6(d)

SW4



**Figure 2.6** Waterfall displays of sequential click spectra, showing power magnitude data over approximately the first 120 clicks from male click sequences (c) SW3 and (d) SW4. Cascade axes show time elapsed since the first click of the respective sequences.

Fig 2.6(e)

SW5

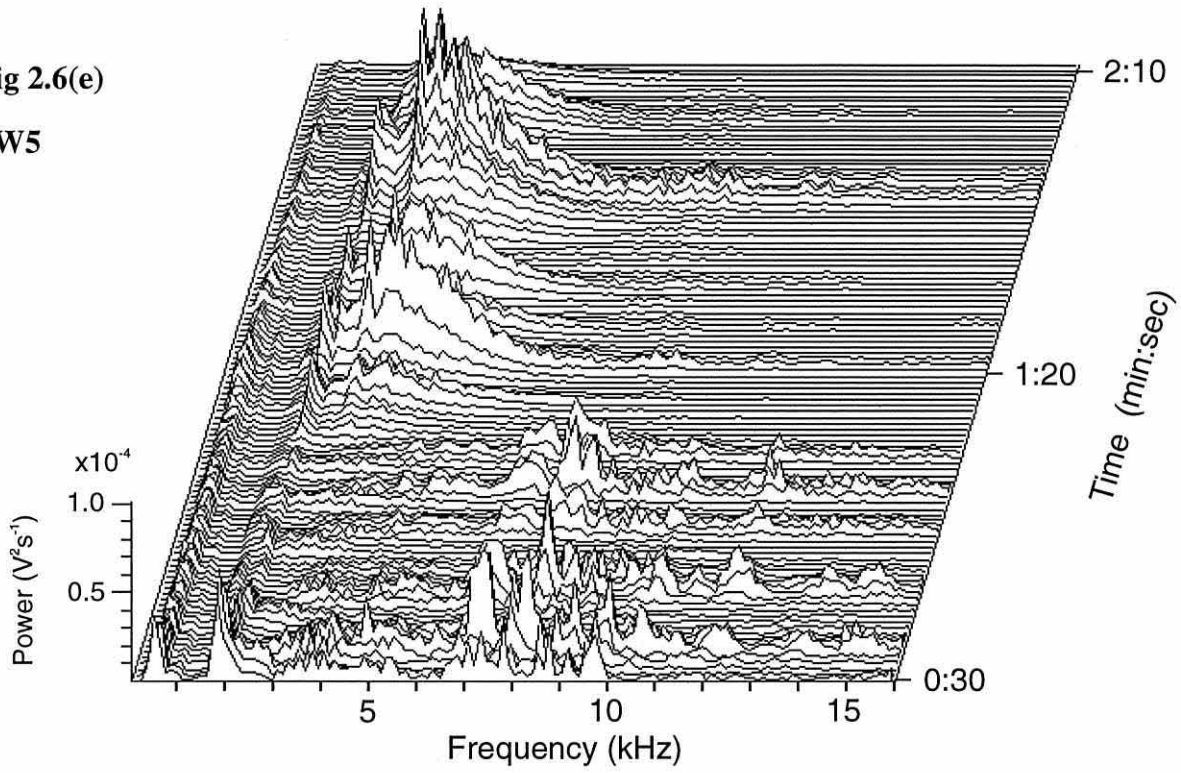


**Figure 2.6** Waterfall display of sequential click spectra, showing power magnitude data over approximately the first 120 clicks from male click sequence (e) SW5. Cascade axis shows time elapsed since the first click of the sequence.

Fig 2.7(a)

SW1

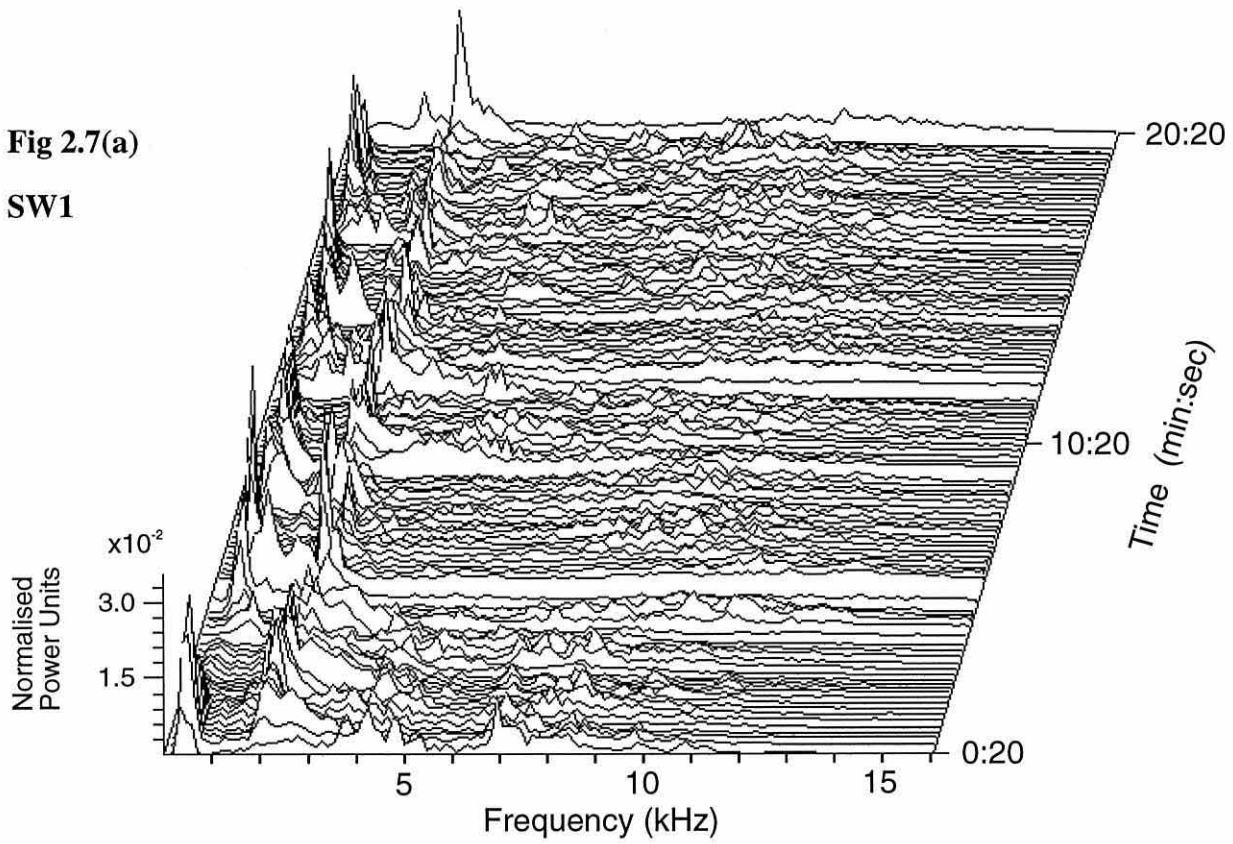
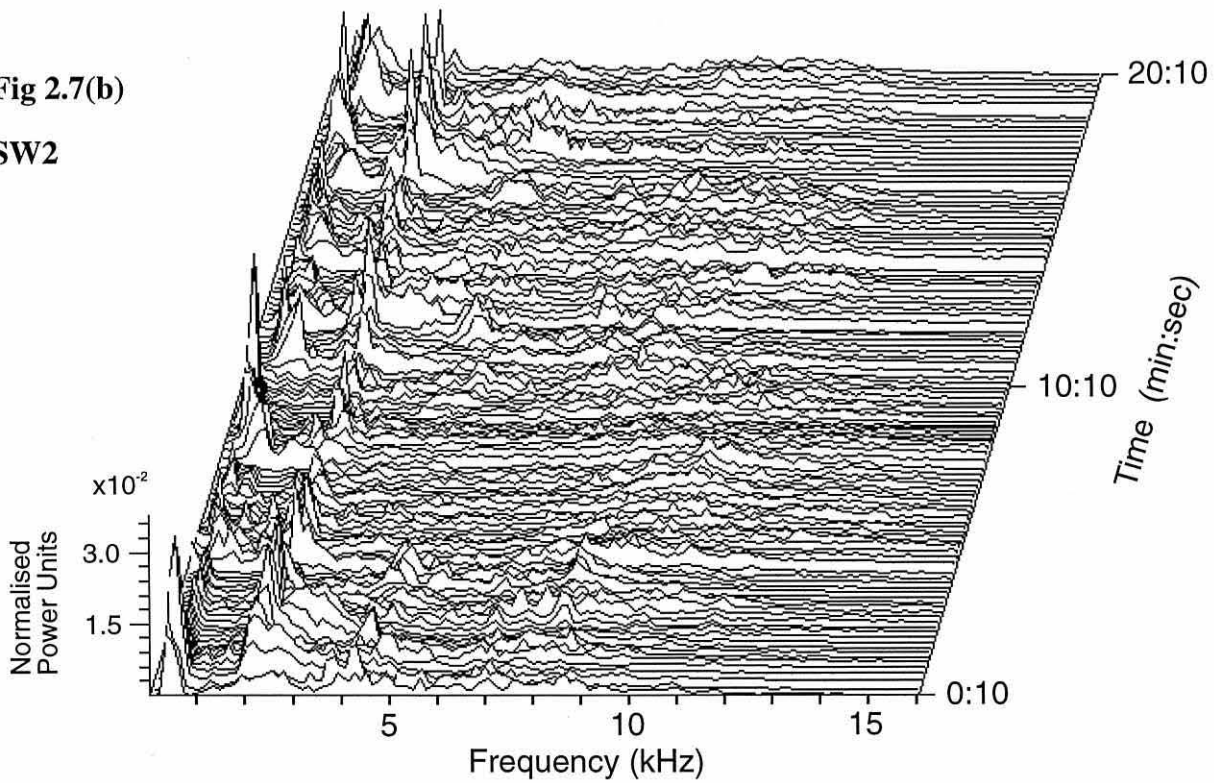


Fig 2.7(b)

SW2



**Figure 2.7** Waterfall displays of normalised and averaged click spectra, showing overall power spectral distribution over the full duration of male click sequences (a) SW1 and (b) SW2. Each individual graph in a cascade is the average of ten sequential normalised power spectra.

Fig 2.7(c)

SW3

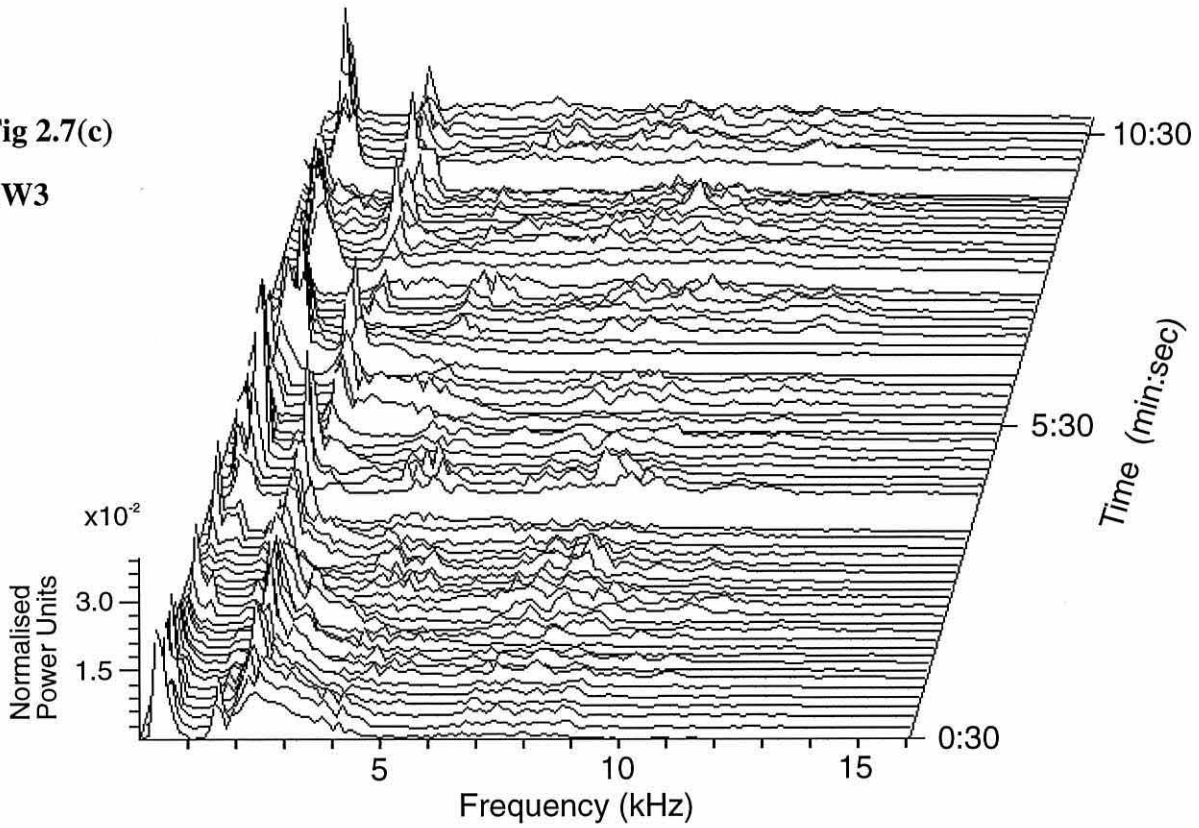
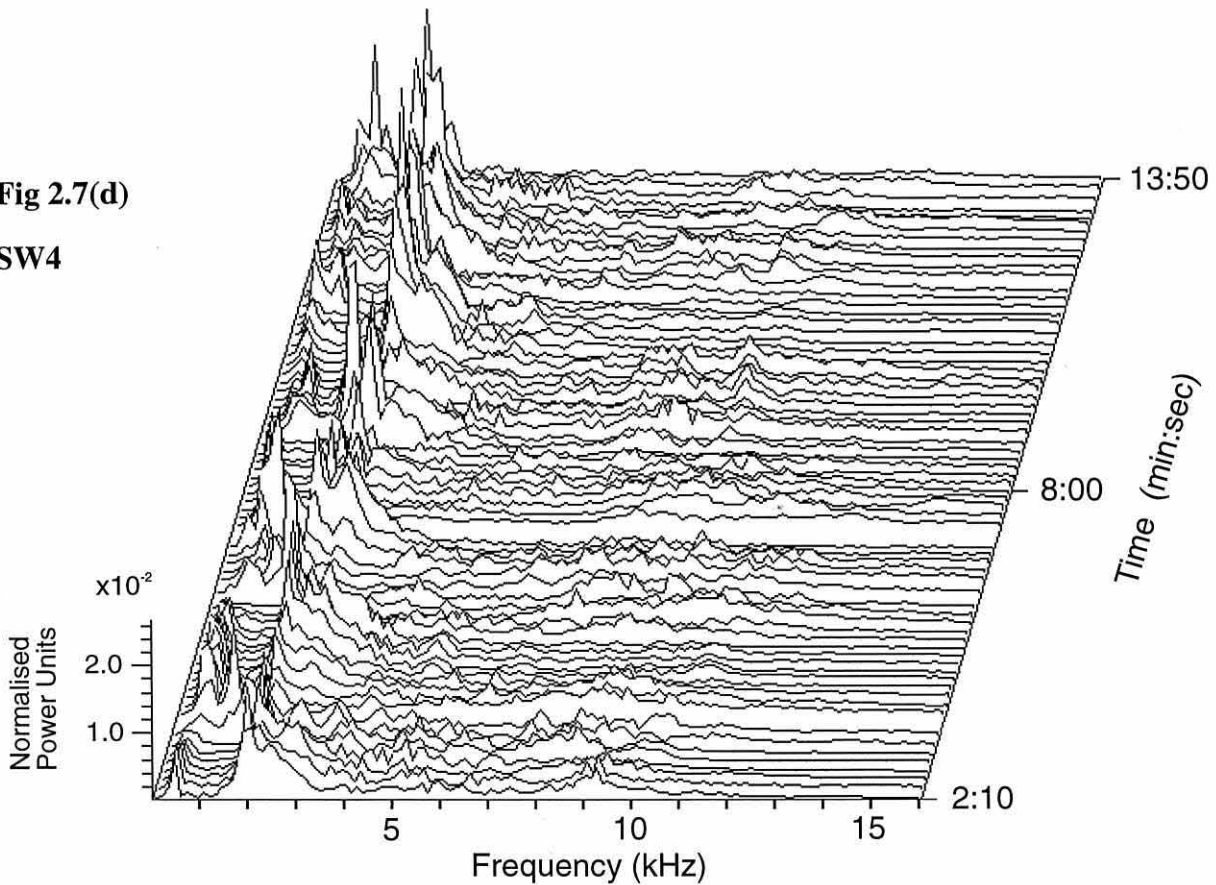


Fig 2.7(d)

SW4



**Figure 2.7** Waterfall displays of normalised and averaged click spectra, showing overall power spectral distribution over the full duration of male click sequences (c) SW3 and (d) SW4. Each individual graph in a cascade is the average of ten sequential normalised power spectra.

Fig 2.7(e)

SW5

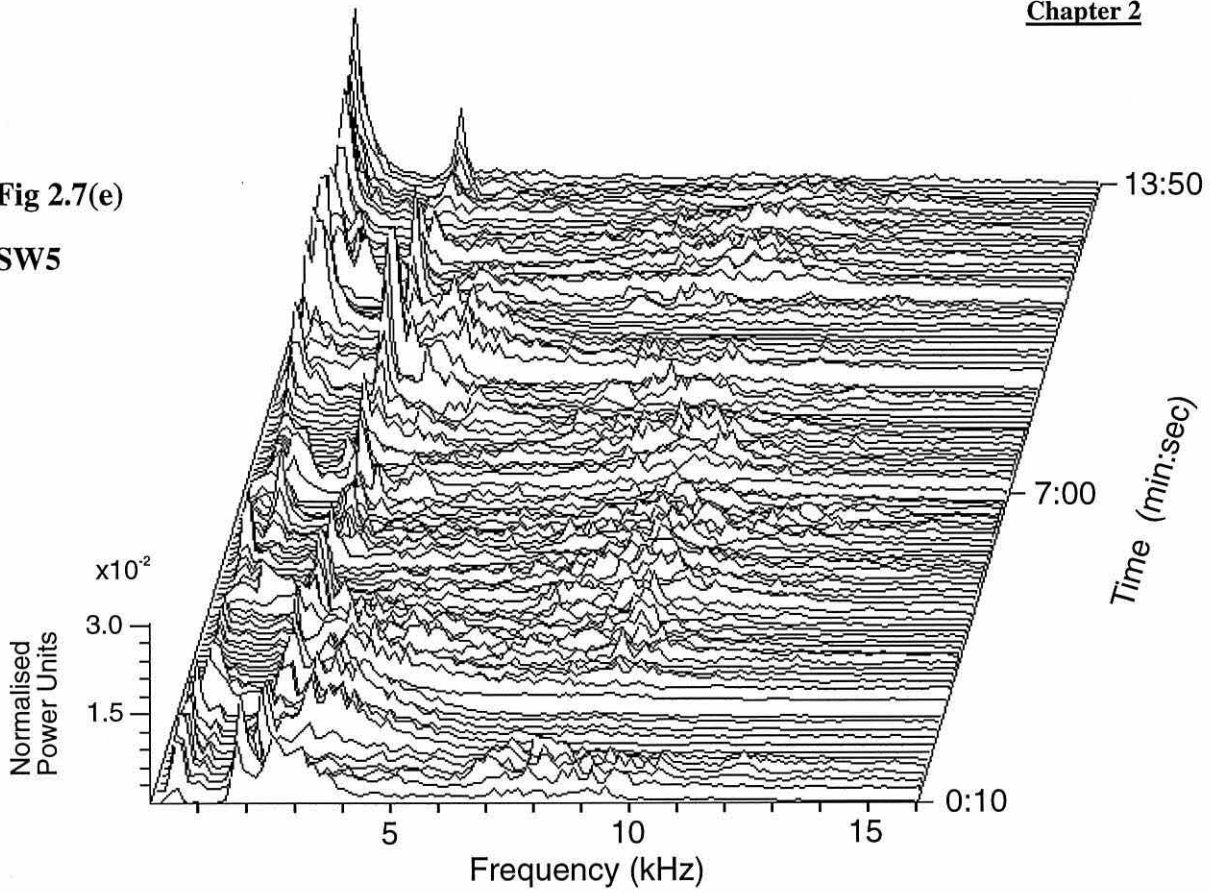


**Figure 2.7** Waterfall displays of normalised and averaged click spectra, showing overall power spectral distribution over the full duration of male click sequence (e) SW5. Each individual graph in a cascade is the average of ten sequential normalised power spectra.

that the power level of the low frequency peak (400 Hz) tends to decay fairly rapidly with time over the first twenty or thirty clicks, whereas the 2 kHz peak does not follow a similar pattern over the same range of clicks. Exceptions are again evident such as SW4 [Fig 2.6(d)] in which the 400 Hz peak does not decay greatly at any point over the first hundred or so clicks. When looking at the 2 kHz peak it is generally the case that power around the 2 kHz peak actually increases, or at least fluctuates around an approximately constant level, across the first 100 or so clicks. This can be clearly seen in the cascade plots of SW1 - SW3 and SW5 [Figs 2.6(a) - 2.6(c) and 2.6(e)]. All five cascade plots [Figs 2.6(a) - (e)] show that energy in male click spectra is present throughout the higher frequency range up to 15 kHz, but not concentrated at any sharply defined frequency above 2 kHz. These cascade plots give clear illustrations of early click characteristics for bull male sperm whales as recorded behind diving animals by surface hydrophones; the original recordings were of very high signal to noise ratio. As the signals were recorded from behind diving whales and off the centre of the main transmission beam they are likely to appear heavily weighted against the higher frequency components present in the on-axis signals. Figure 2.7(a) - (e) shows normalised and averaged power spectra of all clicks in the five male click sequences SW1 - SW5, giving an overview of the power spectral distribution within clicks over extended time periods. It can be seen that the 400 Hz and 2 kHz peaks are largely stable features throughout the duration of the click sequences over tens of minutes.

Figure 2.8 shows waterfall displays of power spectra of the clicks from the early stages of female sperm whale click sequences SW6 - SW9. As with the males there is a concentration of energy at the lower end of the spectrum, but the spectral peaks are not as clearly defined. All four click spectra cascades of SW6 - SW9 [Fig 2.8(a) - (d)] are

Fig 2.8(a)

SW6

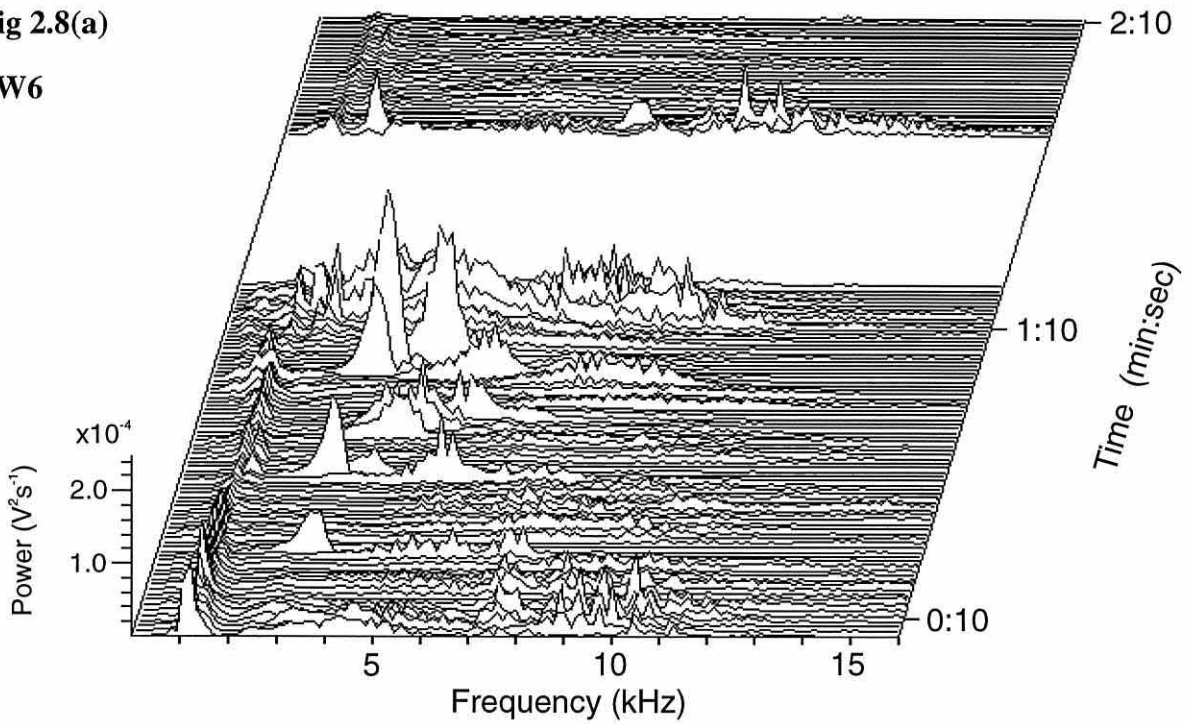
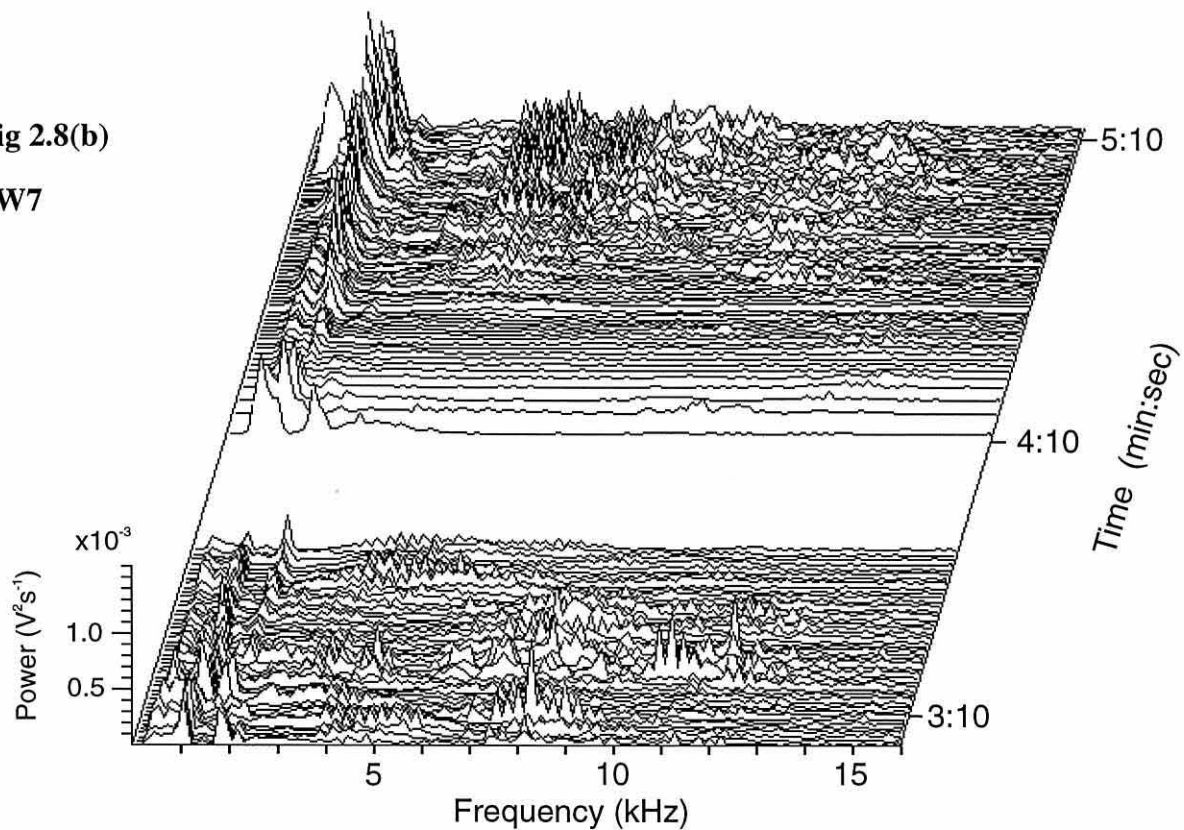


Fig 2.8(b)

SW7



**Figure 2.8** Waterfall displays of sequential click spectra, showing power magnitude data over approximately the first 120 clicks from female click sequences (a) SW6 and (b) SW7. Cascade axes show time elapsed since the first click of the respective sequences.

Fig 2.8(c)

SW8

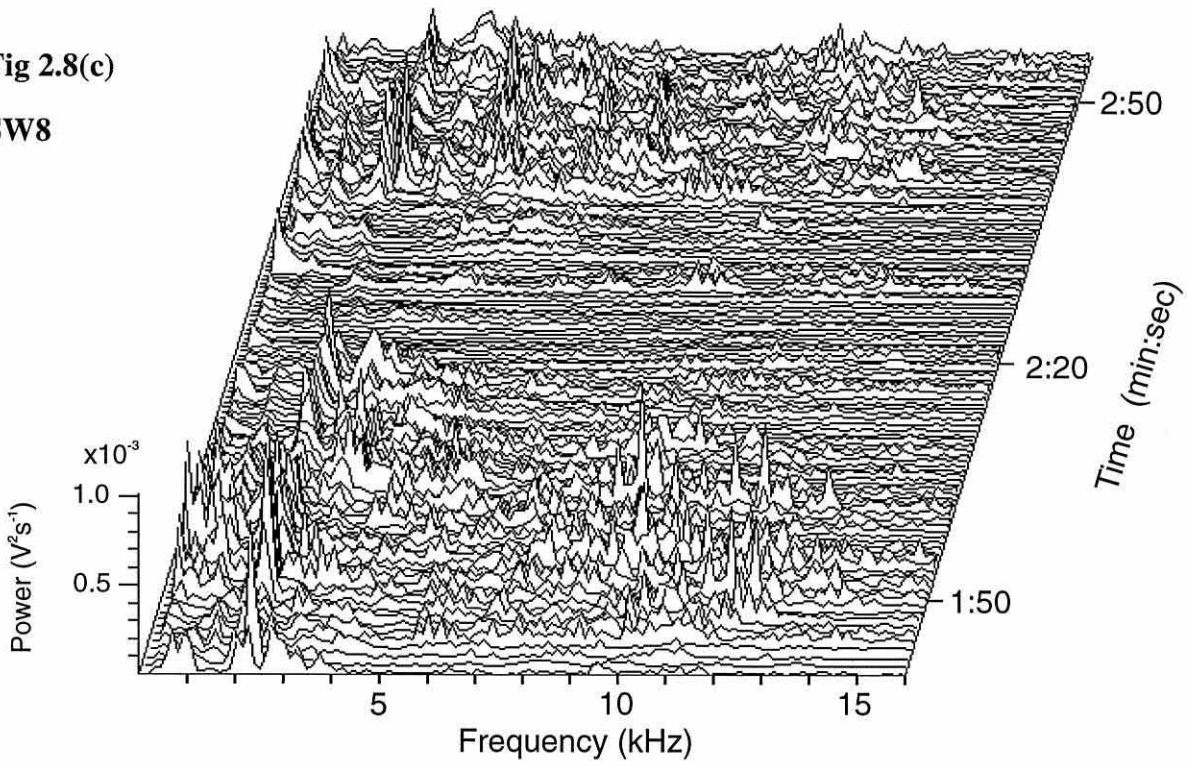
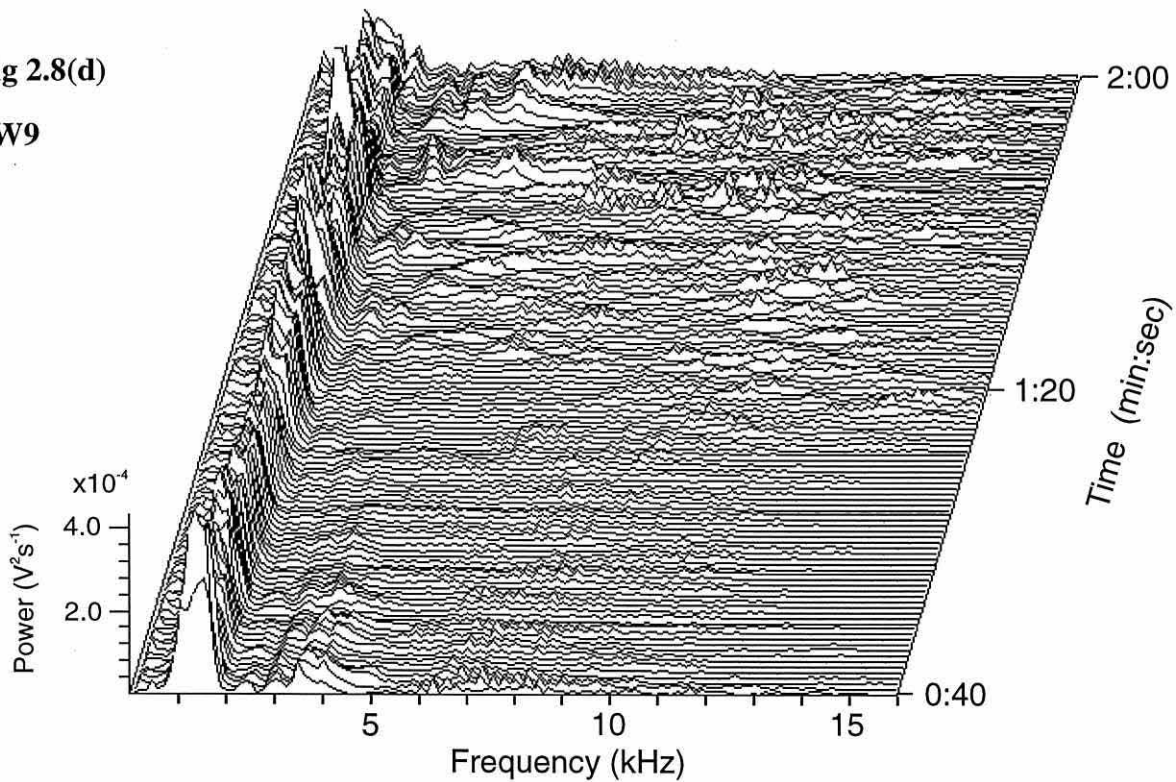


Fig 2.8(d)

SW9



**Figure 2.8** Waterfall displays of sequential click spectra, showing power magnitude data over approximately the first 120 clicks from female click sequences (c) SW8 and (d) SW9. Cascade axes show time elapsed since the first click of the respective sequences.

Fig 2.9(a)

SW6

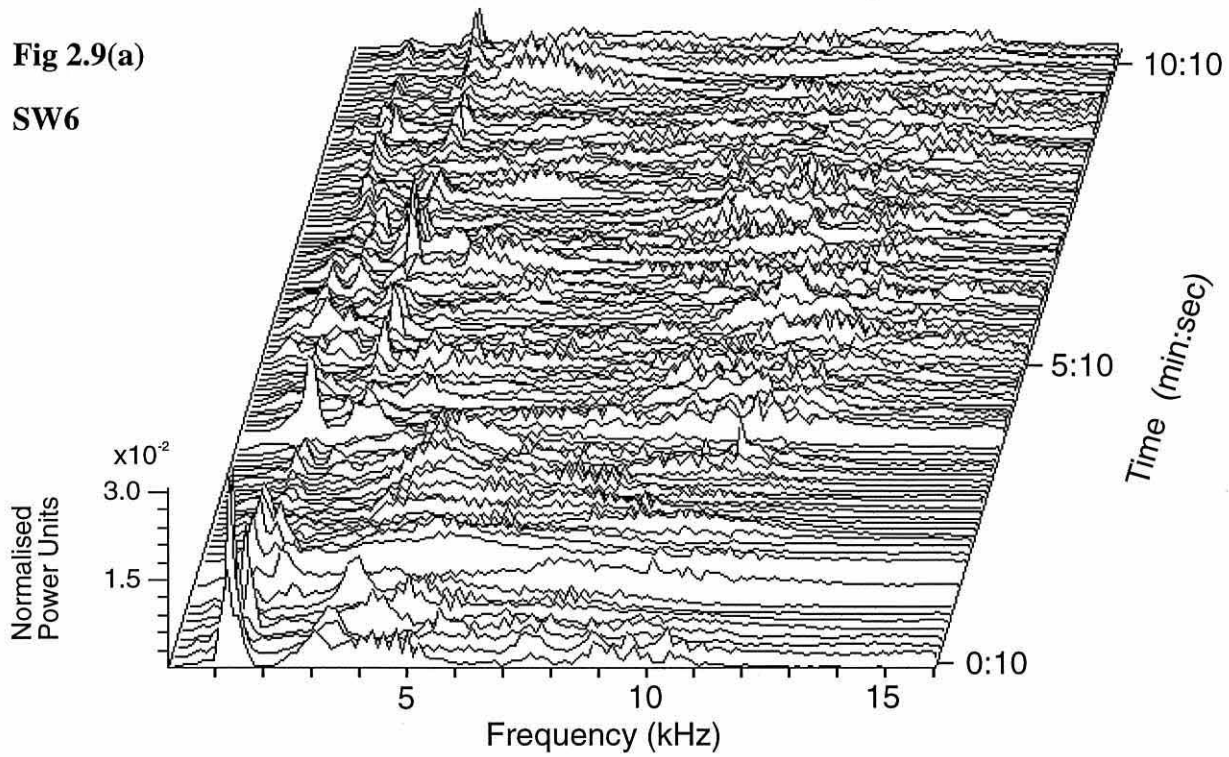
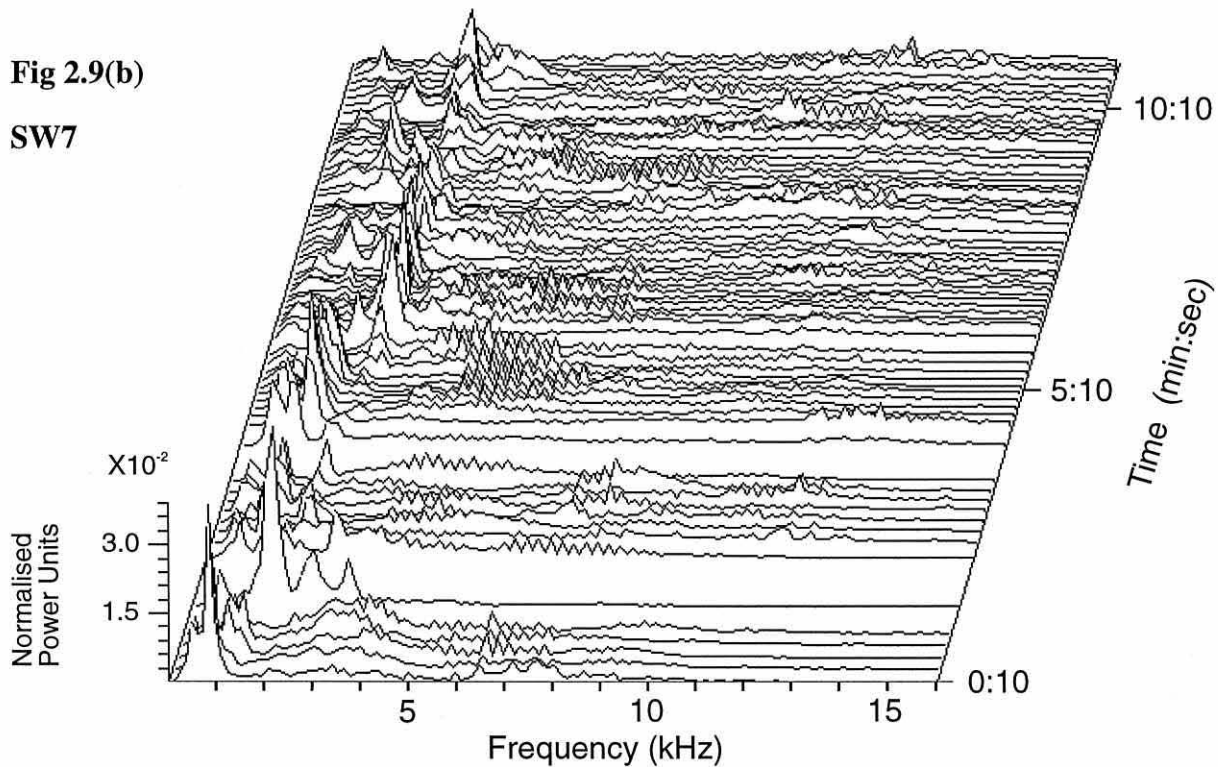


Fig 2.9(b)

SW7



**Figure 2.9** Waterfall displays of normalised and averaged click spectra, showing overall power spectral distribution over the full duration of female click sequences (a) SW6 and (b) SW7. Each individual graph in a cascade is the average of ten sequential normalised power spectra.

Fig 2.9(c)

SW8

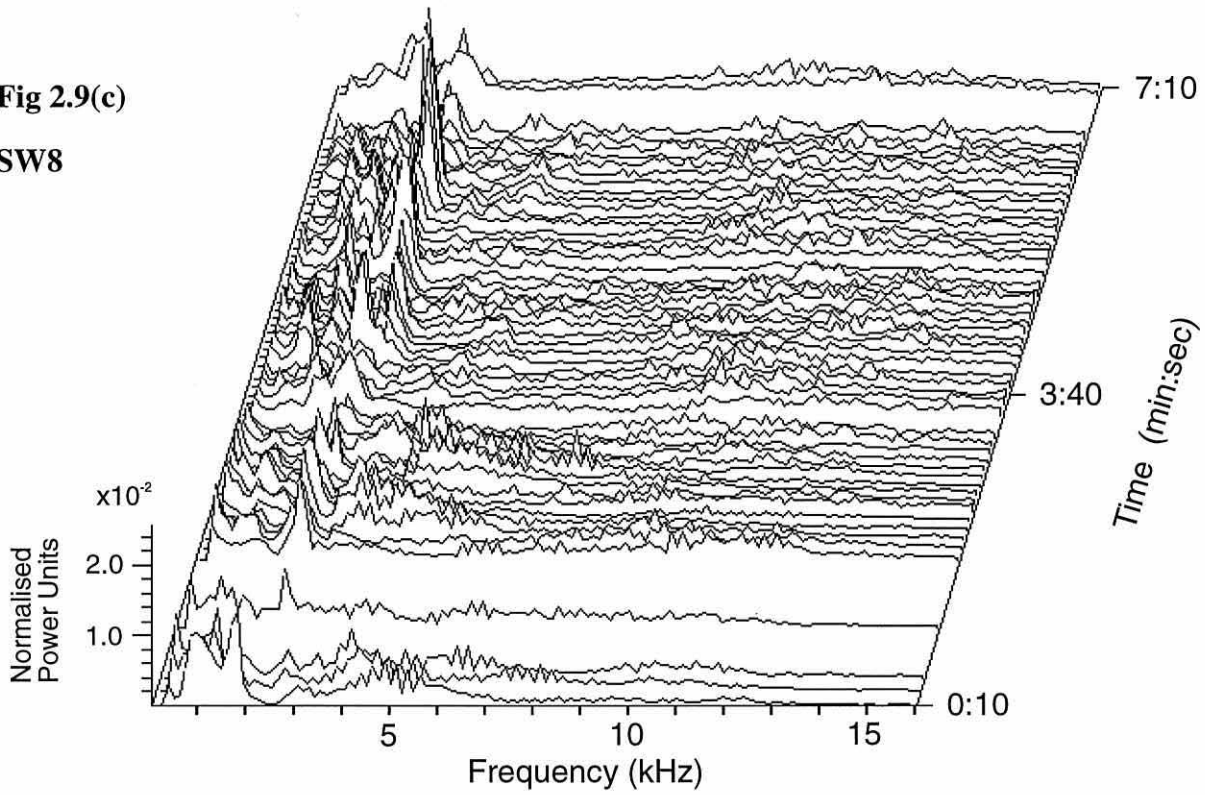
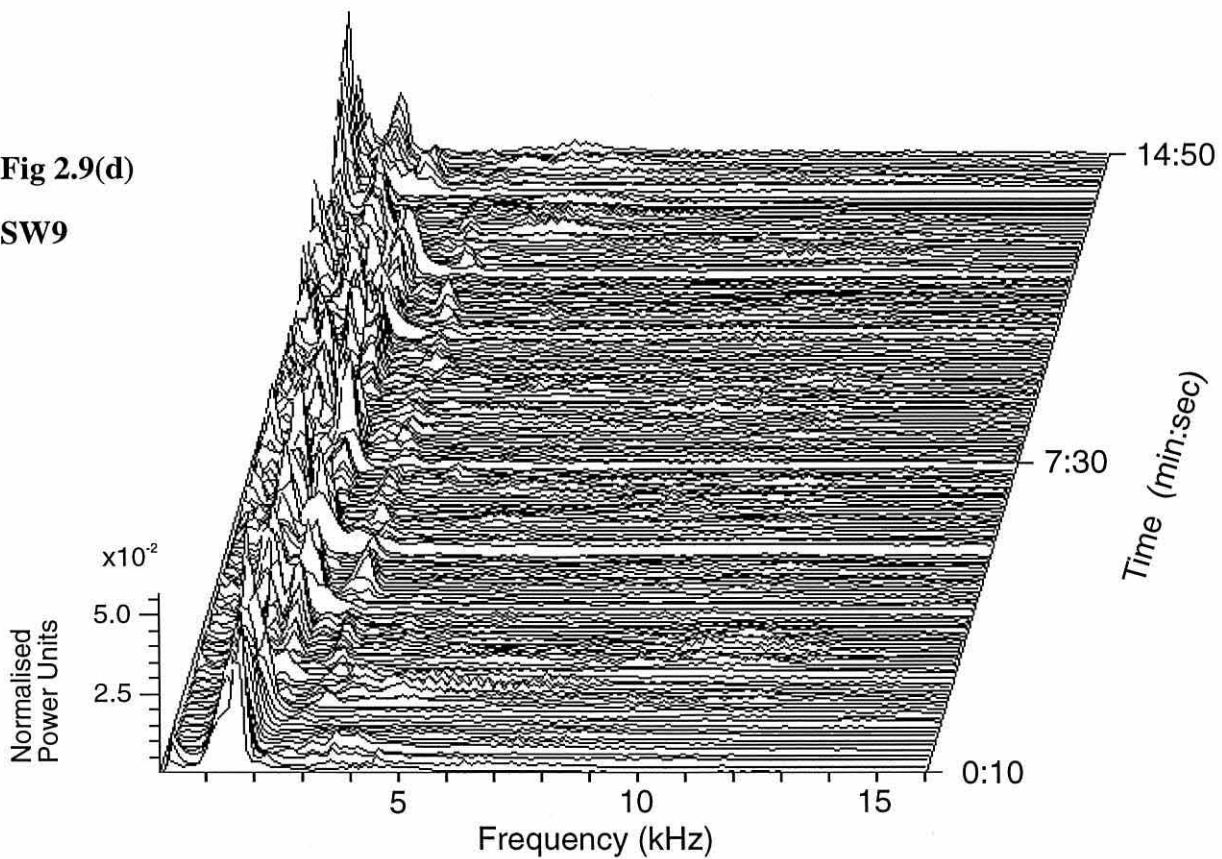


Fig 2.9(d)

SW9



**Figure 2.9** Waterfall displays of normalised and averaged click spectra, showing overall power spectral distribution over the full duration of female click sequences (c) SW8 and (d) SW9. Each individual graph in a cascade is the average of ten sequential normalised power spectra.

suggestive of a strong peak in the region of 1 kHz. The corresponding normalised and averaged spectral cascades clarify these features over the duration of the respective click sequences [Fig 2.9(a) - (d)]. There is a tendency for energy to concentrate at about 1 kHz as noted from the individual click cascades. However the normalised and averaged spectra are variably suggestive of a second peak at around 3 kHz, most evident in the cascades of SW6, SW7 and SW8 [Fig 2.9(a) - (c)]. However these peaks appear less sharply defined and less stable with time in terms of magnitude and frequency than the prominent peaks in the male spectra. Even the normalised and averaged cascade of SW9 [Fig 2.9(d)], which has such prominence of power around 1 kHz, also shows a small but consistent series of peaks at 3 kHz spanning virtually the entire 15 minutes of the sequence (constituting 1,711 clicks). The spectral peak observations are consistent with the distal sac acting as a circular transducer. The distal sac diameter is estimated at approximately 0.5 m in female sperm whales and approximately 0.75 m in male sperm whales. Sound velocity in the whale head tissue (essentially aqueous) can be approximated as  $1500 \text{ ms}^{-1}$  and the half beam width for a circular transducer is given as  $30\lambda/D$ . A 3 kHz pulse in the female head gives a wavelength of 0.5 m and a 2 kHz pulse in male head gives a wavelength of 0.75 m. It is clear that these values will give half beam widths of sperm whale click components at 2 and 3 kHz in males and females respectively of  $30^\circ$ . This is a broad beam-width and hence the small but visible fluctuations in the 2 kHz peaks of males, and to a lesser extent the 3 kHz peaks of females, may be explained by the changing orientation of the whales with respect to the surface hydrophone, i.e. the directional transmission beam is sweeping past the hydrophone as the whales orientation changes. Although the on-axis signal ahead of the sperm whale, to which the directivity estimate strictly pertains, is not being measured it is to be expected that a similarly directional rearward transmission lobe will be present. For the 1 kHz components

in female clicks and the 400 Hz components in male clicks the wavelengths are greatly in excess of the estimated distal sac diameters and the  $30\lambda/D$  relationship shows these components to be omnidirectional.

### **2.3(iii) Time domain analysis**

Figure 2.10 shows the results of filtering the click of a large bull male sperm whale in several incremental frequency bands. Figure 2.10(a) shows the unfiltered signal and (b) shows isolation of the low frequency component (approx 400 Hz) with a 500 Hz lowpass FIR filter. The waveform of this component is a heavily damped sinewave, and represents the typical waveform of the sub kilohertz components of clicks from large males. There is no evidence of a repeating series of pulses, which is to be expected as the wavelength at this frequency, approximately 2.8 m in spermaceti oil (assuming  $c_{\text{spermaceti}} = 1400 \text{ ms}^{-1}$ ), is much larger than the dimensions of the proposed reflective surfaces of the nasofrontal and distal air sacs (less than 1 m). The cascades of male spectral plots [Figs 2.6 & 2.7] indicate very little energy in the band between 500 Hz - 1.5 kHz, and Figure 2.10(c) shows the fairly formless, low level waveform components in this frequency band.

The second prominent peak in the male click spectrum occurs at approximately 2 kHz, and encompasses a slightly broader range of frequencies, from about 1.5 kHz - 3 kHz. These components were isolated with a bandpass FIR filter centred on 2.25 kHz with -3 dB points at 1.5 kHz and 3 kHz. Figure 2.10(d) shows a typical waveform that results from isolation of this narrow frequency band. The initial burst of waveform energy at about 2 kHz

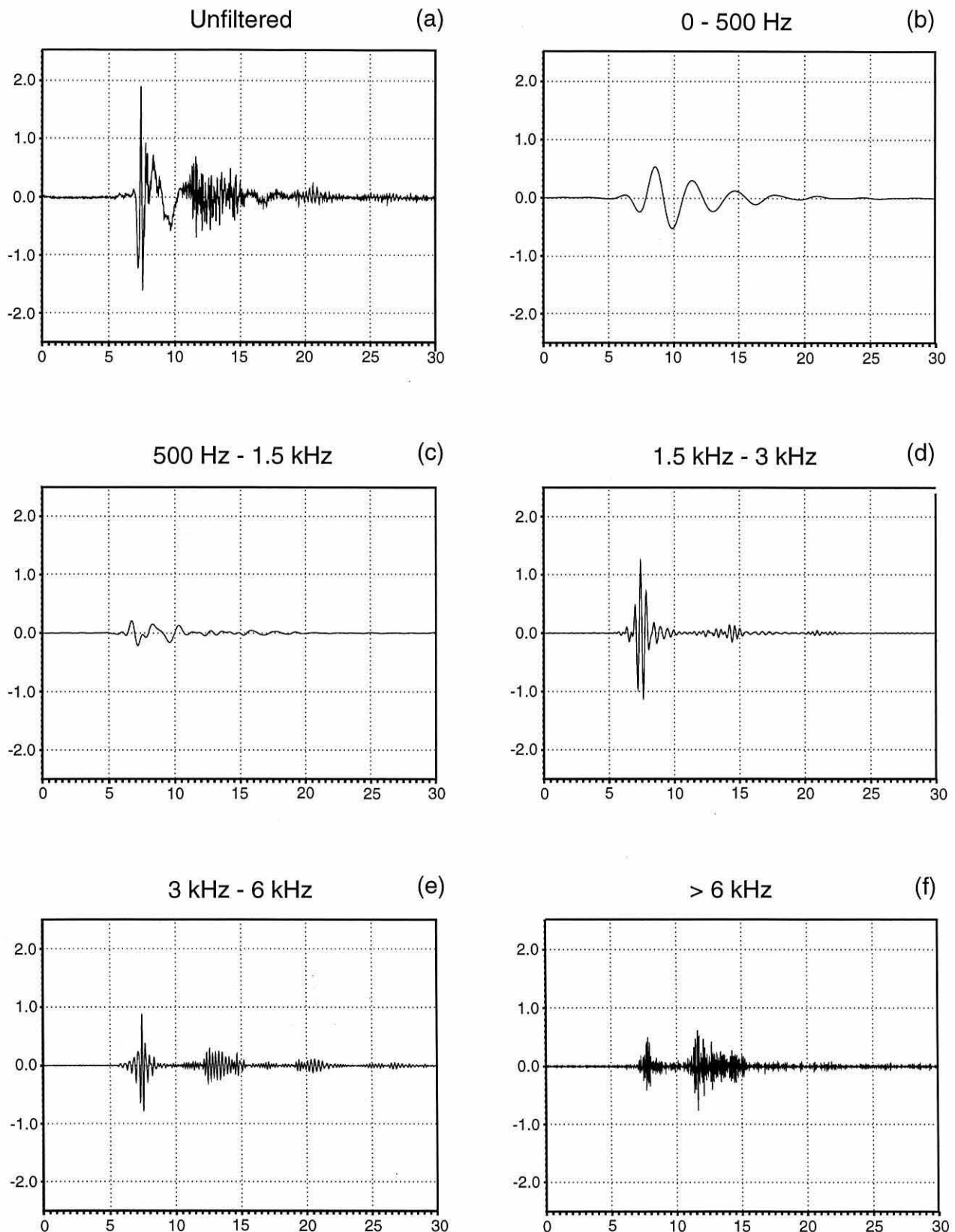


**Figure 2.10** Isolation of incremental frequency components within a bull male sperm whale click. The unfiltered signal is shown in (a) with subsequent plots showing isolation through various incremental frequency band filters as labelled on each plot. Time base is 30 ms in each plot, waveform units are in volts.

constitutes much of the sharp onset of the click, and the bulk of energy at this frequency is largely confined to the click onset of some 2 - 3 ms duration. Note also that a decaying pulse train is becoming visible, the wavelength of sound now approximately 0.7 m in spermaceti oil, at which reflection of sound from the frontal and distal air sacs is more feasible. The decay in energy with successive pulses is very rapid, as might be expected, and the pulse spacing is very regular, approximately 7 ms, which conforms with the Norris & Harvey (1972) hypothesis for an animal of this size (approximately 16 - 18 metres). However, it was observed that a clearly defined pulsed structure in this frequency band did not persist as dive time progressed, although visual definition of pulsed structure would sharpen and degenerate intermittently. As previously mentioned in the context of beam widths, the variable definition of the click waveforms is most likely an effect of a whales' changing orientation.

Above 2 kHz there are no particularly prominent peaks in the male click spectrum, so waveform components at higher frequencies were visualised by progressively widening the filter bandwidths, namely 3 - 6 kHz and finally 6+ kHz. A bandpass FIR filter centred at 4.5 kHz, with -3 dB points at 3 kHz & 6 kHz, and a highpass FIR filter with -3 dB point at 6 kHz were used respectively. In the 3 - 6 kHz band the pulse structure is quite well defined and generally persists throughout the dive [Fig 2.10(e)]. However, it is notable that the envelope of the first and second pulses in the click become dissimilar, with the first pulse envelope retaining a short spike form of some 2 - 3 ms duration, and the second pulse envelope becoming more spread across some 4 - 5 ms. In addition it can be seen that the amplitude of successive pulses decay less rapidly than in the 1.5 kHz - 3 kHz band. Inspection of the components above 6 kHz revealed a marked dissimilarity between the

envelopes of first and second pulses in the click [Fig 2.10(f)]. The first pulse envelope is still confined to some 2 - 3 ms, whereas the second pulse now spreads across some 5 - 6 ms. There is also a large concentration of energy in the high amplitude, long duration second pulse relative to the first, but multiples following this second pulse are of extremely low amplitude. These effects are consistent with increasing directionality of click components as frequency increases.

Figure 2.11 shows the result of applying identical filters to the click of a smaller female sperm whale. It can be seen [Fig 2.11(b)] that waveform components below 500 Hz are virtually absent, whereas in the male click a significant sinewave component can be isolated. The approximate equivalent to this sinewave is to be found in the 500 Hz to 1.5 kHz band [Fig 2.11(c)], representing the low frequency component of the 1 kHz peak seen in the spectral cascades [Figs 2.8 & 2.9]. Waveform components isolated in the band 1.5 kHz - 3 kHz [Fig 2.11(d)] show no evidence of a pulsed structure, unlike the male click. This might be expected as the dimensions of a mature female sperm whale head are considerably less than those of a bull male, and as such the potentially reflective air sacs will also be proportionately smaller. A decaying pulsed structure emerges when viewing waveform components in the 3 kHz - 6 kHz band [Fig 2.11(e)], corresponding to sound wavelengths in spermaceti oil of between 0.5 m and 0.25 m respectively. Waveform components above 6 kHz [Fig 2.11(f)] show, similar to male clicks, a marked dissimilarity of pulse envelope between first and second pulses and a high amplitude second pulse. The click waveforms portrayed in these figures, while merely snap shots of the whole, show features that are generally representative of the majority of male and female sperm whale clicks sampled during this study.

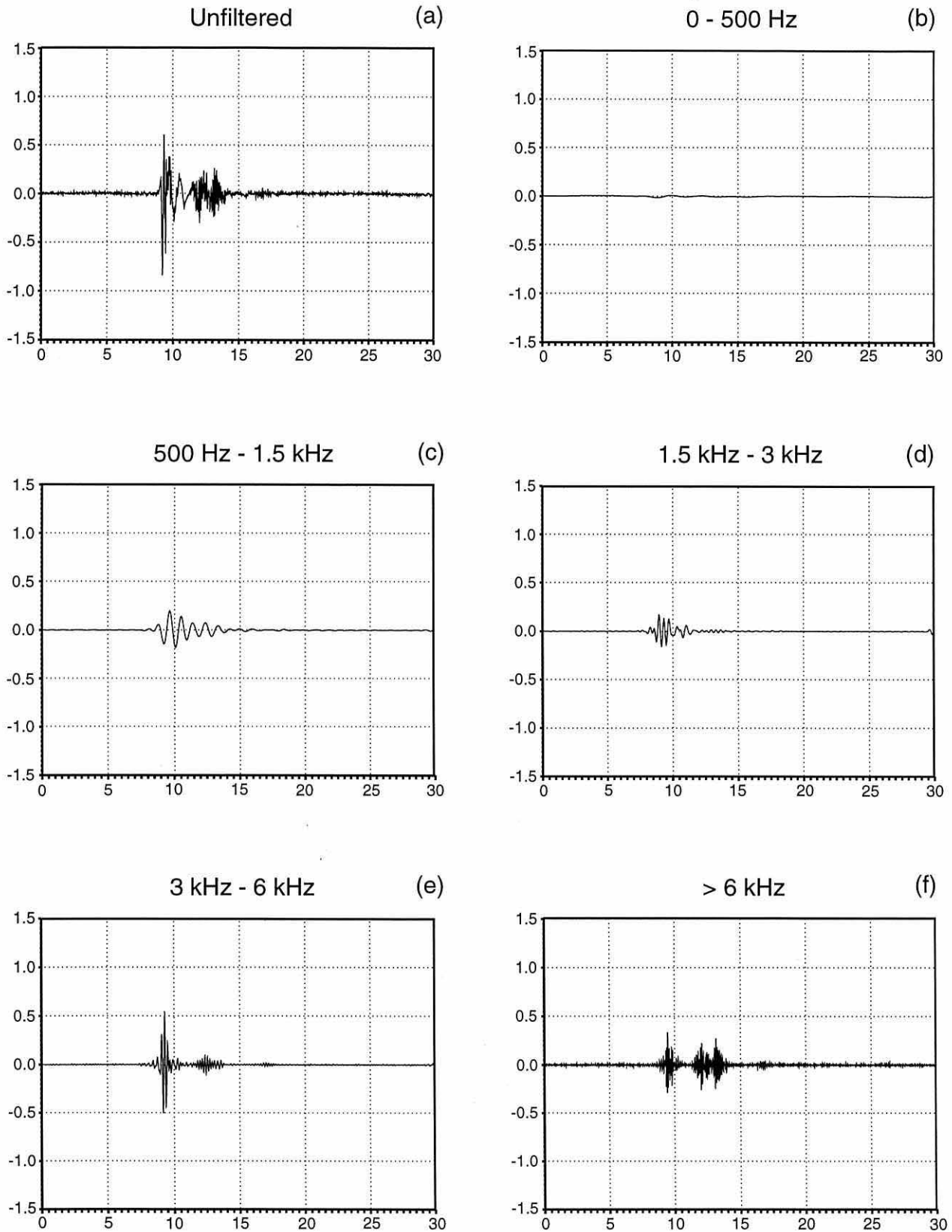


**Figure 2.11** Isolation of incremental frequency components within a female sperm whale click. The unfiltered signal is shown in (a) with subsequent plots showing isolation through various incremental frequency band filters as labelled on each plot. Time base is 30 ms in each plot, waveform units are in volts.

**2.3(iv) Time-Frequency analysis**

Figure 2.12 shows the time-frequency cascade that resulted from a STFT performed on one of the first clicks from the bull male sequence SW2. The picture confirms the complex time-frequency structure already visualised by digital filtering. The onset of the click shows energy at approximately 400 Hz and 2 kHz. The underlying 400 Hz sinewave can be seen to peak about 2 ms after the 2 kHz component peaks. The initially strong 2 kHz component decays very rapidly whereas the 400 Hz component persists for several ms, these features are evident in the waveform plots [Fig 2.10(b) & (d)]. Frequencies from 3 - 12 kHz can be seen to dominate some 6 ms after the initial click onset, with a peak at about 4 kHz. These high frequency components have energy levels greater than occurred at the click onset in the corresponding bands. Again these latter features are evident in the time domain plots [Fig 2.10(e) & (f)] which show the emergence of considerable waveform energy above 3 kHz in the second pulse of the click.

**2.4 Discussion**

The results of the analyses in this chapter show that sperm whale clicks are indeed broad band in a general sense, but that their spectra contain one or two distinct peaks. These peaks are particularly evident in the spectra of male sperm whale clicks. Clicks are emitted almost constantly by submerged sperm whales during feeding dives and click rates tend to oscillate

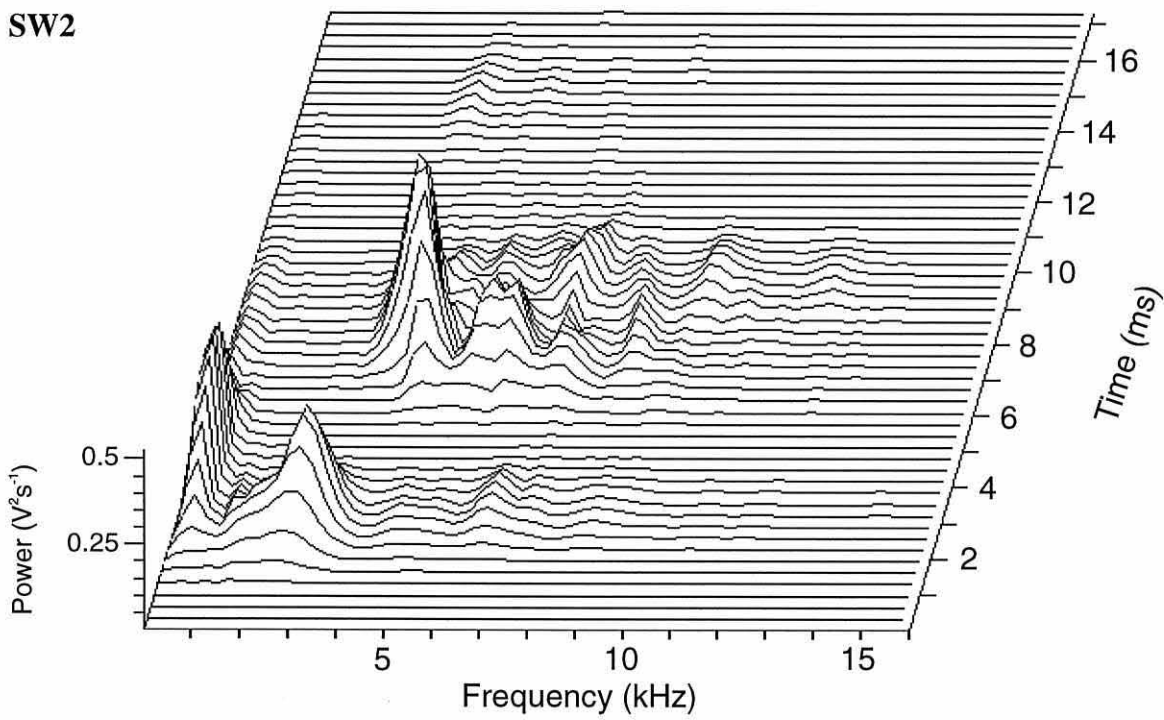


**Figure 2.12** Waterfall display showing short-time fourier transform sequence across the duration of a click from bull male sperm whale SW2. Cascade axis indicates time shift of the FFT window from a point immediately preceding the click onset.

around an equilibrium level after the first few minutes of the dive. Pulsed waveform structure is evident from inspection of individual clicks as observed by other workers, but the threshold frequency at which this pulsed structure emerges clearly differs between the clicks of male and female sperm whales. Sperm whales exhibit extreme sexual dimorphism, with mature bull males growing to almost twice the length of mature females. There is an equivalent dimorphism between the head sizes of males and females, and it is very noticeable that male clicks have longer intra-pulse interval and overall duration than female clicks. It has been observed during the course of this chapter that the clicks of large male sperm whales have almost twice the duration and IPI of female sperm whale clicks [Figs 2.3, 2.10 & 2.11]. Given that the male head has larger dimensions than the female head, some 5 metres in length as opposed to the females 3 metres, the associated spermaceti and air sac structures will be proportionately larger in overall dimension. Sound energy is only reflected effectively when its wavelength is equivalent to, or preferably smaller than, the dimensions of the reflective surface presented to it. Therefore the approximate 2.8 m wavelength of a 400 Hz sound wave in spermaceti oil will be greatly in excess of the lateral dimensions of either the nasofrontal or distal air sacs in either male or female sperm whale head. As a result, very little reflection of sound energy will occur at either air sac and at this low frequency the energy can not be collimated effectively by the spermaceti sac so this component will radiate with little directivity. An absence of pulsed structure is indeed observed in both male and female sperm whale clicks in the sub-kilohertz range [Figs 2.10(b) and 2.11(b)]. Precise dimensions of the nasofrontal and distal air sacs are not a matter of record for either male or female sperm whales, indeed the nasofrontal air sac has been notoriously difficult to observe in carcasses flensed aboard whaling ships (Clarke, personal communication). However, just considering the dimensions of the amphitheatre

skull [Fig 1.3] it is clear that the nasofrontal sac lateral dimension in a large male sperm whale would be in the order of 1 metre diameter. Figure 1.5 shows the nasofrontal sac from a sperm whale of undetermined length exposed during whaling operations. Although there is no precise reference scale the height of the man in the foreground suggests the aforementioned dimension of the nasofrontal sac to be reasonable. The distal sac in the male sperm whale head would probably be slightly smaller than 1 m across, perhaps in the order of 0.75 m. Wavelength of sound in spermaceti oil at a frequency of 2 kHz, observed as a peak in male click spectra, would be about 0.7 m and is a frequency at which pulsed structure is evident in male sperm whale clicks. The 0.7 m wavelength of sound approximates to the likely dimensions of the nasofrontal and distal air sacs, and it is feasible that sound of this wavelength will undergo reflection from air sacs of the aforementioned dimensions, resulting in the pulsed click structure observed. By the same reasoning it is to be expected that click pulsed structure will only emerge in the clicks of smaller female sperm whales at higher frequencies than are observed in the males. Pulsed structure is indeed observed to emerge in female clicks only within the higher frequency bands of 3 - 6 kHz and upwards [Fig 2.11(e) & (f)], and does not emerge in the 1.5 - 3 kHz band [Fig 2.11(d)]. If anything these observation supports the original Norris and Harvey (1972) hypothesis which explains the click pulsed structure as the result of passive reflection of an initial sound pulse between the nasofrontal and distal sacs.

It is assumed that the clicks of diving sperm whales are produced for the purposes of echolocation and food finding in the abyssal depths of the open ocean where little or no light penetrates. Indeed it is difficult to imagine how a sperm whale would be able to sense its environment without the aid of a sonar system and the high frequency components of the

clicks in the region of 10 kHz are appropriate for resolution of the sperm whale prey given the wavelength of a 10 kHz pulse in seawater and the size distribution of sperm whale prey items. Clarke (1993) reported on the various families and size ranges of sperm whale prey off the Azores and found that the majority of contributors to the diet were the Octopoteuthidae, Histioteuthidae, Architeuthidae, Ommastrephidae, Pholidoteuthidae and the Cycloteuthidae. Mean mantle lengths of these groups ranged from 0.11 m - 1 m, and comparing this with the 0.15 m wavelength of a 10 kHz sound pulse in seawater (taking  $c_{\text{seawater}} = 1476 \text{ ms}^{-1}$ : value for 600 m depth, 4°C and 35 ppt salinity [Bark et al, 1964]) it is clear that even individual prey items at the lower end of the size range are at least equivalent in size to the incident wavelength, below which point they become Rayleigh scatterers and hence poor acoustic targets. Smith (1954) demonstrated echo-returns off squid *Loligo pealei* (mantle length = 0.15 m) at 10 kHz, the squid having target strength of -40 dB re 1 $\mu$ Pa. Selivanovsky and Ezersky (1996) state that typical TS for squid of 0.15 to 0.25 m mantle length is between -45 dB re 1 $\mu$ Pa and -55 dB re 1 $\mu$ Pa at 20 kHz, further demonstrating the presence of detectable echo-returns from only moderately high frequency pulses. In addition it should be noted that sperm whales are very unlikely to be searching out individual prey items at long range but rather aggregations of prey. Multiple discrete targets reflecting within the same range resolution cell of a sonar beam increase the individual target strength by approximately 3 dB for every doubling of the numbers present, hence prey aggregations will be much easier for the sperm whale to resolve at long range. The click rate plots [Figs 2.4 & 2.5] indicate that a fairly constant rate of clicking is maintained for the majority of sperm whale dive time. Assuming that sperm whale clicks are active sonar pulses the click rate plots obtained in deep ocean near anechoic conditions suggest that increased rate of clicking with decreasing range to target is unnecessary, at least

when targets are not within immediate striking distance. Such an observation is not inconsistent with a sonar functioning at long ranges of hundreds or thousands of metres, as target information will change very little from one echo-return to the next. The observed click rates strongly suggest that individual squid are not being separated as individual targets during the initial dive. It is quite probable that a clicking whale is only responding to the presence of the large numbers of shoaling prey and/or the scattering layers on which they feed. At close ranges, however, the angular position of a target, especially escaping prey, will change more rapidly and information on its position must be gained at an increasing rate to aid capture (Suga, 1990). Increased click rates preceding creaks, and the creaks themselves, may be indicative of the final stages of prey pursuit.

Figures 2.4 & 2.5 show that click rates approximately doubled from the beginning of each click sequence to a point some 4 minutes or so into the sequence (with the exception of SW7 [Fig 2.5(b)]). This time period represents the initial stages of the dive where sperm whales are usually descending in a near vertical posture towards the seabed. Initial click rates at the beginning of click sequences for both males and females are in the region of  $0.5 - 1 \text{ s}^{-1}$ , implying maximum ranges of useful echo-return between 1476 and 738 m respectively (taking  $c_{\text{seawater}}=1476 \text{ ms}^{-1}$ ), assuming that the whale emits a click upon immediate reception of the echo from its previous click. These ranges are comparable to the water depths in which the animals were feeding, and therefore the seabed proximity appears to have had some influence on the increase in click rate during the early dive stages. Sperm whales off the Azores dive almost vertically towards the seabed during these first few minutes and typical descent rates were measured by echo sounder at approximately  $1.6 \text{ ms}^{-1}$  (100 m/min). Thus in 4 minutes a descending whale is 400 m closer to the seabed,

shortening the total transmission path of a signal in the vertical plane by 800 m and thus the round trip time for a signal-echo from the seabed by about 0.5 s. The water depths and proposed transmission ranges certainly bear a feasibly close relationship, and a large expanse of seabed presents a very strong target to a sperm whale sonar receiver. After the first few minutes of the dive sperm whales may have reached an “operating depth” at which they assume a new aspect and direct their bodies (and transmit and receive beams) more horizontally into the water column than toward the seabed. Under these circumstances the inter-click interval may represent a time window in which they expect to receive a desired target echo-return (i.e. prey).

Overall mean click rates, discounting the initial 4 minute rises in click rate, have been calculated for bull males at  $1.1713 \text{ s}^{-1}$  and for females at  $1.9455 \text{ s}^{-1}$  using the click rate data from SW1 - SW4 and SW6 - SW9 from 4 minutes onwards. These equilibrium rates imply maximum ranges of useful echo-return of about 630 m for large males and about 380 m for females (taking  $c_{\text{seawater}}=1476 \text{ ms}^{-1}$ ). One possible explanation for the difference is that, being physically much larger than females and having more massive heads, bull males can produce more powerful source level clicks and thereby gain target information over greater ranges than females. One might expect the interval between clicks to be representative of the potential (or anticipated) maximum target detection range. The 2 kHz component of the male sperm whale click and/or the 3 kHz component of the female click are unlikely to be of great utility in close range echolocation and target discrimination, given the respective wavelengths in seawater and that fact that the reflected energy vs geometric size falls very rapidly ( $4^{\text{th}}$  power) as target size falls below one wavelength.

Returning to the subject of beam forming it has been mentioned that directional transmission of the high frequency sperm whale click components may largely explain the observed trends in pulse envelope within the various frequency bands. Indeed it is possible to visualise the frequency dependent variation of click spectral density with dive time by computing  $\frac{1}{3}$ <sup>rd</sup> octave band levels from the power spectral cascade data (illustrated in Figs 2.6 & 2.8). This has been done for (i) the first 3 minutes of sequences SW1, SW2 and SW3 and (ii) minutes 9 to 12 of the same sequences, by summing power data bins in  $\frac{1}{3}$ <sup>rd</sup> octave bands (as close as possible given the FFT bin resolution) centred on 500 Hz, 2.5 kHz, 5 kHz and 10 kHz and dividing by the respective  $\frac{1}{3}$ <sup>rd</sup> octave bandwidths. Figures 2.13 - 2.15 show the resulting  $\frac{1}{3}$ <sup>rd</sup> octave band levels across the first 3 minutes of the sequences. It is immediately obvious that spectral density in the band centred on 500 Hz decays with time (an unquantified but increasing function of distance in these cases) in a manner largely consistent with spreading loss from a constant sound source level as distance increases between source and receiver. Figures 2.13(a) and 2.15(a) suggest power output in the band at source to be approximately constant and the received signal to be attenuating with distance, and the transmission to be either omnidirectional or otherwise directional but continually on axis to the hydrophone (the latter being less likely). At higher frequencies the patterns are markedly different, suggesting either varying power output and/or a directional transmission beam varying in aspect with respect to the surface hydrophone. Curiously in some cases spectral density in the high frequency bands increases with time (distance), perhaps suggesting a gradual alignment of the on axis beam with the hydrophone or a real increase in source power. Figure 2.15(b) is particularly striking in that it shows oscillating spectral density, as if the whale were systematically “sweeping” its transmit beam - with the power maximum of the on-axis signal sweeping back and forth across the hydrophone. The

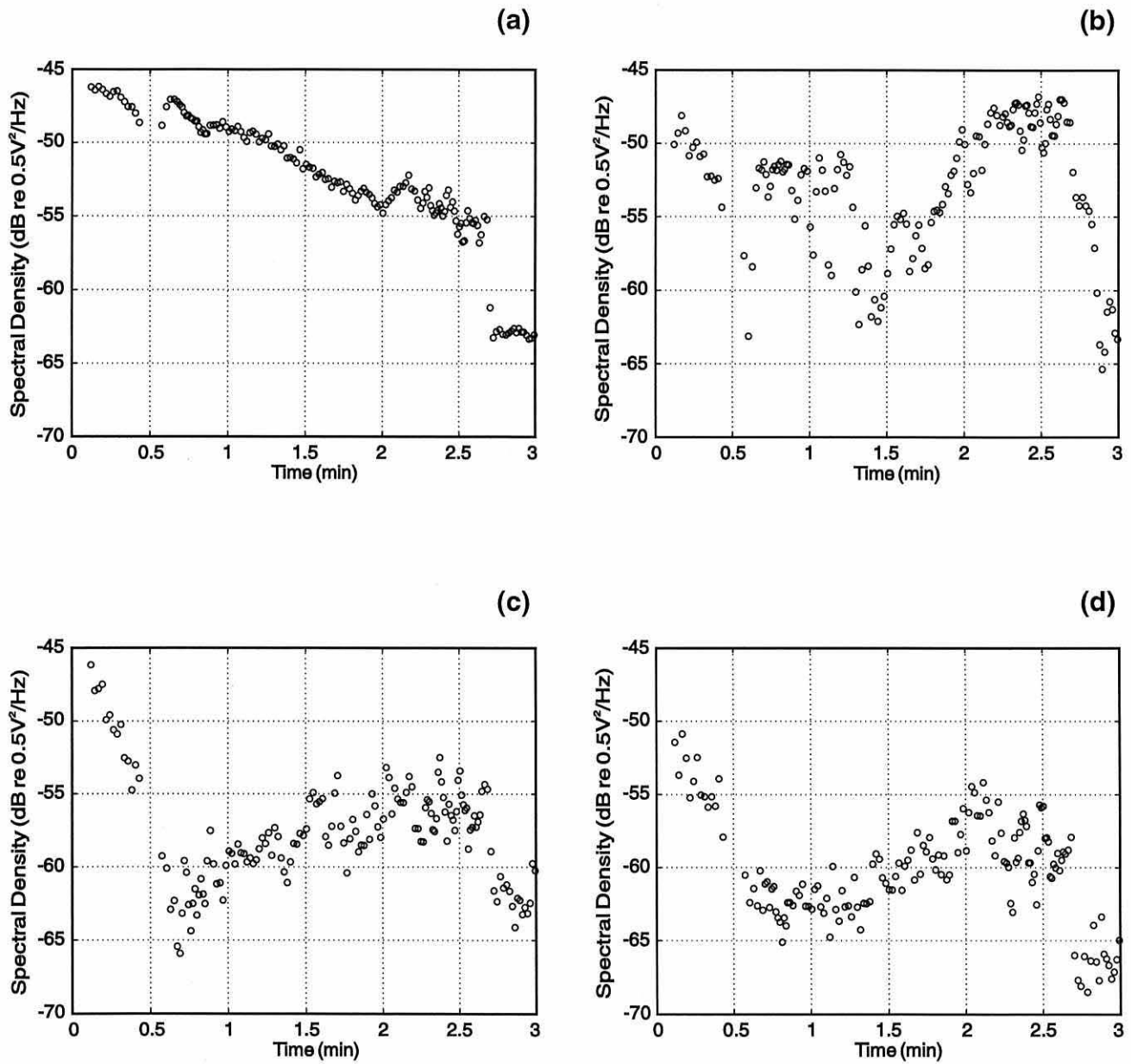


**Figure 2.13** Plots showing spectral density in  $\frac{1}{3}^{\text{rd}}$  octave bands from clicks across the first 3 minutes of sequence SW1. Abscissae show time since first click, centre frequencies of  $\frac{1}{3}^{\text{rd}}$  octave bands are (a) 500 Hz, (b) 2.5 kHz, (c) 5 kHz and (d) 10 kHz; background noise levels are below scale in all plots.

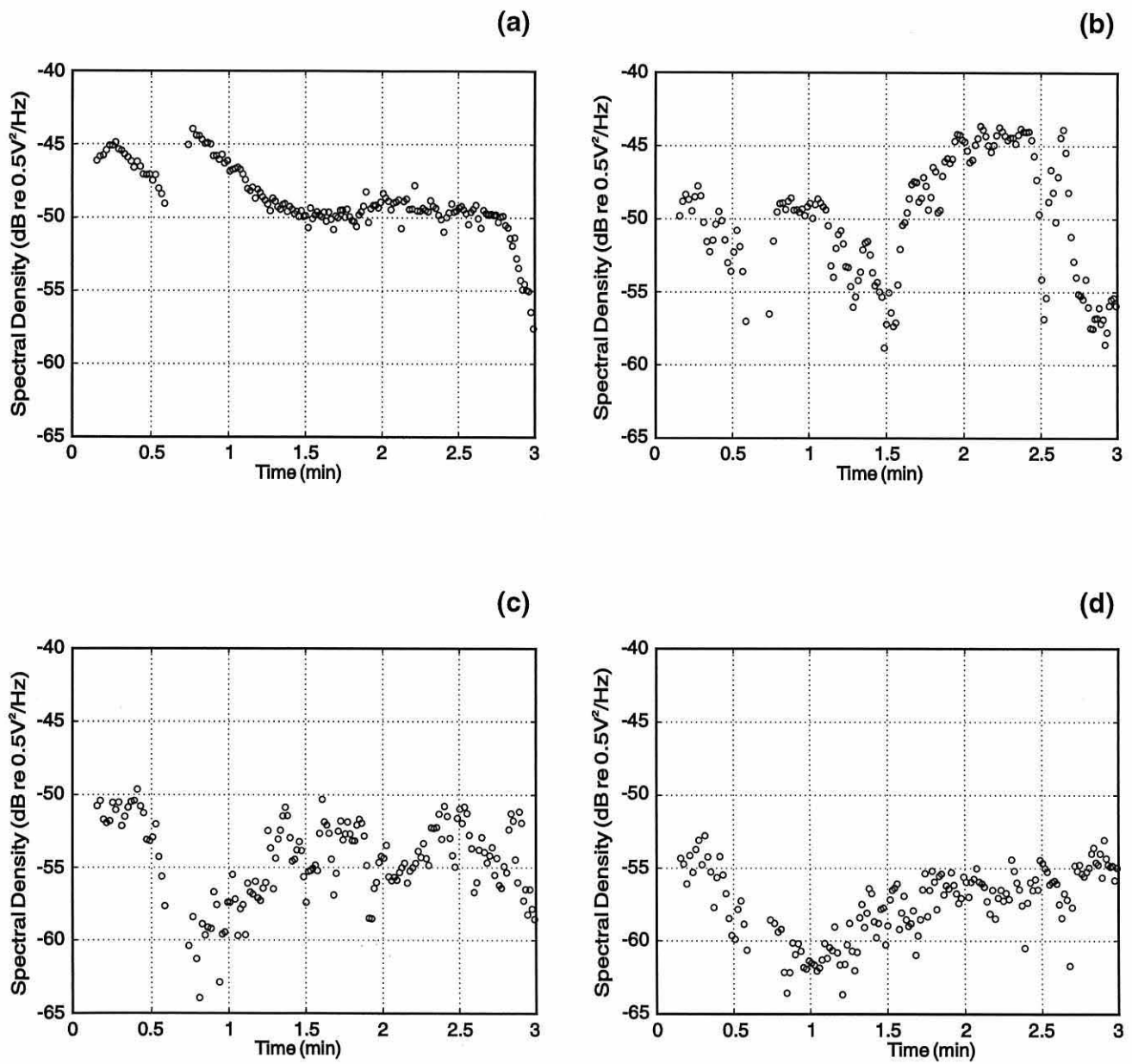


**Figure 2.14** Plots showing spectral density in  $\frac{1}{3}^{\text{rd}}$  octave bands from clicks across the first 3 minutes of sequence SW2. Abscissae show time since first click, centre frequencies of  $\frac{1}{3}^{\text{rd}}$  octave bands are (a) 500 Hz, (b) 2.5 kHz, (c) 5 kHz and (d) 10 kHz; background noise levels are below scale in all plots.

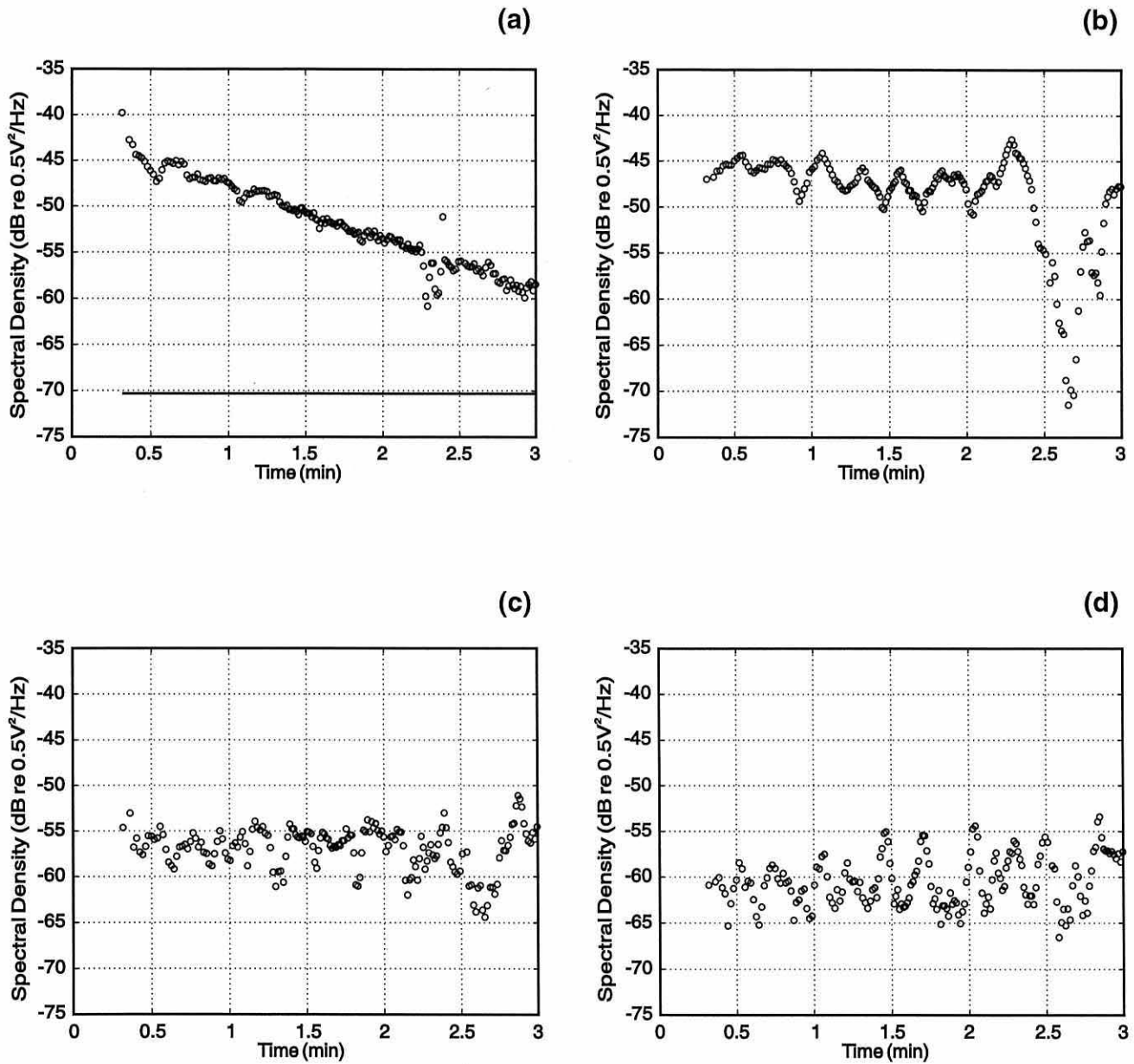


**Figure 2.15** Plots showing spectral density in  $\frac{1}{3}^{\text{rd}}$  octave bands from clicks across the first 3 minutes of sequence SW3. Abscissae show time since first click, centre frequencies of  $\frac{1}{3}^{\text{rd}}$  octave bands are (a) 500 Hz, (b) 2.5 kHz, (c) 5 kHz and (d) 10 kHz; background noise level is indicated by horizontal line in (a), but is below scale in (b)-(d).

pattern also appears similar at higher frequencies in this same click sequence [Fig 2.15(c) & (d)], indeed possibly more pronounced in (d) suggesting a more tightly focused beam as might be expected. From minutes 9 to 12 the whales are at depth and the transmit beams, especially at high frequency, cannot be expected to direct towards the surface hydrophone. There is somewhat more similarity between the low and high frequency band levels, variation in the band centred on 500 Hz may now represent more variability in received power than spreading loss with increasing range would account for, and the variability is clearly no longer systematic. There are, however, still differences in the pattern of variation between low and high frequency bands, e.g. Figure 2.16(a) & (b). At approximately 10.5 minutes in Figure 2.16(b) spectral density dips considerably whereas this does not occur at the low frequencies in part (a). Again this could be the result of receiving a directional beam at varying aspect, whereas the low frequency is essentially omnidirectional and power output at source may be the major cause of variability - in part (c) there is also a dip in power. Similarly in Figure 2.17(a) spectral density decreases between 9 and 10.5 minutes, whereas in parts (b) and (c) power increases and in (d) is approximately level. Notably, however, the variation in all bands in Figure 2.18 is similar.

Assuming that sperm whale clicks become directional at frequencies upwards of 3 kHz, consider the case of a diving sperm whale emitting clicks which are recorded by surface hydrophones directly above it - which is the case for sperm whale sounds analysed in this dissertation. Sound energy would radiate outwards from the monkey lips with the low and sub-kilohertz components radiating omnidirectionally, but with the higher frequency components forming progressively narrower beams along the long axis of the whale. A proportion of the sound energy in the expanding wavefront of the initial pulse, i.e. a

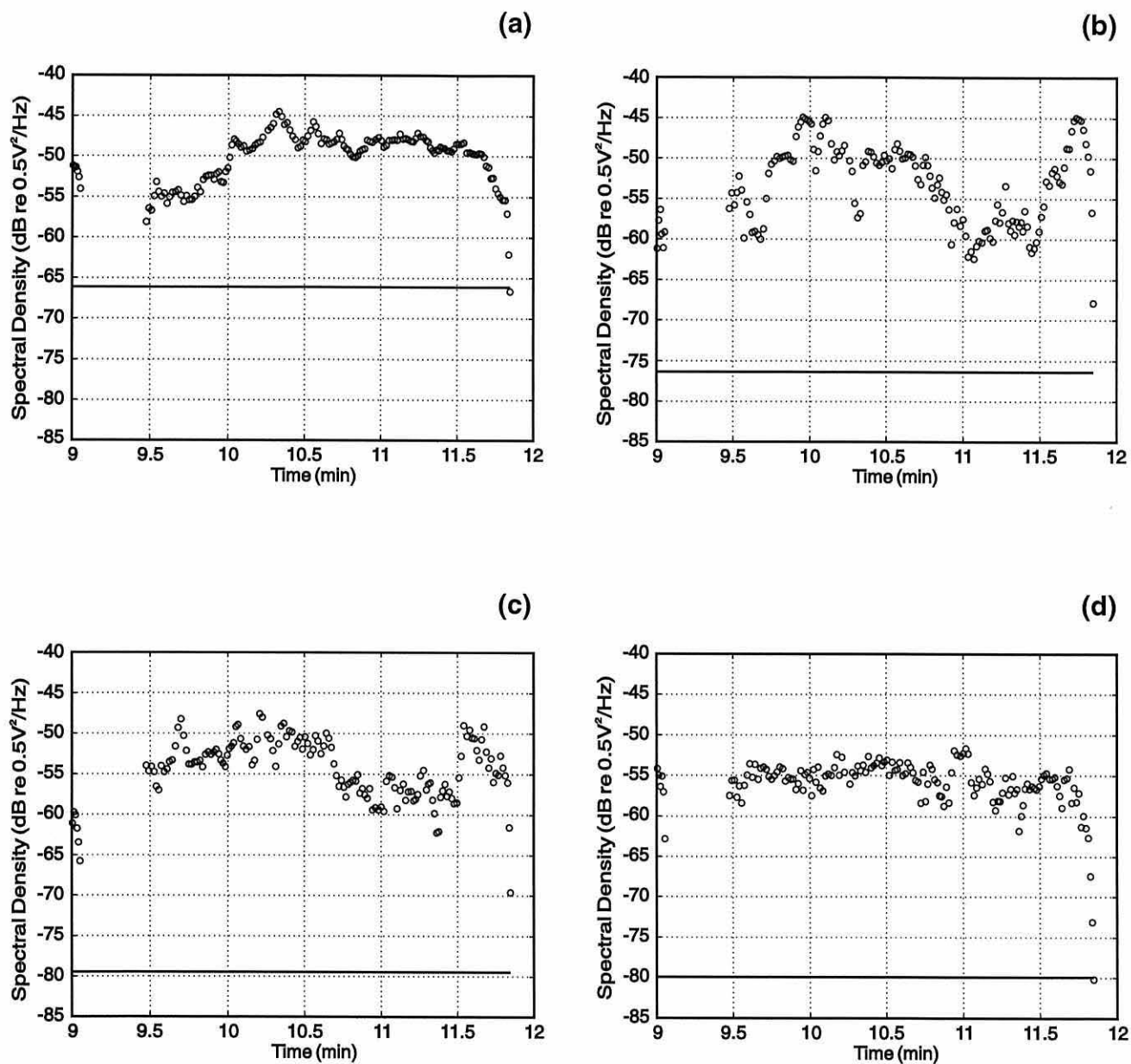


**Figure 2.16** Plots showing spectral density in  $\frac{1}{3}^{\text{rd}}$  octave bands from clicks across minutes 9 to 12 of sequence SW1. Abscissae show time since first click, centre frequencies of  $\frac{1}{3}^{\text{rd}}$  octave bands are (a) 500 Hz, (b) 2.5 kHz, (c) 5 kHz and (d) 10 kHz; horizontal line in each plot indicates the average background noise level.

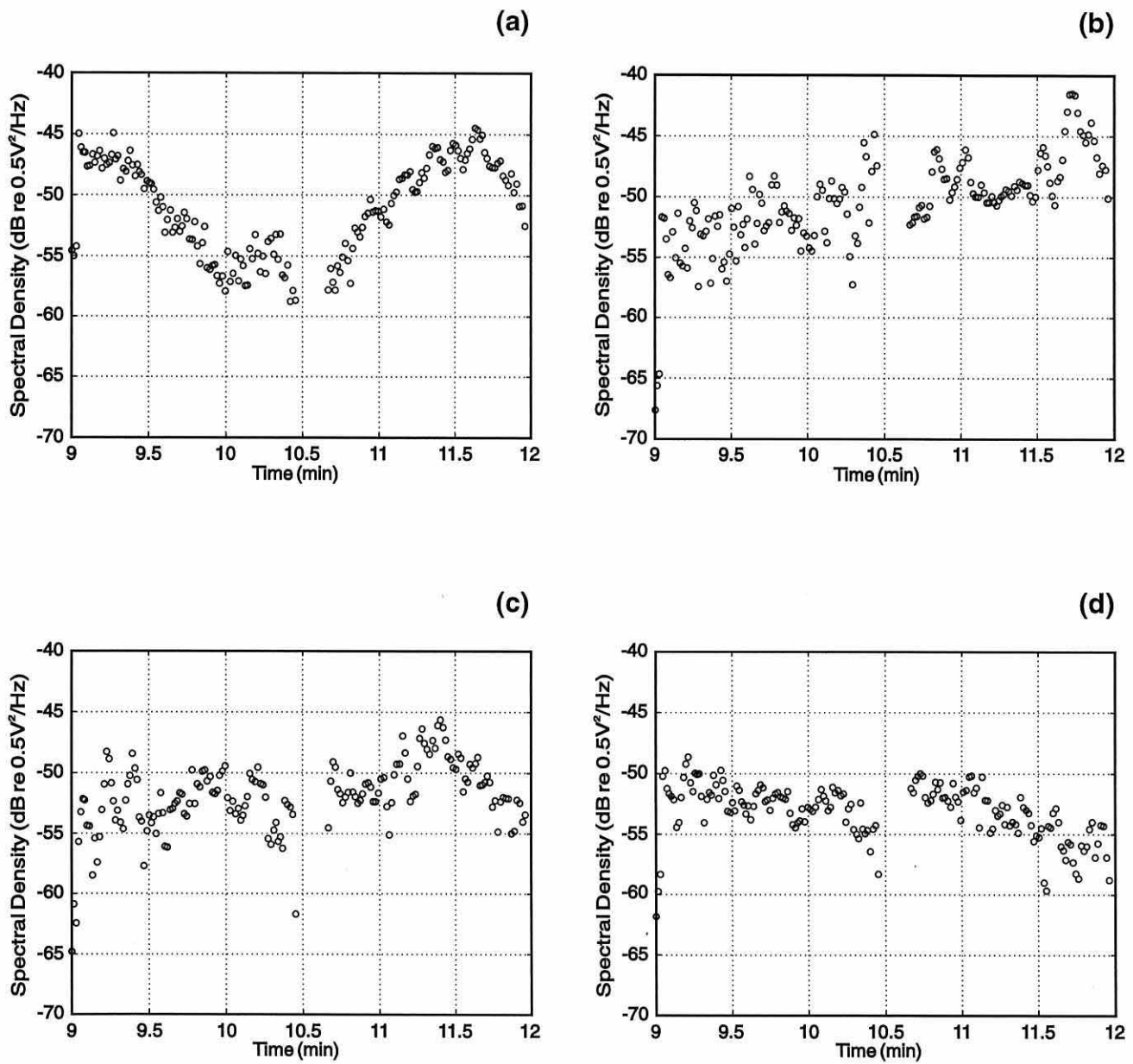


**Figure 2.17** Plots showing spectral density in  $\frac{1}{3}^{\text{rd}}$  octave bands from clicks across minutes 9 to 12 of sequence SW2. Abscissae show time since first click, centre frequencies of  $\frac{1}{3}^{\text{rd}}$  octave bands are (a) 500 Hz, (b) 2.5 kHz, (c) 5 kHz and (d) 10 kHz; background noise level is below scale in each plot.

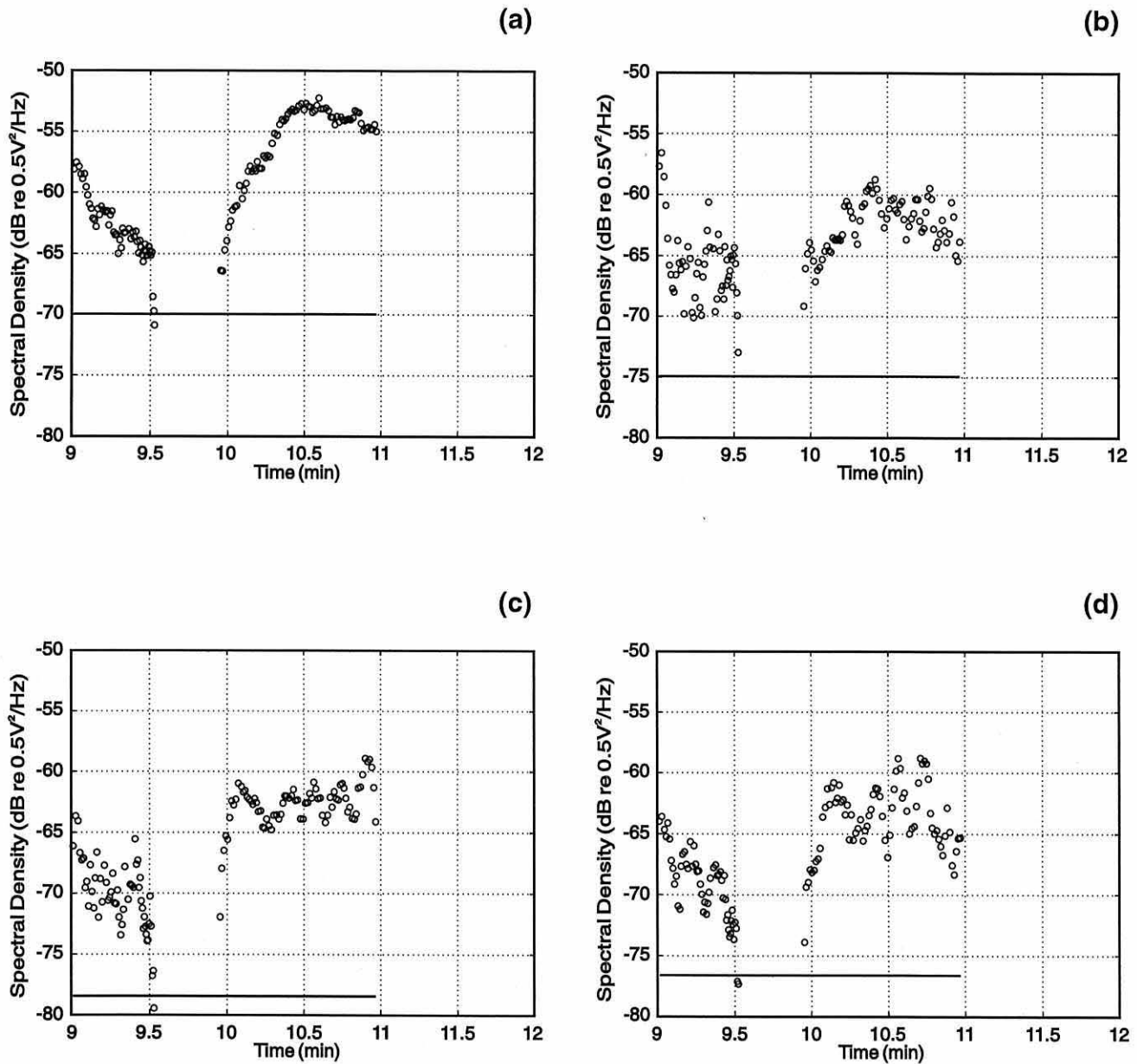


**Figure 2.18** Plots showing spectral density in  $1/3^{\text{rd}}$  octave bands from clicks across minutes 9 to 12 of sequence SW3. Abscissae show time since first click, centre frequencies of  $1/3^{\text{rd}}$  octave bands are (a) 500 Hz, (b) 2.5 kHz, (c) 5 kHz and (d) 10 kHz; background noise is indicated by horizontal line in each plot.

composite of all transmit beam patterns of the initial pulse, would reach the surface hydrophones directly. Assuming the hydrophone is not oriented exactly with the long axis of the diving whale (a very likely assumption) a different composite of beam patterns will be directed posteriorly through the lipid of the spermaceti sac and impact the air filled nasofrontal sac. The sound will partially reflect and travel anteriorly through the spermaceti sac where it will impact the distal air sac at the anterior end of the head. A section of wavefront from the outward radiating reflection from the distal sac directed towards the surface hydrophone will almost certainly be received as a different composite of beam patterns to the initial pulse. In other words, the rearward radiation pattern across the spectrum of the initial sound pulse and that of the first reflection from the distal sac are likely to be dissimilar from the point of origin along the path to the surface hydrophone. If the initial pulse signal had a major rearward transmission lobe along the axis of the whale, and the animal were oriented such that the surface hydrophones were outside this major lobe, then one might expect to receive energy from the initial pulse at a level somewhat reduced from the condition where a similar signal is received on axis. These speculations are supported by the observations made in this chapter.

One observation made by Cranford et al (1996) is the fact that dolphin species with asymmetrical monkey lip/bursal complexes tend to produce echolocation clicks which are generally more broadband than the clicks of porpoises or sperm whales. Porpoises have largely symmetrical monkey-lip/bursal complexes and sperm whales have only one pair of monkey lips. Cranford speculates that the broad bandwidth of energy contained in dolphin clicks results from interference patterns in the sound waves generated by the asymmetric monkey lip complexes, and that dolphins may even be able to alter this interference pattern

to achieve the desired output characteristic of their clicks. Porpoises are known to produce short transient clicks that are very narrow band in comparison to the dolphin clicks (Goodson and Sturtivant, 1996), and Cranford speculates that the apparent symmetry of the harbour porpoise monkey lip pairs does not allow for interference patterns which may give rise to a broadband sound characteristic. Similarly Cranford also points to the fact that sperm whale clicks have previously been observed to exhibit narrow band spectral peaks (e.g. Weilgart & Whitehead, 1988) and implicates the single pair of monkey lips as a possible reason for this, since there is no second sound source to generate an interference pattern. The observations in this chapter [Figs 2.6 & 2.7] clearly show that there are distinct, narrow-band spectral peaks in male sperm whale clicks which would be consistent with Cranford's speculations.

## **Chapter 3**

### **Sound Velocity Measurements in Spermaceti Oil under the combined influences of Temperature and Pressure.**

#### **3.1 Introduction**

The anatomical layout of oil sacs and air spaces within the sperm whale head [Fig 1.4] almost certainly has some influence on the structure of sperm whale clicks, and in all probability gives rise to the multiple pulsed structure. The intra-pulse interval within clicks is hypothesised to be a function of the longitudinal air sac separation and velocity of sound in spermaceti oil. If one has good estimates of the velocity of sound in spermaceti oil, and can measure IPI's to reasonable precision, the air sac separation (essentially head length) can be determined by simple algebra. Head lengths of sperm whales can be used to extrapolate total body lengths (Gordon, 1991), and such information would be of great value to population biologists if it could be obtained through passive acoustics during oceanic surveys. As sperm whales dive to great depths the barometric pressure on the head and spermaceti oil contained therein will undergo considerable variation, and there is also the possibility that temperature of the oil may be altered during dives (Clarke, 1978c). For these reasons it is important to measure, and ultimately predict, the effects that varying temperature and pressure will have on sound velocity in spermaceti oil.

Spermaceti oil is a mixture of wax esters and triglycerides (Morris 1973, 1975) and undergoes a transition between solid and liquid states at a threshold temperature of

approximately 29°C. At 30°C the oil is a pale, relatively low viscosity liquid with a density of about 862 Kgm<sup>-3</sup> at atmospheric pressure. As temperature drops below the 29°C threshold the oil crystallises into a waxy solid reaching a density of about 889 Kgm<sup>-3</sup> at 22.5°C (Clarke, 1978b). It has been argued (by Clarke, 1978c) that sperm whales use this property of spermaceti oil to adjust their buoyancy during deep dives and at different geographical locations. Clarke argues that the complex system of airways in the head, in intimate contact with the oil, can be used to flush cold seawater for heat exchange, thereby cooling the oil to effect phase change and density increase. Clarke further hypothesises that the oil would be reheated by blood flow through a dense capillary network, using stored muscular heat from swimming. Clarke (personal communication) has some indirect evidence of this latter mechanism in a series of photographs of freshly dissected spermaceti tissue showing areas crimson red with vascularisation, while adjoining tissue remains pale yellow and devoid of blood - suggesting control of blood flow through spermaceti tissue.

Clarke's buoyancy hypothesis remains unproven and direct measurement of in-situ spermaceti temperature in living, diving sperm whales presents extreme practical difficulties. However, if IPI's within sperm whale clicks are indeed a function of sound velocity in spermaceti oil, and if sound velocity in the oil is significantly affected by temperature, observation of trends in IPI over dive time may need to take account of possible temperature fluctuations within the head. Flewellen and Morris (1978) made measurements of sound velocity in spermaceti oil at temperatures from 29°C to 40°C, yielding an inverse linear relationship between the two. Valuable as these measurements were the investigators only measured sound velocity in the oils' liquid phase at atmospheric pressure. Since sperm whales undertake dives to extreme depths it is important to

understand the effects that elevated pressures will have on sound velocity in the oil. To account for every possibility it is also important to understand the effect that solid-liquid transition will have on sound velocity in spermaceti oil. This chapter describes original measurements of sound velocity in spermaceti oil under the combined influences of temperature and pressure using purpose built apparatus.

**SECTION 3A - 1994 Measurements : Sound Velocity in Spermaceti Oil**  
**from *Physeter macrocephalus***

**3A.1 Methods**

**3A.1.1 Spermaceti Oil Sampling**

On 15<sup>th</sup> December 1993 a 15.6 metre male sperm whale carcass washed ashore on the East coast of England, some 10 miles south of Bridlington. The carcass was intact and externally undamaged, indicating that the animal had not been dead for too great a length of time; a rough estimate was 48 hours. During an official autopsy approximately 1 litre of spermaceti oil was sampled through a single penetration along the dorsal surface of the head, approximately midway between the eyes and the “snout” [Fig 3A.1]. Flensing knives and a chain saw were used to cut a hole approximately 30 cm square through the tough muscle and tissues of the head and case. Spermaceti tissue containing semi-liquid oil, along with impurities of blood and small quantities of extraneous tissue, were pulled by hand from the peripheral region of the spermaceti sac (within half a metre of the dorsal surface of the head)

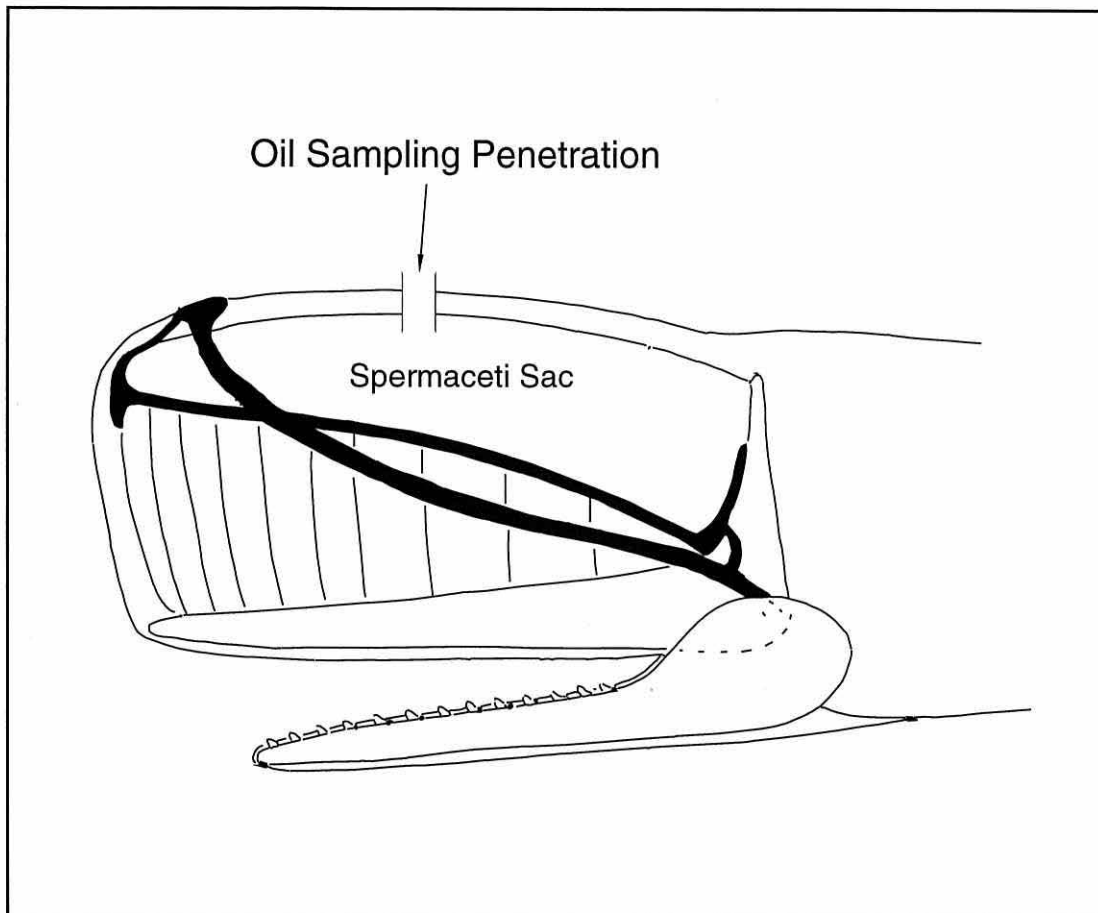


**Figure 3A.1** Schematic of sperm whale head showing approximate position of spermaceti sac penetration through which oil was sampled. Carcass lay on its right side enabling oil sampling horizontally through penetration.

and sealed in clean glass jars. The carcass was lying on its right side, so oil could be sampled horizontally through the penetration. During sampling, liquid spermaceti oil trickled from the penetration in the whales' head and solidified on the cold outer surface. Much of this solidified oil was collected by simply pulling it from the head with a knife and dropping it into the sample jars. The samples were deep frozen to  $-20^{\circ}\text{C}$  within 24 hours of collection. When taking sub-samples of oil for experimentation reasonably clean pieces of solid spermaceti oil were cut from the main sample while still frozen. Gently melting and decanting the oil provided a final means of removing obvious, macroscopic impurities (e.g. small pieces of extraneous tissue). Although the oil was not from a freshly dead animal it did exhibit the expected physical characteristics, with a phase change between  $28^{\circ}\text{C}$  and  $29^{\circ}\text{C}$ .

### **3A.1.2 Velocity Measurement Apparatus**

To measure variation of sound velocity in spermaceti oil as a function of both temperature and pressure, a thermally conductive pressure cell assembly was constructed from CZ121 free cutting brass. This assembly consisted of a thick walled brass cylinder designed to hold the oil samples with an internal bore diameter of 29 mm, a maximum depth of 101 mm and a wall thickness of 8 mm. A solid brass ram was machined precisely to fit the bore and complete the liquid enclosure. A hydraulic rubber lip seal (Lockheed 2782) with a 12 mm diameter hole punched through its centre was fitted to the front face of the ram to minimise fluid seepage past the ram at high pressure. The entire pressure cell assembly was similar in construction to an automobile hydraulic brake cylinder-piston assembly, with spermaceti oil

replacing hydraulic fluid [Fig 3A.2]. A vent machined into the cylinder wall at the base of the bore enabled trapped air to be expelled after the ram had been fitted by simply turning the apparatus on its side to allow air bubbles into the vent tube, from where they could be expelled. Sound transduction was provided by two 500 kHz piezoelectric disc transducers (Morgan Matroc Limited, Transducer Products Division, Southampton). The active transducer was sealed into the face of the ram and sound pulses emitted from this transducer were received by an identical transducer sealed in the cylinder base.

In essence, sound pulses were fired by the ram transducer down through the sample and received by the base transducer, enabling a time of flight measurement through a known sample length of spermaceti oil. The transducers were squat, cylindrical piezoelectrics (PZT4D) with a diameter of 10 mm and a height of 5 mm. A circular recess 12 mm in diameter was machined into the face of the ram to accommodate the transducer, and a small centre hole was bored the entire length of the ram for electrical wiring. The rear face of the transducer was glued to the exposed brass lip at the bottom of the recess with electrically conductive silver paint, and the live connecting wire brought round to the front face of the transducer via a keyhole cut in the edge of the recess [Fig 3A.3]. The live wire was soldered to the front face of the transducer, the main ram-cylinder body was used as a common electrical earth for both transducers. The peripheral ring of space between the edge of the transducer and the recess wall was packed with non-toxic modelling clay (Tebro TB 856). The remainder of the recess was then filled with epoxy resin-hardener mix (Resin: Ciba Geigy MY753, Hardener: Ciba Geigy HY951) such that the front face of the transducer and clay ring was completely covered by a plug of compound approximately 2 mm thick. The resin-hardener mix ensured a good seal, bonding to the walls of the recess and prevented

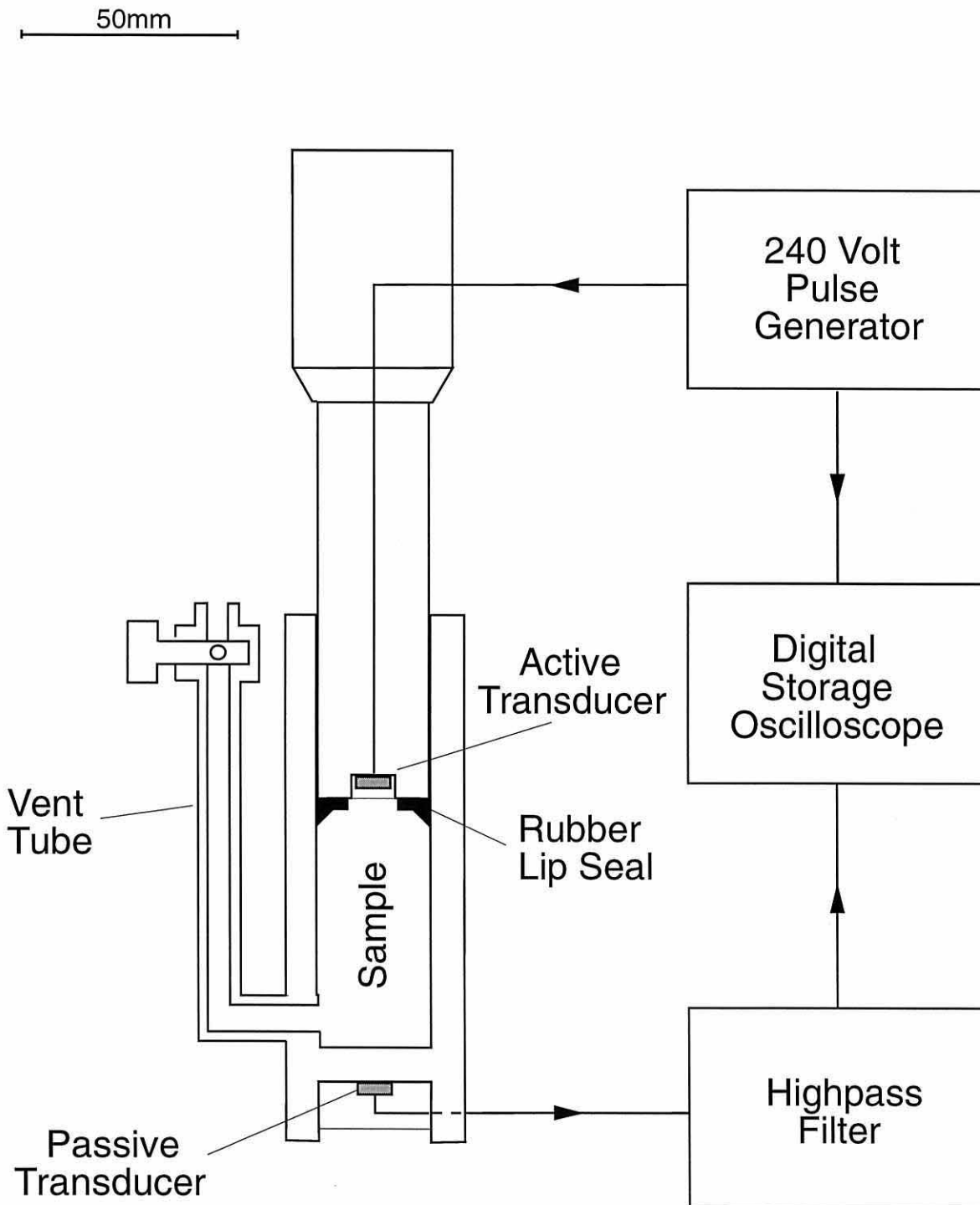


**Figure 3A.2** Schematic of cell assembly used for measuring sound velocity in spermaceti oil under varying temperature and pressure regimes; scale bar refers to cylinder & ram dimensions.

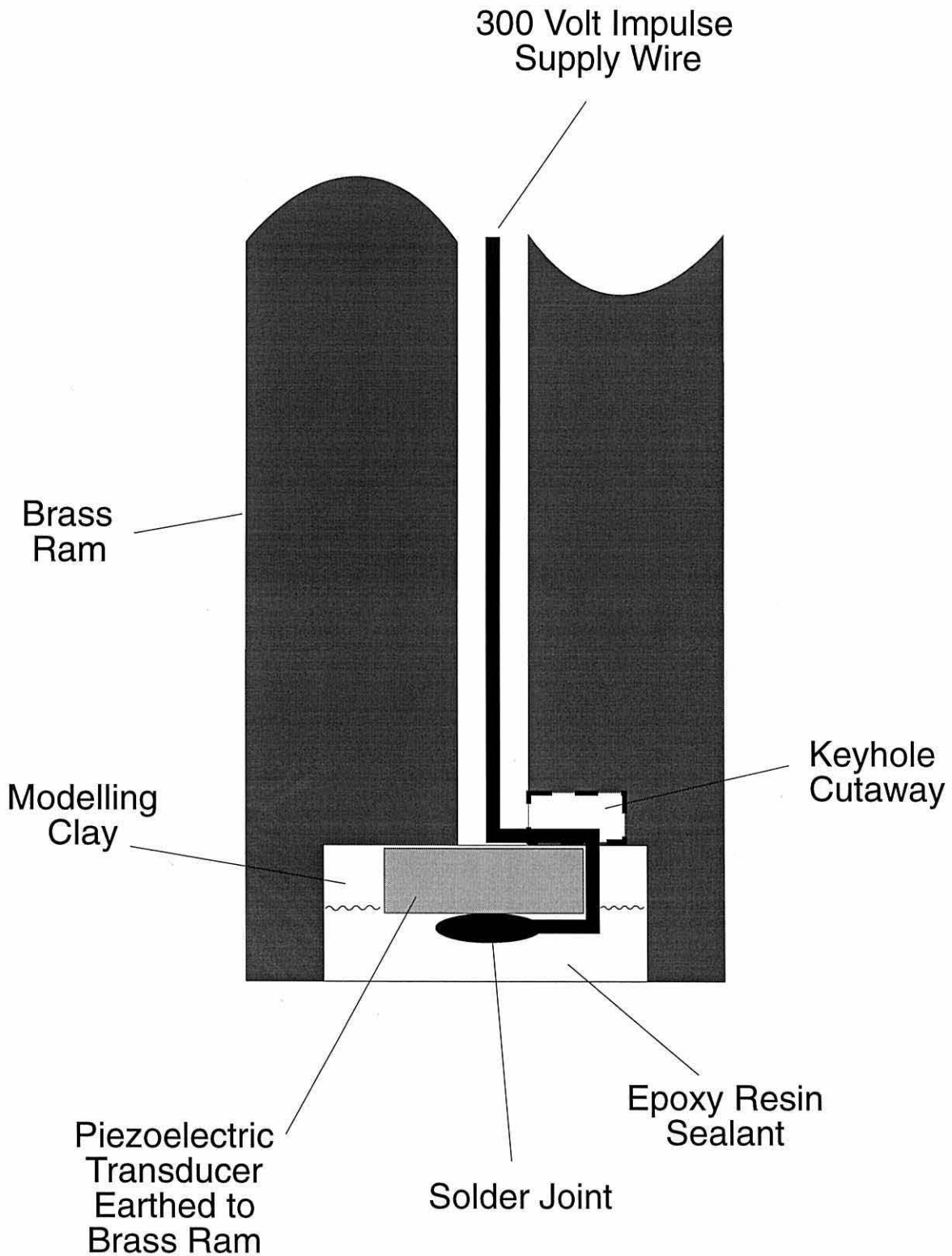


**Figure 3A.3** Schematic of active transducer mounting and connection in the face of the velocimeter ram

fluid seepage into the transducer space. The clay around the edge of the transducer acted as a soft filler in order to allow freer transducer oscillation than would have been the case had epoxy resin-hardener mix been used to totally enclose the transducer. The wiring hole, running the length of the ram behind the transducer, was filled completely with epoxy resin-hardener mix. Applying a 300 Volt spike to the transducer caused it to excite into resonance at its natural frequency and provided the pulsed sound source.

A large exterior recess was bored into the base of the cylinder to accommodate the receive transducer. Unlike the ram transducer, which was within the liquid enclosure and subject to increased barometric pressures, the cylinder transducer was mounted on an exterior surface of the cylinder and hence only subject to ambient atmospheric pressure in the laboratory. The front face of the receive transducer was bonded with silver paint to the top of the recess to achieve good acoustic and electrical contact. The signal wire was soldered to the rear face of the transducer and fed out through a small hole in the recess wall. The recess was then filled with silicone rubber to create a water-tight seal around the transducer [Fig 3A.4].

The active transducer in the ram face was supplied with stimulus by an electronic spike generator (Simpkin, Model 1), firing a 300 Volt spike 50 times per second and exciting the ram transducer into resonance as previously described. Each spike was essentially a unit impulse followed by an exponential decay (effective pulse-width 4  $\mu$ s, peak amplitude 300 Volts) and each also triggered, via the external trigger port, a sweep on a digital storage oscilloscope (Gould, Model DSO 1602). The waveform channel input of the scope was connected to the receive transducer in the cylinder base through a high pass filter unit (Krohn Hite, Model 3100). The filter stage was required as the active transducer had two

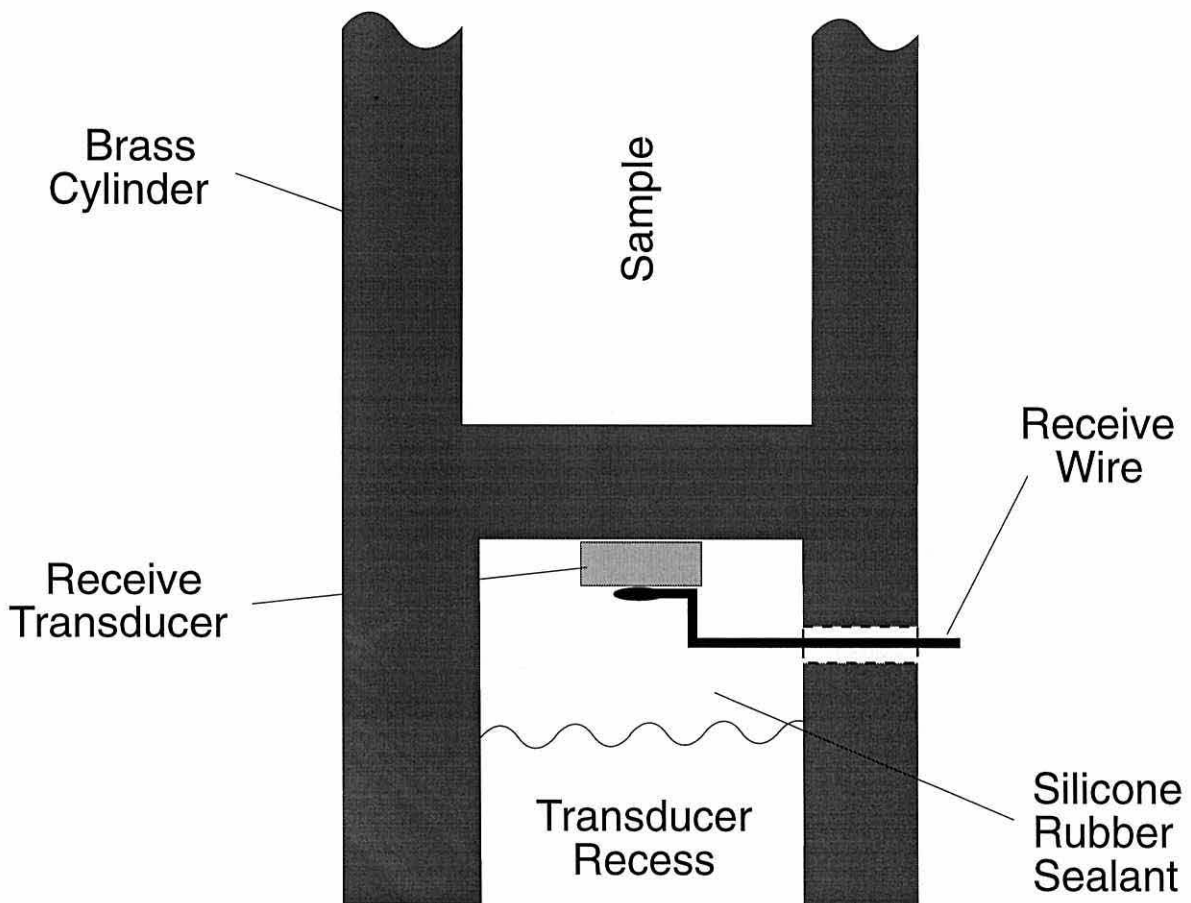


**Figure 3A.4** Schematic of passive transducer mounting and connection in the base of the velocimeter cylinder (for 1994 measurements).

primary modes of oscillation, one longitudinal and the other radial. The longitudinal oscillation produced the desired, direct path sound pulse down through the sample to the receive transducer. Although the free resonant frequency of the transducer was 500 kHz, in practice the mechanical constraints of fixing, potting and the characteristics of the fluid sample lowered the effective frequency of longitudinal sound pulses to some 200 kHz. The radial mode of oscillation coupled well to the metal walls of the cell, the frequency was ill defined in the time domain but seemingly between 100 - 200 kHz. Given that sound velocity in brass was higher than in the oil samples, the radial sound components arrived at the base transducer ahead of the longitudinal components and interfered with reception of the main path signal. High pass filtering the received signal, with a sharp roll-off (5<sup>th</sup> order attenuation) just below 200 kHz, greatly improved the signal to noise ratio of the direct path signal. The oscilloscope was set with a threshold level to capture images of the direct path waveforms, which were updated 50 times per second in accordance with the triggering rate and produced a stable display. A vertical timebase cursor on the oscilloscope display was used to measure the time elapsed between transmission (trigger) event and the leading edge features of the received sound pulse waveform. Leading edge features were the pulse onset followed by first peak, first trough and second peak.

### **3A.1.3 Pressure Cell Calibrations**

Sample temperature was controlled by immersing the pressure cell assembly in a water jacket, fed from a temperature regulated water bath. This arrangement allowed stable cell temperatures to be maintained for extensive periods, and for temperatures to be raised and

lowered by altering the thermostirrer settings at the water bath. The thermostirrer (Gallenkamp Thermo-Stirrer 85) had a heating coil but no cooling coil, so it was not possible to lower cell temperature below ambient room temperature - approximately 22°C. The entire assembly was placed in a modified oedometer, an apparatus normally used for applying vertical loads to sediment-soil samples in soil mechanics consolidation testing, and the oedometer was used to apply a downwards force on the top of the ram [Fig 3A.5]. The entire pressure-cell/waterjacket assembly was placed on a raising flatbed in the oedometer frame and the top of the ram abutted to a fixed shaft. Loading calibrated weights onto the distal end of the oedometer lever arm pushed the pressure cell assembly up against the fixed shaft, thereby creating the large downward forces on the ram and enabling stepwise increase of pressure within the cell.

The thermal response of the cell was assessed by filling the cylinder with distilled water and measuring the time taken for the sample to reach equilibrium temperature with the water jacket. From these measurements it was decided to allow a minimum of 45 minutes for each sample to reach thermal equilibrium after a change in water jacket temperature. Pressure calibration was performed by connecting a Budenberg analogue pressure gauge to the cell vent and measuring the internal cell distilled water pressure as each weight was loaded. The loading of each weight produced an increase in pressure of 1.52 MPa (15 atmospheres), reaching a maximum pressure of 9.1 MPa (90 atmospheres) above ambient atmospheric pressure before the apparatus was considered unstable. The Budenberg gauge had a scale limit of 1500 psi (10.3 MPa or 102 atmospheres [1 MPa = 145 psi]) with the smallest scale division and claimed accuracy being 10 psi; the gauge itself was calibrated using an ELE dead weight tester. The pressure range of 0 - 9.1 MPa (above ambient

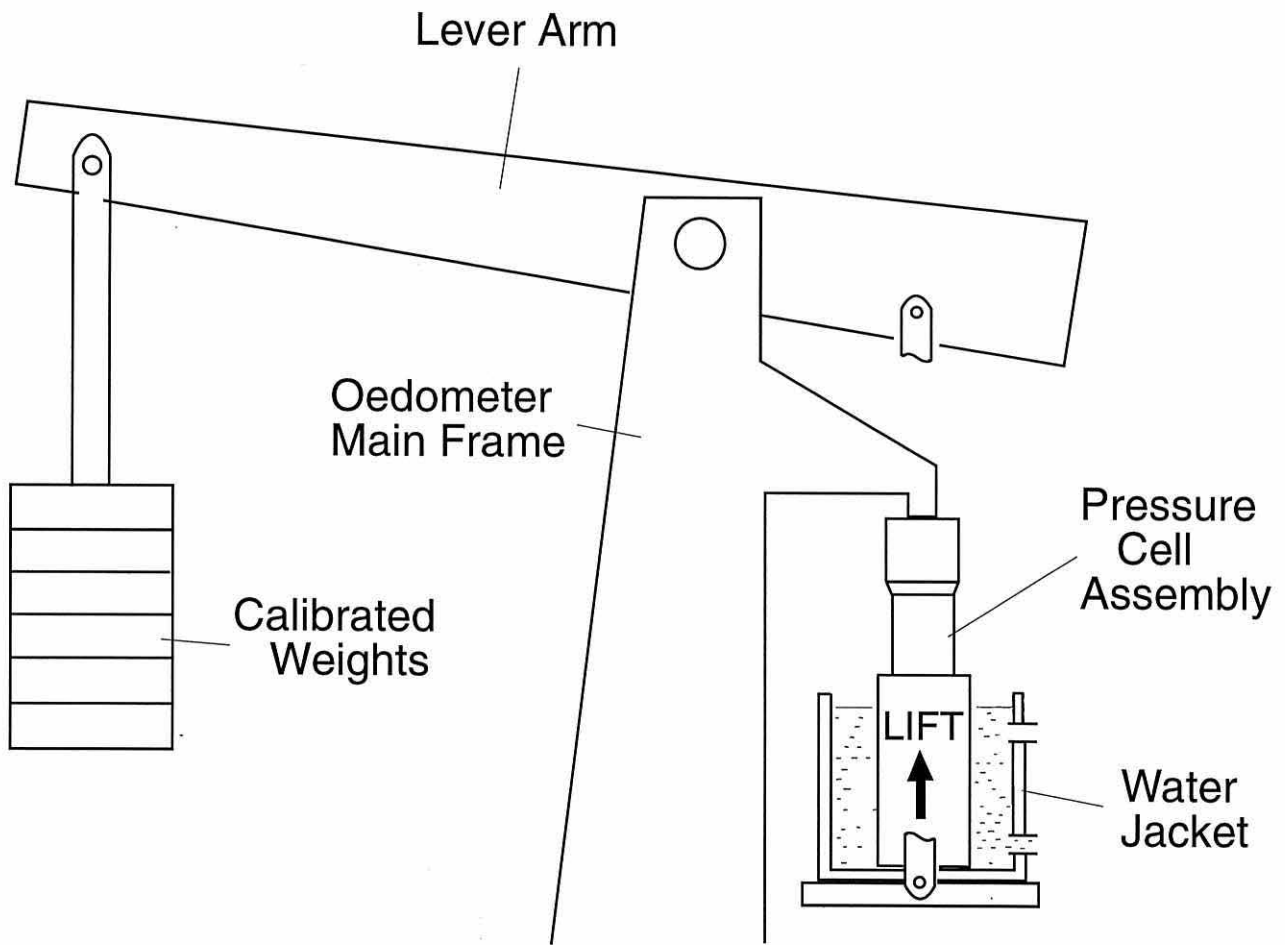


**Figure 3A.5** Schematic of oedometer apparatus used for pressurising temperature regulated oil samples in the cell

atmospheric pressure of 0.1 MPa) represents conditions experienced by a sperm whale between 0 and 900 m water depth, which is a realistic vertical range for sperm whales.

Sound pulse time-of-flight measurements were made in known column lengths of distilled water as a reference calibration for subsequent spermaceti oil measurements. The cell was filled with distilled water, and brought to a stable equilibrium temperature, and sound transmission-reception engaged. The oscilloscopes' timebase cursor was used to measure time elapsed (in 0.05  $\mu$ s steps) between trigger event ( $t=0$ ) and features in the received sound pulse waveform (namely the onset when visible, first peak, first trough and second peak - [see Fig 3A.6]). The distilled water column length in the cell was reduced in steps by bleeding the cell through the vent tap, and at each step the time elapsed and column length of sample were measured. Sample length was determined from the length of the exposed ram, measured with a pair of vernier callipers to 0.05 mm precision. Onset times (i.e. time elapsed between trigger event and received pulse onset) of the received pulse waveforms were extrapolated as  $t_{\text{peak2}} - (1.25 * (t_{\text{peak2}} - t_{\text{peak1}}))$ , i.e. essentially subtracting 1.25 times the "temporal wavelength" (for want of a better description) from the second peak time. The whole procedure was repeated at a number of different temperatures across the range 20°C - 33°C. Sets of extrapolated onset times at fixed temperature were then plotted against sample length [examples shown in Fig 3A.7] to illustrate the discrepancy between onset time and sample length. This discrepancy resulted from the inset transducer mounting, yielding a non-zero time delay with zero sample length. Linear regression analysis of each data set, with sample length as the independent variable, produced near perfect straight line relationships with small positive intercepts in each case corresponding to the time correction applicable at a given temperature [Appendix 5]. These time corrections were plotted against

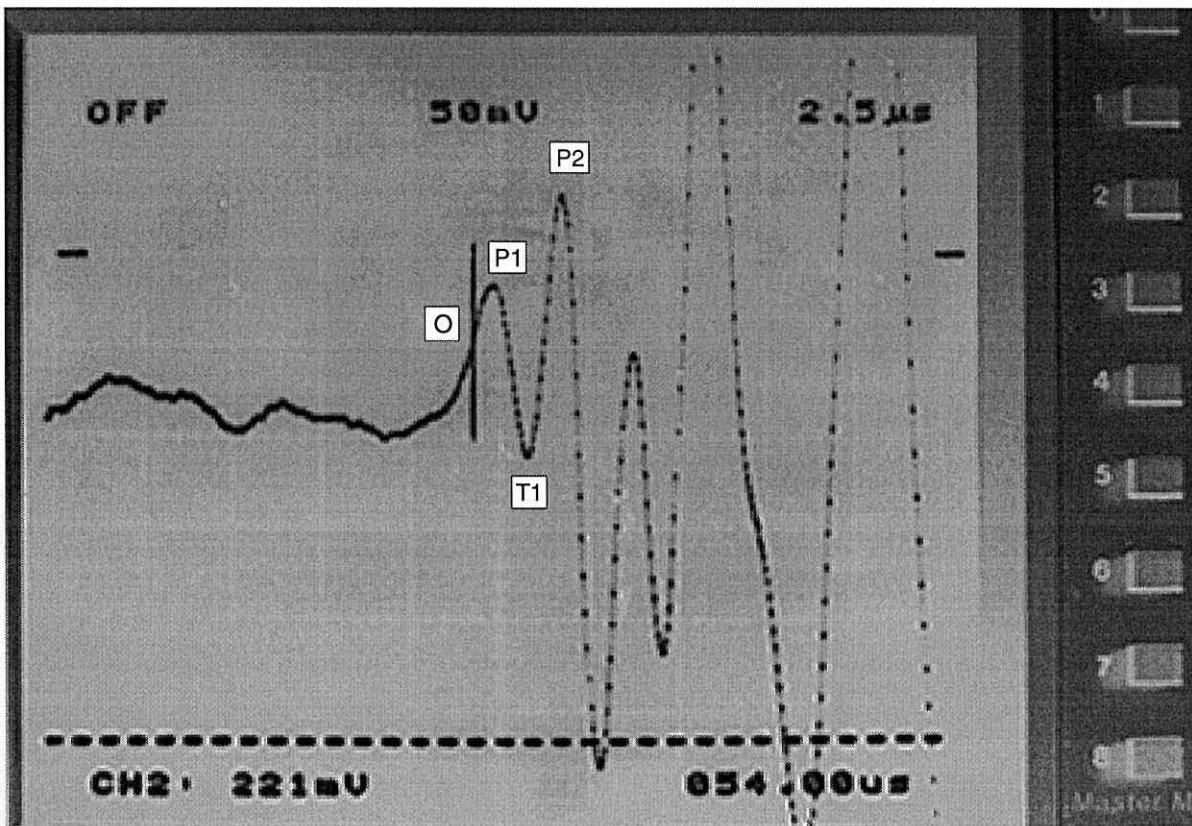


**Figure 3A.6** Negative photographic image of oscilloscope screen showing reception of sound pulse at cylinder base transducer. The onset and subsequent waveform peaks/troughs, denoted O, P1, T1 and P2, of the direct path signal through the oil are distinguishable from the preceding lower frequency interference. The oscilloscope's timebase cursor is visible at the pulse onset, reading 54 microseconds (screen bottom right) from trigger event.

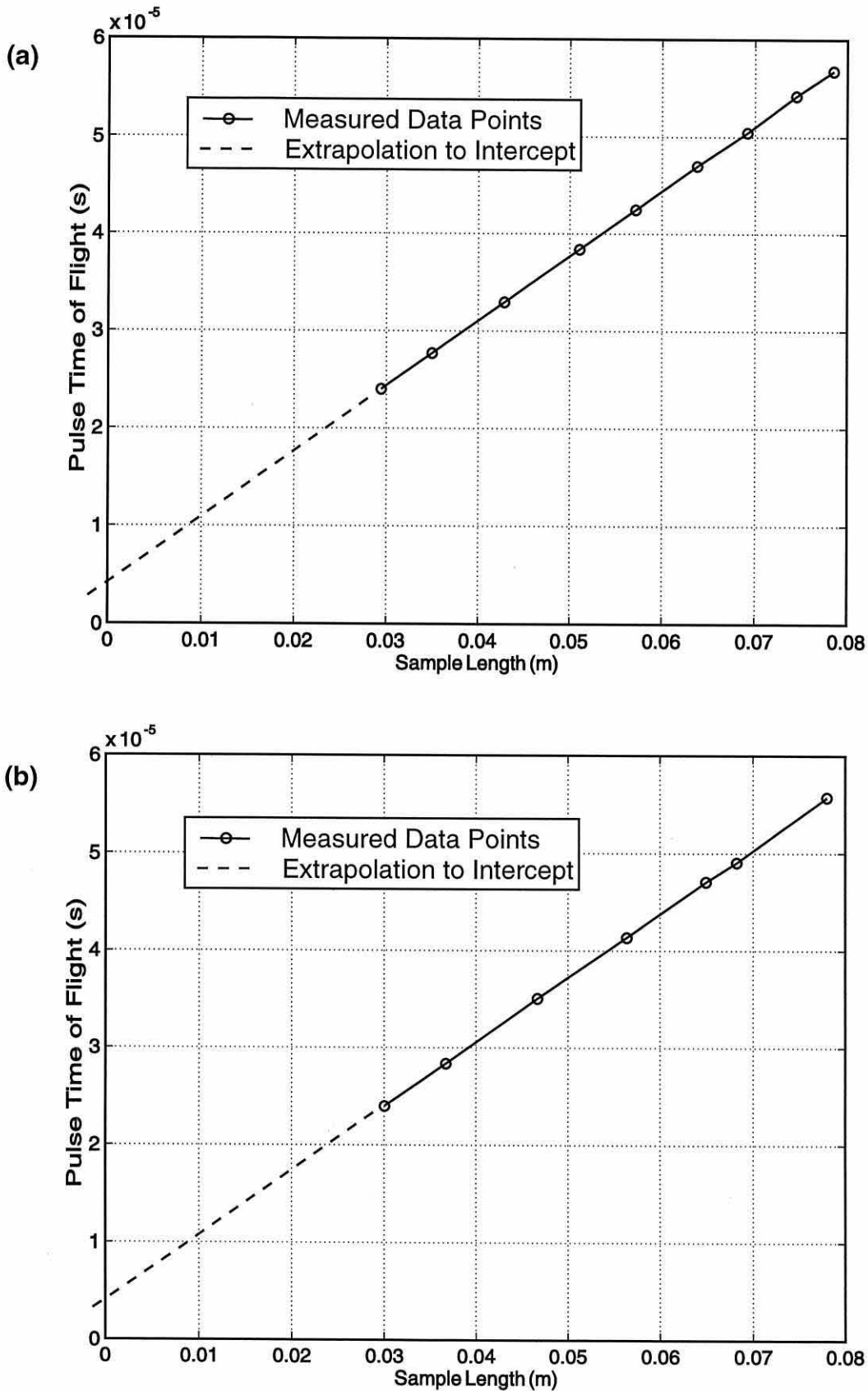


**Figure 3A.7** Two example calibration plots to obtain cell end correction time (a) distilled water at 21.7°C and (b) distilled water at 32.2°C. Temperature has negligible effect on the intercept at zero sample length, which always shows +ve time at zero sample length.

temperature but were too few and widely scattered [Fig 3A.8(a)] to determine a statistically meaningful relationship with temperature; the time correction factor was therefore set at a constant  $4.1\mu\text{s}$  from inspection. The reciprocal of the onset-time/sample-length regression gradient at each temperature was a source of absolute sound velocity in distilled water at that temperature, and values obtained in this way [Fig 3A.8(b)] were in reasonable agreement with tabulated standards (Bark et al, 1964).

#### **3A.1.4 Oil Velocity Measurements**

Prior to filling the pressure cell with spermaceti oil, the cell was heated in the water jacket to a temperature of approximately  $38^{\circ}\text{C}$ . Melted spermaceti oil at the same temperature was then poured into the open bore and the cylinder filled to the brim. The ram and rubber lip seal were then fitted into the bore, with care being taken to exclude as much air as possible, and pushed some 30 mm into the bore with the vent open allowing discharge of excess oil. The vent tap was then closed and the cell turned on its' side, with the vent hole in the cylinder wall uppermost, and shaken carefully to encourage any remaining air into the vent tube. The cell was then set vertical, the vent tap opened and trapped air expelled by slight depression of the ram. This process was repeated until a clear transmission signal showed on the oscilloscope. Initial heating of the cell and spermaceti oil was essential to prevent premature oil solidification and blockage of the vent, which would have prevented the discharge of unwanted air.

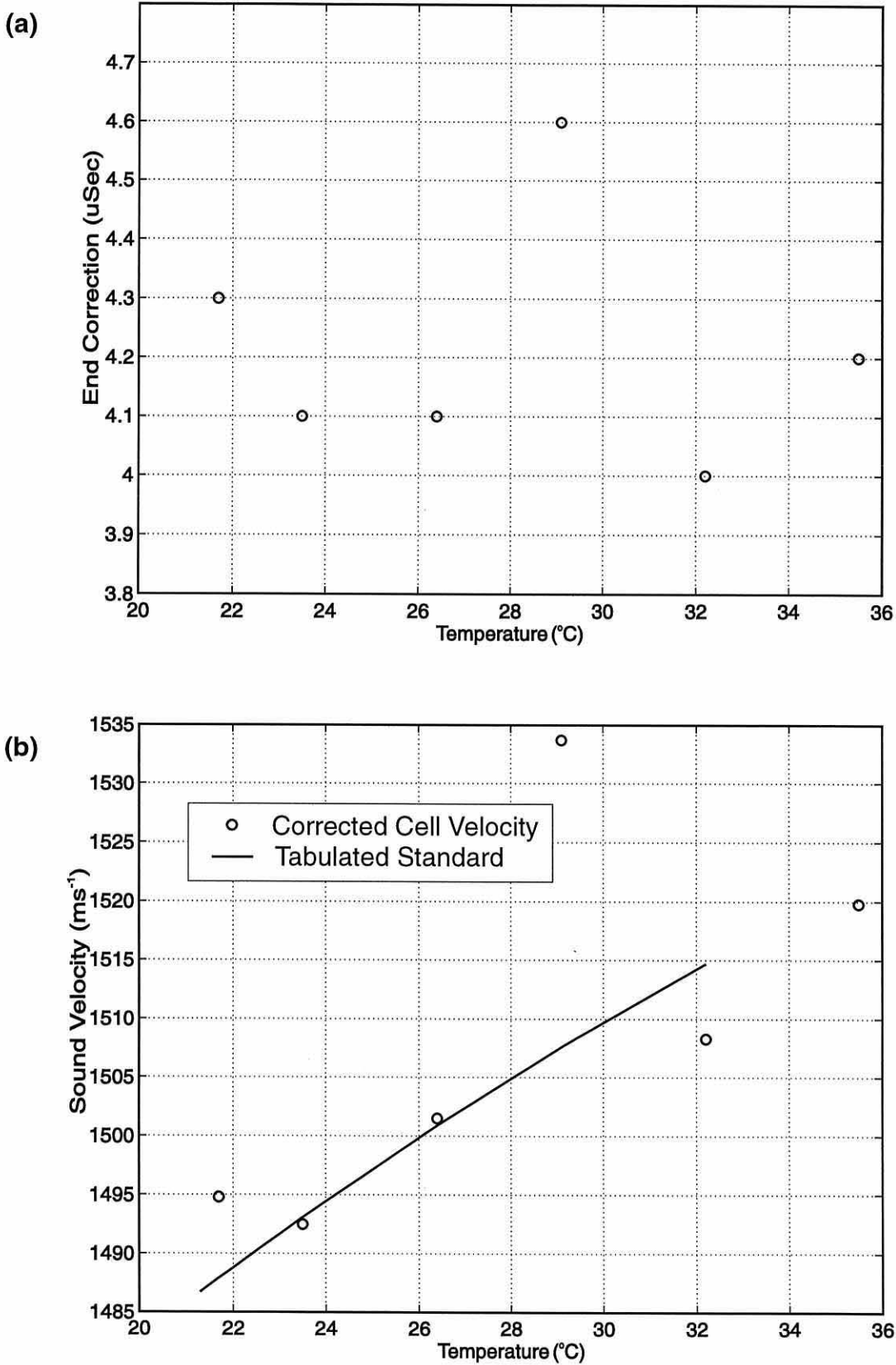


**Figure 3A.8** (a) Cell end correction times vs temperature obtained by cell venting technique with distilled water. (b) Regression distilled water sound velocities from cell plotted with tabulated standard line.

Once the oil sample was successfully enclosed, the pressure cell was immersed in the water jacket and the whole assembly placed in the oedometer frame. The waterbath was set for the maximum experimental temperature and the whole apparatus left to reach thermal equilibrium. Once equilibrium was reached the sound velocity measurements began. The oscilloscopes' timebase cursor was used to measure the time elapsed from trigger event to the same peak-trough features of the received sound pulse waveform as measured during calibration (i.e. onset when visible, first peak, first trough and second peak). Cell pressure was increased in steps of 1.52 MPa (to a maximum of 9.1 MPa above atmospheric pressure) at each temperature by loading individual weights onto the lever arm. For each pressure step, the exposed length of ram was measured using the vernier callipers and used to determine the exact sample length corresponding to the time-of-flight measurement being made. This was necessary as compression of the sample also resulted in slight compression of the rubber seal and therefore a slight decrease of sample length. Compression of the rubber seal did not introduce errors in sample length measurement because the ram was always in contact with the fluid column via the hole in the centre of the rubber seal. Therefore measurement of the exposed ram length was always a known function of the actual fluid column length below the face of the ram, regardless of the state of compression of the rubber seal. Extrapolated onset times [from  $t_{\text{peak2}} - (1.25 * (t_{\text{peak2}} - t_{\text{peak1}}))$ ] were corrected by subtracting the 4.1 $\mu$ s constant in each case, and absolute sound velocity values obtained simply as sample-length divided by corrected-time.

Once a pressure series of measurements was complete the waterbath thermostirrer setting was reduced to the next desired temperature and the apparatus left to reach a new thermal equilibrium, upon reaching which the above steps were repeated. This cascading series of

measurements was continued in decrementing temperature steps of 1 to 2°C, from 30°C right through the spermaceti phase change and down close to room temperature (about 22°C). The entire experiment was run twice using two separate sub-samples of spermaceti oil.

### **3A.2 Results**

Tables 3A.1(a) & (b) detail the sound velocity data. Measured sound velocities in spermaceti oil were in the range 1390 ms<sup>-1</sup> to 1530 ms<sup>-1</sup> depending upon the temperature and pressure variables. In the liquid phase at 30°C sound velocity at atmospheric pressure was about 1410 ms<sup>-1</sup>, some 20 ms<sup>-1</sup> higher than the values obtained by Flewellen and Morris (1978). Figure 3A.9 illustrates variation of sound velocity with temperature in both sub-samples of spermaceti oil at incremental pressures. It is clear from these plots that the relationship between velocity and temperature is non-linear, with sound velocity increasing more rapidly per °C as temperature decreases below the phase change. However, the relationship between velocity and pressure is approximately linear, with a stepwise increase in velocity across the temperature range for each discrete pressure change. It is interesting to note that the velocity-temperature graphs follow approximately smooth curves, with only slight irregularity at the phase change temperature. A sharp increase in velocity as the oil changed from liquid to solid state might have been expected, but this evidently does not occur. The second sample run [Fig 3A.9(b)] was conducted over a slightly wider temperature range than the first sample and produced a smoother set of curves.

HUMBERSIDE SPERMACETI OIL : SUB-SAMPLE A							
Temp (°C)	0 MPa	1.52 MPa	3.03 MPa	4.55 MPa	6.07 MPa	7.58 MPa	9.10 MPa
35.5	1400	1403	1409	1414	1419	1425	1429
33.8	1400	1408	1413	1417	1423	1429	1432
32.2	1404	1410	1416	1423	1428	1432	1439
30.5	1409	1416	1422	1427	1434	1438	1444
29.2	1420	1426	1429	1434	1441	1445	1451
28.0	1425	1427	1434	1440	1445	1452	1460
27.1	1433	1438	1446	1454	1471	1479	1489
25.9	1463	1469	1486	1496	1502	1504	1508
24.2	1498	1501	1505	1519	1522	1533	

**Table 3A.1(a)** Sound velocity ( $\text{ms}^{-1}$ ) at discrete temperatures and pressures in *Physeter spermaceti* oil, sub-sample A.

HUMBERSIDE SPERMACETI OIL : SUB-SAMPLE B							
Temp (°C)	0 MPa	1.52 MPa	3.03 MPa	4.55 MPa	6.07 MPa	7.58 MPa	9.10 MPa
37.1	1387	1391	1396	1403	1409	1417	1421
35.6	1389	1395	1401	1408	1415	1422	1426
33.7	1395	1399	1408	1415	1422	1427	1432
32.5	1397	1406	1414	1421	1425	1430	1434
30.8	1405	1411	1419	1424	1429	1437	1439
29.6	1409	1417	1422	1429	1434	1444	1449
28.2	1421	1434	1449	1451	1451	1455	1456
26.8	1438	1445	1450	1454	1457	1462	1467
24.7	1465	1469	1472	1478	1481	1488	1492
22.7	1486	1497	1505	1510	1526	1524	1528

**Table 3A.1(b)** Sound velocity ( $\text{ms}^{-1}$ ) at discrete temperatures and pressures in *Physeter spermaceti* oil, sub-sample B.

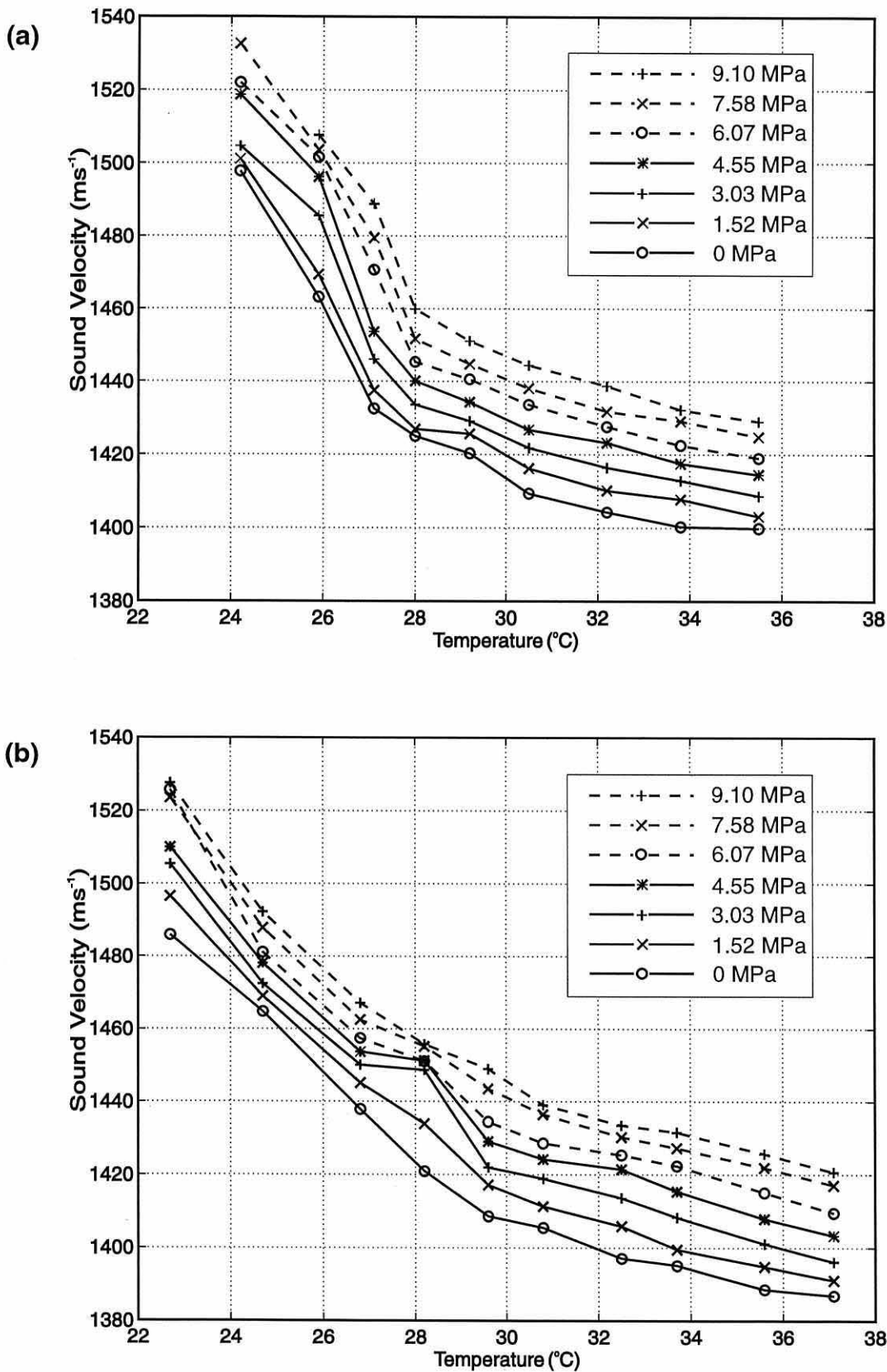


**Figure 3A.9** (a) Sound velocity vs temperature at incremental pressures in sub-sample A of spermaceti oil, (b) Sound velocity vs temperature at incremental pressures in sub-sample B of spermaceti oil

Velocity-temperature data sets at fixed pressure were extracted and used to test fit polynomial relationships with temperature. Nag™ Fortran Library Routines were used to calculate sets of second, third and fourth order polynomial coefficients that best fitted each data set. The predicted curves were then compared with measurements to examine their behaviour. Using this approach it was judged that second order predictive equations best described the data overall. Having established that a second order polynomial in temperature was most appropriate, multi-variant regression analysis was performed on the complete data sets, using MINITAB statistical package. In each case the regression equation was highly significant [see Appendix 5], and best fit (least-squares) regression equations obtained for each of the two data sets were:

$$C_{\text{spermaceti}} = 2710 + 4.2P - 78.4T + 1.17T^2 \quad (3.1)$$

$$(\pm 64) \quad (\pm 0.274) \quad (\pm 4.33) \quad (\pm 0.073)$$

$$R^2 = 96.5\%$$

$$C_{\text{spermaceti}} = 2093 + 3.88P - 38.6T + 0.528T^2 \quad (3.2)$$

$$(\pm 23) \quad (\pm 0.159) \quad (\pm 1.53) \quad (\pm 0.025)$$

$$R^2 = 98.7\%$$

where numbers in brackets denote standard deviations for each coefficient.

Plotting the relationship in equation (3.1) alongside the measured data showed the best fit curve to be an unrealistic predictor at the low and high temperature ends, with a strong inflexion of the curve above 33°C. Equation (3.2) showed a much more realistic trend, with sound velocity “levelling out” at the higher temperatures.

Given the discrepancy between the two sets of curves, and the desire to formulate a generalised predictive equation, both data sets were pooled and multi-variant regression analysis performed on the combined data. The resulting best fit regression equation was:

$$c_{\text{spermaceti}} = 2196 + 3.95P - 44.7T + 0.621T^2 \quad (3.3)$$

$$(\pm 41) \quad (\pm 0.246) \quad (\pm 2.75) \quad (\pm 0.046)$$

$$R^2 = 93.9\%$$

$$22 < T < 38$$

$$0 < P < 9.1$$

The output from equation (3.3) follows the smooth trend of equation (3.2) with varying temperature and curves fall between the two data sets. Equation (3.3) was considered to be the best working equation for the prediction of sound velocity in spermaceti oil with respect to temperature and pressure variables, between the temperature limits 22 - 38°C, and the pressure limits 0 - 9.1 MPa above atmospheric.

**SECTION 3B - 1996 Measurements : Sound Velocity in Castor Oil, Spermaceti Oil from *Kogia simus* and Spermaceti Oil from *Physeter macrocephalus***

**3B.1 Introduction & Methods**

Sound velocity in spermaceti oil was further investigated during 1996 using the same pressure cell apparatus and experimental setup as in 1994 (section 3A of this chapter). For the new measurements the original apparatus was brought out of storage and set up as previously described. Initially it was found that the cell transducers would not function effectively, producing weak and largely indiscernible signals though distilled water - which given past experience should have provided clear and unambiguous signals. Eventually the problem was traced to degraded electrical contacts and transducer earthing. Both transducers were removed from their respective recesses, cleaned, re-earthed with silver paint and repotted in position. A further improvement was made regarding the passive transducer in the cylinder base. Rather than sealing the chamber with silicone rubber, which inevitably restricted the transducers' ability to oscillate freely, the large recess in which it was housed was converted into a water-tight air chamber. This was achieved by closing off the base recess with a large screw fitting brass plug with a semi-inset rubber o-ring seal [Fig 3B.1]. It was then merely necessary to seal the wire exit hole in the recess wall with epoxy resin-hardener mix to make the transducer recess water-tight during water jacket immersion.

Clear signals through liquid samples were obtained with the apparatus thereafter. The

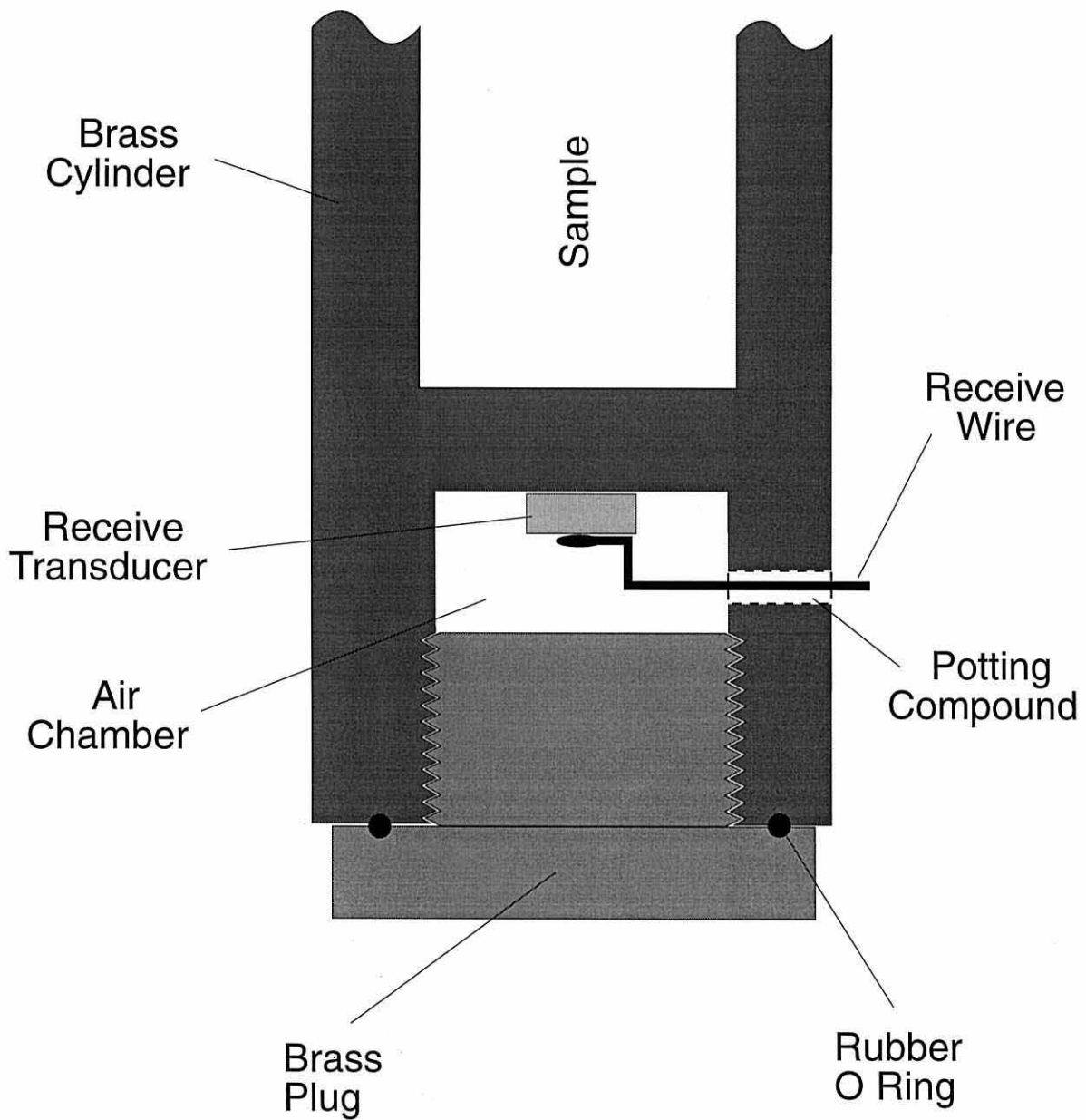


**Figure 3B.1** Schematic of passive transducer mounting and connection in the base of the velocimeter cylinder (for 1996 measurements)

rubber lip seal on the face of the ram was replaced, and a different water bath (Grant LTD6) was used to supply the cell assembly water jacket for temperature regulation. The Grant LTD6 water bath had both heating and cooling coils, allowing sound velocity measurements in samples across a wider temperature range.

As the cell hardware had been considerably reworked it was decided to recalibrate the apparatus with a distilled water medium, even though the transducers were reset in approximately their original positions. The new calibration did not use the venting method of section 3A which, with hindsight, was considered perhaps not the best method for cell calibration. Distilled water calibrations were made by directly measuring time elapsed from trigger event to reception of direct path sound pulses through known sample column lengths of distilled water - i.e. the same protocol as actual spermaceti measurements in section 3A of this chapter. Sample length measurements divided by raw time-of-flight measurements gave uncorrected sound velocities in distilled water. Similar to section 3A, time elapsed from trigger event was measured to features of the received sound pulse front end, with these features being the onset (when visible) followed by first, second and third peaks [Fig 3B.2] - troughs were not measured. Sound pulse onset times were again extrapolated as  $t_{\text{peak2}} - (1.25 * (t_{\text{peak2}} - t_{\text{peak1}}))$ , onsets were always extrapolated for consistency regardless of whether they had been measured or not. Two sample-length/time-of-flight measurements were made at ambient atmospheric pressure at each temperature step, the first made when the sample reached thermal equilibrium, the second a few minutes later after pressurising and releasing the sample - the idea being to cause mechanical disturbance to an otherwise stationary apparatus and obtain a realistic spread of measurements. These measurements were made in distilled water at temperatures between 5°C and 33°C at atmospheric pressure,

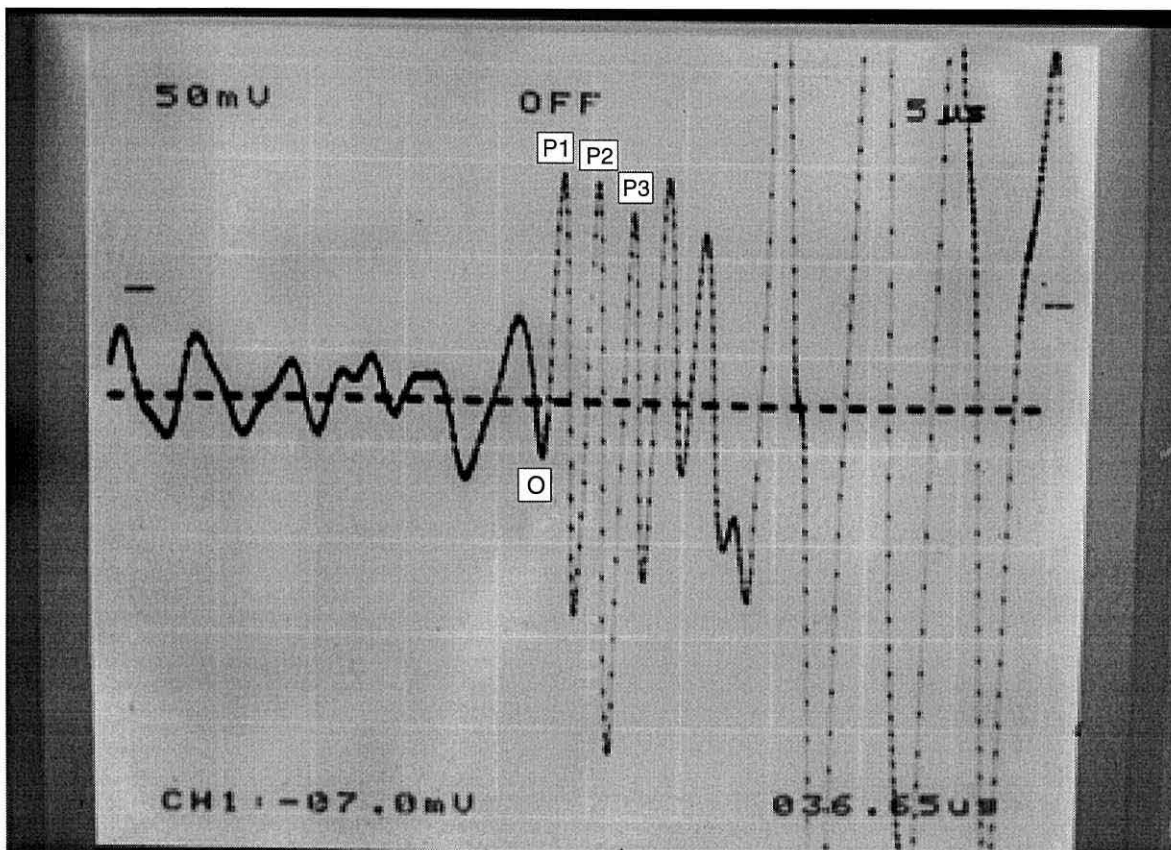


**Figure 3B.2** Negative photographic image of oscilloscope screen showing reception of sound pulse at cylinder base transducer. The onset and subsequent waveform peaks, denoted O, P1, P2 and P3, of the direct path signal through the oil are clearly distinguishable from the preceding lower frequency interference.

resulting in uncorrected sound velocity values which could be referenced to tabulated standards and a correction generated from the discrepancy.

Uncorrected sound velocities in distilled water are plotted in Figure 3B.3(a), alongside tabulated values for sound velocity in distilled water from Bark et al (1964). It is clear that both curves are following almost identical tracks, but with an offset due to mismatch between true liquid column length and the actual separation between the transducers. The tabulated values of Bark et al (1964) are stated to have a precision of  $\pm 0.5 \text{ ms}^{-1}$ , somewhat better than that theoretically attainable with the pressure cell apparatus ( $\pm 4 \text{ ms}^{-1}$ ). Although sound velocity in distilled water is not strictly a linear function with respect to temperature across the range measured, it is sufficiently close that linear regression analysis of both measured and tabulated data sets produced near perfect fits [see Appendix 6]. The respective regression equations for the two data sets are:

$$c_{\text{tabulated}} = 3.123T + 1417.7 \quad (3.4)$$

$$c_{\text{measured}} = 2.749T + 1289.1 \quad (3.5)$$

The difference in intercept approximates to a correction constant (in  $\text{ms}^{-1}$ ) that must be added to the raw velocity data to give a true reading. The difference in gradient amounts to a temperature correction (in  $\text{ms}^{-1} \text{ per } ^\circ\text{C}$ ) that must also be added to the raw data. This latter correction was not evident from the calibrations of section 3A, but the wider range of temperatures and greater number of sample values used here show it to exist. This temperature effect is likely due to thermal expansion of the cell and its components, thereby

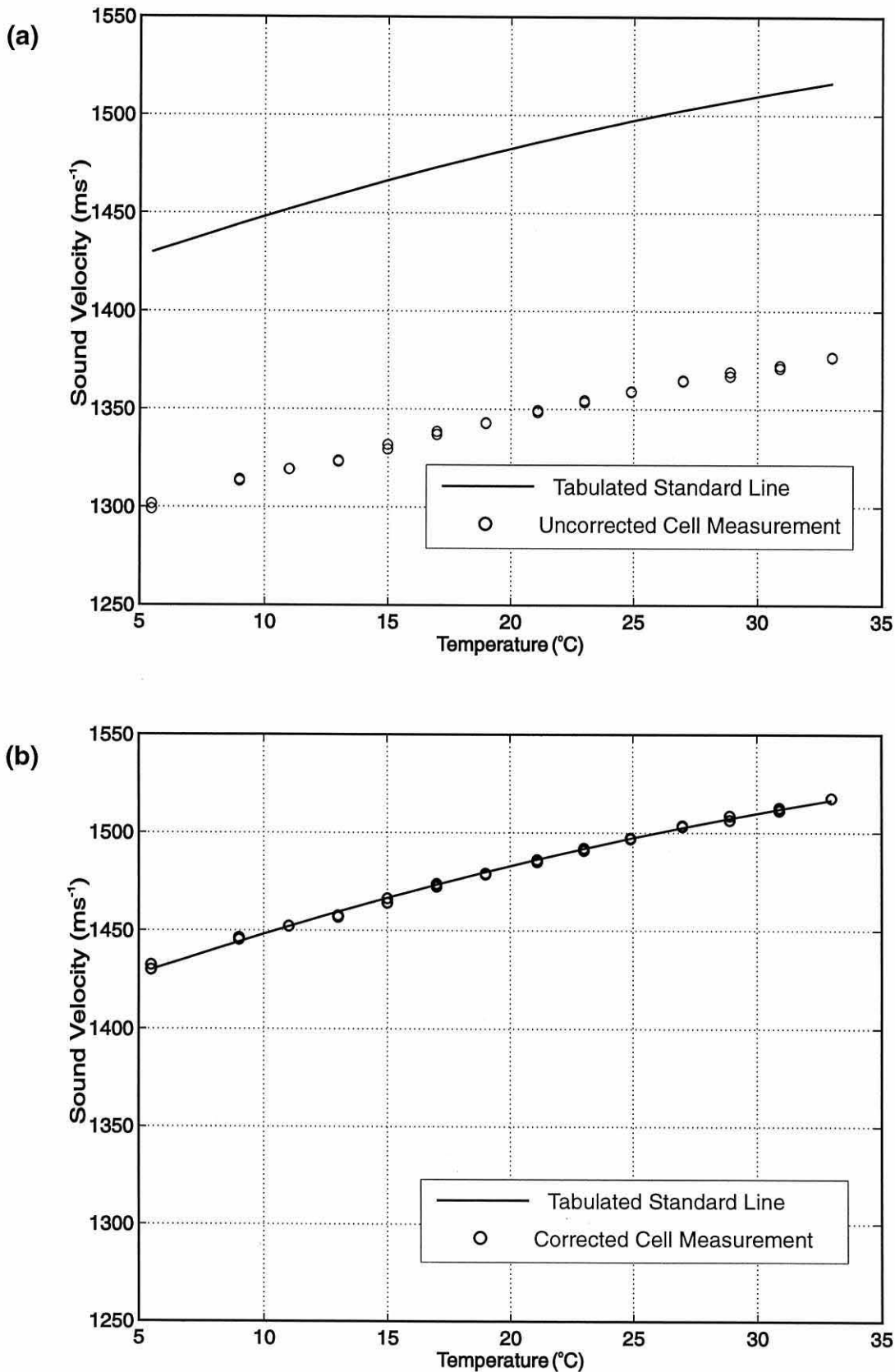


**Figure 3B.3** Calibration curves for velocimeter cell showing (a) uncorrected sound velocity measurements in distilled water from the apparatus compared to true sound velocity standard line plotted from tabulated values and (b) comparison of corrected cell values with the true standard line.

altering the sound path length to the passive transducer. Subtracting the regression equations (3.4) and (3.5) gives coefficients needed to formulate the cell correction equation:

$$c_{\text{corrected}} = c_{\text{measured}} + 128.6 + 0.374T \quad (3.6)$$

The effect of applying equation (3.6) to the uncorrected distilled water sound velocities is illustrated in Figure 3B.3(b). It is clear that the measured points now lie almost perfectly along the tabulated line. Uncorrected sound velocity measurements were made in castor oil and spermaceti oil by the same procedure as in distilled water, and the data subsequently corrected to absolute sound velocity using equation (3.6). In both castor oil and spermaceti oil a range of measurements were made between 0 - 9.1 MPa pressure and 5°C - 40°C temperature. Time elapsed between trigger event and reception of the first three peaks in the waveform front-end was measured as with distilled water. The “temporal wavelength” was evaluated as  $0.5 * ((t_{\text{peak3}} - t_{\text{peak2}}) + (t_{\text{peak2}} - t_{\text{peak1}}))$  and the values at fixed temperature averaged to give a mean “temporal wavelength” at the given temperature. Received sound pulse onset times were then extrapolated by subtraction of this mean from each individual  $t_{\text{peak2}}$  value - onset times were always extrapolated for consistency. This procedure differed slightly from that of section 3A where individual  $1.25 * (t_{\text{peak2}} - t_{\text{peak1}})$  values were used in isolation for subtraction from the respective  $t_{\text{peak2}}$  times.

## **3B.2 Results**

### **3B.2.1 Castor Oil**

Table 3B.1 details the castor oil sound velocity data, and Figure 3B.4(a) illustrates sound velocity in castor oil vs temperature at incremental pressures. It is clear from Figure 3B.4(a) that sound velocity exhibits an approximately linear relationship with both temperature and pressure. From inspection, sound velocity at atmospheric pressure in the oil at 20°C is about 1510 ms<sup>-1</sup>, and the velocity/temperature gradient is approximately -1.6 ms<sup>-1</sup>/°C. These values are rather different to those presented by Kaye and Laby (1966), where sound velocity is given as 1500 ms<sup>-1</sup> in castor oil at 20°C with a velocity/temperature gradient of -4.1 ms<sup>-1</sup>/°C. However, these values too are at odds with more recent measures of sound velocity in castor oil which put the temperature gradient at -2.5 ms<sup>-1</sup>/°C (Capps, 1989), -3.1 ms<sup>-1</sup>/°C (Timme, 1972), -3.6 ms<sup>-1</sup>/°C (Selfridge, 1985) and -4.3 ms<sup>-1</sup>/°C (del Grosso, in Timme, 1972). Indeed Timme (1972) and Capps (1989) present equations for predicting sound velocity in castor oil that contain squared terms in both temperature and pressure. It seems that castor oil itself is the variable factor, rather than there being any serious discrepancy in experimental methods to measure it. Castor oil varies in composition, and hence to some extent physical characteristics, between different manufacturers and with age. The oil used in the spermaceti cell was manufactured by BHP Chemical Limited, Poole, England (product number 33220). In addition it was approximately 10 years old at the time of testing and would likely have undergone some chemical degradation.

CASTOR OIL							
Temp (°C)	0 MPa	1.52 MPa	3.03 MPa	4.55 MPa	6.07 MPa	7.58 MPa	9.10 MPa
39.8	1487	1495	1497	1499	1506	1510	1515
37.4	1488	1495	1470	1499	1508	1513	1517
34.8	1490	1495	1500	1506	1510	1514	1519
32.8	1495	1498	1500	1504	1512	1516	1519
31.1	1497	1500	1500	1508	1513	1517	1519
28.8	1502	1505	1508	1512	1517	1521	1527
26.1	1500	1505	1509	1513	1519	1522	1528
23.9	1508	1510	1513	1519	1523	1526	1530
21.2	1509	1513	1516	1522	1526	1532	1537
19.0	1514	1520	1527	1529	1535	1538	1542
16.5	1515	1525	1528	1534	1536	1537	1544
14.0	1524	1529	1531	1537	1539	1542	1547
11.5	1531	1531	1536	1540	1544	1547	1553
8.9	1538	1540	1545	1549	1551	1555	1559
6.3	1542	1544	1548	1551	1556	1560	1564

**Table 3B.1** Sound velocity ( $\text{ms}^{-1}$ ) at discrete temperatures and pressures in castor oil.

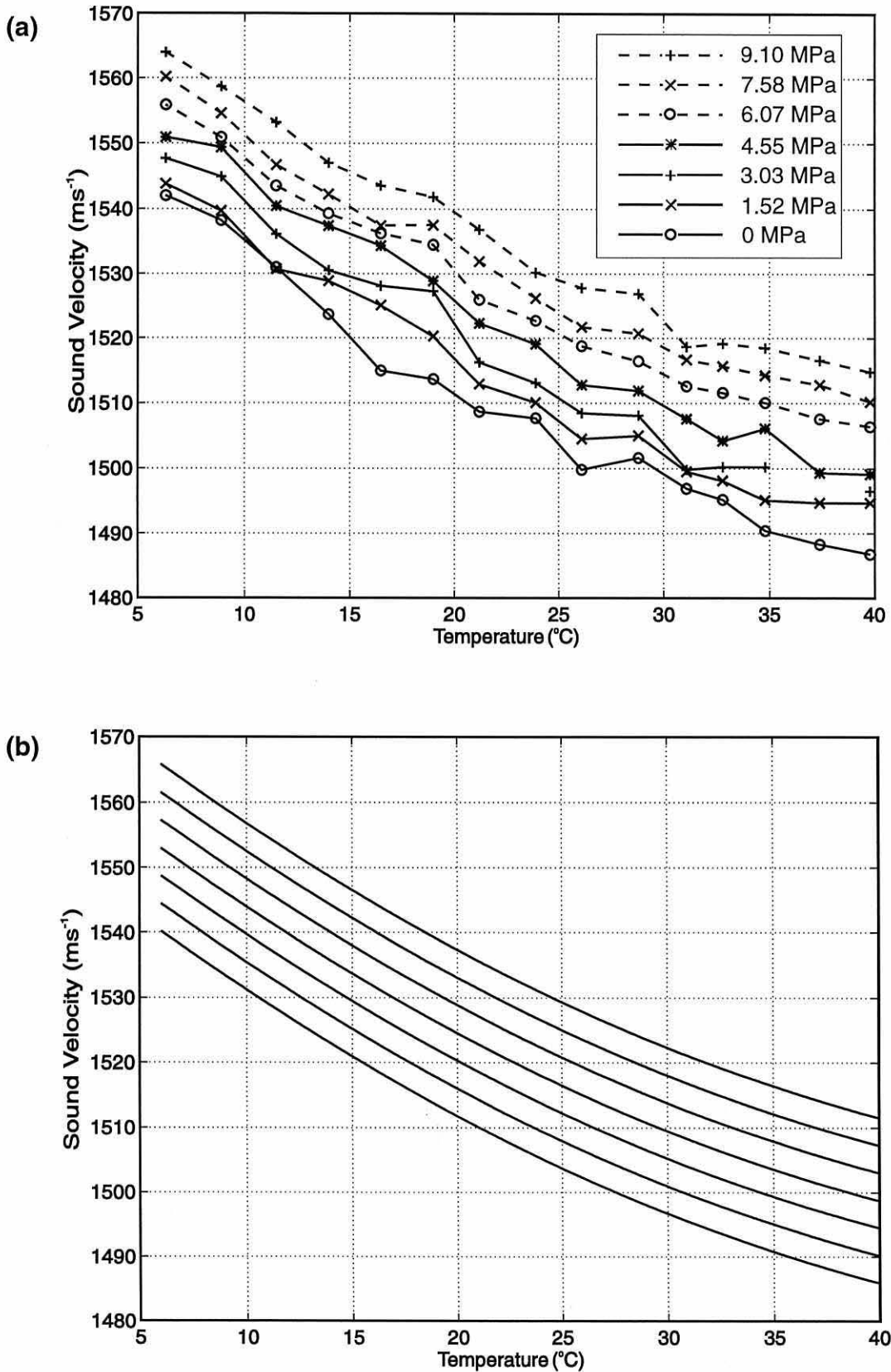


**Figure 3B.4** (a) Sound velocity vs temperature at incremental pressures in BHP castor oil and (b) best fit curves from multi-variant regression analysis of the data, bottom curve is at 0 MPa pressure and subsequent curves are at increasing steps of 1.52 MPa.

It is for the above reasons that the castor oil sound velocity data in this chapter are not comparable to other data. It can at least be said, however, that measured sound velocities are close to that found in other castor oils, and the velocity/temperature gradient is negative and approximately linear. To test the linearity assumption, multi-variant regression analysis was performed on the castor oil data, first with P & T only, then with P, T and T<sup>2</sup>. Both analyses produced very good least squares fits to the data [see Appendix 6], although the T<sup>2</sup> regression actually produced the better fit of the two analyses. The two equations obtained were:

$$c_{\text{castor}} = 1546 + 2.82P - 1.6T \quad (3.7)$$

$$(\pm 1) \quad (\pm 0.125) \quad (\pm 0.037)$$

$$R^2 = 95.8\%$$

$$6 < T < 40$$

$$0 < P < 9.1$$

$$c_{\text{castor}} = 1555 + 2.82P - 2.6T - 0.0218T^2 \quad (3.8)$$

$$(\pm 2) \quad (\pm 0.107) \quad (\pm 0.163) \quad (\pm 0.003)$$

$$R^2 = 96.9\%$$

$$6 < T < 40$$

$$0 < P < 9.1$$

From equation (3.7) it can be seen that the velocity/temperature gradient is exactly -1.6 ms<sup>-1</sup>/°C. However, as equation (3.8) fits the data slightly better it is the one that should more

appropriately apply. Figure 3B.4(b) shows sound velocity vs temperature at incremental pressures in the BHP castor oil, derived from the output of equation (3.8).

### **3B.2.2 *Kogia simus* Spermaceti Oil**

Samples of spermaceti oil taken from specific locations in the melons of two specimens of *Kogia simus* (Dwarf Sperm Whale) were supplied by Professor Malcolm Clarke. The animals, designated as KS16 and KS9525B, had stranded on the Florida Coast (USA) and were deep frozen post mortem. The largest volume oil samples were obtained from KS16, one sample was taken from the inner core of the melon and one sample was taken from the periphery of the melon [Fig 3B.5]. Two smaller samples were taken from the melon core of KS9525B, one from the inner core and one from the outer core (such definitions as inner and outer core are subjective and do not represent definite physical boundaries). The two core samples from KS9525B were mixed together to provide the required volume of oil for sound velocity measurement. The individual core and peripheral samples from KS16 were of sufficient volume individually. Sound velocity was measured in the three discrete oil samples - namely KS16 core, KS16 peripheral and KS9525B composite core. Sound velocity was measured through the samples at discrete temperatures across the range 7 - 38 °C, and at discrete pressures across the range 0 - 9.1 MPa above ambient atmospheric pressure for each temperature. The measurement protocol was identical to that used in the castor oil experiment.

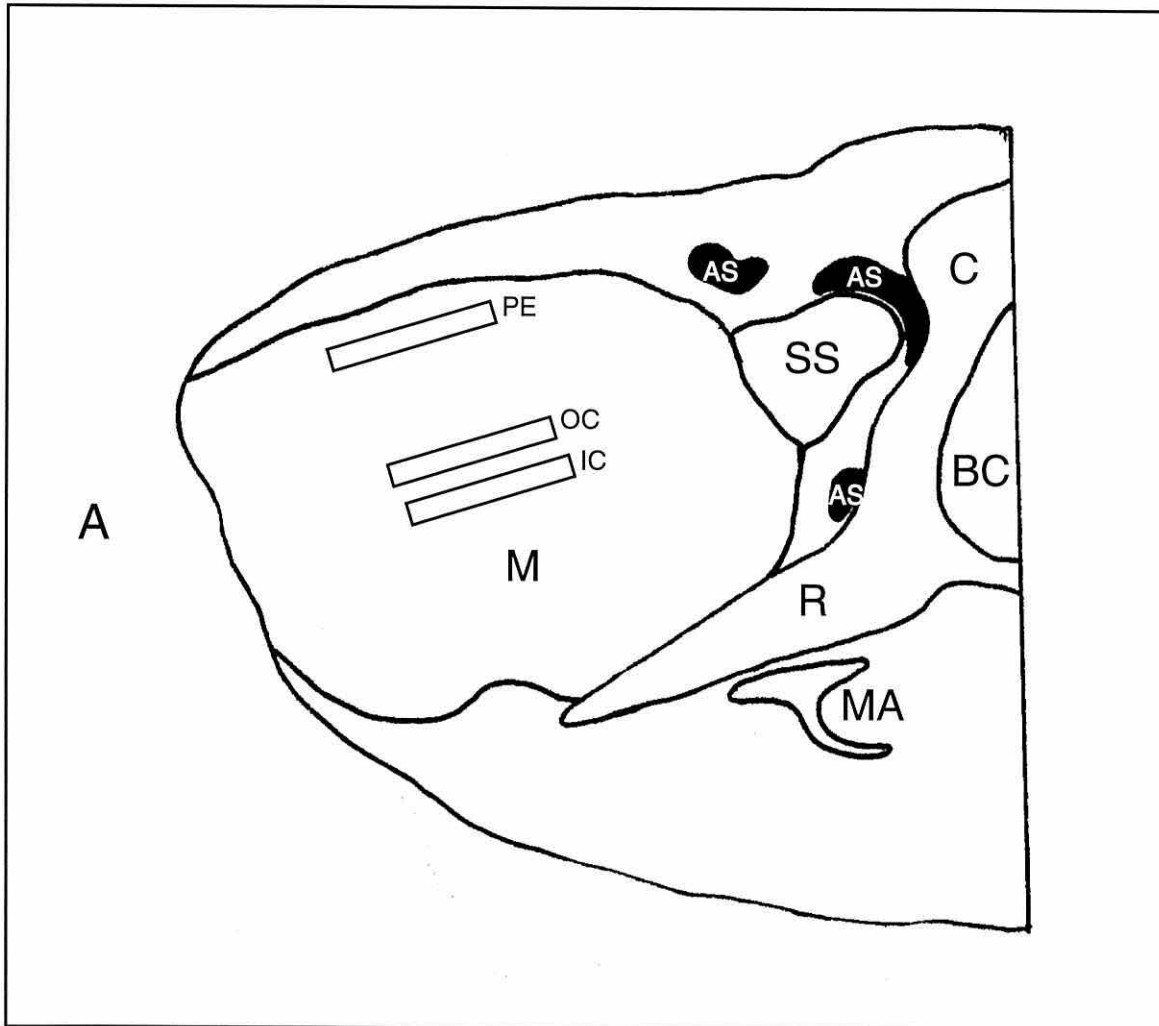


**Figure 3B.5** Schematic of sagittal section through the head of *Kogia*, drawn after Cranford et al (1996). M, melon; SS spermaceti sac; C, cranium; BC, braincase; MA mandible; AS airsacs; R, rostrum; A, anterior end of head. Oil sampling locations equivalent to those from which Clarke extracted melon spermaceti are superimposed: IC, inner core; OC outer core; PE peripheral.

Tables 3B.2(a) - (c) detail the sound velocity data obtained from the three samples - KS16 core, KS16 peripheral and KS9525B core respectively - and Figures 3B.6(a) - (c) illustrate the trends in the data. It is clear that in all cases an inverse non-linear relationship exists between temperature and sound velocity, similar to the case of *Physeter* spermaceti oil demonstrated in section 3A of this chapter. In general sound velocity in all samples increases linearly with increasing pressure, but decreases non linearly with increasing temperature, across the ranges measured. In the case of peripheral spermaceti [Fig 3B.6(b)] velocity-temperature curves essentially “level out” above 22°C, in fact it is arguable that the curves show a slight increase in sound velocity towards the higher temperatures.

An interesting comparison can be made by superimposing the velocity-temperature curves from different samples. Figure 3B.7(a) shows the superimposition of velocity-temperature curves of all three samples at a uniform pressure of 1.52 MPa. The peripheral oil has the shallowest gradient, with velocities ranging between approximately 1490 ms<sup>-1</sup> and 1435 ms<sup>-1</sup> (between 7°C and 38°C). The core samples have the steepest gradients with velocities ranging between approximately 1550 ms<sup>-1</sup> and 1410 ms<sup>-1</sup> (between 17°C and 38°C) for KS16 core oil, and between approximately 1645 ms<sup>-1</sup> and 1400 ms<sup>-1</sup> (between 9°C and 38°C) for KS9525B composite core oil. It is also notable that both of the core velocity curves cross the peripheral curve between 25°C and 27°C. At temperatures below 25°C - 27°C sound velocity is faster in core spermaceti oil than in peripheral spermaceti oil. At temperatures above 25°C - 27°C sound velocity in peripheral spermaceti oil is faster than that in core spermaceti. At the body temperature of *Kogia simus* (38°C - Clarke, personal communication) this difference appears to be in the range 20 - 35 ms<sup>-1</sup> (1.4 to 2.4 % of the highest velocity). Figure 3B.7(b) shows a similar set of curves for all three samples, but this

KS16 MELON CORE SPERMACETI							
Temp (°C)	0 MPa	1.52 MPa	3.03 MPa	4.55 MPa	6.07 MPa	7.58 MPa	9.10 MPa
37.9	1411	1415	1418	1423	1426	1433	1433
36.4	1404	1409	1417	1419	1424	1428	1432
34.4	1413	1419	1425	1428	1437	1447	1436
30.9	1418	1424	1430	1442	1437	1441	1445
28.9	1420	1426	1432	1441	1433	1440	1446
26.9	1427	1432	1437	1447	1443	1447	1449
25.0	1461	1465	1461	1470	1474	1480	
23.2	1484	1491	1488	1495	1495	1498	1503
21.1		1496	1495	1508	1510	1517	1519
18.9		1516	1516	1523	1529	1536	1537
16.9		1547	1550	1554	1558	1563	1564

**Table 3B.2(a)** Sound velocity ( $\text{ms}^{-1}$ ) at discrete temperatures and pressures in *Kogia* KS16 melon core spermaceti oil.

KS16 MELON PERIPHERAL SPERMACETI							
Temp (°C)	0 MPa	1.52 MPa	3.03 MPa	4.55 MPa	6.07 MPa	7.58 MPa	9.10 MPa
37.9	1429	1433	1439	1447	1452	1456	1460
35.6		1435	1440	1444	1451	1458	1461
33.0	1427	1437	1442	1444	1450	1457	1459
30.9	1429	1436	1441	1445	1453	1457	1459
28.9	1426	1434	1440	1444	1450		
26.9	1423	1435	1439	1442	1448	1451	1454
24.9	1428	1436	1438	1444	1446	1453	1453
22.9	1429	1436	1439	1445	1450	1456	1457
20.9	1431	1436	1442	1446	1453	1452	1456
19.1	1447	1450	1455	1459	1464	1467	1470
17.0	1447	1452	1460	1463	1465	1468	1476
15.0	1456	1460	1468	1473	1477	1480	1483
13.0	1463	1471	1476	1479	1483	1487	1490
10.9	1465	1477	1481	1487	1489	1491	1496
9.0		1482	1489	1494	1495	1501	1503
6.9		1491	1495	1498	1501	1503	1507

**Table 3B.2(b)** Sound velocity ( $\text{ms}^{-1}$ ) at discrete temperatures and pressures in *Kogia* KS16 melon peripheral spermaceti oil.

KS9525B COMPOSITE MELON CORE SPERMACETI							
Temp (°C)	0 MPa	1.52 MPa	3.03 MPa	4.55 MPa	6.07 MPa	7.58 MPa	9.10 MPa
38.3	1395	1399	1405	1410	1415	1419	1424
35.2	1401	1406	1411	1416	1420	1425	1429
32.2	1408	1412	1418	1423	1427	1430	1435
29.8	1413	1417	1423	1427	1431	1436	1439
27.2	1416	1420	1425	1430	1434	1438	1443
24.8	1428	1432	1436	1440	1445	1449	1453
22.2	1450	1448	1452	1456	1460	1464	1469
20.0	1467		1476	1483	1488	1492	1498
17.9	1494	1492	1496	1497	1501	1505	1509
15.1	1515	1518	1518	1519	1520	1523	1525
11.8		1573	1576	1578	1579	1579	1580
9.2	1646	1642	1646	1653	1660	1668	1669

**Table 3B.2(c)** Sound velocity ( $\text{ms}^{-1}$ ) at discrete temperatures and pressures in *Kogia* KS9525B melon composite core spermaceti oil.

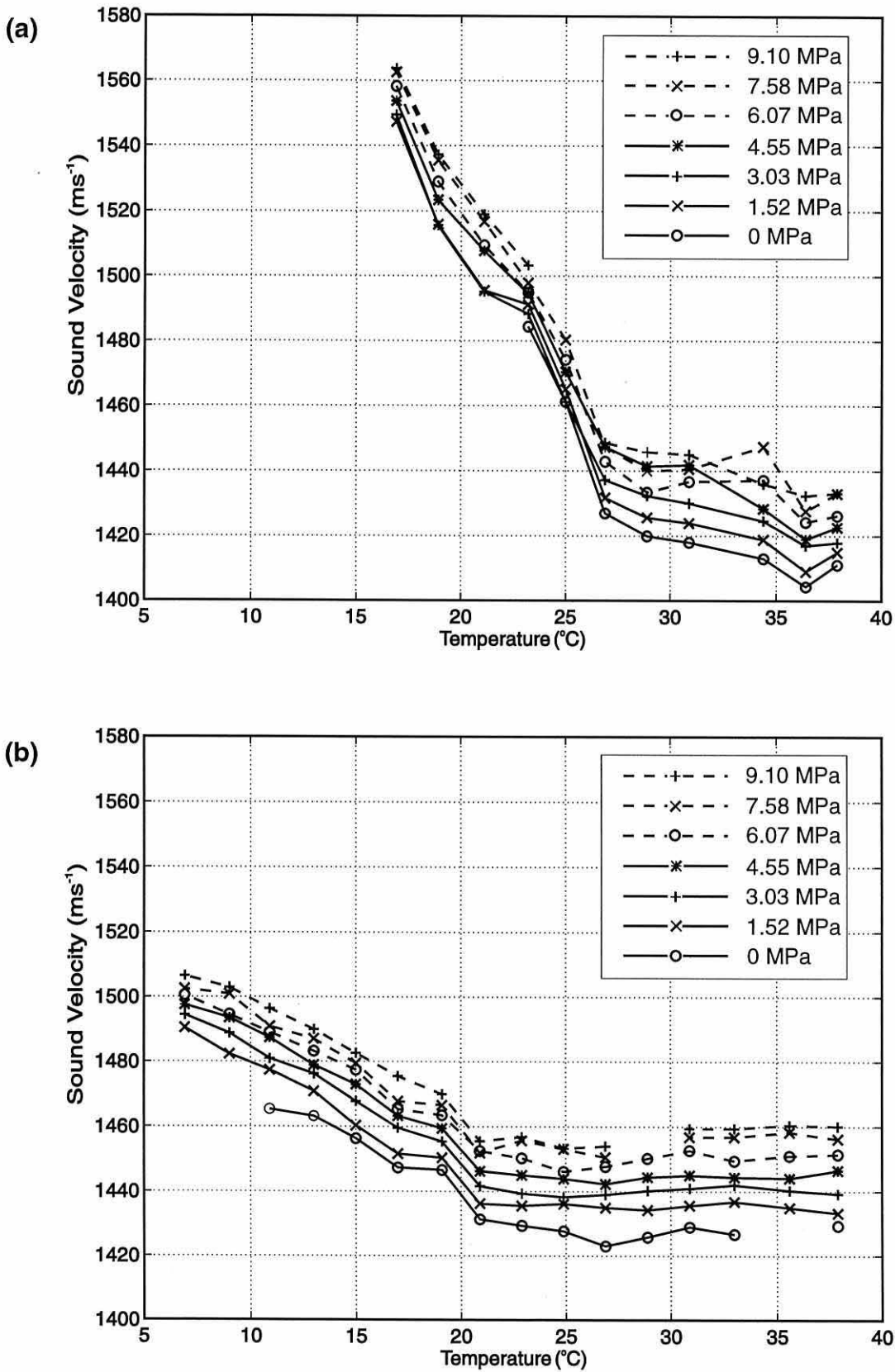
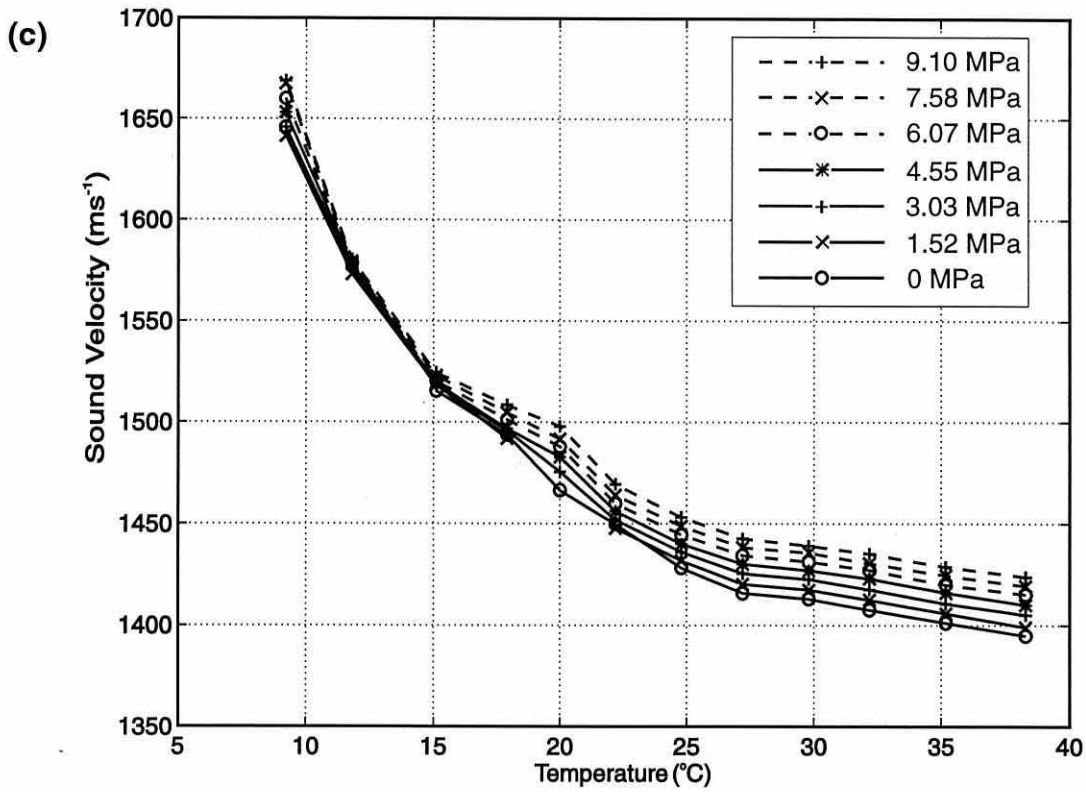
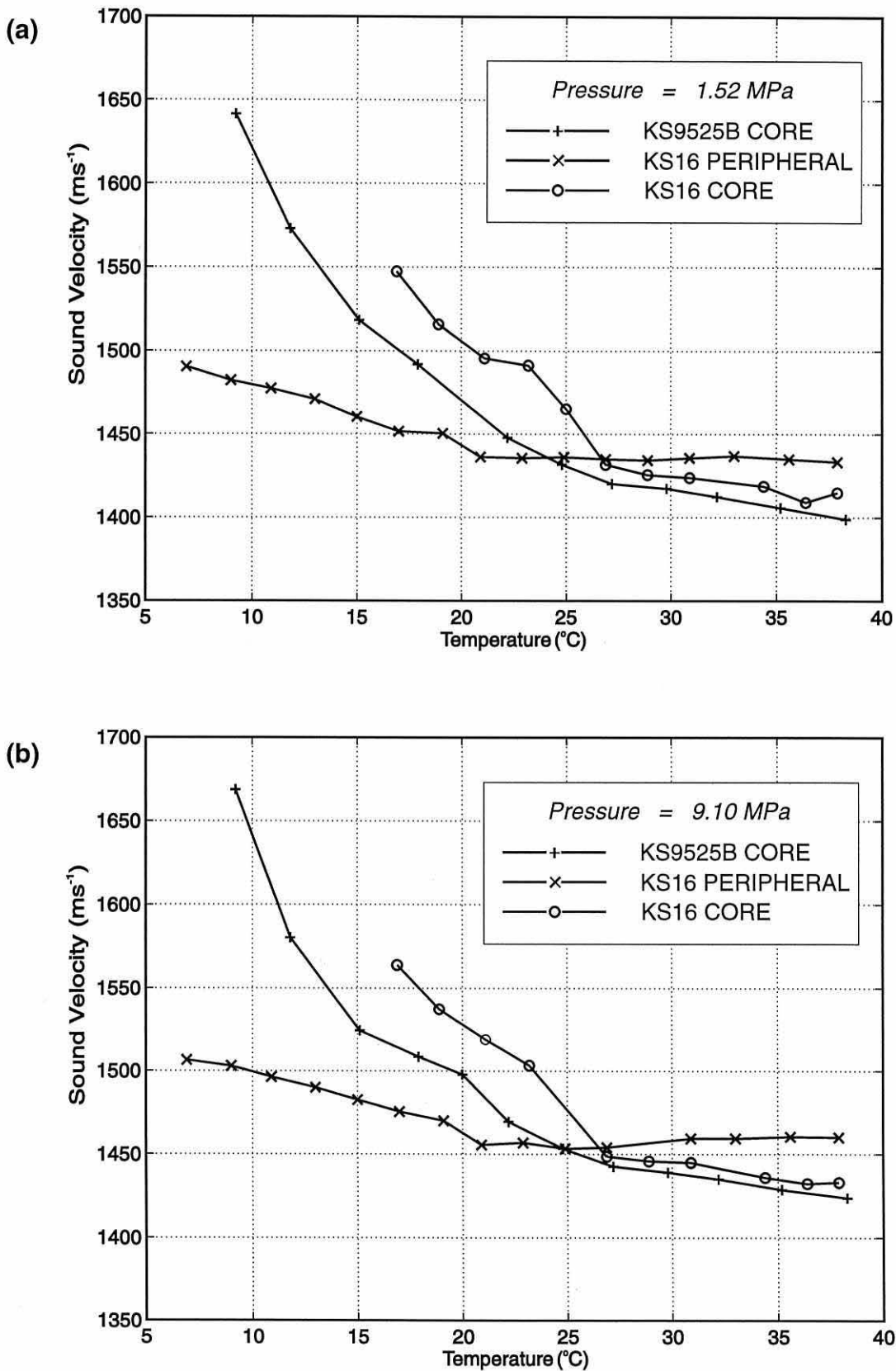


Figure 3B.6 Sound velocity vs temperature at incremental pressures in (a) KS16 Core Spermaceti Oil, and (b) KS16 Peripheral Spermaceti Oil



**Figure 3B.6** Sound velocity vs temperature at incremental pressures in (c) KS9525B Composite Core Spermaceti Oil



**Figure 3B.7** Superimposition of temperature-velocity curves for KS16 Core, KS16 Peripheral and KS9525B Composite Core Spermaceti Oil at (a) 1.52 MPa and (b) 9.1 MPa.

time at the elevated pressure of 9.1 MPa. As expected the trends and interactions are the same, with all curves simply displaced upwards by some 20 - 25 ms<sup>-1</sup>.

Multi-variant regression analysis was applied to the data sets using the parameters P, T and T<sup>2</sup>. Equation (3.9) is a polynomial generated from the combined data sets of KS16 core and KS9525B composite core. Equation (3.10) is a polynomial generated from the data set of KS16 peripheral.

$$C_{\text{core}} = 1796 + 2.7P - 21.7T + 0.302T^2 \quad (3.9)$$

$$(\pm 11) \quad (\pm 0.427) \quad (\pm 0.925) \quad (\pm 0.018)$$

$$R^2 = 93.4\%$$

$$9 < T < 38$$

$$0 < P < 9.1$$

$$C_{\text{peripheral}} = 1527 + 3.01P - 6.5T + 0.107T^2 \quad (3.10)$$

$$(\pm 2) \quad (\pm 0.123) \quad (\pm 0.208) \quad (\pm 0.005)$$

$$R^2 = 96.9\%$$

$$7 < T < 38$$

$$0 < P < 9.1$$

Equations (3.9) and (3.10) can be used to estimate sound velocity in *Kogia* melon core spermaceti and melon peripheral spermaceti, given values of T and P within the prescribed limits. Combining the data sets of KS16 core and KS9525B composite core gave a more general estimate of core velocity, given that both curves were similar in shape but slightly displaced from one another [Fig 3B.7]. Figure 3B.8 shows example predictive curves at 1.52 MPa pressure for melon core and peripheral spermaceti, derived from the output of equations (3.9) and (3.10).

### **3B.2.3 *Physeter macrocephalus* Spermaceti Oil**

Sound velocity was measured in a further sub-sample of the original Humberside spermaceti oil of Section 3A, which had been retained in deep freeze. Instead of cutting lumps of solid oil from the jar, which contained spongy spermaceti tissue laden with oil, the entire oil content of the jar was melted by immersing the sealed jar in the water bath at 38°C. The liquid oil freed from the tissue by this process was decanted from the jar to a measuring cylinder, from where it was poured into the pressure cell cylinder. Sound velocity measurements were made across a full temperature and pressure range applied to the castor oil and *Kogia* spermaceti oil. The resulting sound velocities are tabulated in Table 3B.3 and the trends illustrated in Figure 3B.9. Sound velocities are in the range 1420 ms<sup>-1</sup> to 1530 ms<sup>-1</sup> between 12°C - 38°C and 0 - 9.1 MPa. The magnitude of the sound velocity values are similar to those obtained in section 3A of this chapter, but despite the wider temperature range sound velocities display an almost linear variation with temperature. Multi-variant regression analysis was performed on the data, first with P & T only, then with P, T and T<sup>2</sup>

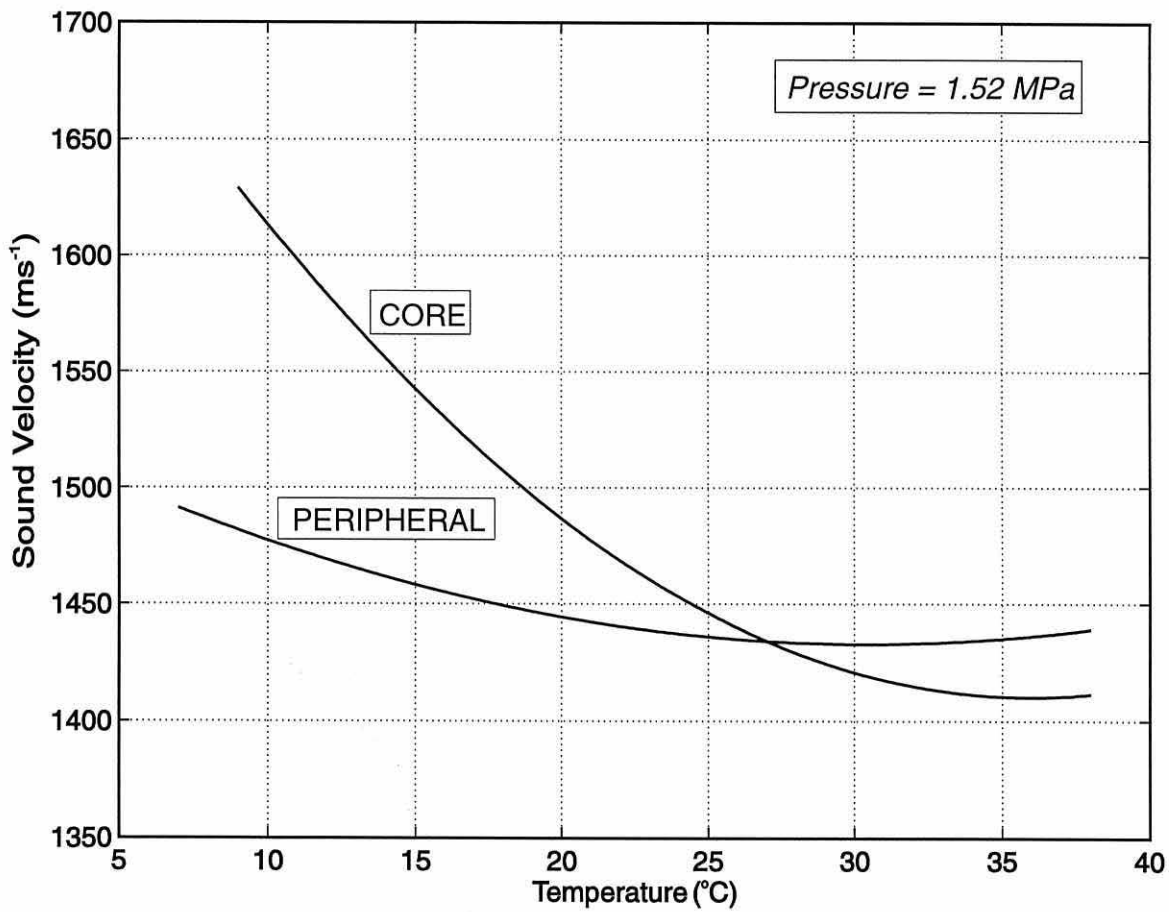


**Figure 3B.8** Generalised predictive curves for *Kogia melon* Core and Peripheral Spermaceti Oil. Curves derived at  $0.1^{\circ}\text{C}$  steps from output of equations (3.9) and (3.10), pressure = 1.52 MPa.

HUMBERSIDE SPERMACETI : HOMOGENISED SAMPLE							
Temp (°C)	0 MPa	1.52 MPa	3.03 MPa	4.55 MPa	6.07 MPa	7.58 MPa	9.10 MPa
38.5	1418	1422	1429	1434	1438	1442	
36.9	1422	1426	1433	1437	1441	1447	
33.0	1428	1431	1434	1441	1446	1450	1455
31.0	1433	1434	1440	1446	1451	1455	1462
28.9	1437	1440	1445	1451	1456	1462	1466
28.3	1440	1443	1449	1454	1459	1464	1469
26.8	1442	1446	1452	1457	1463	1466	1471
25.0	1445	1448	1454	1459	1465	1467	1473
22.8	1453	1457	1463	1467	1472	1476	1480
19.9	1469	1470	1475	1480	1483	1488	1492
17.9	1478	1478	1483	1487	1491	1493	1497
16.0	1486	1485	1489	1493	1497	1502	1508
14.0	1490	1492	1495	1502	1507	1511	1515
12.0	1494	1498	1506	1508	1512	1517	1521

**Table 3B.3** Sound velocity ( $\text{ms}^{-1}$ ) at discrete temperatures and pressures in *Physeter* spermaceti oil, homogenised sample.

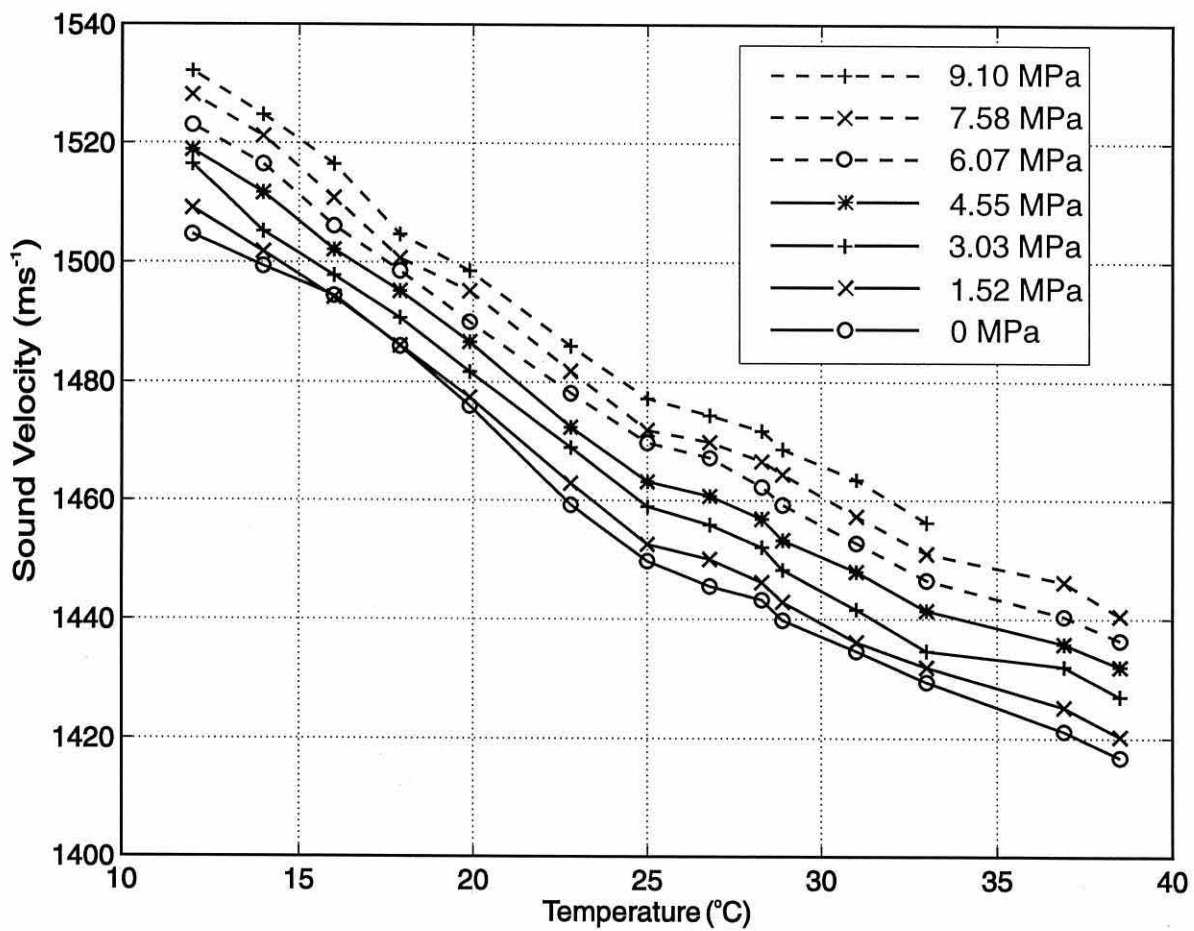


**Figure 3B.9** Sound velocity vs temperature at incremental pressures in homogenised sample of *Physeter spermaceti* oil.

[see Appendix 6]. The regression with  $T^2$  produced the better fit and the polynomial obtained was:

$$C_{\text{spermaceti}} = 1560 + 2.99P - 6.0T + 0.061T^2 \quad (3.11)$$

$$(\pm 2) \quad (\pm 0.068) \quad (\pm 0.168) \quad (\pm 0.003)$$

$$R^2 = 99.4\%$$

$$12 < T < 38$$

$$0 < P < 9.1$$

It might be argued that the oil had degraded during its two year storage since the 1994 measurements and hence this may have contributed to the marked difference in curve shape from the section 3A measurements. While some degradation may well have occurred there is another possibility which may be considered in light of the *Kogia* data and which will be addressed in the following discussion.

### **3B.3 Discussion**

The sound velocity curves obtained for the *Kogia spermaceti* oil are similar in magnitude and shape to those obtained for spermaceti oil of *Physeter* in section 3A of this chapter. The observation of the *Kogia* core and peripheral sound velocity curves crossing between 25°C and 27°C is interesting. At the high body temperatures of 38°C these results imply that sound velocity at the periphery of the melon will be faster than in the melon core. A

consequence of this may be some anterior convergence or focusing of sound, assuming that the temperature profile throughout the melon is constant and that sound is produced by the monkey lips behind the melon.

Perhaps the “shallow” sound velocity gradient of peripheral *Kogia spermaceti* [Fig 3B.6(b)] suggests that cooling of the outer melon layers may occur without greatly altering sound velocity, and hence any focusing or waveguide function the melon may have. For instance, if a temperature of 38°C were maintained throughout the melon sound velocity in the peripheral oils would be about 21 ms<sup>-1</sup> faster than in the core oils [from equations (3.9) & (3.10)]. If the core temperature of 38°C were maintained but the peripheral temperature reduced to 25°C, sound velocity in the peripheral oils would still be faster than in the core oils by almost exactly the same amount [22 ms<sup>-1</sup> from equations (3.9) & (3.10)]. If there were to be any substantial loss of heat from peripheral oils to the cool seawater environment this characteristic of the curves would ensure that sound velocity profile inversion would not occur, provided core temperature was maintained. If the temperature were to drop uniformly across the melon to 25°C or below the sound velocity profile of the melon would invert and anteriorly radiating sound waves from a monkey lip source would diverge rather than converge during passage through the melon.

The works of Morris (1973, 1975) and Flewellen and Morris (1978) found evidence of graded chemical composition and associated sound velocity within the spermaceti sac of the sperm whale, *Physeter macrocephalus*. Their observations suggested a difference of about 1% between sound velocity at the core and the periphery of the sac. Peripheral oil was found to be faster than core oil, again suggesting some form of a waveguide. In the case of

*Physeter*, however, the proposed sound source is at the front of the spermaceti sac so sound channelling through the oils would initially occur in an anterior-posterior direction before partial reflection from the nasofrontal sac. Reflection of sound between the nasofrontal and distal sacs in the head of *Physeter* are proposed to give rise to the pulse intervals within *Physeter* clicks (Backus & Schevill, 1966; Norris & Harvey, 1972; Mohl et al, 1981; Alder-Fenchel, 1980; Gordon, 1991), although the function of these (if any) remain undetermined. In *Kogia* the proposed sound source is posterior to the melon and smaller spermaceti sac, hence sound would be channelled in a posterior-anterior direction through the oils and would not be substantially reflected back from the water/soft-tissue interface at the front of the head.

The sound velocity data for *Physeter* spermaceti oil presented in this chapter are similar in magnitude to those of Flewellen and Morris (1978) although the individual velocity values differ slightly. In section 3A velocities are some  $20 \text{ ms}^{-1}$  higher overall and the extended measurements into the oils' solid phase revealed a non-linear relationship between velocity and temperature, which would not have become apparent had the measurements been restricted to the same temperature range of Flewellen and Morris' work. The  $20 \text{ ms}^{-1}$  discrepancy between this work and the work of Flewellen and Morris is most likely a result of different oil sample composition and the fact that Flewellen & Morris' samples were frozen fresh whereas those used in this work may well have undergone some chemical degradation in the dead whale prior to sampling. Diercks (in Norris and Harvey, 1972) is quoted as finding extraordinarily high sound velocities of over  $2600 \text{ ms}^{-1}$  in spermaceti oil. In light of the data presented in this chapter, and the work of Flewellen and Morris, such high values must be considered questionable. The section 3B *Physeter* sound velocity data

[Table 3B.3, Fig 3B.9] are of similar magnitude to the section 3A data [Table 3A.1, Fig 3A.9] except that the velocity-temperature relationship is approximately linear. The difference in cell calibration does not account for this discrepancy, the correction constant in section 3A and the correction equation (3.6) in section 3B are linear functions. Even if the correction equation (3.6) were applied to the section 3A data it would only have the effect of displacing the curves - it would not alter their shape (i.e. a non-linear relationship between temperature and sound velocity would persist). It seems that the discrepancy between the *Physeter* curve shapes of sections 3A and 3B is a real property of the oil. Aside from the possibility of oil degradation during the two year interval between the respective *Physeter* spermaceti measurements another possible explanation exists for the discrepancy in curve shapes.

When spermaceti oil was originally sampled from the hole in the whales head it was not done in a clinical manner, rather the sampling was opportunistic during the post-mortem operation. It is possible that a mixture of oils from different depths within the spermaceti sac were sampled unintentionally through the single penetration. Spongy spermaceti tissue was scooped out by hand and placed in the sample jars. Liquid spermaceti (that trickled from the hole and solidified on the surface of the head) was picked off and placed on top of the tissue samples in the jars. It is stated in section 3A that pieces of solid spermaceti were cut from the jar prior to melting and pouring into the pressure cell. These pieces of solid oil would probably have been primarily the previously liquid oil that trickled from the head - which had solidified on the skin, been pulled away with a knife and dropped on the top of the spermaceti tissue samples in jars. As this oil was originally liquid within the whale, retaining a temperature of 30+°C, it may have originated from deeper within the sac than

was possible to reach by hand - and hence was trickling out whilst the more peripheral oil was semi-solidified and retained in the spermaceti tissue. It is stated in section 3B that the entire contents of the jar were melted and homogenised before pouring into the velocity measurement cell. When the jar was heated all oil contents duly melted, but the spermaceti tissue remained intact. Therefore the free oil may have been coming from primarily this tissue, which was definitely retrieved from the peripheral region of the spermaceti sac. It is therefore possible that the samples tested in section 3A originated closer to the core of the sac than did the sample tested in section 3B.

It is clear from the *Kogia* data [Figs 3B.7 & 3B.8] that sound velocity-temperature characteristic in core and peripheral oil samples differ, with sound velocity faster in peripheral oils than in core oils under the expected conditions of temperature and pressure. Flewellen and Morris (1978) also showed that sound velocity in the peripheral regions of the *Physeter* spermaceti sac was faster than that at the core. One might expect such a result if the spermaceti sac were to act in any way as a wave-guide or sound focusing medium. If typical *Physeter* sound velocity-temperature curves from sections 3A and 3B are plotted together this possibility can be further considered. The best fit polynomials of (3.3) and (3.11) were used to generate sound velocity curves for *Physeter* oil at a fixed pressure of 1.52 MPa - Figure 3B.10 shows the two curves generated. There is remarkable similarity with the combined plot of *Kogia* peripheral and core oils [Fig 3B.8], i.e. the *Physeter* curves cross in the same manner (and at the same temperature) as the *Kogia* curves with sound velocity higher in (assumed) peripheral spermaceti than in (assumed) core spermaceti at body temperature. This remarkable plot suggests that the aforementioned supposition regarding oil origins from the beached *Physeter* carcass may be correct, given the

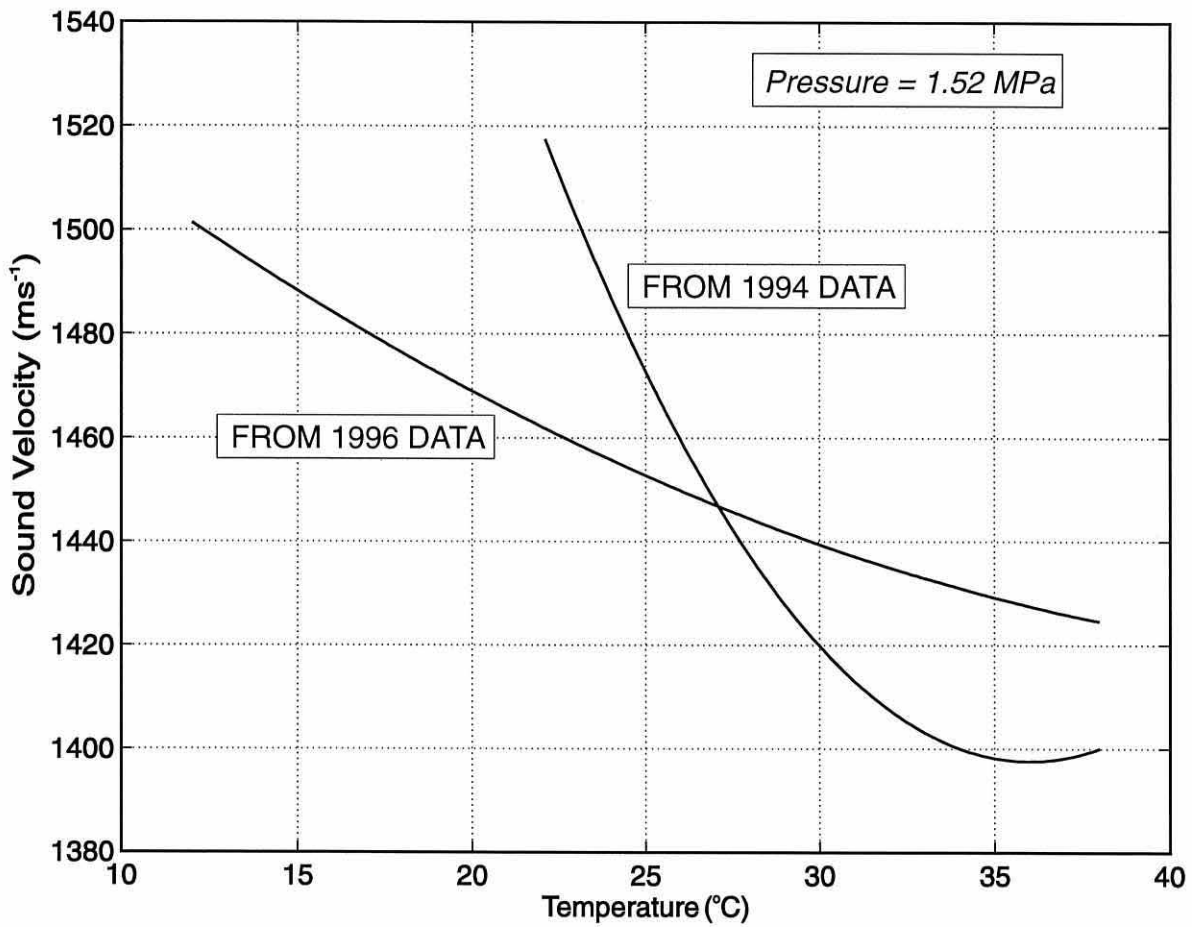


**Figure 3B.10** Generalised predictive curves for *Physeter Spermaceti* Oil, from 1994 & 1996 experiments. Curves derived at 0.1°C steps from output of equations (3.3) and (3.11) .

comparative evidence of the *Kogia* curves. The difference in sound velocity between the two *Physeter* curves ( $T = 38^{\circ}\text{C}$ ) is about 1.5 - 2%, a result largely consistent with the findings of Flewellen and Morris (1978) and the new *Kogia* data in this chapter. Assuming this result is due to the oil origins (i.e. peripheral and core) the plot suggests that the sound velocity profile of the spermaceti sac will invert at low temperatures, although such a situation is unlikely to occur in the head of a living sperm whale and again the characteristics of (assumed) peripheral oil will mediate to a certain extent if cooling occurs from the outside in a graded manner.

Given these results one can envisage the spermaceti sac acting as a sound wave guide. Sound guiding or focusing in the spermaceti sac would act differently to the case of the dolphin melon, as the sound production apparatus in *Physeter* is at the anterior end of the head, and therefore also anterior to the major oil (spermaceti) sac. Sound cannot be projected from a position posterior to the spermaceti sac as the mechanism does not seem to exist for this. Rather, sound may project in all directions (although presumably with some directional characteristics at high frequencies) from the monkey lips, with a section of the wavefront travelling posteriorly through the spermaceti sac. If focusing occurs it will initially occur posteriorly, perhaps concentrating sound or at least flattening the wavefront onto the amphitheatre skull and nasofrontal sac. An initially spherical wavefront would be flattened by its passage through an oil sac of faster peripheral velocity than core velocity, and this could help it guide onto the potentially reflecting surface of the nasofrontal sac. High frequency sound components, i.e. components with wavelengths smaller than the dimensions of the nasofrontal sac, may be reflected forwards and a section of the returning

wavefront again ducted by the spermaceti oil. Such a mechanism would enhance the multiple pulsed structure of sperm whale clicks, at least when received from certain aspects.

Moving on from the specifics of sound velocity gradients within the spermaceti sac, the results have application in the wider context of sperm whale studies in the open ocean. Sperm whale click intra-pulse intervals (IPI's) can be measured by analysis of hydrophone recordings of animals in the deep ocean. If a target animal can be identified at the surface and then tracked through its dive cycle, it may be possible to determine trends in IPI with dive time. It is possible to actively track the descent of a sperm whale using an echosounder, and hence the pressure variable could in theory be determined for a given click. Depth could also be determined more directly using transponders (Watkins et al, 1993). However, other factors are difficult to quantify. The pulsed structure of sperm whale clicks is seldom clear enough for straightforward measurement (usually waveform inspection) of IPI's to high precision. In fact the entire range of sound velocities measured for *Physeter* in this chapter would only produce a change in IPI of about 0.7 ms in the click of a large bull male, which typically have IPI's of about 7 ms. In addition one cannot be certain that the dimensions of the sperm whale head remain unchanged during a deep dive. The huge maxillonasilis muscle, which enshrouds much of the spermaceti complex, is arranged such that its contraction would cause considerable longitudinal compression of the head, thereby shortening the anterior-posterior sound path within the spermaceti sac and reducing IPI's accordingly. The purpose for which sperm whales use the maxillonasilis muscle is not clear, but the size of the muscle does indicate an important function. It may be that body length estimates can only be reliably determined by analysing IPI's of a large number of clicks from a given animal, and obtaining a mean value over time. The situation

might be improved by developing signal processing techniques to improve precision of IPI measurement, or at least semi-automating the process over a large number of clicks. Measurement of IPI's by waveform inspection is a laborious task, and signal processing methods to measure sperm whale click IPI's are the subject of the next chapter.

## **Chapter 4**

### **Measurement of Sperm Whale Click Intra-Pulse Intervals**

#### **4.1 Introduction**

Since Norris & Harveys' 1972 hypothesis of the function of the spermaceti complex in sound production, the intra-pulse interval within sperm whale clicks has been viewed as a key to making remote measurements of sperm whale body lengths. IPI's of mature bull male sperm whale clicks are typically some 7 ms, whereas IPI's of mature female sperm whale clicks are typically some 4 ms. This observation in itself suggests, given the extreme sexual dimorphism of mature sperm whales, that IPI is linked to whale size. If, as seems likely, intra-pulse intervals are a function of spermaceti sac length and velocity of sound in spermaceti oil, body length estimates should be possible to ascertain from IPI's, if they can be reliably measured. This chapter aims to measure IPI's using signal processing techniques, and ultimately estimate whale body lengths based on the resulting data.

While it would seem a straightforward process to measure IPI's from sperm whale clicks by inspection of the time domain signal, in practice it is often difficult to measure time elapsed from feature to feature within a click to high precision. Chapter 2 illustrated that filtering can improve clarity of the pulsed structure in certain frequency bands, and this makes IPI's easier to measure by waveform inspection. Although it is quite possible to distinguish large males from smaller females on the basis of waveform inspection, more subtle variations of

intra-pulse interval can be difficult to detect, and analysing a large number of clicks by waveform inspection is a laborious task. For these reasons signal processing techniques are investigated for their ability to measure IPI's

## **4.2 Concepts and Methods**

### **4.2.1 IPI Measurement using Waveform Autocorrelation**

One possible approach to improving, and semi automating, IPI estimates is to use waveform autocorrelation. By taking a filtered click waveform and repeatedly correlating it with a progressively time shifted replica of itself, peaks in the correlation function should occur when the time shift of the replica is equal to an integer multiple of the intra-pulse interval - i.e. when the first and second pulses in the replica waveform align with the second and third pulses of the original waveform. Figure 4.1 illustrates the concept of waveform autocorrelation as applied to sperm whale clicks. Autocorrelation analysis was used on sequences of clicks from both male and female sperm whales. As the technique relies, in this case, on the alignment of discrete bursts of waveform energy, the clicks were first filtered to remove low frequency non-pulsed sinusoids, thereby clarifying the high frequency pulsed structure. Clicks were filtered in the same three frequency bands used in Chapter 2, namely 1.5 - 3 kHz, 3 - 6 kHz, and 6+kHz; examples of this filtering can be seen in Figures 2.10 & 2.11. Only the 3 - 6 kHz and 6+kHz bands were used with female sperm whale clicks, as pulse structure was shown not to emerge below 3 kHz in these clicks [Fig 2.11].

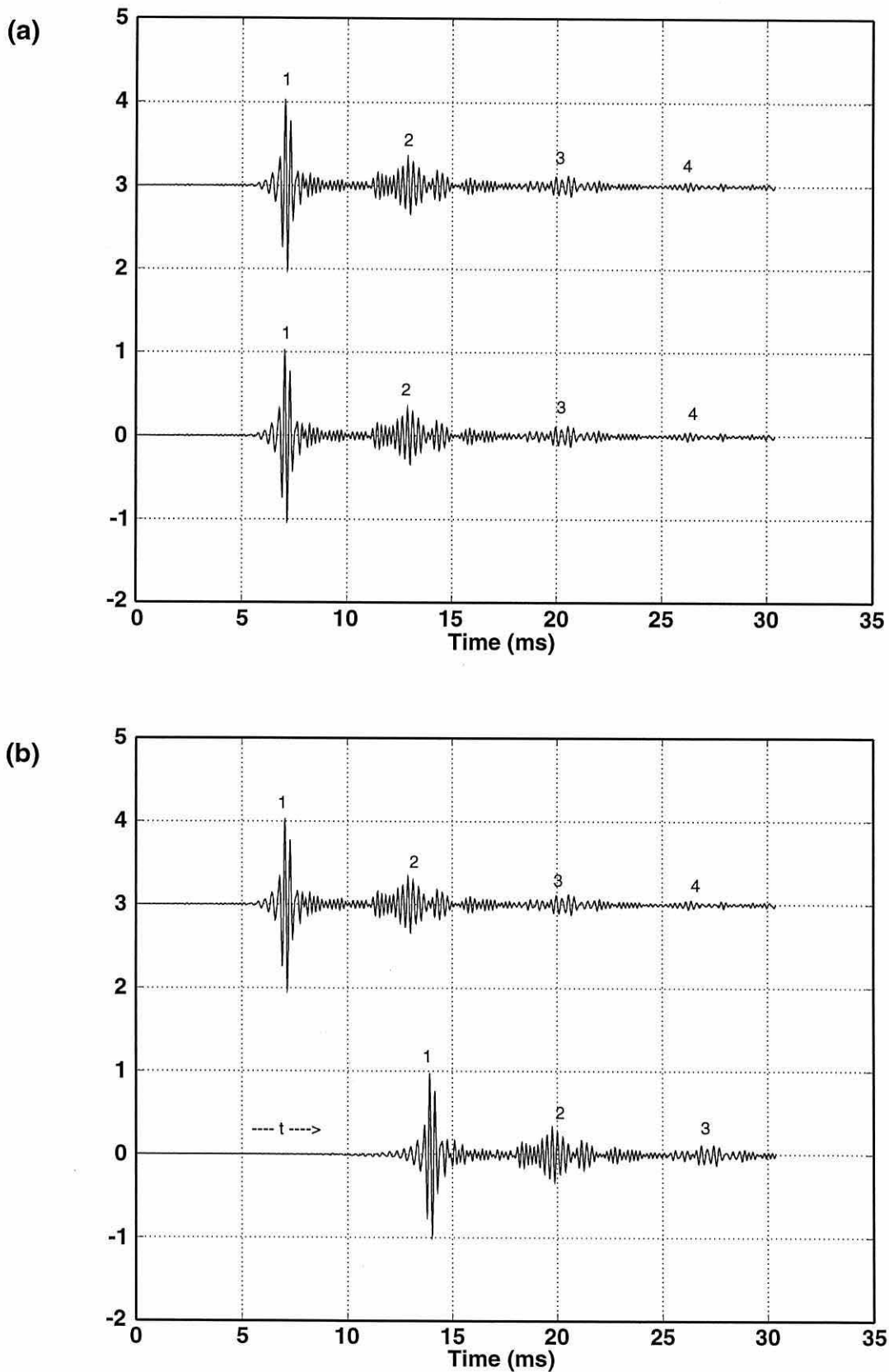


**Figure 4.1** Illustration of waveform autocorrelation applied to sperm whale clicks, pulses are labelled 1 - 4. (a) shows original and replica waveforms in exact alignment at  $t=0$ , which will produce maximum correlation, (b) shows replica time shifted  $t=IPI$  which produces pulse alignments and high correlation value. Ordinate values are displaced for display and have no significance.

Autocorrelation was performed on sequences of clicks from SW2, SW3, SW6 and SW9, i.e. two large bull males and two females. Analysis was conducted by filtering the waveforms with FIR coefficients as described in Chapter 2 and implementing autocorrelation of the sample values through a program written in Turbo Pascal version 6 [Appendix 7]. The following formula was implemented by the program to calculate correlation coefficients  $C_{\Delta t}$  between original and replica waveforms as the replica was time shifted relative to the original.

$$C_{\Delta t} = \frac{\sum_{t=1}^n (X_t Y_{t+\Delta t})}{\sqrt{(\sum_{t=1}^n X_t^2)(\sum_{t=1}^n Y_{t+\Delta t}^2)}} \quad (4.1)$$

Values of  $C_{\Delta t}$  may span the range  $-1 < \Delta t < +1$ . A value of +1 will occur when the two signals being correlated are identical, which occurs when  $\Delta t = 0$ . When  $C_{\Delta t} = 0$  the two signals are orthogonal (i.e. they do not correlate at all). When  $C_{\Delta t} = -1$  the two signals are identical in magnitude but reversed in phase. For the purposes of this analysis only the magnitude correlation was of interest, so only the absolute values of  $C_{\Delta t}$  were computed throughout. The value of  $C_{\Delta t}$  therefore varied between 0 and +1.

Male and female click waveform sections were extracted to ASCII data files after filtering such that they contained the first 4 pulses, about 24 ms of waveform data in the case of males and about 15 ms of data in the case of females. However, only the first 3 pulses were used for autocorrelation. When implementing equation 4.1 on a given click waveform

through the Pascal program the correlation coefficient was stored in an array for each value of  $\Delta t$ . Once correlation on a given click was complete the array was scanned for the highest correlation value between the time limits  $3 \text{ ms} < \Delta t < 11 \text{ ms}$  in the case of male clicks and  $2 \text{ ms} < \Delta t < 6 \text{ ms}$  in the case of female clicks. The time shift  $\Delta t$  corresponding to the highest correlation value between these limits was taken as the intra-pulse interval and saved to a separate disk file.

Given the computational intensity of equation (4.1) for a large number of clicks, several hours were required on a 486 PC to analyse a lengthy series of clicks from each whale in each of the frequency bands described. In addition, disk storage allocation was extremely limited at the time of these analyses and wavedata backup and restore rates were slow. To reduce computational time and maximise the effectiveness of available disk storage space, the original wavedata files were downsampled by a factor of 2 during FIR filtering. This yielded an effective sampling interval of  $32 \mu\text{s}$ , which was adequate for detecting small variations in IPI.

#### **4.2.2 IPI Measurement using Rippled Magnitude Spectra**

An alternative approach to time domain autocorrelation may be found via the frequency domain in the form of rippled magnitude spectra. When a broadband signal is delayed by time  $t$  and added back on itself, the resulting spectrum of the composite signal exhibits ripples with a period equal to  $1/t$  (Yost et al, 1978). This phenomenon can be demonstrated in its most extreme form using unit impulses. Figure 4.2(a) shows a section of a digital

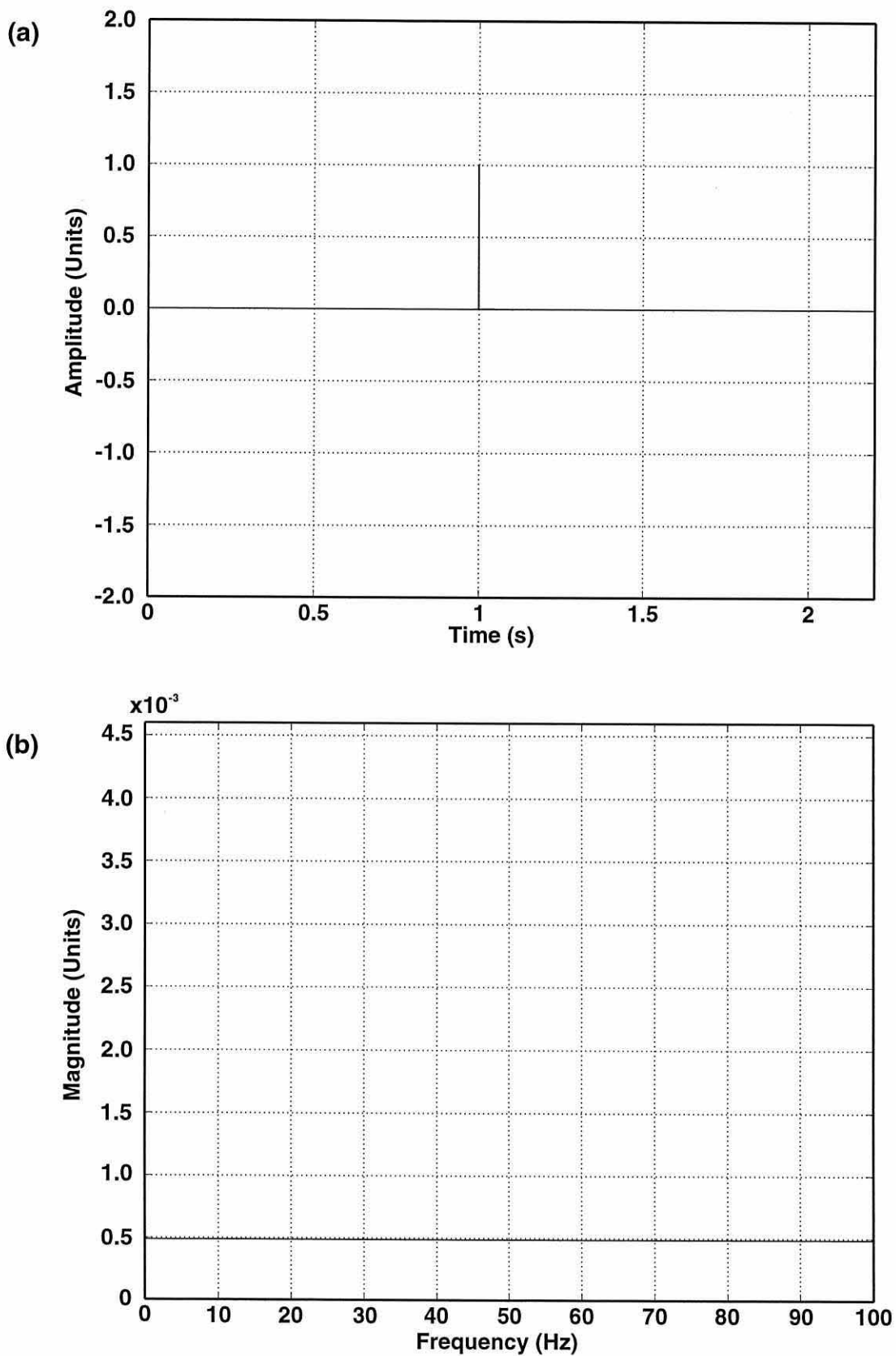


**Figure 4.2** (a) Section of a digital signal with all sample values set at zero except for a single unit impulse; sampling interval = 10 ms, total number of samples in entire signal = 2048. (b) Full 2048 point magnitude spectrum of single unit impulse signal, frequencies above 50 Hz are aliased.

signal sampled at 100 Hz with 2048 samples in the whole sample length, all of which are zero except for a single sample with a value of 1 (i.e. the unit impulse). In digital signal processing the unit impulse is the ultimate broadband stimulus and delivers equal amounts of all frequencies to a processor, in this case the Fourier Transform shown in Figure 4.2(b). As expected Figure 4.2(b) shows a completely flat spectrum with equal magnitude at all frequencies. As the full transform is shown frequencies greater than 50 Hz are a mirror image of those below 50 Hz, an alias due to the ambiguity of sampled digital signals. Although not normally shown in spectral analysis, mirror images are retained for consistency of signal length for the remaining analyses described in this chapter. Figure 4.3(a) shows a similar signal to that in Figure 4.2(a), but this time with an additional unit impulse delayed by  $t=0.1$  s relative to the original impulse. The magnitude spectrum of this new signal is shown in Figure 4.3(b) and has the form of a DC shifted sine wave. Figure 4.3(b) is in fact a rippled magnitude spectrum, with the ripple period equal to  $1/t$  (i.e. 10 Hz). The unit impulse is the ultimate broadband signal, and its use in Figure 4.3 produces a perfect rippled spectrum. Fourier analysis of real world, time delayed broadband signals will produce similar results but not to such an extreme.

It has already been shown that sperm whale clicks are broadband signals. Further, individual pulses constituting the click can be considered as broadband signals separated by a time  $t$  equal to the intra-pulse interval. Therefore the magnitude spectrum of an entire click should also contain ripples with a period equal to  $1/t$  (i.e.  $1/IPI$ ). As large bull male clicks typically have IPI's of some 7 ms the magnitude spectrum ripples should have a period of about 140 Hz, whereas female clicks typically have IPI's of some 4 ms and hence the ripple period should be about 250 Hz. When looking for ripples in the spectra of real

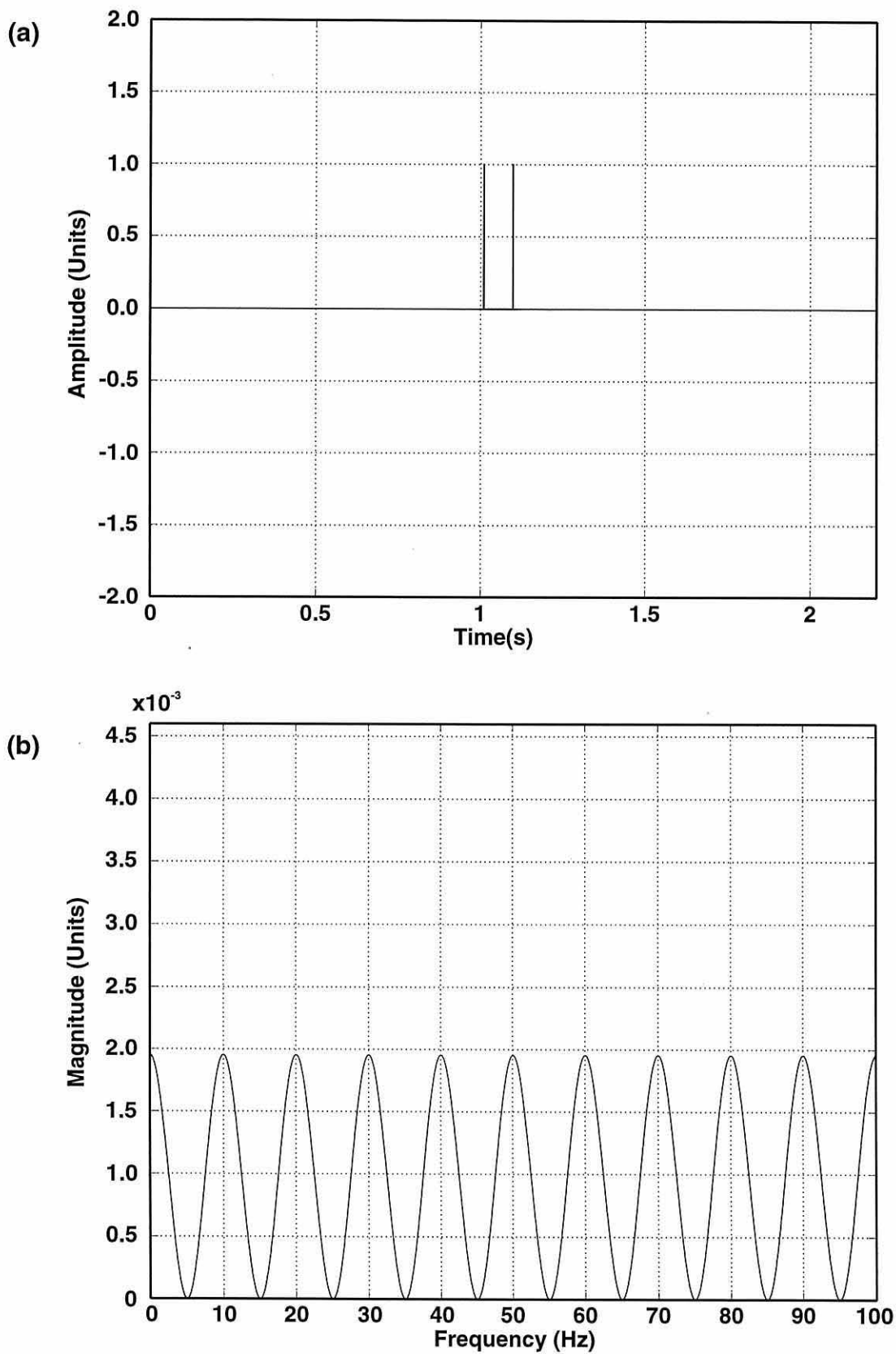
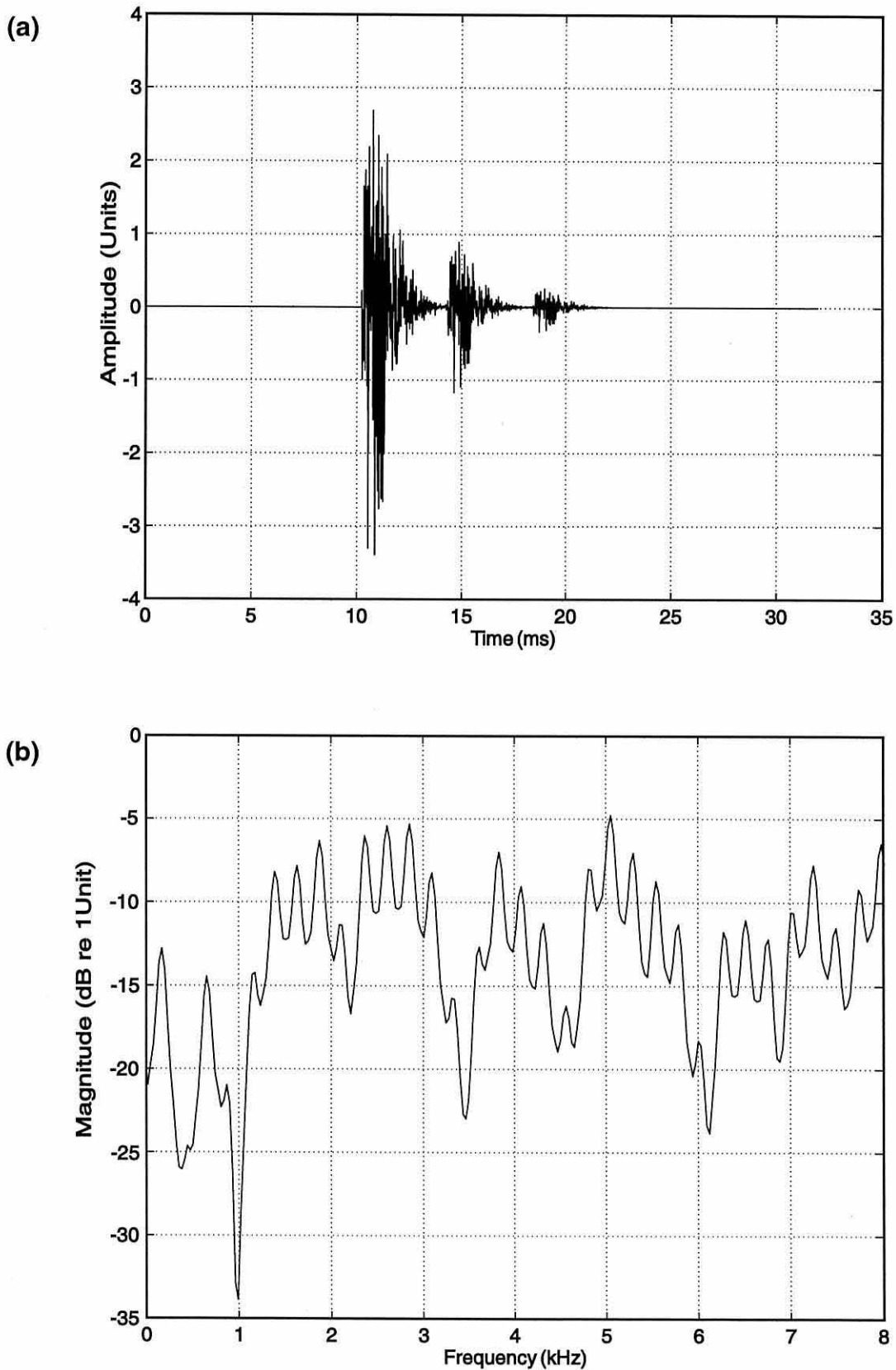


**Figure 4.3** (a) Section of a digital signal containing two unit impulses separated by  $t=0.1s$ , (b) Full 2048 point magnitude spectrum of two unit impulse signal showing ripples with a period equal to  $1/t$ , frequencies above 50 Hz are aliased.

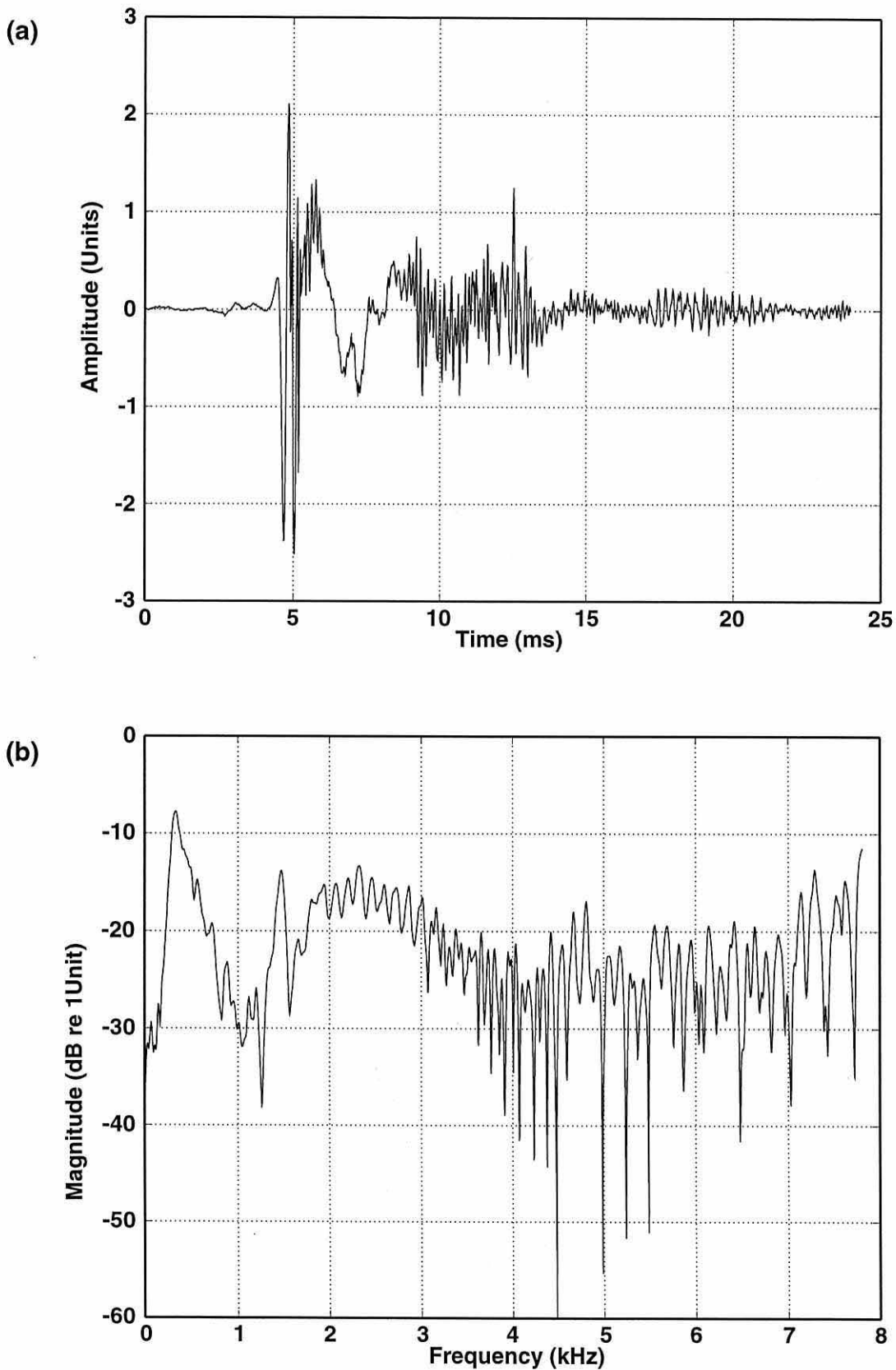
world signals it is usual to display the magnitude units on a logarithmic scale, although this was not necessary for such an unambiguous signal as that in Figure 4.3. The concept is demonstrated further by generating an artificial sperm whale click with three identical, but decayed, pulses [Fig 4.4(a)]. The artificial click was constructed by generating an initial 4 ms signal packet of broadband random noise and windowing it to simulate the envelope of the first pulse in a sperm whale click. This artificial pulse was then copied twice at 4 ms intervals after the initial pulse onset, finally creating three identical broadband pulses with a spacing of 4 ms. The composite signal was then decayed with time using an exponential function to produce a composite waveform not dissimilar to a real sperm whale click. The final signal was zero padded either side of the three pulses to give a total sample length of 2048 points for FFT analysis. Figure 4.4(b) shows a section of the magnitude spectrum computed from this artificial click, with magnitude units converted to a logarithmic scale. The spectrum is not as “level” and “well behaved” as the two unit impulse signal, but ripples can clearly be seen with a period of 250 Hz, corresponding to the time spacing of the artificial pulses - i.e. the artificial intra-pulse interval.

Figure 4.5 shows a real click from a male sperm whale and its' associated magnitude spectrum. The magnitude is displayed on a logarithmic scale across the frequency range 0 - 8 kHz. Ripples in the male click spectrum are quite clear between 2 and 3 kHz, and are also apparent at higher frequencies. Indeed above 3.5 kHz the ripples have considerable amplitude, although they are corrupted by ripples with other periods. Looking closely at the ripples between 2 and 3 kHz the ripple period does indeed appear to be about 140 Hz.

Figure 4.6 shows a real click from a female sperm whale and its associated magnitude



**Figure 4.4** (a) Artificial sperm whale click generated from broadband signal components repeating at 4 ms intervals, windowed and decayed exponentially. (b) magnitude spectrum of artificial click showing distinct ripples with the expected period of 250 Hz.



**Figure 4.5** (a) Male sperm whale click with IPI of approximately 7 ms, (b) logarithm of magnitude spectrum of male sperm whale click showing ripples above 2 kHz with a period of approximately 140 Hz, which is in accordance with  $1/\text{IPI}$ .

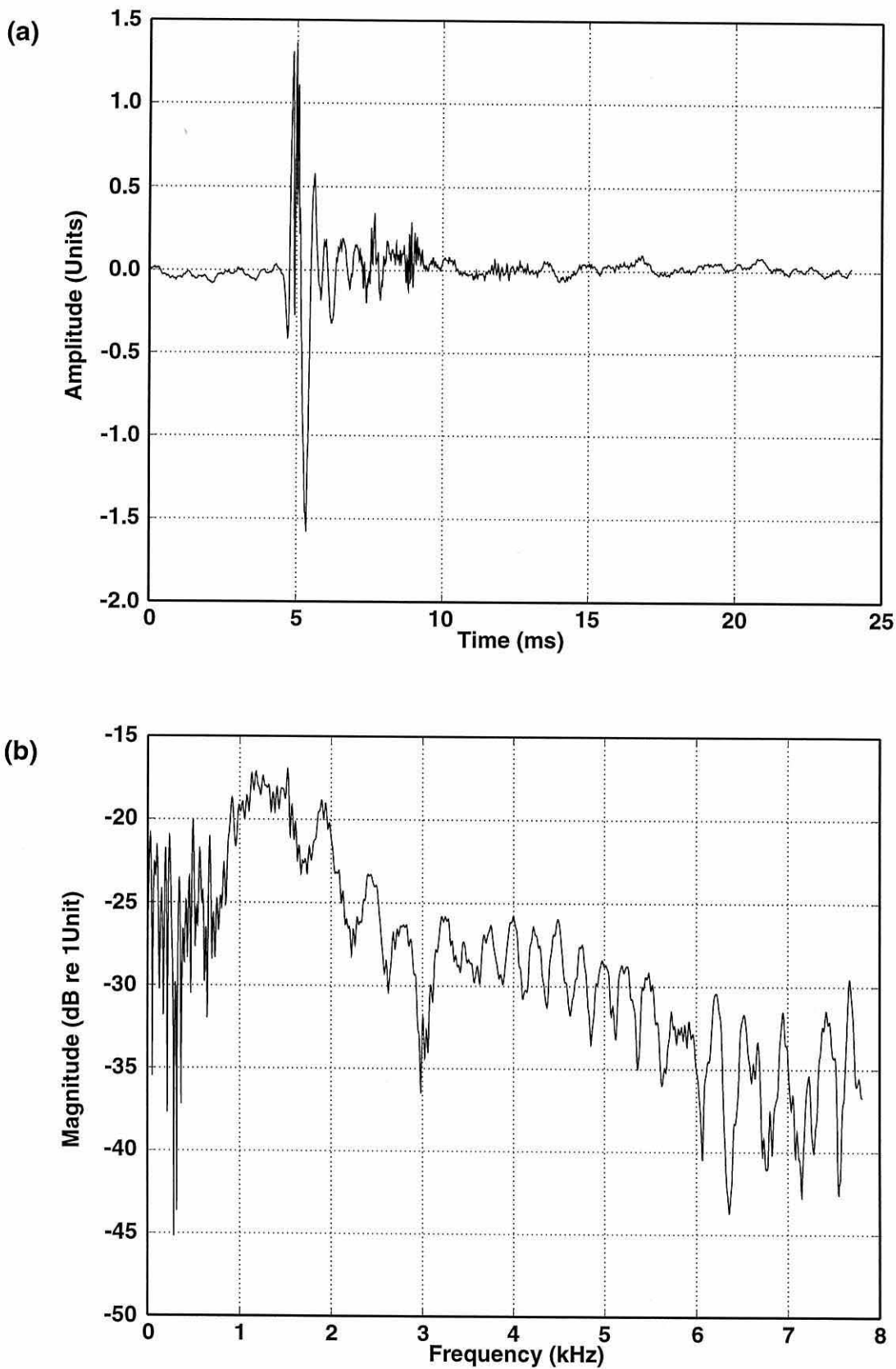


**Figure 4.6** (a) Female sperm whale click with IPI of approximately 4 ms, (b) logarithm of magnitude spectrum of female sperm whale click showing ripples above 3 kHz with a period of approximately 250 Hz, which is in accordance with  $1/\text{IPI}$ .

spectrum. Again ripples can be clearly seen above 3 kHz and the ripple period conforms with that expected, in this case about 250 Hz.

A technique used in speech processing (Noll, 1967) is to compute the magnitude spectrum of the logarithm of the magnitude spectrum. The resulting function is known as the *cepstrum*, a name derived by paraphrasing the word spectrum (Bogert et al, 1963). The independent variable has dimensions of 1/frequency (i.e. time) and is termed the *quefreny*. Essentially the *cepstrum* treats the logarithm of the magnitude spectrum of the original signal as a second signal, and computes the magnitude of oscillations with respect to frequency. This technique is useful in measuring the *quefreny* of ripples in a magnitude spectrum, as the *quefreny* of these ripples corresponds to the original delay  $t$  between the broadband signals in the time domain. Figure 4.7 illustrates the *cepstrum* of the two unit impulse signal shown in Figure 4.3(a). Not surprisingly the function returns one sharp peak at a *quefreny* corresponding to the delay  $t=0.1$  between the original two impulses, a strong DC component was also present but has been zeroed to clarify the 0.1 s peak.

Sperm whale clicks consist of several broadband pulses and unit impulses can again be used to demonstrate the effect of multiple delayed broadband signals on spectrum ripples, although it has already been shown that the expected ripples occur in the spectra of sperm whale clicks. Figure 4.8(a) shows three unit impulses, each delayed by 0.1 s relative to the previous impulse, and part (b) shows the *cepstrum* of this signal. Figure 4.9(a) shows another three impulse signal, but this time the impulses following the first unit impulse are decayed in amplitude with values of 0.5 and 0.25 respectively, and the associated *cepstrum* is shown in part (b). Quite clearly the two *cepstra* are very similar, the major difference

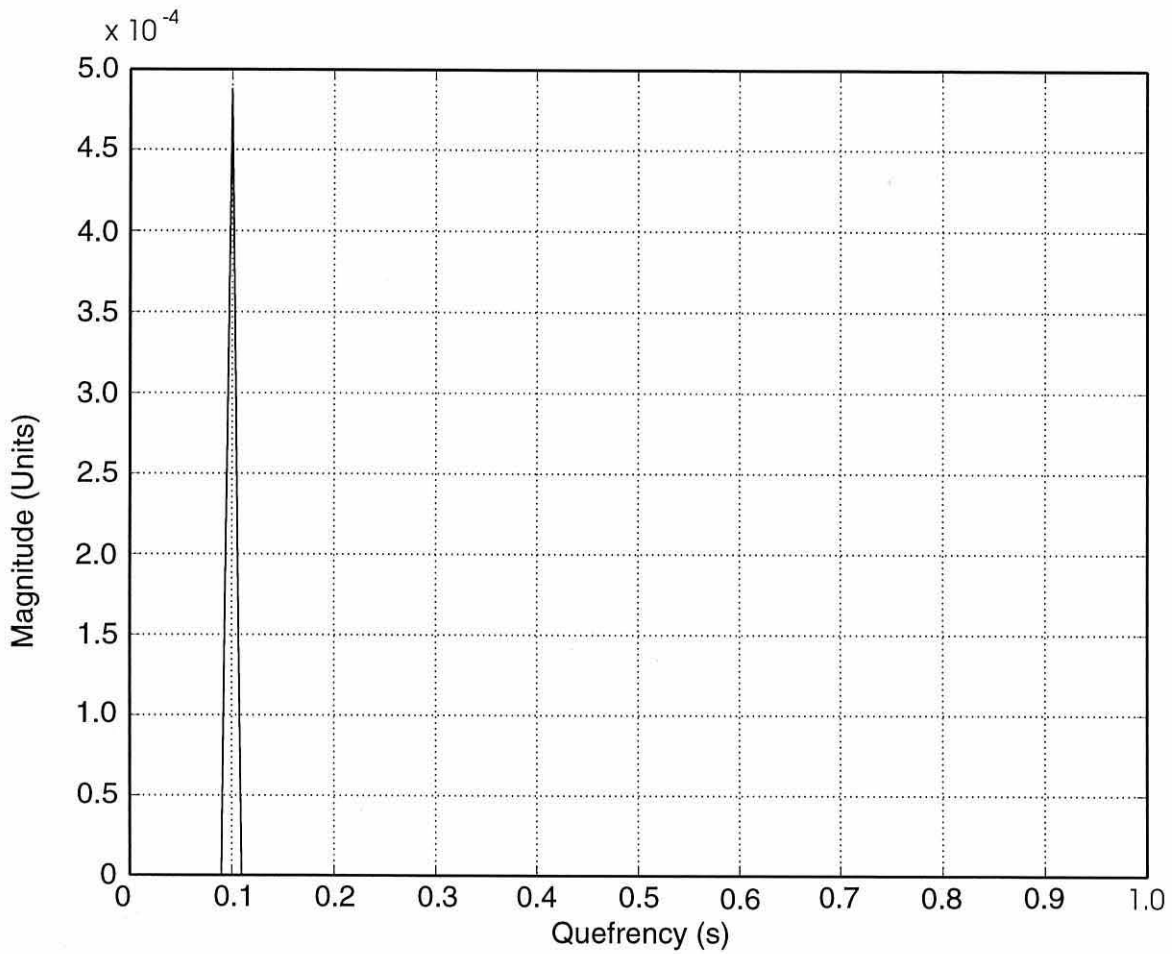


**Figure 4.7** *Cepstrum* obtained from two unit impulse signal; note the peak occurring at a *quefrency* (time) of 0.1s, corresponding to the time delay between the two impulses

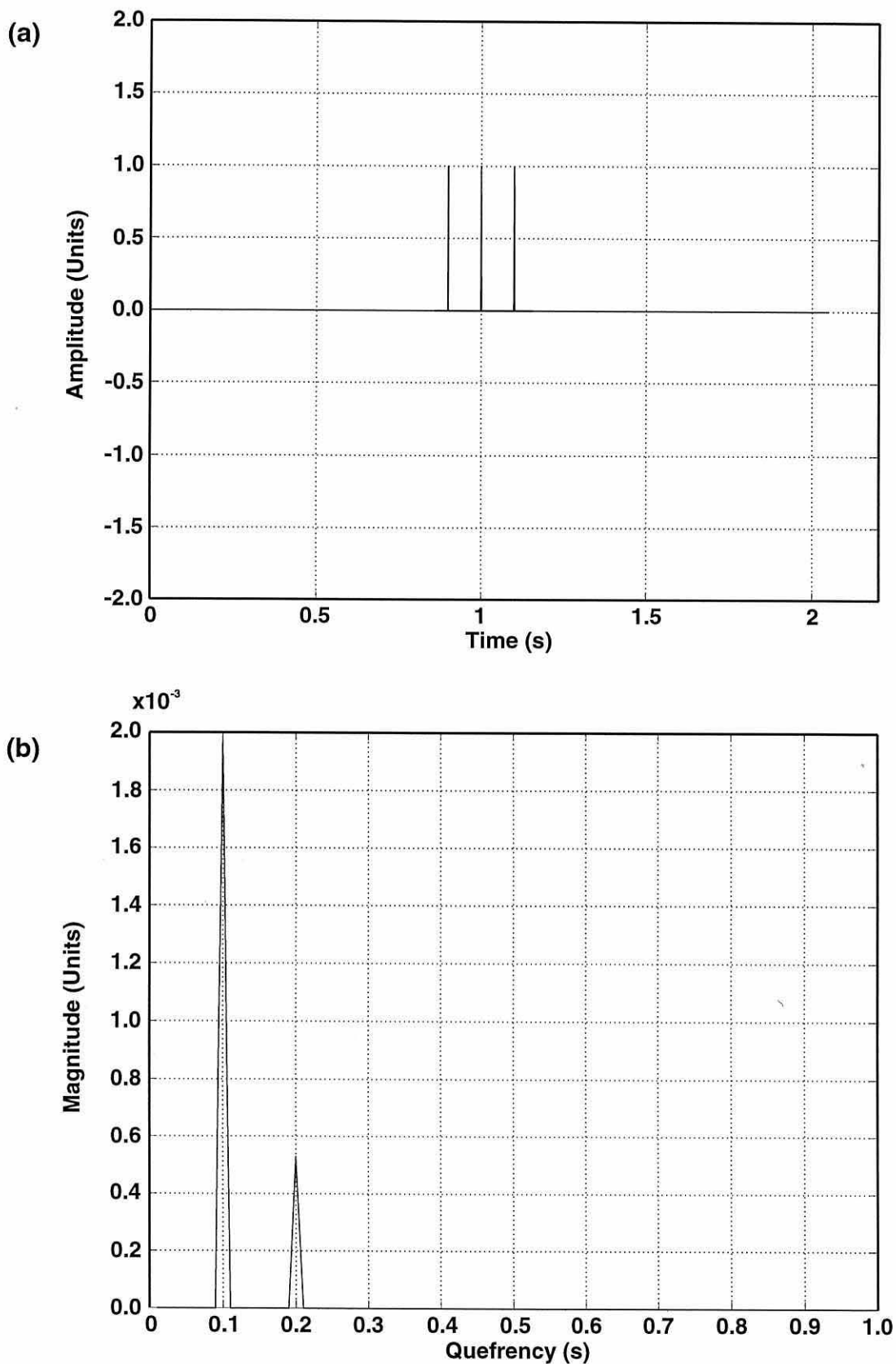


**Figure 4.8** (a) Signal containing three unit impulses with a time separation of 0.1 s between each impulse. (b) Cepstrum of three unit impulse signal showing a primary peak at 0.1 s and a small secondary peak at 0.2 s.

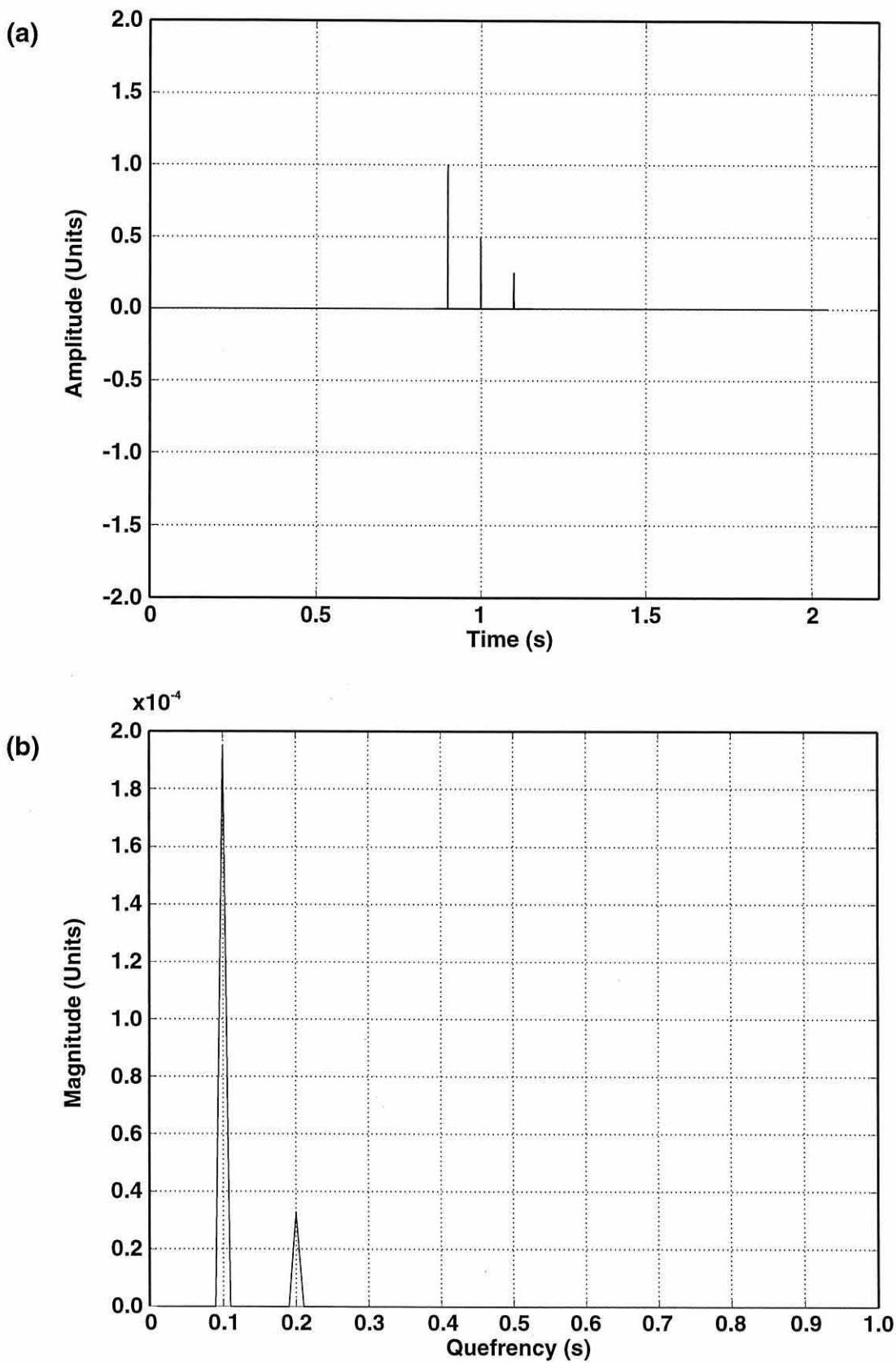


**Figure 4.9** (a) Signal containing three decaying unit impulses with a time separation of 0.1s between each impulse, amplitudes are 1, 0.5 and 0.25 units respectively. (b) Cepstrum of decaying three unit impulse signal showing a primary peak at 0.1 s and a small secondary peak at 0.2 s

being different overall magnitude due to different total signal strengths. In both cases there is a strong peak at 0.1 s, corresponding to the primary delay time. There is also a second, smaller peak at 0.2 s which is due to the delay time between first and third pulses. The 0.1 s delay time, which would correspond to the IPI if this example is taken as a model of a sperm whale click, is the dominant feature in the 3 impulse *cepstrum*. Figure 4.10 illustrates the *cepstrum* computed from the artificial sperm whale click in Figure 4.4(a). Although the *cepstrum* contains noise, a strong peak at 4 ms (corresponding to the IPI) clearly dominates. The *cepstrum* analysis method was therefore chosen as suitable for application in the measurement of sperm whale click intra-pulse intervals.

### 4.2.3 Cepstrum Methods

Selection of the most effective method of extracting IPIs from sperm whale click spectra involved a certain degree of experimentation. Processing was performed using MATLAB version 4.2C; click waveforms were not downsampled for *cepstrum* analysis, thereby retaining the original sampling interval of 16  $\mu$ s. From the point of view of a FFT algorithm the male click spectrum [Fig 4.5(b)] is a signal containing a large, negative DC shift from zero. As only the relatively high *quefrequencies* (i.e. rapid oscillations) in the magnitude spectrum are of interest, the whole magnitude spectrum can be treated as a signal and highpass filtered without losing the IPI component of the signal. To illustrate this a highpass FIR filter was generated to pass only *quefrequencies* greater than 1 ms. This filter was applied to the full magnitude spectrum of the sperm whale click (including mirror image) and a 2048 point FFT performed on the resulting signal to yield the *cepstrum*. The resulting

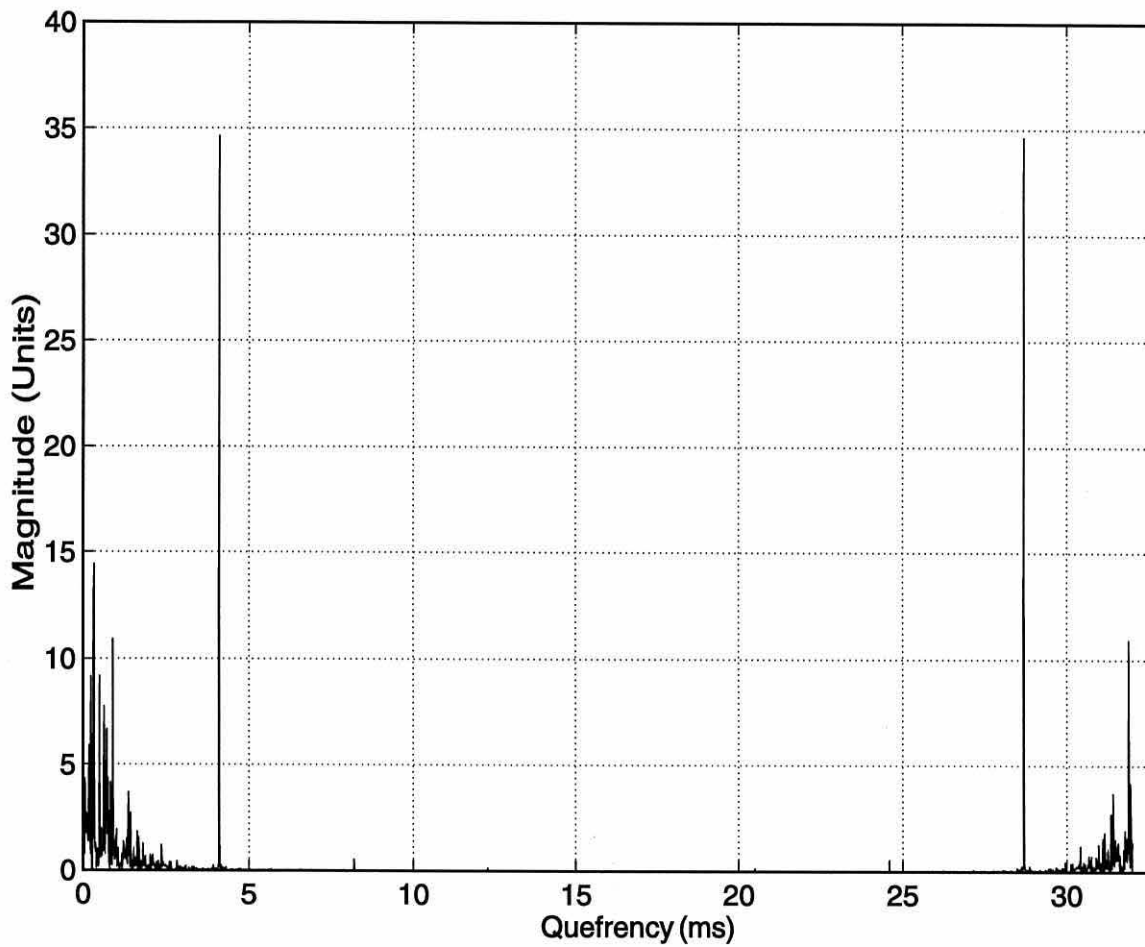


**Figure 4.10** *Cepstrum* obtained from a artificial sperm whale click; note the peak occuring at a *quefrecy* (time) of 4 ms, corresponding to the actual IPI generated. Quefrecies above 16.384 ms on the abscissa are aliased and the mirror image is obvious.

*cepstrum* is shown in Figure 4.11; note the peak occurring at a *quefreny* of approximately 7.5 ms, corresponding to the intra-pulse interval apparent from inspection of the source click waveform [Fig 4.5(a)].

Although the IPI peak is distinct and offers a feature that can be measured, there is considerable noise in the click spectrum and the magnitude of peaks at *quefrenies* other than that corresponding to the IPI may be sufficient to mask it in some instances. The decaying series of pulses will give rise to weaker ripples in the spectrum than would be the case if the pulses were all of similar amplitude in the time domain. In addition spurious multiples within the click may give rise to strong and distinct ripples in the click spectrum. It was decided to experiment with various windows in the time domain to try and enhance the spectrum ripple amplitude at the desired *quefreny*. As a standard a boxcar window was used with unity values across the section of click to be analysed and zero at all other values. For comparison various forms of the chi-squared distribution were chosen as windows to modulate the clicks prior to FFT analysis. The use of chi-squared windows is demonstrated in Au (1993) to accentuate power spectrum ripples in the spectra of delayed pulse signals.

#### **4.2.4 Generating Windows**

Chi-squared type distributions were generated using the following formula:

$$\chi^2(n) = \frac{1}{2^{k/2} \Gamma(k/2)} n^{(k/2)-1} e^{-(n/2)} \quad (4.2)$$

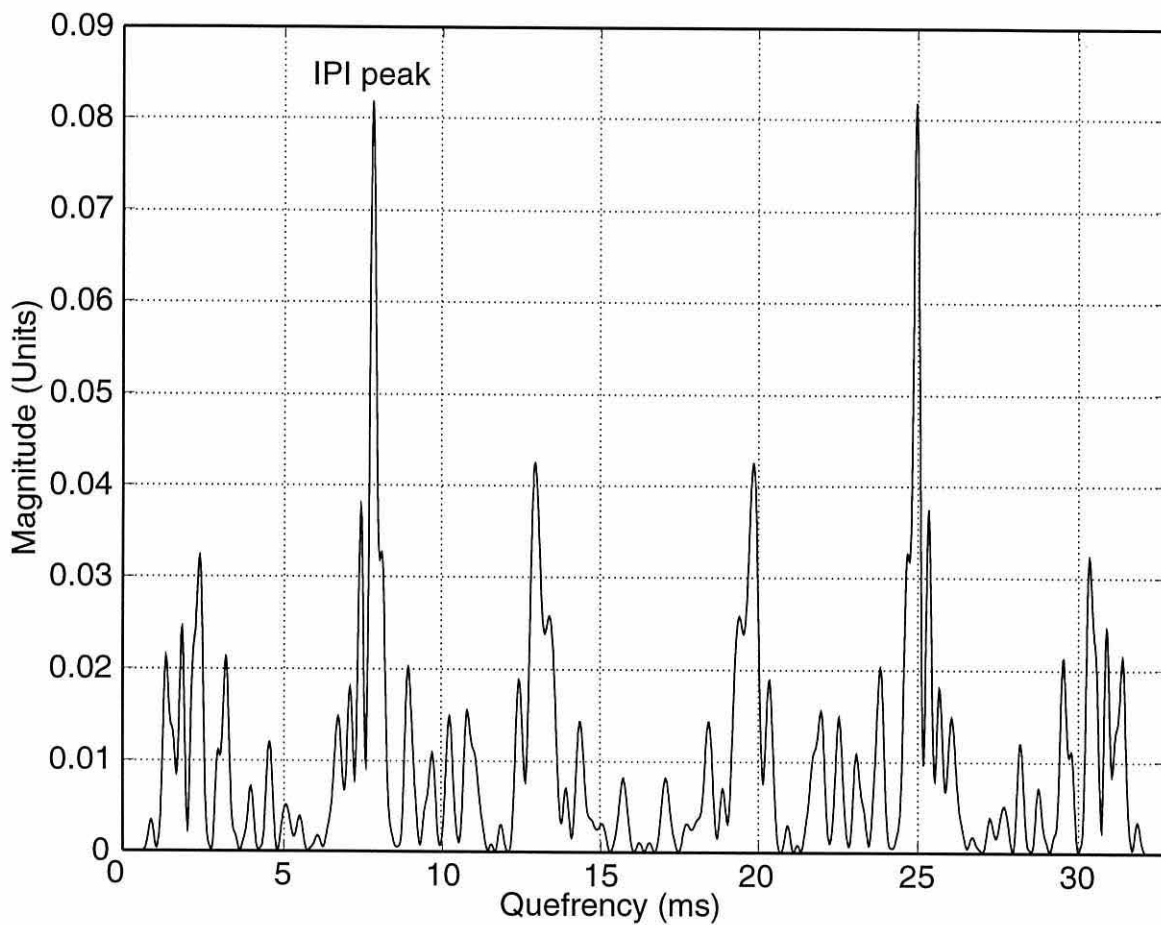


**Figure 4.11** Example of a *cepstrum* obtained from a male sperm whale click; note the peak occurring at a *quefrequency* (time) of  $\sim 7.5$  ms, corresponding to the IPI observed from waveform inspection. *Quefrequencies* above 16.384 ms on the abscissa are aliased and the mirror image pattern is obvious. *Quefrequencies* below 1 ms were filtered out of the click spectrum from which this plot was obtained.

where gamma was calculated as a factorial of k-1 thus:

$$\Gamma(k) = (k - 1)! \quad (4.3)$$

Strictly speaking equation (4.2) will not always result in mathematically true chi-squared distributions as k was used with values of 2, 3, 4, 5 and 6, whereas gamma should only be defined as a factorial when k/2 in equation (4.2) is a positive integer. However, equation (4.2) produced the desired window shapes through the factorial method shown, which was considered more important than the mathematical purity of the distributions. The term chi-squared will continue to be used for convenience but the above statement should be borne in mind.

The number of samples in the active window section (i.e. the section overlaying the click waveform itself) was varied depending upon the length of the click waveform section to be modulated. The value of n/2 in the  $e^{-(n/2)}$  term of equation (4.2) was always modified to step between 0 and 5 whatever the number of window samples, in order to maintain a constant window shape for different active window section lengths at a given value of k. Once generated the final value in the window tail was used to scale the window. This final window samples' ratio to unity was calculated and used as a multiplier for all other sample values in the window, essentially scaling them up. Finally the window was inverted left to right and positioned within a 2048 sample frame such that its unity start value coincided

with the click onset in a matching 2048 sample waveform section. All values either side of this active window section, to a total window length of 2048 samples, were set to zero.

Once in this form windows could be used to modulate 2048 sample waveform sections containing the clicks. Figure 4.12 shows the six windows used for initial investigation of IPIs. A chi-squared window with  $k=2$  is an exponential, but with  $k=3$  the window takes on the chi-squared shape, and as  $k$  increases the window becomes more symmetric and has lower peak amplitude. The windows are effectively used as skewed amplifiers to boost the weaker signal level of successive pulses in the click. Figure 4.13(a) shows a full 2048 point waveform segment containing a male sperm whale click, and part (b) shows the associated chi squared window ( $k=3$ ) aligned to modulate the first three pulses. Figure 4.13(c) shows the result of this modulation on the waveform, and the spectrum in part (d) can be seen to contain ripples of enhanced amplitude relative to the non-windowed case [Fig 4.5(b)].

The six windows were used on all clicks during the first 6 minutes of sequences SW3 and SW9, and *cepstra* computed in each case. Through a process of trial and error it was discovered that IPI values could best be extracted by a combination of processes. First the click waveform was shifted to begin 6 ms into the time view and then modulated with the appropriate window. A full 2048 point FFT was performed and the spectrum converted to a logarithmic scale. The full spectrum, including mirror image, was then filtered with a FIR filter to pass only *quefrequencies* between 5 and 9 ms in the case of male clicks, and 3 - 6 ms in the case of female clicks. For male click spectra, components below 2 kHz and above 6 kHz were then zeroed. For female click spectra, components below 3 kHz and above 12 kHz were zeroed. Finally a further full 2048 point FFT was performed on the resulting

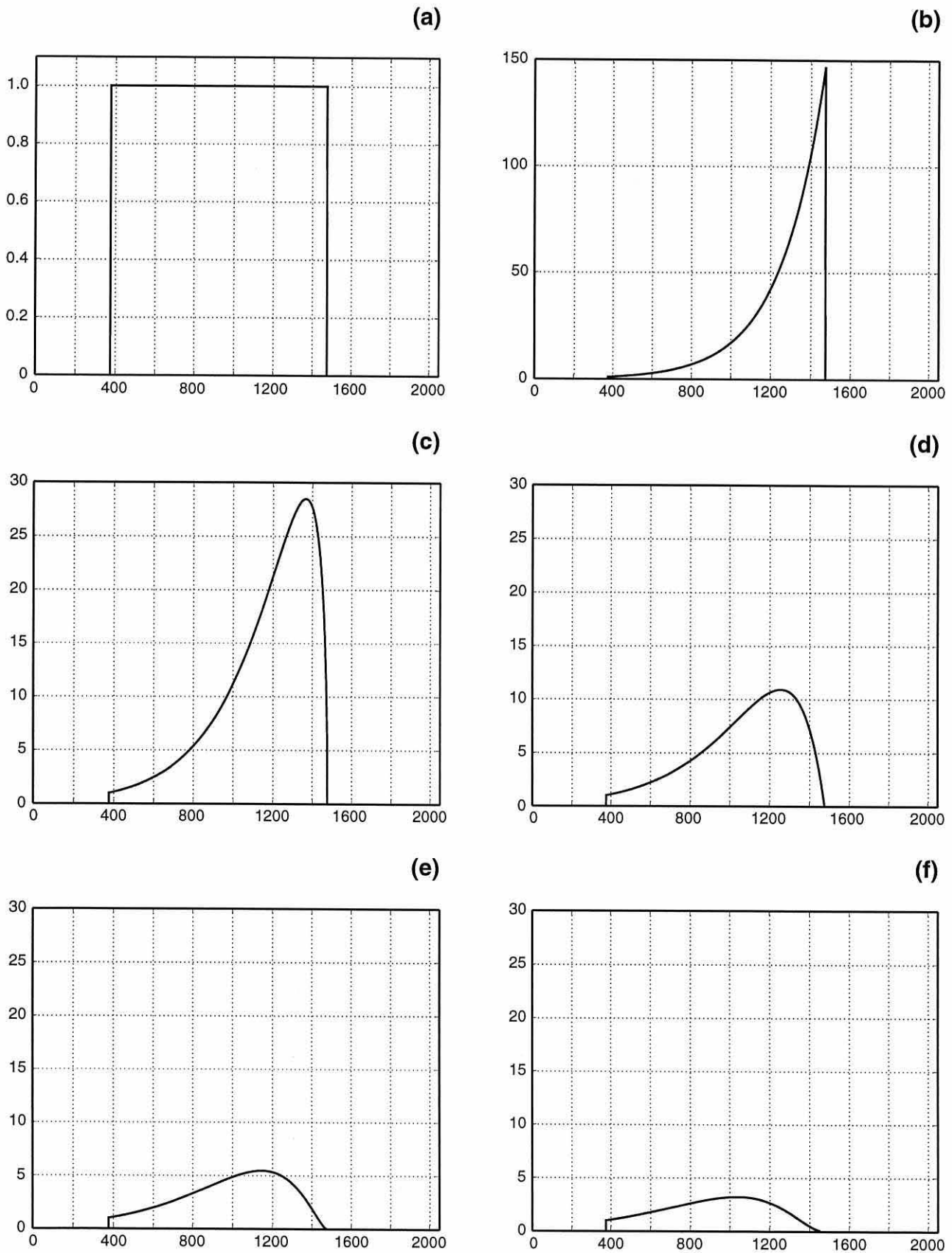


**Figure 4.12** Various windows used to modulate clicks (a) boxcar, (b) exponential (chi squared  $k=2$ ), (c) chi squared  $k=3$ , (d) chi squared  $k=4$ , (e) chi squared  $k=5$  and (f) chi squared  $k=6$ . Ordinates show window coefficients, abscissae show window points.

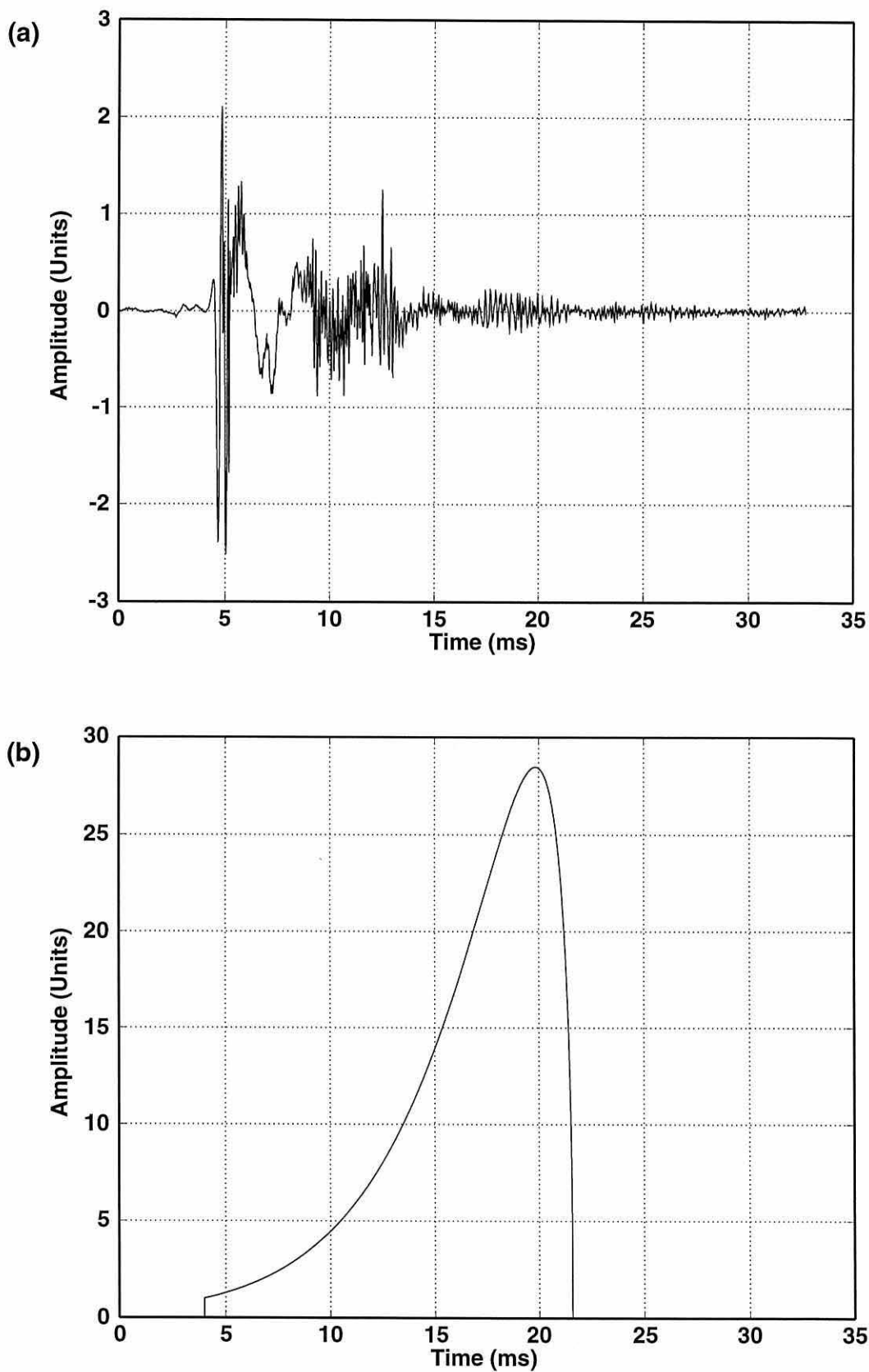


**Figure 4.13** (a) 2048 point waveform section containing male sperm whale click showing several pulses and (b) corresponding chi squared window with  $k=3$  used for modulation of waveform section prior to FFT processing.

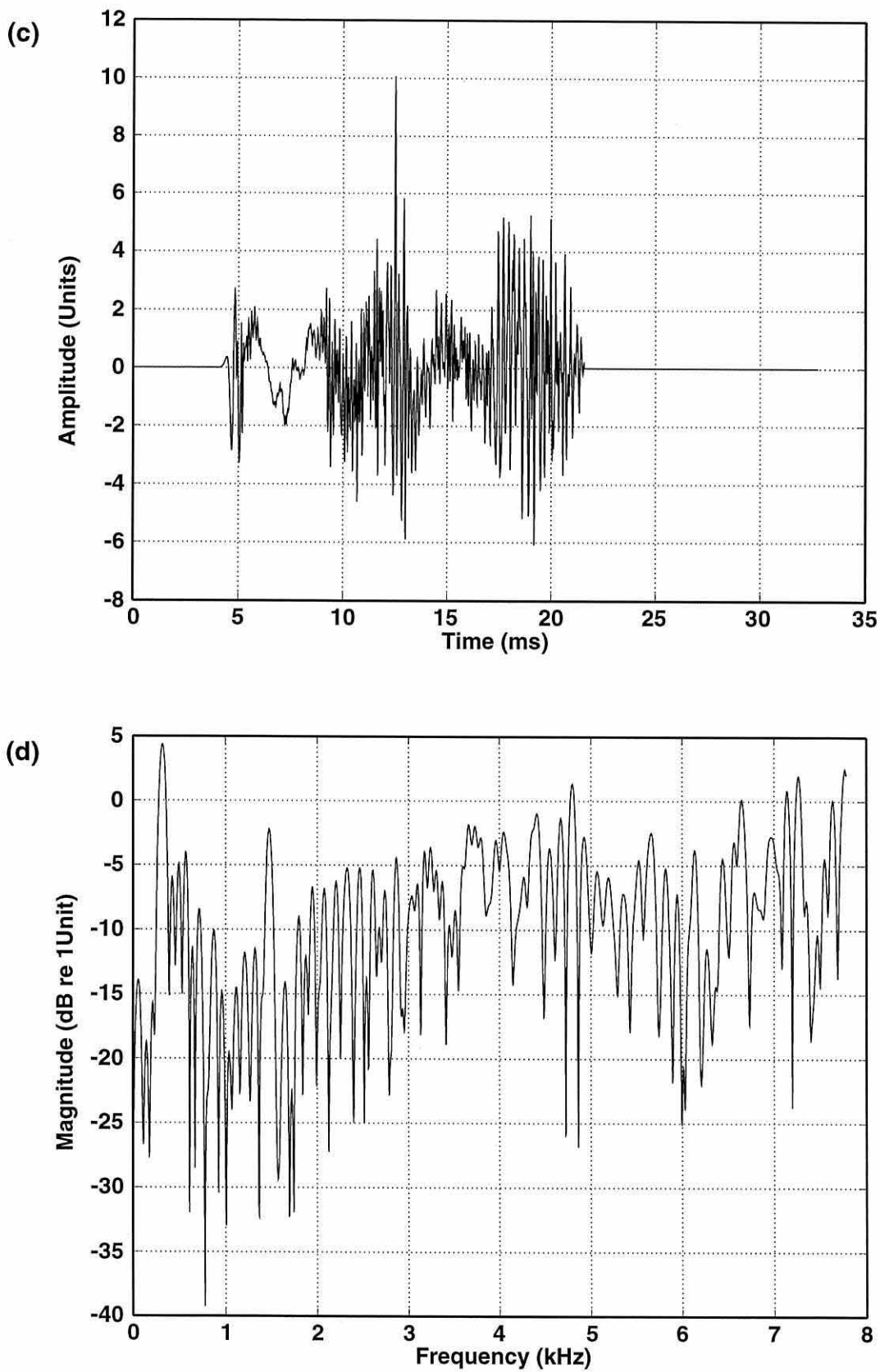


**Figure 4.13** (c) Male sperm whale click waveform from (a) after modulation with chi squared window in (b). (d) logarithmic magnitude spectrum of modulated click showing increased ripple magnitude as compared to a non modulated case.

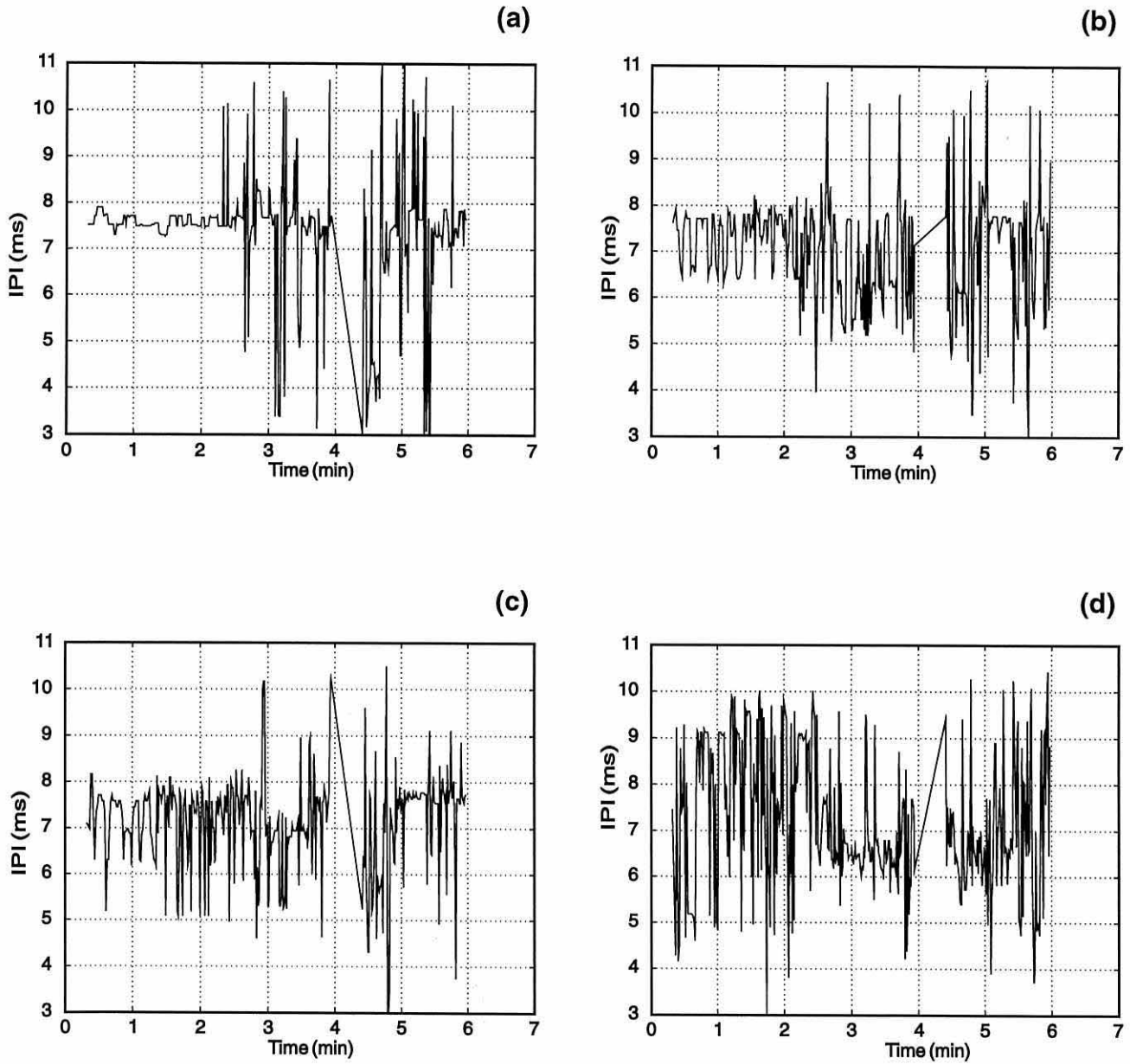
signal to produce the *cepstrum*. The *cepstrum* was scanned for a peak value, the corresponding *quefreny* of which was taken as the intra-pulse interval and saved to a disk file.

### **4.3 Results**

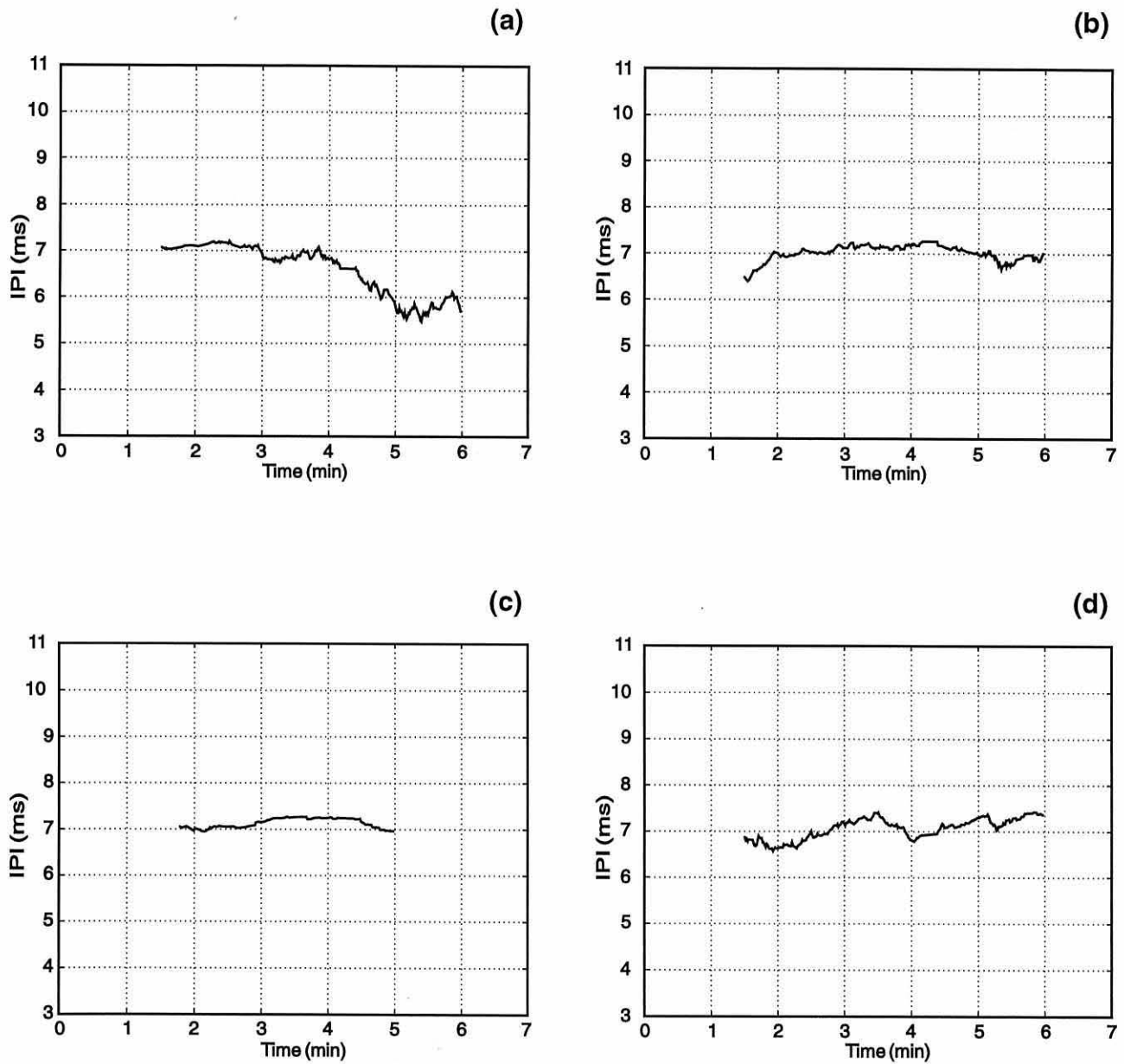
#### **4.3.1 Autocorrelation Analysis Results**

Figure 4.14 shows plots of raw IPI values obtained from autocorrelation analysis across the first 6 minutes of male click sequence SW3. During the first 2.5 minutes of clicking IPI's maintain a fairly stable value at about 7.5 ms as measured in the 1.5 - 3 kHz band [Fig 4.14(a)]. As the dive progresses, however, the data becomes considerably more scattered, most likely as a result of distortion producing spurious multiples within the click which are being detected as the strongest peak values in the autocorrelation function. This general picture is similar when correlation is performed on the same clicks filtered in the higher frequency bands, although the scatter appears to become progressively worse [Fig 4.14(b)-(d)]. The plots do show, however, that IPI values oscillate around an equilibrium level of approximately 7.5 ms, which corresponds to the IPI obtained by visual inspection of the click waveforms. The scatter in the data may be reduced substantially and the IPI trend more clearly visualised by applying a simple moving average filter.

Figures 4.15 - 4.18 show the results of applying a 50 point moving average filter to the sets of IPI values obtained through autocorrelation analysis for sequences SW2, SW3, SW6 and



**Figure 4.14** Raw plots of IPI data obtained from autocorrelation through sequence SW3. Plots result from autocorrelation analysis of waveform data in the bands (a) 1.5-3 kHz pulses 1-3, (b) 3-6 kHz pulses 1-3, (c) 3-6 kHz pulses 2-4, (d) 6+ kHz



**Figure 4.15** Plots showing smoothed trends in IPI for autocorrelation in different frequency bands through sequence SW2. Smoothing is performed with a 50 point moving average filter, (a) 1.5-3 kHz pulses 1-3, (b) 3-6 kHz pulses 1-3, (c) 3-6 kHz pulses 2-4, (d) 6+ kHz pulses 1-3

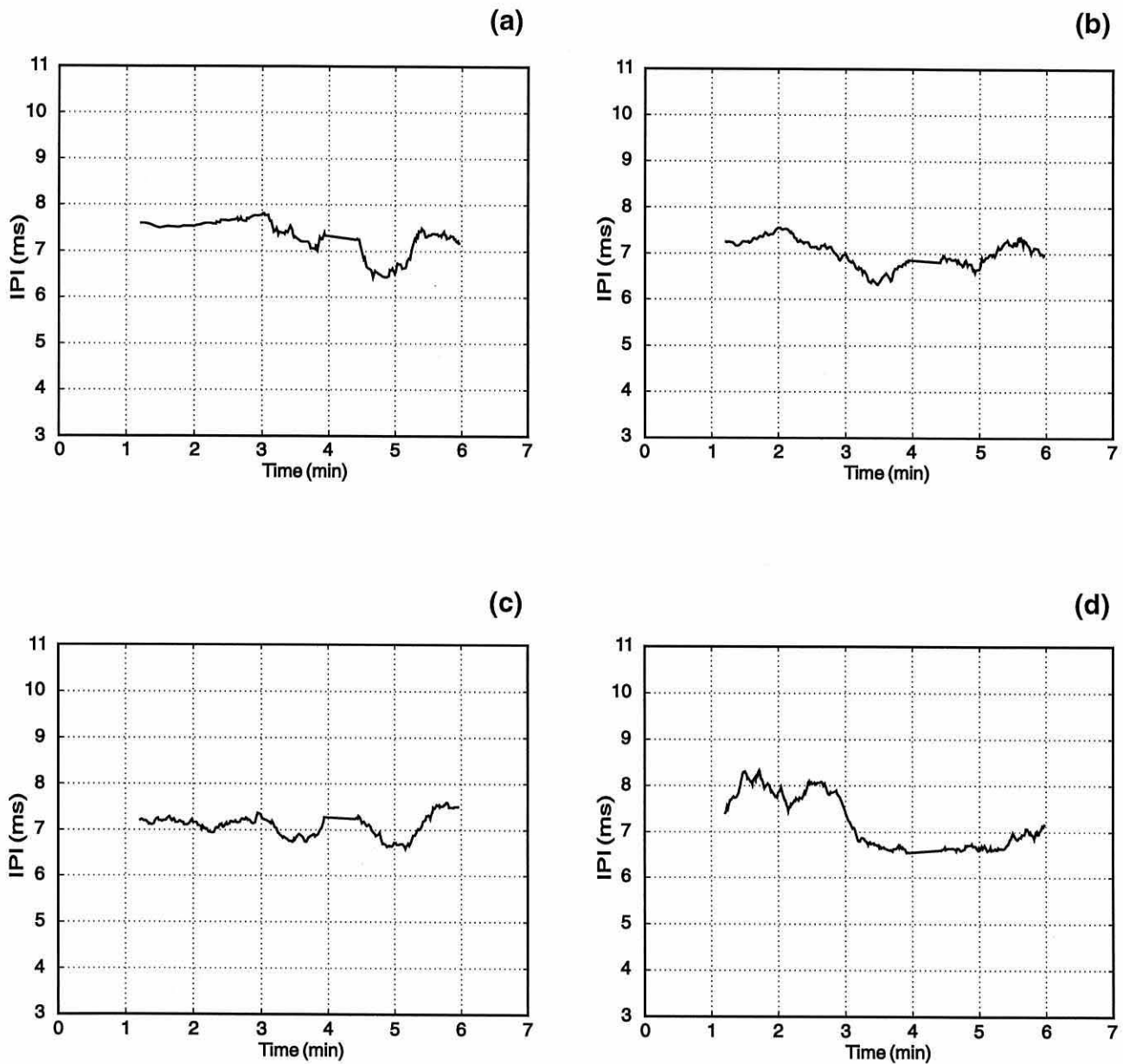


**Figure 4.16** Plots showing smoothed trends in IPI for autocorrelation in different frequency bands through sequence SW3. Smoothing is performed with a 50 point moving average filter, (a) 1.5-3 kHz pulses 1-3, (b) 3-6 kHz pulses 1-3, (c) 3-6 kHz pulses 2-4, (d) 6+ kHz pulses 1-3

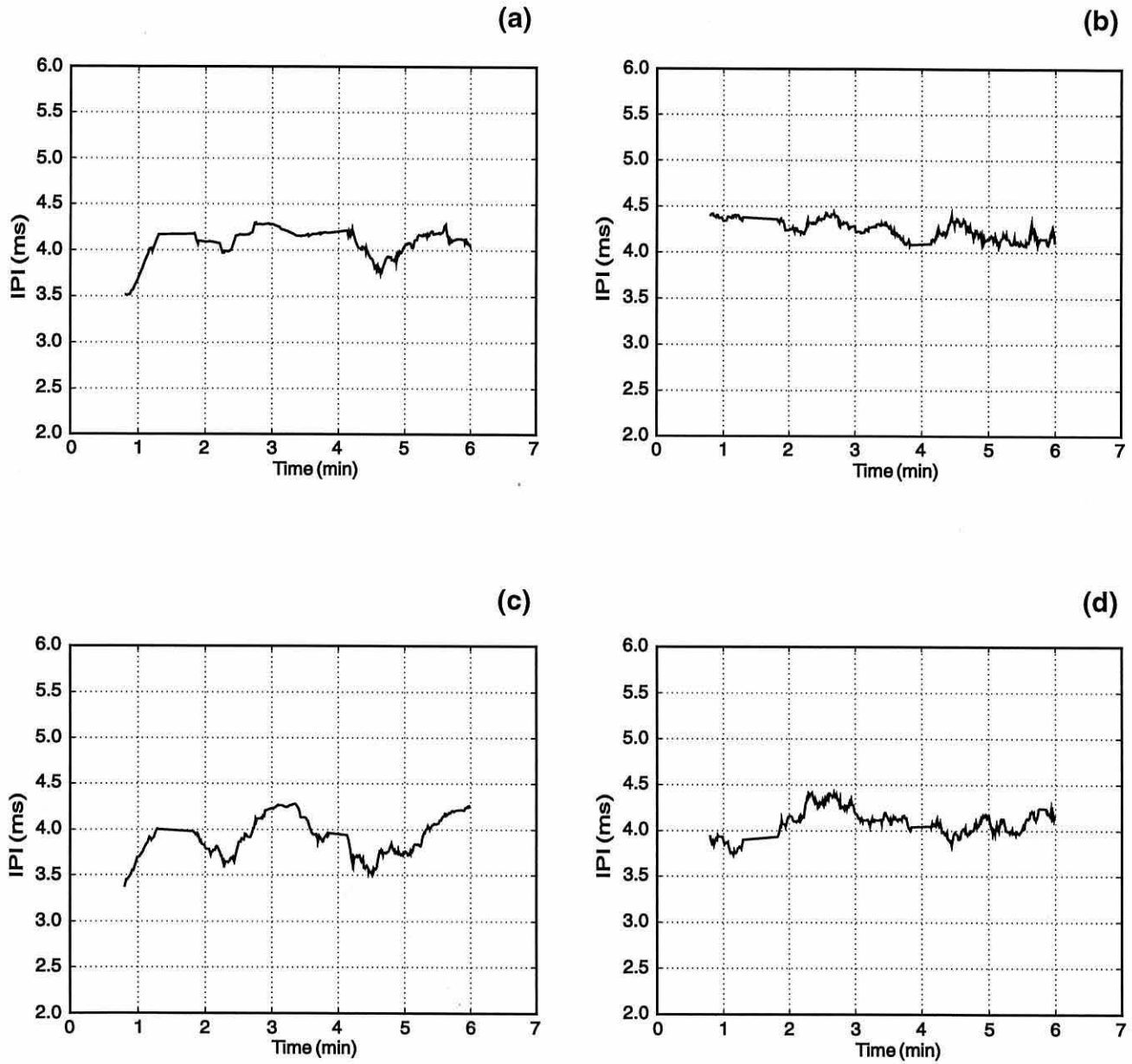


**Figure 4.17** Plots showing smoothed trends in IPI for autocorrelation in different frequency bands through sequence SW6. Smoothing is performed with a 50 point moving average filter, (a) 3-6 kHz pulses 1-3, (b) 3-6 kHz pulses 2-4, (c) 6+ kHz pulses 1-3, (d) 6+ kHz pulses 2-4

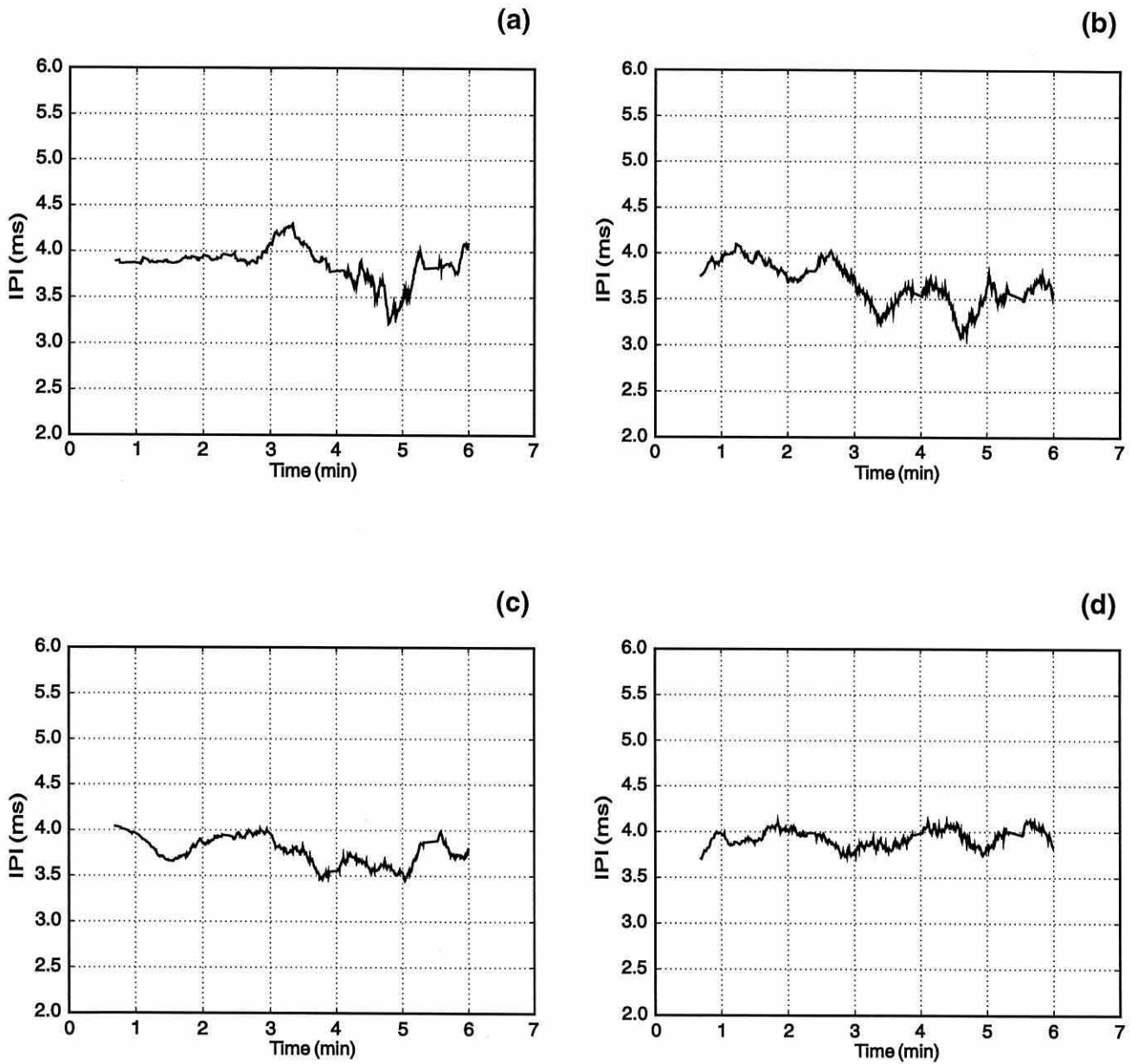


**Figure 4.18** Plots showing smoothed trends in IPI for autocorrelation in different frequency bands through sequence SW9. Smoothing is performed with a 50 point moving average filter, (a) 3-6 kHz pulses 1-3, (b) 3-6 kHz pulses 2-4, (c) 6+ kHz pulses 1-3, (d) 6+ kHz pulses 2-4

SW9. Autocorrelation was performed on all clicks across the first 6 minutes of each sequence, which produced enough IPI values for subsequent smoothing. It is a reasonable assumption that the whales were diving at a fairly constant rate during these sequences, depth sounder traces from other whales suggest descent rates of about  $1.6 \text{ ms}^{-1}$  (approximately 100 m per minute). Therefore all the whales were likely to have been at depths between 0 and 900 metres whilst their clicks were being recorded. Referring to Chapter 3, equation (3.3) can be used to determine the likely range of sound velocities in spermaceti oil under these conditions, and hence the likely range of variation in IPI. At the lowest temperature of  $22^\circ\text{C}$  and highest pressure of 9.1 MPa,  $c_{\text{spermaceti}} = 1549 \text{ ms}^{-1}$ , whereas at the highest temperature of  $38^\circ\text{C}$  and lowest pressure of 0 MPa,  $c_{\text{spermaceti}} = 1395 \text{ ms}^{-1}$ . According to these values, and assuming a large male sperm whale to have a spermaceti sac length of 5 m, IPI should have a minimum value of approximately 6.5 ms and a maximum value of approximately 7.2 ms, a total variation of only 0.7 ms. Therefore one would ideally expect the IPI data to exhibit only this much variation between any two extremes of IPI. Figures 4.15 - 4.18 show the total variation in IPI of the averaged data to be largely within the range expected, although there are instances when the theoretical extremes are exceeded.

Figures 4.15(a) and 4.16(a) show IPIs measured from male click waveforms in the band 1.5 to 3 kHz. Pulse structure is easiest to measure visually in this band and will produce some of the best correlations, but unfortunately the pulse decay is very rapid and a well defined pulse structure does not persist with increasing dive time. Nevertheless both these plots suggests a downward trend in IPI with dive time. A reduction in IPI would be expected from a diving whale as increasing pressure will increase sound velocity in the oil. Figures 4.15(b) and 4.16(b) show IPI values from male clicks bandpass filtered between 3 kHz and

6 kHz. While the pulse train in this band is usually more evident visually, the signals were likely being recorded outside the main transmission lobe as dives progressed, hence introducing distortion which may cause the autocorrelation analysis to produce lower coefficient values when comparing first and second pulses than would be the case for the 1.5 kHz - 3 kHz band. However the plots are fairly stable with at least an initial reduction in IPI [Fig 4.16(b)]. Figures 4.15(c) and 4.16(c) show IPI's for male clicks filtered in the same frequency band but this time IPI is obtained by ignoring the first pulse in the train and correlating with the following three. These pulses may all have had similar transmission lobes and be less distorted with respect to one another, but signal strength and hence signal to noise ratio is weaker. Again the IPI trend is fairly stable, although reduction in IPI with increasing dive time is less obvious. Figures 4.16(a)-(c) show IPI's to increase at about 5 minutes dive time, suggesting that the autocorrelation is tracking similar features in each case. In Figures 4.15(d) and 4.16(d) the results are more difficult to interpret, with an increase of IPI with time [Fig 4.15(d)] and large values in the early dive stages [Fig 4.16(d)]. These may be spurious readings due to the marked dissimilarity between envelopes of first and second pulses at very high frequencies, and the very low signal to noise ratio of successive pulses.

Figures 4.17 and 4.18 show the smoothed IPI results from autocorrelation of female click sequences SW6 and SW9. The mean equilibrium value appears to be approximately 4 ms which would be expected from animals of this size. Figures 4.17 and 4.18 parts (a) and (b) are in the 3 to 6 kHz band, (a) being correlation of pulses 1 - 3 and (b) being correlation of pulses 2 - 4. Parts (c) and (d) are in the 6+ kHz band with pulse numbers corresponding to parts (a) and (b) respectively. The figures suggest that autocorrelation in the 3 - 6 kHz band

produces slightly more realistic trends in IPI than does correlation in higher frequency bands, probably by virtue of a higher signal to noise ratio of successive pulses in this band. Female clicks were not bandpass filtered between 1.5 and 3 kHz, as pulse structure does not emerge below 3 kHz in female clicks.

### **4.3.2 Cepstrum Analysis Results**

Using sequences SW3 and SW9 as test sequences, it was found that generally *cepstrum* analysis with chi-squared windows produced IPI results with less scatter than analysis with boxcar windows, and chi squared windows with  $k=4$  produced acceptable values throughout. It was therefore decided to use chi-squared windows with  $k=4$  to extend analyses to sequences SW2 and SW6. Trial and error also showed that *cepstrum* analysis encompassing the first 3 pulses of the clicks, as opposed to pulses 2 - 4 or pulses 1 and 2 only, produced the best results with least scatter. *Cepstrum* analysis was therefore applied consistently with chi-squared ( $k=4$ ) windows across the first 3 pulses of each click analysed, through the first six minutes of sequences SW2, SW3, SW6 and SW9. Figure 4.19 shows plots of raw IPI values obtained from the first six minutes of sequences SW2, SW3, SW6 and SW9 by *cepstrum* analysis with  $k=4$  chi-squared windows. The scatter within the plots is obvious but in comparison to the raw autocorrelation plots [Fig 4.14] the scatter is clearly much less. Moving average filters were applied to the *cepstrum* IPI data and Figure 4.20 shows the results of applying a 50 point moving average filter to the first six minutes of IPI data from the four sequences SW2, SW3, SW6 and SW9. In the case of male sperm whale clicks [Figs 4.20(a) & (b)] IPIs are quite stable between 7 and 7.5 ms and certainly exhibit

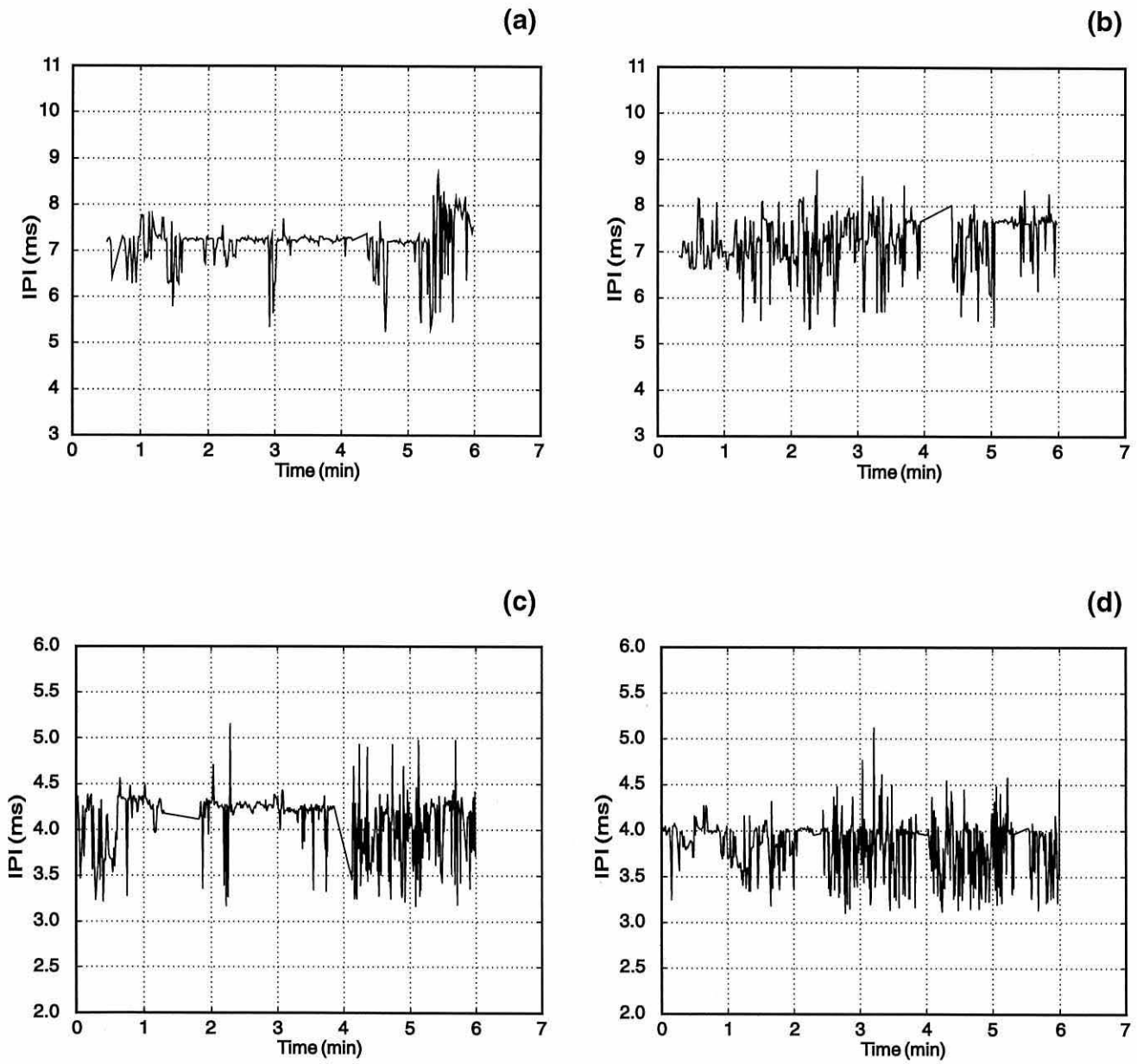


**Figure 4.19** Raw plots of IPI data obtained from cepstrum analysis through sequences (a) SW2, (b) SW3, (c) SW6 and (d) SW9.

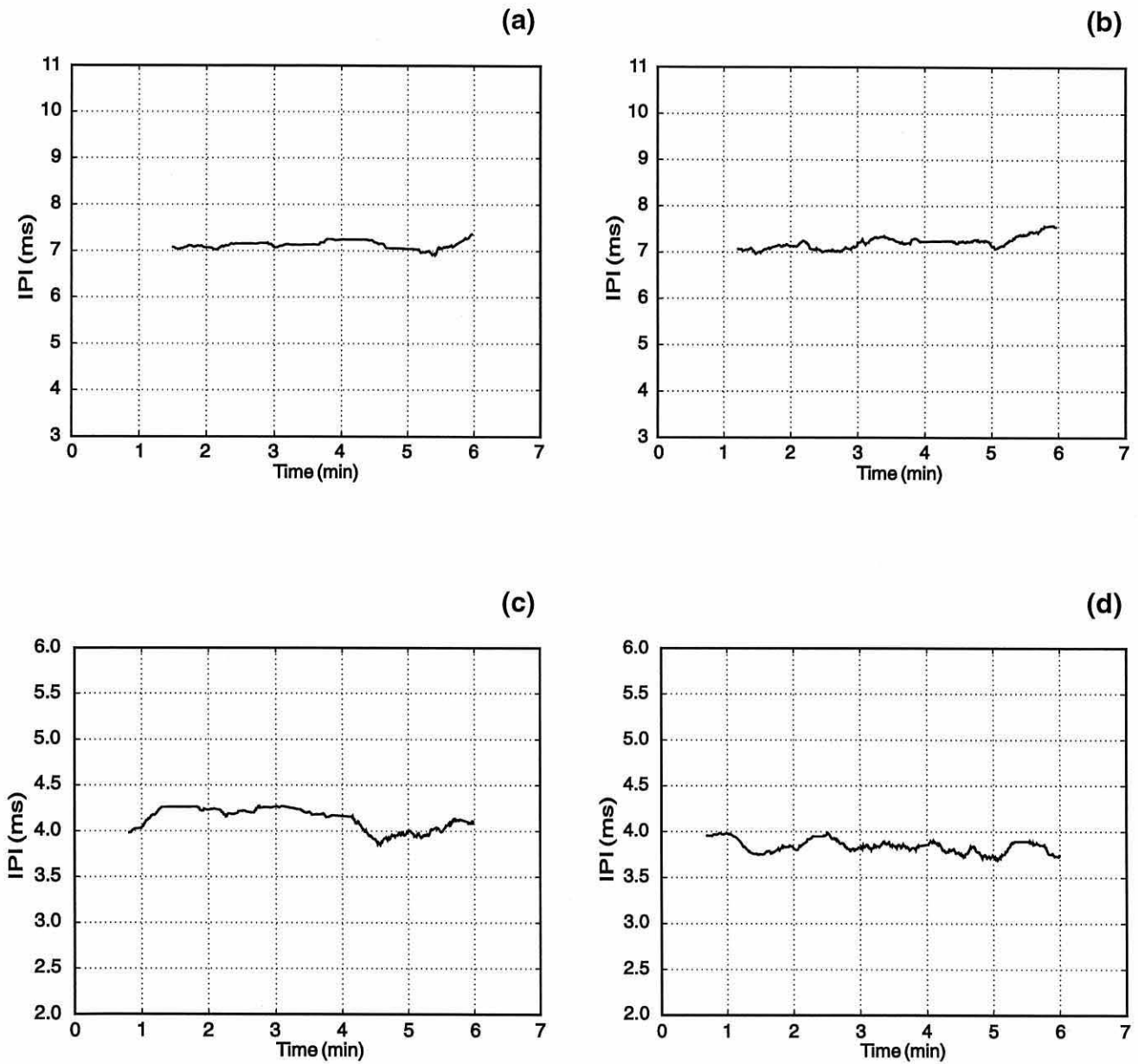


**Figure 4.20** Plots showing smoothed trends in IPI for cepstrum analysis through sequences (a) SW2, (b) SW3, (c) SW6 and (d) SW9. Smoothing is performed using a 50 point moving average filter.

less variation than the equivalent autocorrelation plots [Figs 4.15 & 4.16], although there is little indication of decreasing IPI with time. Figures 4.20(c) and (d) show IPI trends for the two female sequences SW6 and SW9, which show IPI decreasing slightly with dive time as expected. SW6 begins with an increase in IPI but also appears to have a slightly greater overall IPI than SW9, suggesting the former to be a slightly larger animal.

Results from the *cepstrum* analysis were used to calculate mean IPI's from the first six minutes of each of the four click sequences, and the results are summarised in Table 4.1. One way analysis of variance showed that all four data sets were significantly different from each other at the 95% level with an F value of 8306 and P value of 0. Gordon (1991) gives a polynomial for calculating sperm whale body lengths from spermaceti sac lengths thus:

$$L = 9.75 - 0.521S + 0.068S^2 + 0.057S^3 \quad (4.4)$$

where S is given by

$$S = IPI_x \frac{c_{spermaceti}}{2} \quad (4.5)$$

From Chapter 3, equation (3.3), an estimate of mean sound velocity in spermaceti oil during the first six to ten minutes of the dive can be made by using mid range values of temperature and pressure - yielding  $c_{spermaceti} \approx 1430 \text{ ms}^{-1}$ . Assuming this value of sound velocity,

Click Sequence Code	Number of clicks analysed	Mean IPI (ms)	Lower 95% Confidence Limit (ms)	Upper 95% Confidence Limit (ms)
SW2	327	7.09	7.03	7.15
SW3	356	7.31	7.25	7.37
SW6	502	4.10	4.08	4.12
SW9	629	3.83	3.81	3.85

**Table 4.1** Mean values of IPI for the first six minutes of each click sequence; IPI's obtained by *cepstrum* analysis. Upper and lower 95% confidence limits indicate that all means are significantly different from each other.

equations (4.5) and (4.4) can be used to estimate the body lengths of the four sperm whales in this study, using mean IPI values from Table 4.1. These calculations result in body lengths of SW2 = 16.3 m, SW3 = 17.0 m, SW6 = 10.2 m and SW9 = 10.0 m. Such results are consistent with known male and female sperm whale body lengths.

#### **4.4 Discussion and Conclusions**

Both autocorrelation analysis and *cepstrum* analysis show some promise in the measurement of sperm whale click intra-pulse intervals. *Cepstrum* analysis looks likely to be the more favourable technique for development, and with some prior knowledge of IPI for a given animal the method can be tailored to refine results. However, neither method in the form demonstrated is sufficiently robust to yield precise measurement of IPI's for each individual click, although long term smoothed trends and mean values can be obtained with some success. The results do suggest that modulation of click waveforms with chi-squared windows prior to FFT processing helps improve *cepstrum* measurement of IPI's. The smoothed trends in IPI, from both autocorrelation and *cepstrum* analysis, generally suggest that IPI's decrease during the first few minutes of feeding dives in accordance with the expected increase of sound velocity in spermaceti oil under increasing barometric pressure. However, this is not universally the case, and it is unclear whether features such as rapid changes in IPI are spurious readings caused by distorted signals or whether they represent real processes in the sperm whale head. It will be necessary to refine techniques for measurements of click IPI's before such questions can be answered.

The quality of IPI information obtainable from the analysis of sperm whale clicks may depend much upon signal to noise ratio and whale orientation with respect to hydrophones. If off axis distortion corrupts click pulse structure it may prove impossible to obtain reliable IPI information from every click recorded. However the longer term trends, or at least longer term averaged values of IPI, are readily obtainable and have been used to make reasonable estimates of sperm whale body lengths. If ocean going acoustic surveys of sperm whales were to be widely employed, using towed or fixed arrays of hydrophones to localise and count animals from their click vocalisations, the ability to process the received signals and extract IPI information for individual animals should be valuable. Such data would aid in the determination of sperm whale population composition in terms of animal size. Only the adult and sub-adult animals are known to click regularly, and hence calves could not be readily detected by such ocean going surveys. However the extreme sexual dimorphism of sperm whales means that surveys may expect to detect animals of between 10 and 19 metres in length. Such non-invasive monitoring would be a useful tool in the assessment of whale populations for their study and ultimately future conservation.

## Chapter 5

### Overview and Conclusions

The work presented in this thesis has expanded upon previous knowledge of sperm whale clicks. The original hypothesis of Norris and Harvey (1972), that clicks exhibit a multiple pulsed structure due to sound reflection from air cavities within the sperm whale head, is supported. The most likely function of sperm whale clicks is considered to be echolocation. The broadband impulsive nature of the clicks makes this the most likely explanation, and the clicks would seem to be of little value otherwise. When sperm whales are at depth they continue to click at fairly constant rates of between 1 and 2 s<sup>-1</sup>. Given that individual squid are such poor acoustic targets, with individual target strengths possibly in the order of -50 dB re 1μPa, it is possible that sperm whales are using their clicks to search for large shoals of squid, which present larger targets. Indeed Clarke et al (1993) note *“it seems likely that the sperm whale is obtaining 77% of its food by swimming through luminous shoals of slow swimming, neutrally buoyant squids and only about 23% by chasing faster swimming, larger cephalopods”*. If shoals of slow swimming squid luminesce, then perhaps vision has a limited role in feeding at depth - it might even be speculated that sperm whale clicks excite shoals into luminescence, although there is no evidence to support this. The final feeding event is still something of a mystery and has never been witnessed. From an energetic point of view it is unlikely that sperm whales chase and capture small individual prey items; feeding off large shoals of small squid seems a more likely scenario. Large, fast swimming species may have improved detectability to sperm whales as turbulent wakes can

reflect sound energy (Selivanovsky & Ezersky, 1996), however Clarke et al's data indicate that the majority of "Azorean" sperm whale prey is in fact composed of the small, slow swimming cephalopods.

One hypothesis proposes that sperm whales, and indeed other cetaceans, use loud sound pulses to disorient, stun or even kill prey, thus enabling its ease of capture (Norris & Muhl, 1983). Larsen and Johnsen (in Turnpenney and Nedwell, 1994) concluded that mortality of Atlantic Salmon *Salmo salar* and Cod *Gadus morhua* occurs when two critical criteria are met simultaneously, (i) incident peak sound pressure level of 229 dB re 1 $\mu$ Pa and (ii) rise time and decay of sound pulse of  $\leq$  1 ms. From research findings to date, neither of these criteria are met by sperm whale clicks. Squid do not have sensitive hearing structures (Moynihan, 1985) so they are unlikely to be disoriented by sperm whale clicks. Tissue damage arises when shock waves pass through tissues of different density, and high frequency signals where the wavelength is less than the body size can transfer much greater energy than signals where the wavelength exceeds body size. Damage is greatest at interfaces between tissue and gas filled cavities such as fish swim bladders. When signals are applied across such interfaces damage can occur as the reflected energy at the pressure release boundary layer distorts and stresses the tissue. Deep sea squid, however, are largely gelatinous and without bone structure or gas bladders, buoyancy sometimes being afforded by ammonium compounds in the gelatinous body tissue. This makes squid largely transparent to sound in seawater and hence unsusceptible to damage from pressure waves created by sperm whale clicks. Perhaps the most likely explanation is that sperm whales simply find a large aggregation of squid by echolocation, and then lunge through the shoal, sucking in prey with the large muscular tongue. Sperm whales with broken jaws have been

found with full stomachs (Berzin, 1971), and even healthy sperm whales have been found with prey in the stomach contents largely unmarked by the whales teeth. The fact that sperm whales tend to make creaks during their deep dives, which sound very much like rapid bursts of echolocation clicks, may indicate that the whale is tracking the movement of a shoal of squid during its final approach. While chasing individual squid is likely to be impractical, a large shoal may prove more attractive.

It is usually assumed that reception and processing of echolocation signals by odontocetes occurs via the usual auditory pathways, i.e. the ears. An alternative hypothesis was put forward by Goodson & Klinowska (1990) to explain the remarkable discrimination and tracking ability of dolphin sonars at close range during the final stages of food capture. It is hypothesised that dolphin teeth act as echo-receptors matched to the spectral characteristics of the click. The sensory mechanism is hypothesised to involve excitation of nerves within the dentine tubules of the teeth, invoking potentials that are transmitted directly to the higher brain centres independent of the normal auditory pathways. In addition it is hypothesised that the offset alignment of teeth between the left and right sides of the dolphin jaw serves to resolve the lateral ambiguity of received echolocation signals that would otherwise result, i.e. the animal is able to discriminate from which side of its head an echo return originated. Goodson & Klinowska point out that the inter-tooth spacing along either side of the jaw is remarkably consistent and approximates to the wavelength of 130 kHz sonar signal components. It is interesting to note that the inter-tooth spacing of large sperm whales is in the order of 0.15 m, which is approximately the wavelength of a 10 kHz sound wave in seawater. The region of the frequency spectrum around 10 kHz has been suggested as the most effective operating region of sperm whale sonar.

The measurements of sound velocity in spermaceti oil made in this dissertation suggest that the variability of intra-pulse intervals within sperm whale clicks, as a result of changing temperature and pressure within the sperm whale head, will be small compared to the IPI itself. This fact strengthens the case for using sperm whale click IPI's to measure individual whale body lengths during passive acoustic surveys. The results of Chapter 4 indicate that average IPI's can be assessed across several minutes of sequential clicks by applying signal processing techniques. In terms of acoustic censusing of whale populations such techniques could prove extremely valuable. If ocean going vessels were to tow hydrophone arrays across oceanic transects and record sperm whale clicks, it should be possible to determine bearing to individual animals given the appropriate array geometry. The rate of change of bearing could be used to estimate the range of whales from the hydrophone array, by the assumption that sperm whales are approximately stationary in the horizontal plane relative to survey vessels. Such methods would enable the number of "vocalising" whales to be counted across a given area of ocean. Add to this further processing techniques to measure IPI's from sequences of click waveforms from each animal, and one may obtain approximate sizes of the whales being detected, especially if several minutes of sequential clicks can be processed from any given whale.

Such data would be helpful in determining the size (and to some extent age) structure of sperm whale populations. Sperm whale calves do not make deep dives, and hence do not produce long series of echolocation clicks that would be picked up by oceanic surveys. Only adult and sub-adult animals are likely to be detected by acoustic surveys, and the sexual dimorphism of sperm whales means that bull males and females would be relatively

easy to distinguish acoustically. One could expect to collect length data from whales that are anywhere between 10 metres and 19 metres in length. The distribution of sperm whales is such that females and calves remain in tropical and sub-tropical latitudes all year round. As males grow and mature they gradually move to higher latitudes until they become large bull males, at which point they will undertake periodic migrations from high latitudes to the lower latitudes to mate with females. Acoustic surveying across a range of latitudes, with the application of acoustic body length measurement, would help to enhance our understanding of the distribution of sperm whales. Given sufficient survey coverage at low latitudes during the breeding season, it may be possible to assess the number of returning males.

Analysis of sperm whale clicks has the potential to become a useful tool in the benign assessment of sperm whale populations in the open ocean. If methods for tracking, and ultimately size discrimination of individual whales, along oceanic transects could be developed and realised in dedicated hardware for vessels of opportunity, valuable data on sperm whale populations would be obtained.

## References

**Alder-Fenchel H S (1980)** Acoustically derived estimate of the size distribution for a sample of sperm whales, *Physeter catodon*, in the Western North Atlantic. *Canadian Journal of Fisheries and Aquatic Science* 37(12), 2358-2361

**Amundin M and Andersen S H (1983)** Bony nares air pressure and nasal plug muscle activity during click production in the harbour porpoise, *Phocoena phocoena*, and the bottlenose dolphin, *Tursiops truncatus*. *Journal of Experimental Biology* 105, 275-282

**Amundin M (1991)** Sound production in Odontocetes with emphasis on the Harbour Porpoise, *Phocoena phocoena*. *Doctoral Dissertation, Department of Zoology, Stockholm University*

**Au W W L (1980)** Echolocation signals of the Atlantic Bottlenose Dolphin, *Tursiops truncatus*, in open waters. in *Animals Sonar Systems*, edited by R G Bunsel & J F Fish, Plenum Press, New York & London. pp 251-282

**Au W W L (1993)** The sonar of dolphins. *Springer-Verlag, New York and Berlin.*  
277.pp

- Backus R H and Schevill W E (1966)** Physeter Clicks. *in Whales, Dolphins and Porpoises, edited by K S Norris, University of California, Berkeley, pp 510-528*
- Bark L S, Ganson P P and Meister N A (1964)** Tables of the velocity of sound in seawater. *Pergamon Press, Oxford, vol 21, 180 pp*
- Berzin A A (1971)** The Sperm Whale. *Israel Program for Scientific Translations Ltd, Keter Press, Jerusalem, 394 pp*
- Bogert B P, Healy M J R and Tukey J W (1963)** The quefrency analysis of time series for echoes: cepstrum, pseudo-autocovariance, cross-cepstrum and saphe cracking. *in Proceedings of the Symposium on Time Series Analysis, edited by M. Rosenblatt, Wiley New York, pp 209-243*
- Bunsel R G and Dzedzic A (1967)** Observations sur le comportement et les emmissions acoustiques du cachalot lors de la chasse. *Bocagiana 14, 1-15*
- Capps R N (1989)** Elastomeric Materials for Acoustic Applications. *NRL, Orlando, Florida, pp 243-254*
- Clarke M R (1978a)** Structure and proportions of the spermaceti organ in the sperm whale. *Journal of the Marine Biological Association of the United Kingdom 58, 1-17*

**Clarke M R (1978b)** Physical properties of spermaceti oil in the sperm whale. *Journal of the Marine Biological Association of the United Kingdom* 58, 19-26

**Clarke M R (1978c)** Buoyancy control as a function of the spermaceti organ in the sperm whale. *Journal of the Marine Biological Association of the United Kingdom* 58, 27-71

**Clarke M R (1979)** The head of the sperm whale. *Scientific American* 240(1), 106-117

**Clarke M R, Martins H R and Pascoe P (1993)** The diet of sperm whales, *Physeter macrocephalus* Linnaeus 1758, off the Azores. *Philosophical Transactions of the Royal Society of London, series B* 339, 67-82

**Coates R F W (1990)** Underwater acoustic systems. *MacMillan New Electronics, Introductions to Advanced Topics, London, 188 pp*

**Cranford T W, Amundin M and Norris K S (1996)** Functional morphology and homology in the odontocete nasal complex: implications for sound generation. *Journal of Morphology* 228(3), 223-285

**Evans W E and Prescott J H (1962)** Observations of the sound capabilities of the bottlenose porpoise: A study of whistles and clicks. *Zoologica* 47, 121-128

- Flewellen C G and Morris R J (1978)** Sound velocity measurements on samples from the spermaceti organ of the sperm whale, *Physeter catodon*. *Deep Sea Research* 25, 269-277
- Goodson A D and Klinowska M (1990)** A proposed echolocation receptor for the bottlenose dolphin, *Tursiops truncatus*: modelling the receive directivity from tooth and jaw geometry. in *Sensory Abilities of Cetaceans*, edited by J Thomas and R Kastelein, Plenum Press, New York, pp 255-267
- Goodson A D and Sturtivant C R (1996)** Sonar characteristics of the harbour porpoise (*Phocoena phocoena*): source levels and spectrum. *ICES Journal of Marine Science* 53, 465-472
- Gordon J C D (1987)** The behaviour and ecology of sperm whales off Sri Lanka. *PhD Thesis, University of Cambridge*
- Gordon J C D (1991)** Evaluation of a method for determining the length of sperm whales, *Physeter catodon*, from their vocalisations. *Journal of Zoology, London* 224, 301-314
- Hiby A R and Hammond P S (1989)** Survey techniques for estimating abundance of cetaceans. *Reports of the International Whaling Commission, Special Issue 11*, edited by G P Donovan, Cambridge pp 47-80

**Hollien H P, Hollien P, Caldwell D K and Caldwell M C (1976)** Sound production by the Atlantic bottlenose dolphin *Tursiops truncatus*. *Cetology* 26, 1-8

**Kaye G W C and Laby T H (1966)** Tables of Physical and Chemical Constants. *Longmans, 13th Edition, 249 pp*

**Levenson C (1974)** Source level and bistatic target strength of the sperm whale, *Physeter catodon*, measured from an oceanographic aircraft. *Journal of the Acoustical Society of America* 55(5), 1100-1103

**Lockyer C (1977)** Observations on diving behaviour of the sperm whale, *Physeter catodon*. in *A Voyage of Discovery*, edited by M Angel, Pergamon Press, Oxford pp 591-609

**Lynn P A and Fuerst W (1992)** Introductory Digital Signal Processing, with computer applications. *John Wiley and Sons, Chichester, New York, Brisbane, Toronto & Singapore, 371 pp*

**Mackay R S (1980)** A theory of the spermaceti organ in sperm whale sound production. in *Animal Sonar Systems*, edited by R G Bunsel & J F Fish, Plenum Press, New York & London pp 937-940

**Mohl B, Larsen E and Amundin M (1981)** Sperm whale size determination: outlines of an acoustic approach. *FAO Fisheries Series* 5(3), 327-332

- Morris R J (1973)** The lipid structure of the spermaceti organ of the sperm whale (*Physeter catodon*). *Deep Sea Research* 20, 911-916
- Morris R J (1975)** Further studies into the lipid structure of the spermaceti organ of the sperm whale (*Physeter catodon*). *Deep Sea Research* 22, 483-489
- Moynihan M (1985)** Why are cephalopods deaf? *American Naturalist* 125(3), 465-469
- Mutlu E (1996)** Target strength of the common jellyfish (*Aurelia aurita*): a preliminary experimental study with a dual beam acoustic system. *ICES Journal of Marine Science* 53, 309-311
- Noll A M (1967)** Cepstrum pitch determination. *Journal of the Acoustical Society of America* 41(2), 293-309.
- Norris K S, Dormer K J, Pegg J and Leise G T (1971)** The mechanism of sound production and air recycling in porpoises. *A preliminary report in Proceedings of the VIII Conference on Biological Sonar & Diving Mammals, Menlo Park, CA. Stanford Research Institute, pp 113-129*
- Norris K S and Harvey G W (1972)** A theory for the function of the spermaceti organ of the sperm whale, *Physeter catodon*. in *Animal Orientation and Navigation* edited by S R Galler, K Schmidt-Koenig, G J Jacobs and R E Belleville, *NASA special publications* 262, Washington, DC pp 397-417

- Norris K S and Mohl B (1983)** Can odontocetes debilitate prey with sound? *American Naturalist* 122, 85-104
- Prestwich K N (1994)** Energetic constraints on acoustic signalling. *American Zoologist* 34, 625-643
- Purves P E and Pilleri G E (1983)** Echolocation in Whales and Dolphins. *Academic Press, London*
- Ridgway S H, Carder D A, Green R F, Gaunt A S, Gaunt S L L and Evans W E (1980)** Electromyographic and pressure events in the nasolaryngeal system of dolphins during sound production. in *Animal Sonar Systems*, edited by R G Bunsel and J F Fish, Plenum Press, New York & London, pp 239-250
- Ridgway S H and Carder D A (1988)** Nasal pressure and sound production in an echolocating white whale (*Delphinapterus leucas*). in *Animal Sonar Systems: Process and Performance*, edited by P E Nachtigall and P W B Moore, Plenum Press, New York, pp 53-60
- Selivanovsky D A and Ezersky A B (1996)** Sound scattering by the hydrodynamic wake of sea animals. *ICES Journal of Marine Science* 53, 377-381

- Selfridge A R (1985)** Approximate material properties in isotropic materials. *IEEE Transactions on Sonics and Ultrasonics* 32(3), 381-394
- Smith P F (1954)** Further measurements of the sound scattering properties of several marine organisms. *Deep Sea Research* 2, 71-79
- Suga N (1990)** Biosonar and neural computation in bats. *Scientific American* 262, 34-41
- Timme R W (1972)** Speed of sound in castor oil. *Journal of the Acoustical Society of America* 52(3), 989-992
- Turnpenny A W H and Nedwell J R (1994)** The effects on marine fish, diving mammals and birds of underwater sound generated by seismic surveys. *Consultancy Report, Fawley Aquatic Research Laboratories Ltd. 40 pp*
- Urick R J (1975)** Principles of Underwater Sound for Engineers. *McGraw Hill, New York, Revised Edition, 384 pp*
- Watkins W A (1977)** Acoustic behaviours of sperm whales. *Oceanus* 20, 50-58
- Watkins W A, Daher M A, Fristrup K M, Howald T J and Disciara G N (1993)** Sperm Whales tagged with transponders and tracked underwater by sonar. *Marine Mammal Science* 9(1), 55-67

- Weilgart L S and Whitehead H (1988)** Distinctive vocalisations from mature male sperm whales, *Physeter macrocephalus*. *Canadian Journal of Zoology* 66, 1931-1937
- Weilgart L S (1990)** Vocalisations of the sperm whale, *Physeter macrocephalus*, off the Galapagos Islands as related to behavioural and circumstantial variables. *PhD thesis, Dalhousie University, Halifax, Nova Scotia.*
- Whitehead H and Weilgart L S (1990)** Click rates from sperm whales. *Journal of the Acoustical Society of America* 87(4), 1798-1806
- Worthington L V and Schevill W E (1957)** Underwater sounds heard from sperm whales. *Nature* 180, 291
- Yost W A, Hill R, and Perez-Falcon T (1978)** Pitch and pitch discrimination of broadband signals with rippled power spectra. *Journal of the Acoustical Society of America* 63(4), 1168-1173

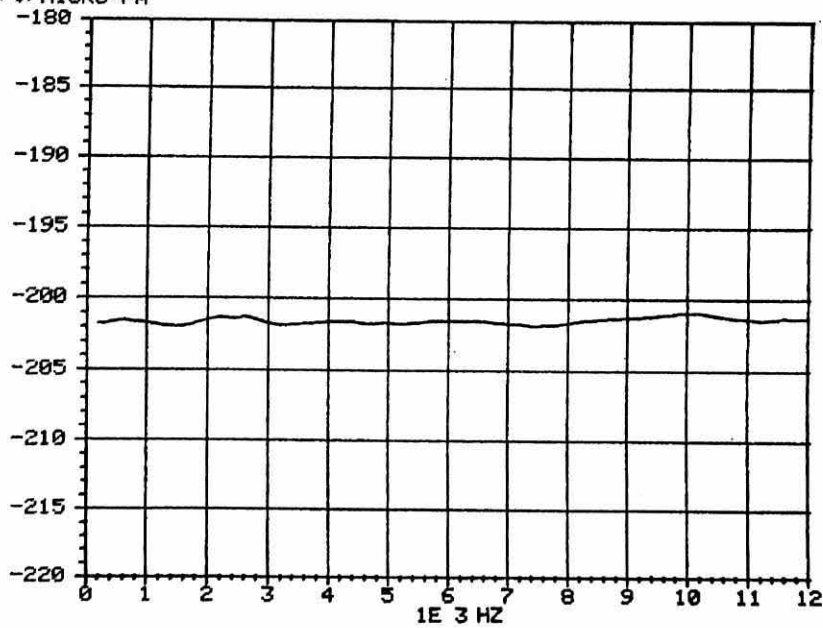
# Appendix 1

## Frequency & Polar Response of Benthos AQ-4 Hydrophone Element

XDCR TYPE: AQ4, S/N: X, REC. VOLT. SENS.  
REMARKS:

18-JUN-85 02:39:41

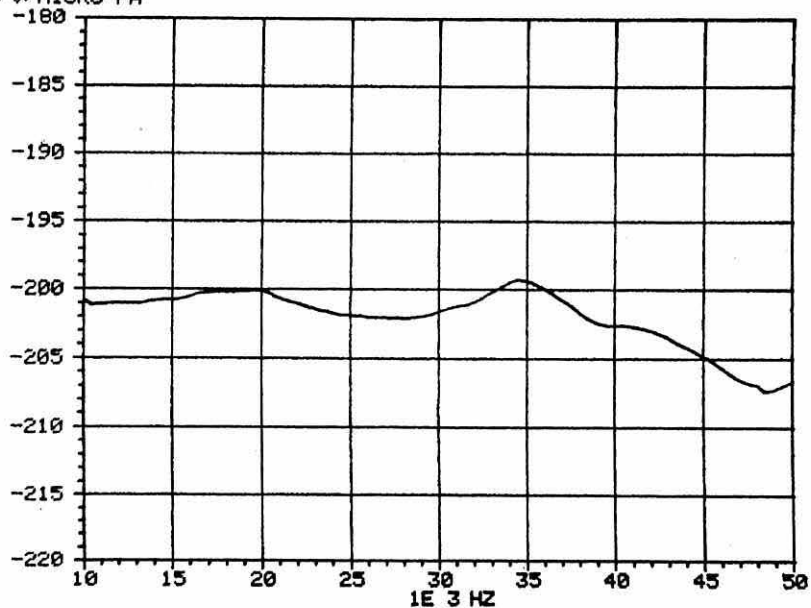
DB//V/MICRO-PA



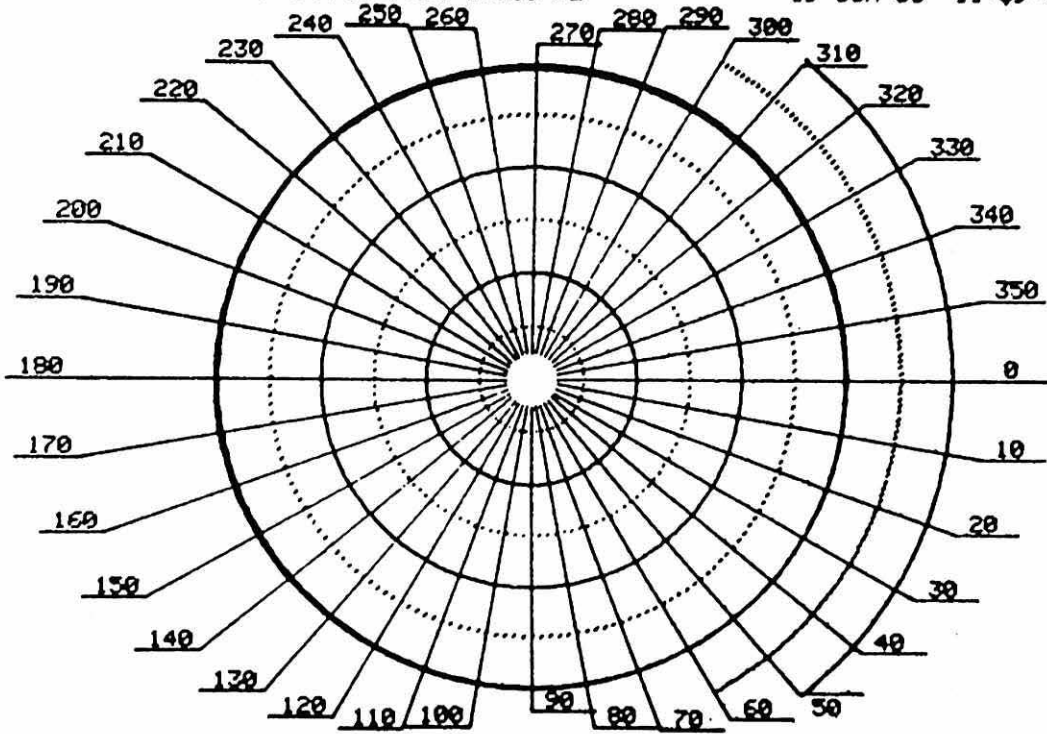
XDCR TYPE: AQ4, S/N: X, REC. VOLT. SENS.  
REMARKS:

19-JUN-85 11:50:45

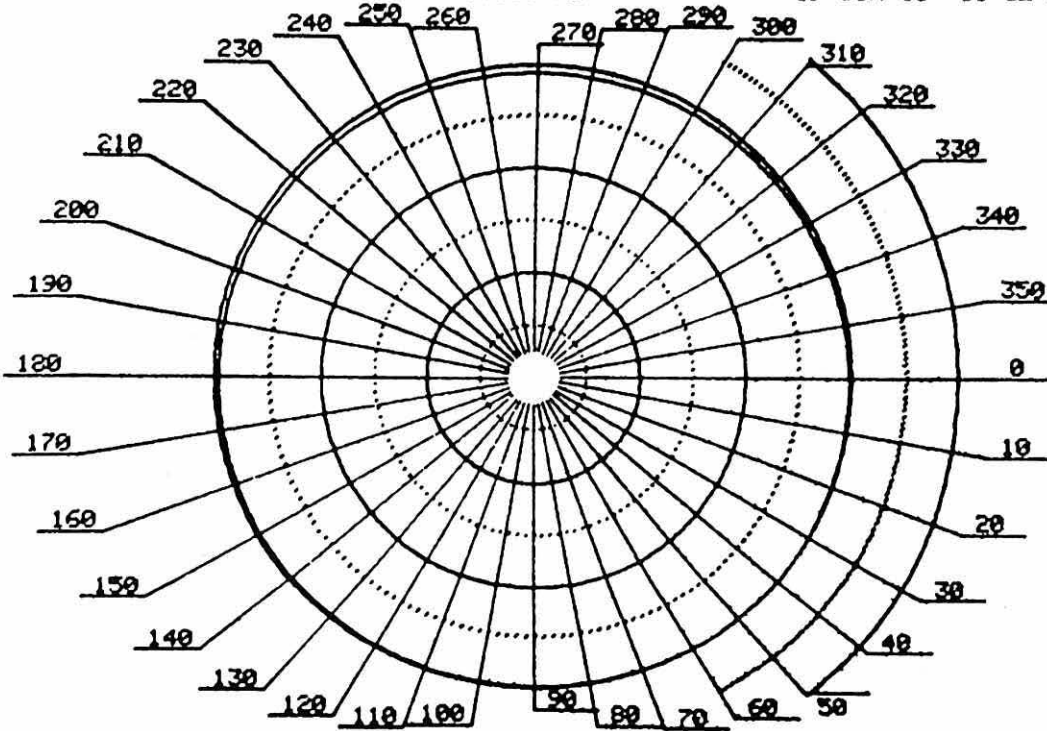
DB//V/MICRO-PA



NUJC NPT, XDR #AQ4, S/N 1, FREQ 10000 HZ 19-JUN-85 11:09:41

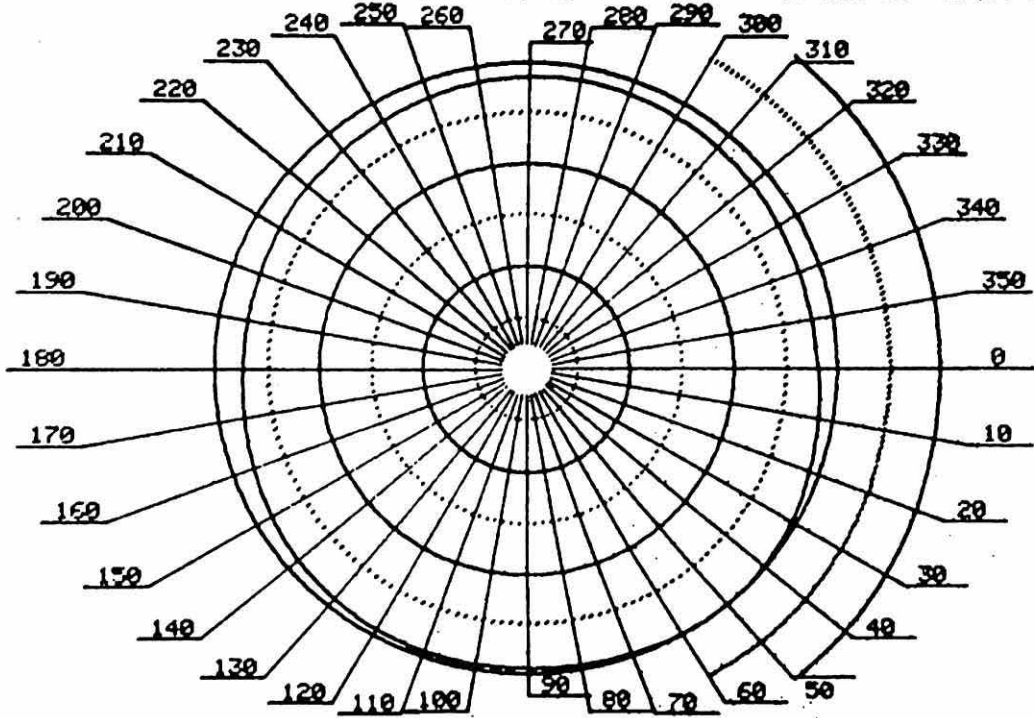


NUJC NPT, XDR #AQ4, S/N 1, FREQ 20000 HZ 19-JUN-85 11:32:24



NUJC NPT, XDR #AQ4, S/N 1, FREQ 37600 HZ

19-JUN-85 11:54:41



## Appendix 2

### Specifications of Nagra IV-SJ Reel-Reel Tape Recorder and Sony TCD-D10 PROII DAT Recorder

#### Nagra IV-SJ Reel-Reel Tape Recorder

##### **Dimensions and Weight**

Overall Dimensions	333 x 242 x 113 mm
Thickness of Anticorodal sheet used for box	2 mm
Thickness of Tape Deck	3 mm
Empty Weight	6.15 Kg
Weight with Ordinary Batteries	7.3 Kg

##### **Power Supply**

Supply voltage, direct current, positive to the ground	12 to 30 V
Current Consumption	
On Test	120 mA
On Line Playback	205 mA
On Record : Direct	260 mA
Mic (1 BK 2619)	465 mA
On Rapid Rewind	305 mA
Type of Batteries Used (12 cells)	
CEI Standard	R 20
ASA Standard	D and L 90
Approximate length of Battery Life	26 hours

##### **Magnetic Tape**

Nominal Width	6.25 mm
Admissible Thickness	12 to 50 $\mu$ m
Maximum reel diameter with lid open	178 mm
Recording time at 19 cm/s (17.5 ips)	45 min
Maximum reel diameter with lid closed	127 mm
Recording time under same conditions	22 min
Rewind time with 35 $\mu$ m tape	2 min

##### **Tape Transport**

Switchable nominal speeds	38.1 cm/s (38.1 ips)
	19.05 cm/s (7.5 ips)
	9.525 cm/s (3.75 ips)
	3.81 cm/s (1.5 ips)

Stability of the nominal speed in relation to the temperature (within the specified range), the position of the recorder, the distribution of the tape between the reels, and the supply voltage (except on 3.81 cm/s)	±0.1%
<b>Wow and Flutter</b>	
Weighted peak-to-peak value, DIN 45 507 standard	38 cm/s ±0.05% 19 cm/s ±0.07% 9.5 cm/s ±0.12% 3.8 cm/s ±0.25%
Unweighted RMS value, NAB standard	38 cm/s ±0.06% 19 cm/s ±0.08% 9.5 cm/s ±0.13% 3.8 cm/s ±0.19%
Starting time	3 s

**Direct Recording Tracks**

Amplifier Chain (without microphone amplifiers)

Input impedance	100 KΩ
Overall accuracy of the attenuator	±0.1 dB
Frequency response (2.5 Hz to 35 kHz)	±0.3 dB
Input voltage for recording at max peak level, max sensitivity	10 mV
Maximum admissible level for a distortion of 1% in relation to the maximum peak level	+8 dB
Signal to noise ratio	66 dB (linear) 74 dB (ASA A weighted)
Crosstalk attenuation at 1 kHz	80 dB
High pass filter attenuation at 20 kHz	3 dB, 12 dB per octave

**Control Instrument**

<b>Peak Indication</b>	
semi-logarithmic scale, usable from -10 to +23 dB	
Frequency response 2.5 kHz	-3 dB
Frequency response 10 Hz to 35 kHz	±0.5 dB
Integration time for 2 dB below reference deviation	5 ms ±20%
<b>RMS (sonometer) indication</b>	
Normalised scale, usable from -10 to +12 dB	
Frequency response from 10 Hz to 35 kHz	±0.5 dB
Fast integration time, 200 ms for 1 dB below ref deviation	±0.5 dB
Slow integration time, 500 ms for 4 dB below ref deviation	±0.5 dB
Fast integration time, 200 ms for -1 dB	±0.5 dB
Reading accuracy below 0 dB	±0.5 dB
Reading accuracy above 0 dB	±0.2 dB

**Recording and Playback**

Nominal recording level, identical to maximum peak level (MPL)	320 nWb/m for NAB 405 nWb/m for CCIR
Bias frequency	150 kHz
Bias switchable according to tape used, five possible values	
Tape used for testing	3M 177 for NAB LPR 35 LH for CCIR
Erase efficiency in relation to MPL	80 dB
Frequency response, recording at 20 dB below MPL	
38 cm/s, 25 Hz to 35 kHz	±1.0 dB
19 cm/s, 25 Hz to 20 kHz	±1.0 dB
9.5 cm/s, 25 Hz to 10 kHz	±1.5 dB
3.8 cm/s, 25 Hz to 3.5 kHz	±1.5 dB
Third harmonic distortion at MPL	1.5%
Signal to noise ratio	
38 cm/s	55 dB NAB (Linear)
38 cm/s	57 dB CCIR (Linear)
38 cm/s	62 dB NAB (A weighted)
38 cm/s	64 dB CCIR (A weighted)
19 cm/s	59 dB NAB (Linear)
19 cm/s	59 dB CCIR (Linear)
19 cm/s	64 dB NAB (A weighted)
19 cm/s	61 dB CCIR (A weighted)
Crosstalk attenuation	60 dB at 1 kHz 50 dB at 10 kHz
Phase fluctuation between tracks at 19 cm/s and 10 kHz	±12°

**Outputs**

Output voltage at MPL on 10 kΩ	1 V
Output voltage for 1% distortion at 1 kHz	2.5V
Output voltage for 200Ω headphones, adjustable	0 to 1 V
Built in loudspeaker, power output of amplifier	1 W
Reference signal level RMS	+10 dB ±0.1 dB

**FM Track**

Working speeds	38 and 19 cm/s
Carrier frequency	17 kHz
Static linearity	2%
Maximum frequency deviation Δfo	±45%
Frequency response at -3 dB	0 to 4 kHz
Signal to noise ratio for deviation of ±20%	44 dB
Peak-to-peak input voltage for deviation of ±20%	2.8 V PILOT 2.0 V CUE

**Operating Conditions**

Temperature with manganese batteries	-20 to +71 °C
Temperature with external power	-55 to +71°C
The recorder functions correctly in any position	

**Sony TCD-D10 PROII DAT Recorder**

**Format**

Tape	Digital audio tape
Head	Rotary head
Recording time	120 minutes (with DT-120)
Tape speed	8.15 mm/s
Drum rotation	Approx 2000 rpm
Error correction	Double Reed Solomon code

**Digital Audio Characteristics**

Number of channels	2-channel stereo
Quantization	16-bit linear
Frequency response ( $\pm 1.0$ dB, line input: +4 dBs, line output: -10 dBs)	20 Hz to 22 kHz +4 dBs line output -10 dBs
Signal-to-noise ratio (line inputs, AWTD)	>85 dB
Dynamic range (line inputs, AWTD)	>85 dB
Total harmonic distortion (1 kHz, line inout: +4 dBs, line output: -10 dBs, 30 kHz LPF)	<0.06%
Channel separation (1 kHz, line input 30 kHz LPF)	>80 dB
Wow and flutter	Below measurable limit ( $\pm 0.001\%$ W Peak)

**Tape**

Track pitch	13.6 $\mu\text{m}$ (20.4 $\mu\text{m}$ )
Sampling frequency, recording (selected automatically)	32 kHz 44.1 kHz (digital input only) 48 kHz
Sampling frequency, playback (selected automatically)	32 kHz 44.1 kHz 48 kHz
Modulation	8-10 Modulation

**Input**

Analog Inputs

MIC

Rated input	-60 dB
Maximum input	-20 dB
Impedance	10 k $\Omega$ balanced
Connector type	XLR-3-31

LINE IN

Rated input	+4 dB
Maximum input	+24 dB
Impedance	47 k $\Omega$ balanced
Connector type	XLR-3-31

Digital Inputs

Digital I/O connector with the supplied digital input/output cable (XLR type connectors): AES/EBU type

**Output**

Analog Outputs

LINE OUT

Rated output	-10 dB
Maximum output (at 10% distortion)	-
Impedance	Z <sub>o</sub> 700 $\Omega$ balanced
Connector type	Phono jack (RCA)

HEADPHONES

Rated output	-
Maximum output	20 mW + 20 mW
Impedance	Z <sub>L</sub> 32 $\Omega$
Connector type	Stereo phone jack

Digital Outputs

Digital I/O connector with the supplied digital input/output cable (XLR type connectors): AES/EBU type

**General**

Power requirements	6 V DC
Power consumption	Approx 7.5 W
Operating temperature	+5°C to +35°C
Operating humidity	<80% (relative humidity)
Storage temperature	-20°C to +55°C
Dimensions	253 x 55 x 191 mm
Weight	Approx 2.0 kg

## Appendix 3

### PASCAL Program to Create Waterfall Spectra Display

#### Program Written in Borland Turbo Pascal version 6 Borland CRT & GRAPH Library Linked Routines Used

```
*****  
* PASCAL Program to Create Waterfall Spectra Display *  
*      from Data in Random Access Files             *  
*                                                                 *  
*      Program by: John C. Goold (1994)             *  
*****
```

```
PROGRAM Binreadr(INPUT, OUTPUT);  
USES CRT, GRAPH;
```

```
TYPE
```

```
  PolyPoints = ARRAY[1..4] OF PointType;
```

```
VAR
```

```
  QUAD : PolyPoints;
```

```
  A, B, X, Y, X1, Y1, X2, Y2, dBFlag, CompFlag, HalfFlag, BinFlag,  
  Top, Bottom, Left, Right, DecPlaces, Zeroes, BoxFlag, BaseLine,  
  GraphDriver, GraphMode, Avg, ErrCode, SlantOffSet, MinuteFlag,  
  CutOff : INTEGER;
```

```
  Slices, Bins, Low, High, LowBin, HighBin, StartTime, EndTime,  
  StartSlice, EndSlice, Freq, FreqLow, FreqHigh, Time, Time1,  
  Time2, Time3, LowMark, MidMark, HighMark, Xinc, Yinc,  
  Xrange, Yrange, Xscale, Yscale, OrdScale, AbsScale, Temp,  
  Mean, N, FreqScale, Resol, Rec, AddTime, FixAxis, Index,  
  T1, T2, T3, dBMinimum, TimeScale : REAL;
```

```
  Bin : ARRAY[1..2048] OF REAL;  
  Comp : ARRAY[1..2048] OF REAL;
```

```
  PathFile, CompFile : TEXT;
```

```
  BGIPATH : STRING[30];
```

```
  ScrNum, Minutes, Seconds, FLNM1, FLNM2 : STRING[30];
```

```
  Ext1, Ext2 : STRING[4];
```

```
  Key : CHAR;
```

```
  TimeFile, BinFile : FILE OF REAL;
```

```
  LABEL 1,2;
```

```

PROCEDURE ReadBins;
BEGIN
  FOR B:=1 TO ROUND(Bins) DO
    BEGIN
      Rec:=((A-1)*BINS)+B+3;
      SEEK (BinFile, ROUND(Rec));
      READ (BinFile, Bin[B]);
      END;
    END;

PROCEDURE Convert;
BEGIN
  dBMinimum:=1000000;
  FOR B:=1 TO ROUND(Bins) DO
    BEGIN
      IF dBFlag=1 THEN
        BEGIN
          IF Bin[B]=0 THEN      (** Convert Power to dB **)
            BEGIN
              Bin[B]:=-120;
              dBMinimum:=-120;
            END
          ELSE
            BEGIN
              Bin[B]:=10*(ln(Bin[B])*(1/ln(10)));
              IF Bin[B] < dBMinimum THEN dBMinimum:=Bin[B];
            END;
          END;
        END;

      IF dBFlag=2 THEN
        BEGIN
          IF Bin[B]=0 THEN      (** Convert dB to Power **)
            BEGIN
              Bin[B]:=0.99;
            END
          ELSE
            BEGIN
              Bin[B]:=EXP((Bin[B]/10)*ln(10));
            END;
          END;
        END; (** FOR **)
      END; (** PROC **)
    END;
  END;

```

```

PROCEDURE Compensate;
BEGIN
  FOR B:=1 TO ROUND(Bins) DO
    BEGIN
      IF CompFlag=1 THEN
        BEGIN
          Bin[B]:=Bin[B]+Comp[B];
        END
      ELSE
        BEGIN
          Bin[B]:=Bin[B]*Comp[B];
        END;
      END; (** FOR **)
    END; (** PROC **)
  END;

```

PROCEDURE Average;

BEGIN

Mean:=0;

FOR B:=1 TO ROUND(Bins) DO

BEGIN

Temp:=B;

Mean:=Mean+Bin[B];

IF Temp/Avg = ROUND(Temp/Avg) THEN

BEGIN

Mean:=Mean/Avg;

Bin[B]:=Mean;

Mean:=0;

END;

END;

END; (\*\* PROC \*\*)

PROCEDURE OrdNosFrac;

BEGIN

HalfFlag:=0;

Temp:=(ln(high))\*(1/ln(10));

DecPlaces:=1+TRUNC(ABS(Temp));

Temp:=TRUNC(High\*Exp(DecPlaces\*ln(10)));

IF Temp/2 <> TRUNC(Temp/2) THEN HalfFlag:=1;

IF High/2 < Low THEN

BEGIN

Low:=0;

YScale:=Yrange/(High-Low);

END;

HighMark:=Temp/Exp(DecPlaces\*ln(10));

LowMark:=(Temp/2)/Exp(DecPlaces\*ln(10));

END;

PROCEDURE DrawOrdFrac;

BEGIN

OrdScale:=(HighMark-LowMark)/5;

IF Low <> 0 THEN

BEGIN

Temp:=TRUNC(Low/OrdScale)+1;

Temp:=Temp\*OrdScale;

END

ELSE

BEGIN

Temp:=OrdScale;

END;

LINE (Left, Bottom, Left, Bottom-ROUND(Yrange));

IF BoxFlag=1 THEN

BEGIN

LINE (Left+SlantOffSet, Top, Left+SlantOffSet, Top-ROUND(Yrange));

LINE (Left, Bottom-ROUND(Yrange), Left+SlantOffSet, Top-ROUND(Yrange));

LINE (Right, Top, Right, Top-ROUND(Yrange));

LINE (Left+SlantOffSet, Top-ROUND(Yrange), Right, Top-ROUND(Yrange));

END;

WHILE Temp <= High DO

BEGIN

Y:=ROUND(Yscale\*(Temp-Low));

```

LINE (Left-5, Bottom-Y, Left, Bottom-Y);
IF BoxFlag=1 THEN
  BEGIN
    LINE (Left+SlantOffset-5, Top-Y, Left+SlantOffset, Top-Y);
    LINE (Right, Top-Y, Right+5, Top-Y);
  END;
Temp:=Temp+OrdScale;
END;

Y:=ROUND (YScale*(HighMark-Low));
LINE (Left-10, Bottom-Y, Left, Bottom-Y);
IF BoxFlag=1 THEN
  BEGIN
    LINE (Left+SlantOffset-10, Top-Y, Left+SlantOffset, Top-Y);
    LINE (Right, Top-Y, Right+10, Top-Y);
  END;
SetTextStyle (0,0,0);
STR (HighMark : (DecPlaces+1) : (DecPlaces), ScrNum);
X:=(DecPlaces+1)*8+20;
OutTextXY (Left-X, Bottom-Y-4, ScrNum);
Y:=ROUND (YScale*(LowMark-Low));
LINE (Left-10, Bottom-Y, Left, Bottom-Y);
IF BoxFlag=1 THEN
  BEGIN
    LINE (Left+SlantOffset-10, Top-Y, Left+SlantOffset, Top-Y);
    LINE (Right, Top-Y, Right+10, Top-Y);
  END;
STR (LowMark : (DecPlaces+1+HalfFlag) : (DecPlaces+HalfFlag), ScrNum);
X:=(DecPlaces+1+HalfFlag)*8+20;
OutTextXY (Left-X, Bottom-Y-4, ScrNum);
END;

PROCEDURE OrdNos;
BEGIN
  IF HIGH <> 0 THEN
    BEGIN
      Temp:=(ln(ABS(HIGH)))*(1/ln(10));
      Temp:=TRUNC(Temp);
      IF Temp <> 0 THEN
        BEGIN
          Temp:=Exp(Temp*ln(10));
          HighMark:=TRUNC(ABS(High)/Temp);
          IF High < 0 THEN HighMark:=HighMark+1;
          HighMark:=HighMark*Temp;
          IF High < 0 THEN HighMark:=-HighMark;
        END
      ELSE
        BEGIN
          HighMark:=0;
        END; (** IF **)
      END; (** IF **)
    IF HIGH = 0 THEN HighMark:=0;

  IF Low <> 0 THEN
    BEGIN
      Temp:=(ln(ABS(Low)))*(1/ln(10));
      Temp:=TRUNC(Temp);
      Temp:=Exp(Temp*ln(10));

```

```

LowMark:=TRUNC(ABS(Low)/Temp);
LowMark:=LowMark*Temp;
IF Low < 0 THEN LowMark:= -LowMark;
END
ELSE
BEGIN
LowMark:=0; (** alternately - LowMark:=HighMark/2; **)
END;

END; (** PROC **)

```

```

PROCEDURE DrawOrd;
BEGIN
OrdScale:=ABS((HighMark-LowMark)/5);
Temp:=LowMark;
WHILE Temp >= Low DO
BEGIN
Temp:=Temp-OrdScale;
END;
Temp:=Temp+OrdScale;

LINE (Left, Bottom, Left, Bottom-ROUND(Yrange));
IF BoxFlag=1 THEN
BEGIN
LINE (Left+SlantOffSet, Top, Left+SlantOffSet, Top-ROUND(Yrange));
LINE (Left, Bottom-ROUND(Yrange), Left+SlantOffSet, Top-ROUND(Yrange));
LINE (Right, Top, Right, Top-ROUND(Yrange));
LINE (Left+SlantOffSet, Top-ROUND(Yrange), Right, Top-ROUND(Yrange));
END;

WHILE Temp <= High DO
BEGIN
Y:=ROUND(YScale*(Temp-Low));
LINE (Left-5, Bottom-Y, Left, Bottom-Y);
IF BoxFlag=1 THEN
BEGIN
LINE (Left+SlantOffSet-5, Top-Y, Left+SlantOffSet, Top-Y);
LINE (Right, Top-Y, Right+5, Top-Y);
END;
Temp:=Temp+OrdScale;
END; (** DO **)

Y:=ROUND(YScale*ABS(HighMark-Low));
LINE (Left-10, Bottom-Y, Left, Bottom-Y);
IF BoxFlag=1 THEN
BEGIN
LINE (Left+SlantOffSet-10, Top-Y, Left+SlantOffSet, Top-Y);
LINE (Right, Top-Y, Right+10, Top-Y);
END;
IF HighMark <> 0 THEN
BEGIN
DecPlaces:=TRUNC((ln(ABS(HighMark)))*(1/ln(10)))+1;
END
ELSE
BEGIN
Decplaces:=1;
END;
SetTextStyle (0,0,0);

```

```

STR (HighMark : (DecPlaces+1) : 0, ScrNum);
X:=DecPlaces*8+20;
OutTextXY (Left-X, Bottom-Y-4, ScrNum);

Y:=ROUND(YScale*(ABS(LowMark-Low)));
LINE (Left-10, Bottom-Y, Left, Bottom-Y);
IF BoxFlag=1 THEN
  BEGIN
    LINE (Left+SlantOffSet-10, Top-Y, Left+SlantOffSet, Top-Y);
    LINE (Right, Top-Y, Right+10, Top-Y);
  END;
IF LowMark <> 0 THEN
  BEGIN
    DecPlaces:=TRUNC((Ln(ABS(LowMark)))*(1/Ln(10)))+1;
  END
ELSE
  BEGIN
    DecPlaces:=1;
  END;
STR (LowMark : (DecPlaces+1) : 0, ScrNum);
X:=DecPlaces*8+20;
OutTextXY (Left-X, Bottom-Y-4, ScrNum);
END; (** PROC **)

```

```

PROCEDURE FreqNosPositive;
BEGIN
  Zeroes:=TRUNC(Ln(FreqHigh)*(1/Ln(10)));
  Temp:=FreqHigh/Exp((Zeroes-1)*Ln(10));
  Temp:=TRUNC(Temp/5);          (** find nice high/low marks **)
                                (** for wide frequency range **)
  HighMark:=(Temp*5)*Exp((Zeroes-1)*Ln(10));
  LowMark:=HighMark/2;

  IF LowMark < FreqLow THEN
    BEGIN
      Index:=TRUNC (Ln(FreqHigh)*(1/Ln(10)))-1;      (** find nice high mark **)
      Temp:=TRUNC (FreqHigh/Exp(Index*Ln(10)));      (** for restricted range **)
      HighMark:=Temp*EXP(Index*Ln(10));

      Temp:=HighMark-((HighMark-FreqLow)/2);      (** find nice low mark **)
      Index:=TRUNC (Ln(Temp)*(1/Ln(10)))-1;      (** for restricted range **)
      LowMark:=TRUNC (Temp/EXP(Index*(Ln(10))));
      LowMark:=LowMark*EXP(Index*Ln(10));

    END;
  END;

```

```

PROCEDURE DrawFreqPositive;
BEGIN
  AbsScale:=(HighMark-LowMark)/10;      (** set scale for ten divisions between markers **)
  IF FreqLow <> 0 THEN
    BEGIN
      Temp:=TRUNC((FreqLow/AbsScale)+1); (** find start division if non-zero **)
      Temp:=Temp*AbsScale;
    END
  ELSE
    BEGIN

```

```

Temp:=AbsScale;
END;
LINE (Left, Bottom, ROUND(Left+XRange), Bottom);

WHILE Temp < FreqHigh DO
BEGIN
X:=Left+ROUND(FreqScale*(Temp-FreqLow));
LINE (X, Bottom+5, X, Bottom);
Temp:=Temp+AbsScale;
END;

SetTextStyle (0,0,2);
X:=Left + ROUND (FreqScale*(HighMark-FreqLow));
Line (X, Bottom+10, X, Bottom);
STR (HighMark : (Zeroes+1) : 0, ScrNum);
OutTextXY (X-30, Bottom+20, ScrNum+' Hz');
X:=Left + ROUND (FreqScale*(LowMark-FreqLow));
LINE (X, Bottom+10, X, Bottom);
STR (LowMark : (Zeroes+1) : 0, ScrNum);
OutTextXY (X-30, Bottom+20, ScrNum);
END;

PROCEDURE TimeAxis;
BEGIN
T1:=TRUNC (StartTime+1);
T3:=TRUNC (EndTime);
T2:=TRUNC (T1+((T3-T1)/2));

Time:=T1;
Temp:=(T3-T1)/2;
SetTextStyle (2,0,6);
WHILE Time <= T3 DO
BEGIN
IF (EndTime-Time) <> 0 THEN
BEGIN
Yinc:=(Bottom-Top)*((EndTime-Time)/(EndTime-StartTime));
Xinc:=(EndTime-Time)/(EndTime-StartTime);
END
ELSE
BEGIN
Yinc:=0;
Xinc:=0;
END;
Xinc:=1-Xinc;
Xinc:=Xinc*((Right-Left)-Xrange);
X:=ROUND((Right-SlantOffSet)+Xinc);
Y:=ROUND(Top+Yinc);
LINE (X, Y, X+8, Y);

IF MinuteFlag=0 THEN
BEGIN
STR (ROUND(Time+AddTime), ScrNum);
OutTextXY (X+16, Y-10, ScrNum);
END
ELSE
BEGIN
T1:=TRUNC((Time+AddTime)/60);
T2:=FRAC((Time+AddTime)/60);

```

```

T2:=ROUND(T2*60);
STR (ROUND(T1), Minutes);
STR (ROUND(T2), Seconds);
IF T2 < 10 THEN Seconds:='0'+Seconds;
ScrNum:=Minutes+':' +Seconds;
OutTextXY (X+16, Y-10, ScrNum);
END;
Time:=Time+Temp;
END;
END; (** PROC **)

```

```

PROCEDURE TimeAxisFrac;
BEGIN

```

```

Temp:=(ln(EndTime))*(1/ln(10));
Temp:=TRUNC(Temp)-1;
Temp:=EXP(Temp*ln(10));
HighMark:=TRUNC(EndTime/Temp);
HighMark:=HighMark*Temp;

TimeScale:=HighMark/10;
Temp:=HighMark;
WHILE Temp > StartTime DO
  BEGIN
    Temp:=Temp-TimeScale;
  END;
Temp:=Temp+TimeScale;

Time:=Temp;
Temp:=(ln(Time))*(1/ln(10));
Temp:=TRUNC(Temp)-1;
DecPlaces:=TRUNC(ABS(Temp));
SetTextStyle (2, 0, 6);
WHILE Time < EndTime DO
  BEGIN
    IF (EndTime-Time) <> 0 THEN
      BEGIN
        Yinc:=(Bottom-Top)*((EndTime-Time) / (EndTime-StartTime));
        Xinc:=(EndTime-Time) / (EndTime-StartTime);
      END
    ELSE
      BEGIN
        Yinc:=0;
        Xinc:=0;
      END;
    Xinc:=1-Xinc;
    Xinc:=Xinc*((Right-Left)-XRange);
    X:=ROUND((Right-SlantOffSet)+Xinc);
    Y:=ROUND(Top+Yinc);
    LINE (X, Y, X+8, Y);

    STR (Time : (DecPlaces+2) : DecPlaces, ScrNum);
    OutTextXY (X+16, Y-10, ScrNum);
    Time:=Time+TimeScale;
  END; (** WHILE **)

```

```

END; (** PROC **)

```

```
PROCEDURE MenuFill;
BEGIN
  IF Key=CHR(49) THEN
  BEGIN
    WRITE ('Enter FileName ');
    READLN (FLNM1);
    GotoXY (20,8); WRITE (' ');
    GotoXY (20,8); WRITE (FLNM1);
    END;
  IF Key=CHR(50) THEN
  BEGIN
    WRITE ('Enter TimeFile Extension ');
    READLN (Ext1);
    GotoXY (20,9); WRITE (' ');
    GotoXY (20,9); WRITE (Ext1);
    END;
  IF Key=CHR(51) THEN
  BEGIN
    WRITE ('Enter BinFile Extension ');
    READLN (Ext2);
    GotoXY (20,10); WRITE (' ');
    GotoXY (20,10); WRITE (Ext2);
    END;
  IF Key=CHR(52) THEN
  BEGIN
    WRITE ('Enter Start Slice ');
    READLN (StartSlice);
    GotoXY (20,12); WRITE (' ');
    GotoXY (20,12); WRITE (StartSlice:3:0);
    END;
  IF Key=CHR(53) THEN
  BEGIN
    WRITE ('Enter End Slice ');
    READLN (EndSlice);
    GotoXY (20,13); WRITE (' ');
    GotoXY (20,13); WRITE (EndSlice:3:0);
    END;
  IF Key=CHR(54) THEN
  BEGIN
    WRITE ('Enter Time Addition (sec) ');
    READLN (AddTime);
    GotoXY (20,14); WRITE (' ');
    GotoXY (20,14); WRITE (AddTime:7:6);
    END;
  IF Key=CHR(55) THEN
  BEGIN
    WRITE ('Enter Bin Average Divisor ');
    READLN (Avg);
    GotoXY (20,16); WRITE (' ');
    GotoXY (20,16); WRITE (Avg);
    END;
  IF Key=CHR(56) THEN
  BEGIN
    WRITE ('Enter Low Axis Limit ');
    READLN (Low);
    GotoXY (20,22);
    WRITE (' ');
    GotoXY (20,22);
```

```

WRITE ('Enter High Axis Limit ');
READLN (High);
FixAxis:=1;
IF Low=0 THEN
  BEGIN
    IF High=0 THEN FixAxis:=0;
  END;
GotoXY (20,17); WRITE (' ');
GotoXY (20,17); WRITE (Low:7:6);
GotoXY (20,18); WRITE (High:7:6);
END;

IF Key=CHR(59) THEN (** F1 **)
  BEGIN
    IF dBFlag=1 THEN dBFlag:=0 ELSE dBFlag:=1;
    GotoXY (60,8);
    IF dBFlag=1 THEN WRITE ('ON ') ELSE WRITE ('OFF');
    GotoXY (60,9);
    WRITE ('OFF');
  END;
IF Key=CHR(60) THEN (** F2 **)
  BEGIN
    IF dBFlag=2 THEN dBFlag:=0 ELSE dBFlag:=2;
    GotoXY (60,9);
    IF dBFlag=2 THEN WRITE ('ON ') ELSE WRITE ('OFF');
    GotoXY (60,8);
    WRITE ('OFF');
  END;
IF Key=CHR(61) THEN (** F3 **)
  BEGIN
    IF BoxFlag=0 THEN BoxFlag:=1 ELSE BoxFlag:=0;
    GotoXY (60,10);
    IF BoxFlag=0 THEN WRITE ('OFF') ELSE WRITE ('ON ');
  END;
IF Key=CHR(62) THEN (** F4 **)
  BEGIN
    IF Compflag=0 THEN
      BEGIN
        Compflag:=1
      END
    ELSE
      BEGIN
        IF CompFlag=1 THEN Compflag:=2 ELSE Compflag:=0;
      END;
    GotoXY (60,12);
    IF Compflag=0 THEN WRITE ('OFF');
    IF Compflag=1 THEN WRITE (' + ');
    IF Compflag=2 THEN WRITE (' x ');
  END;
IF Key=CHR(63) THEN (** F5 **)
  BEGIN
    WRITE ('Enter Compensator Filename ');
    READLN (FLNM2);
    GotoXY (60,13); WRITE (' ');
    GotoXY (60,13); WRITE (FLNM2);
    ASSIGN (CompFile, FLNM2);
    RESET (CompFile);
    READLN (CompFile, Temp);
    FOR B:=1 TO ROUND(Temp) DO (** read compensator **)

```

```

        BEGIN          (** weighting coeffs **)
        READLN (CompFile, Comp[B]);
        END;
        CLOSE (CompFile);
        END;
    IF Key=CHR(64) THEN (** F6 **)
        BEGIN
        WRITE ('Enter Slant Offset ');
        READLN (SlantOffSet);
        GotoXY (60,14); WRITE (' ');
        GotoXY (60,14); WRITE (SlantOffSet);
        END;
    IF Key=CHR(65) THEN (** F7 **)
        BEGIN
        WRITE ('Enter Low Bin ');
        READLN (LowBin);
        GotoXY (20,22);
        WRITE ('Enter High Bin ');
        READLN (HighBin);
        GotoXY (60,16); WRITE (' ');
        GotoXY (60,16); WRITE (ROUND(LowBin),' -> ',ROUND(HighBin));
        END;
    IF Key=CHR(66) THEN (** F8 **)
        BEGIN
        WRITE ('Enter LF Cut Off ');
        READLN (CutOff);
        GotoXY (60,17); WRITE (' ');
        GotoXY (60,17); WRITE (CutOff,' Hz');
        END;
    IF Key=CHR(67) THEN (** F9 **)
        BEGIN
        IF MinuteFlag=0 THEN MinuteFlag:=1 ELSE MinuteFlag:=0;
        GotoXY (60,18);
        IF MinuteFlag=0 THEN WRITE ('Seconds') ELSE WRITE ('Minutes');
        END;

        GotoXY (20,22);
        WRITELN (' ');
        GotoXY (20,22);
        END;

```

```

PROCEDURE TimeLimits;
BEGIN
    RESET (TimeFile);
    READ (TimeFile, N);
    IF EndSlice > N THEN EndSlice:=N;
    IF StartSlice >= (N-1) THEN StartSlice:=1;
    IF StartSlice >= EndSlice THEN EndSlice:=N;

    SEEK (TimeFile, ROUND(StartSlice));
    READ (TimeFile, StartTime);
    SEEK (TimeFile, ROUND(EndSlice));
    READ (TimeFile, EndTime);
    END;

```

```

PROCEDURE BinLimits;

```

```

BEGIN
  RESET (BinFile);
  READ (BinFile, Slices);
  READ (BinFile, Bins);
  IF LowBin >= Bins THEN LowBin:=1;
  IF HighBin > Bins THEN HighBin:=Bins;
  IF HighBin <= LowBin THEN HighBin:=Bins;
  SEEK (BinFile, 3);
  READ (BinFile, Freq);

  IF FixAxis=0 THEN
    BEGIN
      Low:=1000000; High:=-1000000;
      FOR A:=ROUND(StartSlice) TO ROUND(EndSlice) DO
        BEGIN
          ReadBins;
          IF dBFlag <> 0 THEN Convert;
          IF CompFlag <> 0 THEN Compensate;
          IF Avg <> 1 THEN Average;
          B:=Avg;
          WHILE B <= Bins DO
            BEGIN
              IF B >= LowBin THEN
                BEGIN
                  IF B <= HighBin THEN
                    BEGIN
                      IF (B*(Freq/Bins)) >= CutOff THEN
                        BEGIN
                          IF Bin[B] > High THEN High:=Bin[B];
                          IF Bin[B] < Low THEN Low:=Bin[B];
                          END;
                        END;
                      END;
                    B:=B+Avg;
                    END; (** WHILE **)
                  END; (** FOR A **)
                END; (** IF **)
              END; (** PROC **)
            END;
          END;
        END;
      END;
    END;
  END;

PROCEDURE ReadTime;
BEGIN
  SEEK (TimeFile, A);
  READ (TimeFile, Time);
  IF (EndTime-Time) <> 0 THEN
    BEGIN
      Yinc:=(Bottom-Top)*((EndTime-Time)/(EndTime-StartTime));
      END
    ELSE
      BEGIN
        Yinc:=0;
        END;
      END;
    END;

PROCEDURE DrawSlice;
BEGIN
  IF (EndTime-Time) <> 0 THEN
    BEGIN

```

```

Xinc:=(EndTime-Time)/(EndTime-StartTime);
END
ELSE
BEGIN
Xinc:=0;
END;

Xinc:=1-Xinc;
Xinc:=Xinc*((Right-Left)-Xrange);
BaseLine:=ROUND(Top+Yinc);

IF (AVG*Resol) < CutOff THEN
BEGIN
IF dBFlag=0 THEN Bin[B]:=Low;
IF dBFlag=1 THEN Bin[B]:=dBMinimum;
IF dBFlag=2 THEN Bin[B]:=Low;
END;

B:=2*AVG;
WHILE B <= Bins DO
BEGIN
IF (B*Resol) < CutOff THEN
BEGIN
IF dBFlag=0 THEN Bin[B]:=Low;
IF dBFlag=1 THEN Bin[B]:=dBMinimum;
IF dBFlag=2 THEN Bin[B]:=Low;
END;
IF B >= (LowBin+Avg) THEN
BEGIN
IF B <= HighBin THEN
BEGIN
X1:=ROUND(((B-Avg)-LowBin)*Xscale)+Left+Xinc;
Y1:=BaseLine - ROUND(((BIN[B-Avg]-Low)*YScale));
X2:=ROUND(((B-LowBin)*Xscale)+Left+Xinc);
Y2:=BaseLine - ROUND(((Bin[B]-Low)*Yscale));
IF BaseLine - Y1 > Yrange THEN Y1 := BaseLine - ROUND(Yrange);
(** truncate tall **)
(** spikes if Fix **)
IF BaseLine - Y2 > Yrange THEN Y2 := BaseLine - ROUND(Yrange);

IF Y1 > Y2 THEN Temp:=BaseLine-Y2 ELSE Temp:=BaseLine-Y1;
Y:=0;
SETCOLOR (EGABLACK);
WHILE Y < Temp DO
BEGIN
(** wipe out **)
LINE (X1, Y1+Y, X2, Y2+Y); (** descending line **)
Y:=Y+1;
END;
SETCOLOR (EGAWHITE);
LINE (X1, Y1, X2, Y2); (** new line **)

IF B-Avg <= LowBin THEN LINE (X1, BaseLine, X1, Y1); (** close down **)
IF B+AVG > HighBin THEN LINE (X2, BaseLine, X2, Y2); (** loose ends **)

END;
END;
B:=B+AVG;
END; (** WHILE **)
END; (** PROC **)

```

```

PROCEDURE Setup;
BEGIN
  GraphDriver:=VGA;
  GraphMode:=VGAHi;
  INITGRAPH (GraphDriver, GraphMode, BGIPATH);
  IF dBFlag = 1 THEN
    BEGIN
      OrdNos;
      DrawOrd;
    END
  ELSE
    BEGIN
      IF ABS(Low) > 1 THEN OrdNos ELSE OrdNosFrac;
      IF ABS(Low) > 1 THEN DrawOrd ELSE DrawOrdFrac;
    END;
  LINE (Left, Bottom, Left, Bottom-ROUND(Yrange));
  LINE (Left, Bottom, ROUND(Left+SlantOffSet), Top);
  END;

```

PROCEDURE Menu;

LABEL 1;

BEGIN

CLRSCR;

(\*\* TextMode(BW80)\*\*);

GotoXY (5,5);

WRITE ('PARAMETERS');

GotoXY (45,5);

WRITE ('OPTIONS');

GotoXY (1,8); WRITE ('1. FileName: ', FLNM1);

GotoXY (1,9); WRITE ('2. Time Ext: ', Ext1);

GotoXY (1,10); WRITE ('3. Bin Ext: ', Ext2);

GotoXY (1,12); WRITE ('4. Start Slice: ', StartSlice:3:0);

GotoXY (1,13); WRITE ('5. End Slice: ', EndSlice:3:0);

GotoXY (1,14); WRITE ('6. Add Time: ', AddTime:7:6);

GotoXY (1,16); WRITE ('7. Bin Average: ', Avg);

GotoXY (1,17); WRITE ('8. Fix Axis: ', Low:7:6);

GotoXY (1,18); WRITE (' ', High:7:6);

GotoXY (40,8); WRITE ('F1. Power -> dB: '); GotoXY(60,8); IF dBFlag=1 THEN WRITE ('ON ') ELSE WRITE ('OFF');

GotoXY (40,9); WRITE ('F2. dB -> Power: '); GotoXY(60,9); IF dBFlag=2 THEN WRITE ('ON ') ELSE WRITE ('OFF');

GotoXY (40,10); WRITE ('F3. Rear Box: '); GotoXY(60,10); IF BoxFlag=0 THEN WRITE ('OFF') ELSE WRITE ('ON');

GotoXY (40,12); WRITE ('F4. Compensator: '); GotoXY(60,12); IF CompFlag=1 THEN WRITE ('ON ') ELSE WRITE ('OFF');

GotoXY (40,13); WRITE ('F5. CmpFileName: ', FLNM2);

GotoXY (40,14); WRITE ('F6. Slant Offset: ', SlantOffSet);

GotoXY (40,16); WRITE ('F7. Bin Range: ', ROUND(LowBin), '->', ROUND(HighBin));

GotoXY (40,17); WRITE ('F8. LF CutOff: ', CutOff, ' Hz');

GotoXY (40,18); WRITE ('F9. Time Units: '); GotoXY(60,18);

IF MinuteFlag=0 THEN WRITE('Seconds') ELSE WRITE('Minutes');

GotoXY (40,20); WRITE ('F10. RUN');

GotoXY (20,22);

```

1: Key:=ReadKey;
  ScrNum:=Key;
  VAL(ScrNum, B, ErrCode);

  IF Key='#0' THEN Key:=ReadKey;
  IF Key <> CHR(68) THEN
    BEGIN
      MenuFill;
      GOTO 1;
    END;

  END; (** PROC **)

```

```

BEGIN
  ASSIGN (PathFile, 'BGIPATH.TXT');
  RESET (PathFile);
  READLN (PathFile, BGIPATH);
  CLOSE (PathFile);
  Left:=63;
  Right:=575;
  Top:=100;
  Bottom:=431;
  SlantOffSet:=100;
  dBFlag:=0; CompFlag:=0; BinFlag:=0; BoxFlag:=0; MinuteFlag:=1;
  StartSlice:=1; EndSlice:=30;
  Avg:=4; LowBin:=1; HighBin:=788;
  low:=0; High:=0; FixAxis:=0;
  FLNM1:='88NG16BA'; FLNM2:=''; Ext1:='.TR1'; Ext2:='.OR1';
  AddTime:=0; CutOff:=0;
1: Menu;
  ASSIGN (TimeFile, FLNM1+EXT1);
  ASSIGN (BinFile, FLNM1+EXT2);

  CLRSCR;
  GotoXY (22,12); WRITE ('Reading Files - Please Wait !');
  TimeLimits;
  BinLimits;
  XRange:=(Right-Left)-SlantOffSet;
  YRange:=96;
  XScale:=XRange/((HighBin+1)-LowBin);
  Resol:=Freq/Bins;
  FreqScale:=XScale/Resol;
  YScale:=YRange/(High-Low);
  FreqLow:=(LowBin-1)*Resol;
  FreqHigh:=HighBin*Resol;
  Setup;

  A:=ROUND(EndSlice);
  REPEAT
    ReadBins;
    IF dBFlag <> 0 THEN Convert;
    IF CompFlag <> 0 THEN Compensate;
    IF Avg <> 1 THEN Average;
    ReadTime;
    DrawSlice;
    A:=A-1;
  UNTIL A < StartSlice;

```

```
FreqNosPositive;
DrawFreqPositive;
IF TRUNC(EndTime)-TRUNC(StartTime+1) > 5 THEN TimeAxis ELSE TimeAxisFrac;
LINE (Right, Top, ROUND(Left+Xrange), Bottom);

CLOSE (TimeFile);
CLOSE (BinFile);
SetTextStyle (2,0,4);
OutTextXY (0,470,'F2. Run');
OutTextXY (100,470,'F3. Info');
OutTextXY (200,470,'F4. Clr');
OutTextXY (300,470,'F10. Quit');
2: Key:=ReadKey;
ScrNum:=Key;
VAL (ScrNum, B, ErrCode);
IF Key='#0' THEN Key:=READKEY;
IF Key = CHR(60) THEN (** F2 Go **)
  BEGIN
  CloseGraph;
  GOTO 1;
  END;
IF Key = CHR(61) THEN (** F3 Info **)
  BEGIN
  END;
IF Key = CHR(62) THEN (** F4 Clear **)
  BEGIN
  SETCOLOR (EGABLACK);
  FOR B:=470 TO 479 DO
    BEGIN
    LINE (0, B, 639, B);
    END;
  END;
IF Key = CHR(68) THEN (** F10 Quit **)
  BEGIN
  CLOSEGRAPH;
  HALT;
  END;
GOTO 2;
END.
```

## Appendix 4

### Program to create FIR Filter Coefficients Using Kaiser Parameters

#### Program Written in Borland Turbo Pascal version 6 Borland CRT & GRAPH Library Linked Routines Used

```
*****
* Non-Recursive Filter Design with the Kaiser Window *
*                                                    *
*   Program modified by John C. Goold (1994)       *
*****

PROGRAM DSP18 (INPUT, OUTPUT);
USES CRT, GRAPH;
VAR
  SEE : ARRAY[0..1000] OF REAL;
  h : ARRAY[0..1000] OF REAL;
  w : ARRAY[0..540] OF REAL;

  P, Q, R, S, T, A, I, B, C, D, Degrees, NYQUIST, SAMPLING,
  ALPHA, BETA, A0, h0, w0, w1, FREQ, MAX, DB, MREAL : REAL;

  X, N, K, M, Y, SHADE, SIZE,
  GRAPHDRIVER, GRAPHMODE : INTEGER;

  P1, P2 : ^INTEGER;

  FLNM, COMMENT, SDEG, SFREQ : STRING[80];

  Coefffile : TEXT;

  KEY : CHAR;

  LABEL 1,2;

BEGIN
  GRAPHDRIVER:=VGA;
  GRAPHMODE:=VGAHi;
  SHADE:=EGAWHITE;

1: WRITELN;
  WRITE ('Enter Sampling Frequency (Hertz) '); READLN(SAMPLING);
  NYQUIST:=SAMPLING/2;
  WRITE ('Enter Centre Frequency (Degrees) '); READLN(P);
  w0:=P*Pi/180;
  WRITE ('Enter Filter Bandwidth (Degrees) '); READLN(Q);
  w1:=Q*0.5*Pi/180;
  WRITELN;
  WRITELN ('Enter Kaiser Design Parameters:');
```

```

WRITELN;
WRITE ('Ripple (as a fraction): '); READLN (R);
WRITE ('Transition Width (Degrees): '); READLN(S);
T:=S/360;
WRITELN; WRITELN;

(***** Estimate Kaiser Parameters *****)
A:=-20*ln(R)*0.4343;
MREAL:=(A-7.95)/(28.72*T);
M:=TRUNC(MREAL+1);
WRITELN ('No of Impulse Response Terms = ',2*M+1);
WRITELN;
WRITE ('Do you wish to Change Parameters (y/n) ?');
KEY:=READKEY;
IF UPCASE(KEY)='Y' THEN GOTO 1;
WRITELN; WRITELN;

IF A > 49 THEN
  BEGIN
    ALPHA:=0.1102*(A-8.7);
    GOTO 2 END;
IF A > 21 THEN
  BEGIN
    ALPHA:=(0.5842*exp(0.4*ln(A-21))+(0.07886*(A-21)));
    GOTO 2 END;
ALPHA:=0;

2: WRITELN ('For this window, Alpha = ',ALPHA);
WRITELN;
WRITE ('Press any key to start plot');
KEY:=READKEY;
WRITELN; WRITELN; WRITELN;
WRITELN ('      Computing Coefficients - Please Wait!');

(***** Compute Window Values *****)
FOR N:=0 TO M DO
  BEGIN
    BETA:=ALPHA*SQRT(1-(N/M)*(N/M));
    I:=1;
    B:=1;
    FOR K:=1 TO 20 DO
      BEGIN
        C:=B*BETA*BETA/4;
        D:=C/(K*K);
        I:=I+D;
        B:=D;
      END;

    SEE[N]:=I;
  END;

A0:=SEE[0];
FOR N:=0 TO M DO
  BEGIN
    SEE[N]:=SEE[N]/A0;
  END;

```

```

(***** Compute Impulse Response Values *****)
h[0]:=w1/Pi;
FOR N:=1 TO M DO
  BEGIN
    h[N]:=(1/(N*Pi))*SIN(N*w1)*COS(N*w0)*SEE[N];
  END;

(***** Compute Frequency Response *****)
(***** 540 Pixels to Absicca, 1 pixel =0.333 degrees *****)
FOR N:=1 TO 540 DO
  BEGIN
    FREQ:=Pi*(N-1)/540;
    w[N]:=h[0];
    FOR K:=1 TO M DO
      BEGIN
        w[N]:=w[N]+2*h[K]*COS(K*FREQ);
      END;
    END;

(***** Normalise to Unity, Convert to Decibels, and Plot *****)
INITGRAPH (GRAPHDRIVER, GRAPHMODE, 'C:\TP\BGI');
SIZE:=IMAGESIZE(320, 100, 320, 380);
GETMEM (P1, SIZE);
SIZE:=IMAGESIZE(0, 0, 600, 50);
GETMEM (P2, SIZE);
GETIMAGE (0, 0, 600, 50, P2^);

MAX:=0;
FOR N:=1 TO 540 DO
  BEGIN
    IF ABS(w[N]) > MAX THEN MAX:=ABS(w[N]);
  END;
FOR N:=1 TO 540 DO
  BEGIN
    DB:=20*ln(ABS(w[N])/MAX)*0.4343;
    IF DB < -50 THEN DB:=-50;
    LINE (N+50, 350, N+50, ROUND(150-4*DB));
  END;

LINE (51, 350, 591, 350);
LINE (51, 150, 591, 150);      (***** Draw Box *****)
LINE (51, 350, 51, 150);
LINE (591, 350, 591, 150);

LINE (45, 310, 591, 310);
LINE (45, 270, 591, 270);      (***** Draw cross lines *****)
LINE (45, 230, 591, 230);
LINE (45, 190, 591, 190);
SetTextStyle (2, 0, 6);
OutTextXY (10, 340, '-50');
OutTextXY (10, 300, '-40');
OutTextXY (10, 260, '-30');
OutTextXY (10, 220, '-20');
OutTextXY (10, 180, '-10');
OutTextXY (30, 140, '0');

LINE (186, 356, 186, 150);
LINE (321, 356, 321, 150);      (***** Draw X-Marks *****)

```

```

LINE (456, 356, 456, 150);
OutTextXY (176, 360, '45');
OutTextXY (310, 360, '90');
OutTextXY (446, 360, '135');
SetTextStyle (2, 0, 2);
OutTextXY (196, 360, 'o');
OutTextXY (330, 360, 'o');
OutTextXY (476, 360, 'o');

SetTextStyle (2, 0, 6);
OutTextXY (10, 10, 'Do you want to activate the cursor (y/n)?');
KEY:=READKEY;
PUTIMAGE (0, 0, P2^, 0);
IF UPCASE(KEY)='Y' THEN
  BEGIN
  X:=320;
  GETIMAGE (X, 100, X, 380, P1^);
  LINE (X, 100, X, 380);
  REPEAT
    KEY:=READKEY;
    IF KEY=#0 THEN
      BEGIN
      KEY:=READKEY;
      IF KEY=CHR(75) THEN
        BEGIN
        IF X-1 > 50 THEN
          BEGIN
          PUTIMAGE (X, 100, P1^, 0);
          X:=X-1;
          GETIMAGE (X, 100, X, 380, P1^);
          END;
        END;
      IF KEY=CHR(77) THEN
        BEGIN
        IF X+1 < 592 THEN
          BEGIN
          PUTIMAGE (X, 100, P1^, 0);
          X:=X+1;
          GETIMAGE (X, 100, X, 380, P1^);
          END;
        END;
      END;
      END;
      LINE (X, 380, X, 100);
      Degrees:=(1/3)*(X-51);
      FREQ:=NYQUIST*(Degrees/180);
      STR (Degrees:6:3, SDEG);
      STR (FREQ:6:1, SFREQ);
      PUTIMAGE (0, 0, P2^, 0);
      OutTextXY (10, 10, SDEG+' Degrees');
      OutTextXY (10, 25, SFREQ+' Hertz');
    UNTIL KEY=CHR(13);
  END;

  PUTIMAGE (0, 0, P2^, 0);
  OutTextXY (10,10, 'Do you want to create a filter coefficient file (y/n)?');
  KEY:=READKEY;
  CLOSEGRAPH;
  IF UPCASE(KEY)='Y' THEN
    BEGIN

```

```
h[0]:=h[0]/MAX;
FOR N:=1 TO M DO
  BEGIN      (** correct h[N] for unity max gain **)
    h[N]:=h[N]/MAX;
  END;
WRITE ('Enter File Name for filter coefficients '); READLN (FLNM);
WRITE ('Enter File Comment '); READLN (COMMENT);
ASSIGN (Coeffile, FLNM);
REWRITE (COEFFILE);
WRITELN (Coeffile, COMMENT);
WRITELN (Coeffile, 1.0:2:1);
FOR N:=1 TO 3 DO
  BEGIN
    WRITELN (Coeffile);      (** Line feed **)
  END;
WRITELN (Coeffile, (2*M+1));

N:=M;
REPEAT
  WRITELN (Coeffile, h[N]:7:6);
  N:=N-1;
UNTIL N=0;
WRITELN (Coeffile, h[0]:7:6);
N:=1;
REPEAT
  WRITELN (Coeffile, h[N]:7:6);
  N:=N+1;
UNTIL N>M;
CLOSE (Coeffile);
WRITELN; WRITELN;
WRITELN (FLNM, ' created successfully');
WRITELN;
WRITELN ('Impulse Response is Symmetrical & Shifted to n=0');
DELAY (3000);
END;
```

END.

## Appendix 5

### Regression Data & Tables for 1994 (Chapter 3, Section A) Sound Velocity Measurements

#### Distilled Water Calibration : Regression Output from Quattro Pro

Uncorrected Onset Times

Temp = 21.7 C

Sample Length (m)	Extrap Onset (s)
----------------------	---------------------

0.07855	0.0000568
0.0745	5.425E-05
0.0692	5.045E-05
0.0638	0.000047
0.05715	0.0000425
0.05105	0.0000384
0.04285	3.295E-05
0.03495	0.0000277
0.02945	0.000024

Regression Output:

Constant	4.301E-06
Std Err of Y Est	7.306E-08
R Squared	0.9999656
No. of Observations	9
Degrees of Freedom	7
X Coefficient(s)	0.0006687
Std Err of Coef.	1.482E-06

Velocity 1495.5124

Temp = 23.5

0.08815	0.0000631
0.08355	6.015E-05
0.0767	5.565E-05
0.0694	0.0000504
0.0646	4.735E-05
0.05685	4.215E-05
0.0491	3.705E-05
0.04325	0.0000331
0.0362	2.845E-05
0.03035	2.435E-05

Regression Output:

Constant	4.098E-06
Std Err of Y Est	1.096E-07
R Squared	0.9999403
No. of Observations	10
Degrees of Freedom	8
X Coefficient(s)	0.00067
Std Err of Coef.	1.83E-06

Velocity 1492.5065

Temp = 26.4

0.0863	6.175E-05	Regression Output:	
0.0813	5.805E-05	Constant	4.092E-06
0.0756	5.475E-05	Std Err of Y Est	1.775E-07
0.06945	0.0000501	R Squared	0.9998458
0.06305	4.615E-05	No. of Observations	10
0.05555	4.105E-05	Degrees of Freedom	8
0.0495	0.0000372		
0.04115	3.145E-05	X Coefficient(s)	0.0006664
0.0342	2.685E-05	Std Err of Coef.	2.926E-06
0.0273	2.235E-05		
		Velocity	1500.6003

Temp = 29.1

0.08975	0.0000629	Regression Output:	
0.0843	0.0000593	Constant	4.581E-06
0.071	5.085E-05	Std Err of Y Est	2.068E-07
0.06455	4.705E-05	R Squared	0.9998256
0.0578	4.245E-05	No. of Observations	10
0.04685	3.525E-05	Degrees of Freedom	8
0.0416	0.0000317		
0.03545	0.0000276	X Coefficient(s)	0.0006517
0.0292	0.0000235	Std Err of Coef.	3.043E-06
0.0249	2.065E-05		
		Velocity	1534.4311

Temp = 32.2

0.09025	0.000064	Regression Output:	
0.07805	5.575E-05	Constant	4.018E-06
0.06825	4.905E-05	Std Err of Y Est	1.167E-07
0.06495	4.705E-05	R Squared	0.9999371
0.0564	4.135E-05	No. of Observations	8
0.0467	3.505E-05	Degrees of Freedom	6
0.0367	2.835E-05		
0.03005	0.000024	X Coefficient(s)	0.0006629
		Std Err of Coef.	2.147E-06
		Velocity	1508.5392

Temp =35.5

0.09085	0.0000643		Regression	
			Output:	
0.08415	5.925E-05	Constant		4.157E-06
0.07105	5.065E-05	Std Err of		2.051E-07
		Y Est		
0.0653	0.0000471	R Squared		0.9998122
0.05525	0.0000404	No. of		9
		Observation		
		s		
0.0479	0.0000357	Degrees of Freedom		7
0.0423	3.195E-05			
0.0367	2.835E-05	X		0.0006576
		Coefficient		
		(s)		
0.0292	2.345E-05	Std Err of Coef.		3.406E-06
		Velocity		1520.6393

Temp	Corrected Cell Velocity	Tabulated Standard Velocity
21.7	1492.072	1487.9
23.5	1495.429	1493.1
26.4	1500.837	1500.9
32.2	1511.654	1514.7
35.5	1517.809	

**Humberside Spermaceti, Sub-Sample A : Regression Output from MINITAB**

MTB > REGRESS C1 3 C2 C3 C4

Regression Analysis

- \* NOTE \* Temp is highly correlated with other predictor variables
- \* NOTE \* Temp^2 is highly correlated with other predictor variables

The regression equation is  
 Velocity = 2710 + 4.20 Pressure - 78.4 Temp + 1.17 Temp^2

Predictor	Coef	Stdev	t-ratio	p
Constant	2709.94	64.25	42.18	0.000
Pressure	4.1991	0.2741	15.32	0.000
Temp	-78.432	4.328	-18.12	0.000
Temp^2	1.16952	0.07205	16.23	0.000

s = 6.481      R-sq = 96.6%      R-sq(adj) = 96.5%

Analysis of Variance

SOURCE	DF	SS	MS	F	p
Regression	3	70111	23370	556.47	0.000
Error	58	2436	42		
Total	61	72547			

SOURCE	DF	SEQ SS
Pressure	1	7381
Temp	1	51664
Temp^2	1	11066

Unusual Observations

Obs.	Pressure	Velocity	Fit	Stdev.Fit	Residual	St.Resid
29	4.56	1496.00	1482.22	1.26	13.78	2.17R
38	6.08	1502.00	1488.60	1.35	13.40	2.11R

R denotes an obs. with a large st. resid.

MTB > PRINT C1-C4

Data Display

Row	Velocity	Pressure	Temp	Temp^2
1	1498	0.00000	24.2	585.64
2	1463	0.00000	25.9	670.81
3	1433	0.00000	27.1	734.41
4	1425	0.00000	28.0	784.00
.	.	.	.	.
.	.	.	.	.
62	1429	9.11925	35.5	1260.25

**Humberside Spermacti, Sub-Sample B : Regression Output from MINITAB**

MTB > REGRESS C1 3 C2 C3 C4

Regression Analysis

\* NOTE \*      Temp is highly correlated with other predictor variables  
 \* NOTE \*      Temp^2 is highly correlated with other predictor variables

The regression equation is

$$\text{Velocity} = 2093 + 3.88 \text{ Pressure} - 38.6 \text{ Temp} + 0.528 \text{ Temp}^2$$

Predictor	Coef	Stdev	t-ratio	p
Constant	2093.47	22.63	92.52	0.000
Pressure	3.8842	0.1589	24.45	0.000
Temp	-38.568	1.530	-25.21	0.000
Temp^2	0.52775	0.02546	20.73	0.000

s = 4.041      R-sq = 98.7%      R-sq(adj) = 98.7%

Analysis of Variance

SOURCE	DF	SS	MS	F	p
Regression	3	83026	27675	1694.75	0.000
Error	66	1078	16		
Total	69	84104			

SOURCE	DF	SEQ SS
Pressure	1	9759
Temp	1	66249
Temp^2	1	7018

Unusual Observations

Obs.	Pressure	Velocity	Fit	Stdev.Fit	Residual	St.Resid
24	3.04	1449.00	1437.33	0.72	11.67	2.93R
41	6.08	1526.00	1513.52	1.29	12.48	3.26R

R denotes an obs. with a large st. resid.

MTB > PRINT C1-C4

Data Display

Row	Velocity	Pressure	Temp	Temp^2
1	1486	0.00000	22.7	515.29
2	1465	0.00000	24.7	610.09
3	1438	0.00000	26.8	718.24
4	1421	0.00000	28.2	795.24
.	.	.	.	.
70	1421	9.11925	37.1	1376.41

**Combined HumberSide Spermacti, Subsamples A & B : Regression Output from MINITAB**

MTB > REGRESS C1 3 C2 C3 C4

Regression Analysis

- \* NOTE \* Temp is highly correlated with other predictor variables
- \* NOTE \* Temp^2 is highly correlated with other predictor variables

The regression equation is

$$\text{Velocity} = 2196 + 3.95 \text{ Pressure} - 44.7 \text{ Temp} + 0.621 \text{ Temp}^2$$

Predictor	Coef	Stdev	t-ratio	p
Constant	2195.74	40.73	53.91	0.000
Pressure	3.9527	0.2462	16.06	0.000
Temp	-44.723	2.745	-16.29	0.000
Temp^2	0.62132	0.04563	13.62	0.000

s = 8.555      R-sq = 94.1%      R-sq(adj) = 93.9%

Analysis of Variance

SOURCE	DF	SS	MS	F	p
Regression	3	148871	49624	678.11	0.000
Error	128	9367	73		
Total	131	158238			

SOURCE	DF	SEQ SS
Pressure	1	16991
Temp	1	118311
Temp^2	1	13569

Unusual Observations

Obs.	Pressure	Velocity	Fit	Stdev.Fit	Residual	St.Resid
1	0.00	1498.00	1477.30	1.87	20.70	2.48R
10	1.52	1501.00	1483.31	1.68	17.69	2.11R
20	3.04	1486.00	1466.20	1.11	19.80	2.33R
28	4.56	1519.00	1495.32	1.52	23.68	2.81R
29	4.56	1496.00	1472.21	1.06	23.79	2.80R
37	6.08	1522.00	1501.33	1.58	20.67	2.46R
38	6.08	1502.00	1478.22	1.13	23.78	2.80R
46	7.60	1533.00	1507.34	1.71	25.66	3.06R
47	7.60	1504.00	1484.22	1.31	19.78	2.34R
55	9.12	1508.00	1490.23	1.56	17.77	2.11R

R denotes an obs. with a large st. resid.

MTB > PRINT C1-C4

Data Display

Row	Velocity	Pressure	Temp	Temp^2
1	1498	0.00000	24.2	585.64
2	1463	0.00000	25.9	670.81
3	1433	0.00000	27.1	734.41
4	1425	0.00000	28.0	784.00
.	.	.	.	.
.	.	.	.	.
132	1421	9.11925	37.1	1376.41

## Appendix 6

### Regression Data & Tables for 1996 (Chapter 3, Section B) Sound Velocity Measurements

#### Distilled Water Calibration : Regression Output from Quattro Pro

Temp (°C)	0 Pa	0 Pa	
	Uncorr Velocity (m/s)	Uncorr Velocity (m/s)	Tabulated Velocity (m/s)
38.9	1400.8	1388.8	
37	1388.4	1386.8	
35	1383	1383.6	
33	1376.7	1376.5	1516.5
30.9	1372.4	1371	1511.8
28.9	1369.1	1366.9	1507.1
27	1364.4	1364.8	1502.4
24.9	1358.9	1359.3	1496.9
23	1354.7	1353.6	1491.6
21.1	1349.6	1348.5	1486.1
19	1342.9	1343.3	1479.7
17	1338.8	1337.3	1473.2
15	1332.1	1329.8	1466.4
13	1323.4	1324	1459.3
11	1319.4	1319.5	1451.9
9	1314.4	1313.5	1444.1
5.5	1299.2	1301.8	1429.6

Regression Output:	Tabulated Water
Constant	1417.677
Std Err of Y Est	2.669484
R Squared	0.990819
No. of Observations	14
Degrees of Freedom	12

X Coefficient(s)                    3.122972  
Std Err of Coef.                    0.086779

$$\text{Velocity} = 3.123 * \text{Temp} + 1417.7$$

Regression Output:                  Measured Water  
Constant                              1289.129  
Std Err of Y Est                    2.096706  
R Squared                            0.992073  
No. of Observations                28  
Degrees of Freedom                 26

X Coefficient(s)                    2.749174  
Std Err of Coef.                    0.048196

$$\text{Velocity} = 2.749 * \text{Temp} + 1289.1$$

Correction for all velocity values is:

$$+128.6 + 0.374T$$

Corrected Velocity for all data is calculated as:

$$\text{Sample Length} / \text{Extrapolated Onset} + 128.6 + 0.374T$$

**Castor Oil, BHP Chemicals Ltd : Regression Output from MINITAB**

MTB > REGRESS C1 2 C2 C3

Regression Analysis

The regression equation is  
Velocity = 1546 + 2.82 Pressure - 1.60 Temp

Predictor	Coef	Stdev	t-ratio	p
Constant	1546.17	1.11	1393.50	0.000
Pressure	2.8151	0.1254	22.44	0.000
Temp	-1.59662	0.03711	-43.03	0.000

s = 3.907      R-sq = 95.8%      R-sq(adj) = 95.8%

Analysis of Variance

SOURCE	DF	SS	MS	F	p
Regression	2	35947	17974	1177.55	0.000
Error	102	1557	15		
Total	104	37504			

SOURCE	DF	SEQ SS
Pressure	1	7689
Temp	1	28259

Unusual Observations

Obs.	Pressure	Velocity	Fit	Stdev.Fit	Residual	St.Resid
16	1.52	1495.00	1486.90	0.81	8.10	2.12R
32	3.04	1470.00	1495.01	0.67	-25.01	-6.50R

R denotes an obs. with a large st. resid.

MTB > REGRESS C1 3 C2 C3 C4

Regression Analysis

The regression equation is

$$\text{Velocity} = 1555 + 2.82 \text{ Pressure} - 2.60 \text{ Temp} + 0.0218 \text{ Temp}^2$$

Predictor	Coef	Stdev	t-ratio	p
Constant	1555.49	1.75	888.19	0.000
Pressure	2.8151	0.1067	26.38	0.000
Temp	-2.6046	0.1626	-16.02	0.000
Temp^2	0.021833	0.003454	6.32	0.000

s = 3.323      R-sq = 97.0%      R-sq(adj) = 96.9%

Analysis of Variance

SOURCE	DF	SS	MS	F	p
Regression	3	36389	12130	1098.18	0.000
Error	101	1116	11		
Total	104	37504			

SOURCE	DF	SEQ SS
Pressure	1	7689
Temp	1	28259
Temp^2	1	441

Unusual Observations

Obs.	Pressure	Velocity	Fit	Stdev.Fit	Residual	St.Resid
32	3.04	1470.00	1497.18	0.67	-27.18	-8.35R

R denotes an obs. with a large st. resid.

MTB > PRINT C1-C4

Data Display

Row	Velocity	Pressure	Temp	Temp^2
1	1487	0.00000	39.8	1584.04
2	1488	0.00000	37.4	1398.76
3	1490	0.00000	34.8	1211.04
4	1495	0.00000	32.8	1075.84
.	.	.	.	.
.	.	.	.	.
105	1564	9.11925	6.3	39.69

**KS16 Core and KS9525B Composite Core, Combined Data : Regression Output from MINITAB**

MTB > REGRESS C1 3 C2 C3 C4

Regression Analysis

The regression equation is  
 Velocity = 1796 + 2.70 Pressure - 21.7 Temp + 0.302 Temp^2

155 cases used 6 cases contain missing values

Predictor	Coef	Stdev	t-ratio	p
Constant	1796.38	11.17	160.85	0.000
Pressure	2.7043	0.4273	6.33	0.000
Temp	-21.7349	0.9248	-23.50	0.000
Temp^2	0.30249	0.01833	16.50	0.000

s = 15.81      R-sq = 93.5%      R-sq(adj) = 93.4%

Analysis of Variance

SOURCE	DF	SS	MS	F	p
Regression	3	545895	181965	727.62	0.000
Error	151	37762	250		
Total	154	583657			

SOURCE	DF	SEQ SS
Pressure	1	17604
Temp	1	460195
Temp^2	1	68095

Unusual Observations

Obs.	Pressure	Velocity	Fit	Stdev.Fit	Residual	St.Resid
19	1.52	1491.00	1459.05	2.23	31.95	2.04R
89	0.00	1646.00	1622.02	4.84	23.98	1.59X
101	1.52	1642.00	1626.13	4.59	15.87	1.05X
113	3.04	1646.00	1630.24	4.42	15.76	1.04X
135	6.08	1520.00	1553.59	2.20	-33.59	-2.15R
147	7.60	1523.00	1557.70	2.44	-34.70	-2.22R
149	7.60	1668.00	1642.57	4.48	25.43	1.68X
159	9.12	1525.00	1561.81	2.81	-36.81	-2.37R
161	9.12	1669.00	1646.68	4.69	22.32	1.48X

R denotes an obs. with a large st. resid.  
 X denotes an obs. whose X value gives it large influence.

MTB > PRINT C1-C4

Data Display

Row	Velocity	Pressure	Temp	Temp^2
1	1411	0.00000	37.9	1436.41
2	1404	0.00000	36.4	1324.96
3	1413	0.00000	34.4	1183.36
4	1418	0.00000	30.9	954.81
.	.	.	.	.
161	1669	9.11925	9.2	84.64

**KS16 Peripheral Spermacti : Regression Output from MINITAB**

MTB > REGRESS C1 3 C2 C3 C4

Regression Analysis

The regression equation is  
 Velocity = 1527 + 3.01 Pressure - 6.50 Temp + 0.107 Temp^2

107 cases used 5 cases contain missing values

Predictor	Coef	Stdev	t-ratio	p
Constant	1527.25	2.24	683.25	0.000
Pressure	3.0104	0.1225	24.57	0.000
Temp	-6.4972	0.2076	-31.30	0.000
Temp^2	0.106503	0.004545	23.43	0.000

s = 3.747      R-sq = 96.9%      R-sq(adj) = 96.9%

Analysis of Variance

SOURCE	DF	SS	MS	F	p
Regression	3	45867	15289	1088.71	0.000
Error	103	1446	14		
Total	106	47314			

SOURCE	DF	SEQ SS
Pressure	1	11145
Temp	1	27011
Temp^2	1	7712

Unusual Observations

Obs.	Pressure	Velocity	Fit	Stdev.Fit	Residual	St.Resid
89	7.60	1452.00	1460.86	0.66	-8.86	-2.40R
96	7.60	1503.00	1510.37	1.03	-7.37	-2.05R
105	9.12	1456.00	1465.43	0.78	-9.43	-2.57R
112	9.12	1507.00	1514.94	1.10	-7.94	-2.22R

R denotes an obs. with a large st. resid.

MTB > PRINT C1-C4

Data Display

Row	Velocity	Pressure	Temp	Temp^2
1	1429	0.00000	37.9	1436.41
2	*	*	*	*
3	1427	0.00000	33.0	1089.00
4	1429	0.00000	30.9	954.81
.	.	.	.	.
.	.	.	.	.
112	1507	9.11925	6.9	47.61

**Humberside Spermacti, Homogenised Sample : Regression Output from MINITAB**

MTB > REGRESS C1 2 C2 C3

Regression Analysis

The regression equation is  
 Velocity = 1526 + 2.93 Pressure - 2.95 Temp

96 cases used 2 cases contain missing values

Predictor	Coef	Stdev	t-ratio	p
Constant	1525.79	1.60	954.25	0.000
Pressure	2.9254	0.1450	20.18	0.000
Temp	-2.95246	0.05494	-53.74	0.000

s = 4.254      R-sq = 97.3%      R-sq(adj) = 97.3%

Analysis of Variance

SOURCE	DF	SS	MS	F	p
Regression	2	61814	30907	1707.84	0.000
Error	93	1683	18		
Total	95	63497			

SOURCE	DF	SEQ SS
Pressure	1	9557
Temp	1	52257

Unusual Observations

Obs.	Pressure	Velocity	Fit	Stdev.Fit	Residual	St.Resid
22	1.52	1448.00	1456.42	0.61	-8.42	-2.00R
43	4.56	1434.00	1425.46	0.87	8.54	2.05R

R denotes an obs. with a large st. resid.

MTB > REGRESS C1 3 C2 C3 C4

Regression Analysis

The regression equation is

$$\text{Velocity} = 1560 + 2.99 \text{ Pressure} - 6.00 \text{ Temp} + 0.0612 \text{ Temp}^2$$

96 cases used 2 cases contain missing values

Predictor	Coef	Stdev	t-ratio	p
Constant	1559.52	1.98	787.08	0.000
Pressure	2.99190	0.06758	44.27	0.000
Temp	-5.9976	0.1677	-35.75	0.000
Temp^2	0.061230	0.003334	18.37	0.000

s = 1.980            R-sq = 99.4%            R-sq(adj) = 99.4%

Analysis of Variance

SOURCE	DF	SS	MS	F	p
Regression	3	63136	21045	5369.18	0.000
Error	92	361	4		
Total	95	63497			

SOURCE	DF	SEQ SS
Pressure	1	9557
Temp	1	52257
Temp^2	1	1322

Unusual Observations

Obs.	Pressure	Velocity	Fit	Stdev.Fit	Residual	St.Resid
10	0.00	1469.00	1464.41	0.41	4.59	2.37R
11	0.00	1478.00	1471.78	0.42	6.22	3.21R
12	0.00	1486.00	1479.23	0.44	6.77	3.50R
22	1.52	1448.00	1452.40	0.36	-4.40	-2.26R

R denotes an obs. with a large st. resid.

MTB > PRINT C1-C4

Data Display

Row	Velocity	Pressure	Temp	Temp^2
1	1418	0.00000	38.5	1482.25
2	1422	0.00000	36.9	1361.61
3	1428	0.00000	33.0	1089.00
4	1433	0.00000	31.0	961.00
.	.	.	.	.
98	1521	9.11925	12.0	144.00

## Appendix 7

### PASCAL Program to perform Waveform Autocorrelation

#### Program Written in Borland Turbo Pascal version 6 Borland CRT & GRAPH Library Linked Routines Used

```
*****  
* PASCAL Program to perform Waveform Autocorrelation *  
*                                                                 *  
*       Program by: John C. Goold (1994)                   *  
*****
```

```
PROGRAM WaveformCorrelator(INPUT, OUTPUT);  
USES CRT, GRAPH;  
VAR  
  A, N, BINS, t, Dt, COUNT, INDEX1, INDEX2,  
  GRAPHDRIVER, GRAPHMODE, LIMIT, NUM, POINTS : INTEGER;
```

```
  SAMPLE : ARRAY[0..2048] OF REAL;  
  SLIDE : ARRAY[0..2048] OF REAL;  
  CORRFN : ARRAY[0..1024] OF REAL;  
  TIME : ARRAY[0..1024] OF REAL;  
  SIGN : ARRAY[0..2048] OF INTEGER;
```

```
  SUM1, SUM2, SUM3, MAVG, SAMPLEINT, ZONE1, ZONE2,  
  PEAK1, PEAK2, TIME1, TIME2, T1, T2, TIMEADD, TIMEINC,  
  LAST, FDUD, RDUD, DudPoint : REAL;
```

```
  INDEX : CHAR;
```

```
  WAVEFILE, OUTFILE, IPIFILE, TIMEFILE, PARFILE: TEXT;
```

```
  FLNM, TEMP, EXT1, EXT2, EXT3, EXT4, COCKUP : STRING[30];
```

```
BEGIN
```

```
  TIMEADD:=0;  
  GRAPHDRIVER:=VGA;  
  GRAPHMODE:=VGAHi;  
  CLRSCR;  
  WRITE ('Enter Parameter FileName ');  
  READLN (FLNM);  
  ASSIGN (PARFILE, FLNM);  
  RESET (PARFILE);
```

```
REPEAT
```

```
  FOR A:=0 TO 1024 DO  
    BEGIN
```

```
      (** Initialise Arrays **)
```

```
    END
```

```
SAMPLE[A]:=0; SAMPLE[2048-A]:=0;
SLIDE[A]:=0; SLIDE[2048-A]:=0;
SIGN[A]:=0; SIGN[2048-A]:=0;
CORRFN[A]:=0;
TIME[A]:=0;
END;
SUM1:=0;
SUM2:=0;
SUM3:=0;
LAST:=0;

CLRSCR;
READLN (PARFILE, FLNM);
READLN (PARFILE, INDEX1);
READLN (PARFILE, INDEX2);
INDEX:=CHR (INDEX1);
LIMIT:=INDEX2;

READLN (PARFILE, EXT1);
READLN (PARFILE, FDUD);
READLN (PARFILE, RDUD);

READLN (PARFILE, EXT3);
READLN (PARFILE, EXT4);

READLN (PARFILE, SAMPLEINT);

READLN (PARFILE, ZONE1);
ZONE1:=ROUND(ZONE1/SAMPLEINT);
READLN (PARFILE, ZONE2);
ZONE2:=ROUND(ZONE2/SAMPLEINT);

READLN (PARFILE, TIMEADD);
READLN (PARFILE, TIMEINC);

GRAPHDRIVER:=VGA;
GRAPHMODE:=VGAHi;

(***** READ WAVEFORM DATA INTO ARRAY *****)

REPEAT

ASSIGN (WAVEFILE, FLNM+INDEX+EXT1);
RESET (WAVEFILE);
READLN (WAVEFILE, N);
READLN (WAVEFILE, BINS);
ASSIGN (TIMEFILE, FLNM+INDEX+EXT3);
RESET (TIMEFILE);
READLN (TIMEFILE, T1, T2);
ASSIGN (IPIFILE, FLNM+INDEX+EXT4);
REWRITE (IPIFILE);
WRITELN (IPIFILE, N:10, N:10);

COUNT:=1;
REPEAT
  READLN (TIMEFILE, T1, T2);
  TIME[COUNT]:=T1+TIMEADD;
  IF TIME[COUNT] < LAST THEN
```

```

BEGIN
TIMEADD:=TIMEADD+TIMEINC;
TIME[COUNT]:=TIME[COUNT]+TIMEINC;
END;
LAST:=T1+TIMEADD;
INITGRAPH (GRAPHDRIVER, GRAPHMODE, 'C:\TP\BGI');
POINTS:=0;
IF FDUD <> 0 THEN
  BEGIN          (** read front dud points **)
  FOR t:=1 TO ROUND(FDUD) DO
    BEGIN
    READLN (WAVEFILE, DudPoint);
    POINTS:=POINTS+1;
    END;
  END;

FOR t:=0 TO ROUND((BINS-1)-(FDUD+RDUD)) DO
  BEGIN
  READLN (WAVEFILE, SAMPLE[t]);
  POINTS:=POINTS+1;
  SLIDE[t]:=SAMPLE[t];

  IF t=0 THEN
    BEGIN
    MOVETO (ROUND(t*(600/(BINS-(FDUD+RDUD)))), ROUND(200-(50*SAMPLE[t])));
    END
  ELSE
    BEGIN
    LINETO (ROUND(t*(600/(BINS-(FDUD+RDUD)))), ROUND(200-(50*SAMPLE[t])));
    END;
  END;

IF RDUD <> 0 THEN          (** read rear dud points **)
  BEGIN
  FOR t:=ROUND(BINS-RDUD) TO BINS-1 DO
    BEGIN
    READLN (WAVEFILE, DudPoint);
    POINTS:=POINTS+1;
    END;
  END;

DELAY (3000);
CLOSEGRAPH;
INITGRAPH (GRAPHDRIVER, GRAPHMODE, 'C:\TP\BGI');

(** PERFORM CORRELATION **)

STR (COUNT, TEMP);
SetTextStyle (2,0,8);
OutTextXY (300, 360, TEMP);
OutTextXY (200, 420, FLNM+INDEX+EXT1);
OutTextXY (ROUND((ZONE2*(600/(BINS-(FDUD+RDUD))))-140), 20, 'ZONE1');
OutTextXY (ROUND((ZONE2*(600/(BINS-(FDUD+RDUD))))+100), 20, 'ZONE2');
STR (POINTS, COCKUP);
OutTextXY (0, 420, COCKUP);
LINE (ROUND(ZONE1*(600/(BINS-(FDUD+RDUD)))), 0, ROUND(ZONE1*(600/(BINS-
(FDUD+RDUD)))), 300);
LINE (ROUND(ZONE2*(600/(BINS-(FDUD+RDUD)))), 0, ROUND(ZONE2*(600/(BINS-
(FDUD+RDUD)))), 300);

```

```

SUM2:=0;
FOR t:=0 TO ROUND((BINS-1)-(FDUD+RDUD)) DO
  BEGIN
    SUM2:=SUM2+(SAMPLE[t]*SAMPLE[t]);
  END;
FOR Dt:=0 TO ROUND((BINS-1)-(FDUD+RDUD)) DO
  BEGIN
    FOR t:=0 TO ROUND((BINS-1)-(FDUD+RDUD)) DO
      BEGIN
        SUM1:=SUM1+(SAMPLE[t]*SLIDE[t+Dt]);
        SUM3:=SUM3+(SLIDE[t+Dt]*SLIDE[t+Dt]);
      END;

    IF (SUM1*SUM2*SUM3)=0 THEN
      BEGIN
        CORRFN[Dt]:=0;
      END
    ELSE
      BEGIN
        CORRFN[Dt]:=ABS(SUM1/SQRT(SUM2*SUM3));
      END;

    (****   WRITELN (OUTFILE, CORRFN[Dt]);   ***)

    IF Dt=0 THEN
      BEGIN
        MOVETO (ROUND(Dt*(600/(BINS-(FDUD+RDUD)))), ROUND(200-(150*CORRFN[Dt])));
      END
    ELSE
      BEGIN
        LINETO (ROUND(Dt*(600/(BINS-(FDUD+RDUD)))), ROUND(200-(150*CORRFN[Dt])));
      END;

    SUM1:=0;
    SUM3:=0;

    END;

(** LOCATE TWO HIGHEST PEAKS IN UNFILTERED CORRELATION ARRAY **)
PEAK1:=0; PEAK2:=0;
TIME1:=0; TIME2:=0;
FOR Dt:=ROUND(ZONE1) TO ROUND((BINS-1)-(FDUD+RDUD)) DO
  BEGIN
    IF Dt > ZONE2 THEN
      BEGIN
        IF CORRFN[Dt] > PEAK2 THEN
          BEGIN
            PEAK2:=CORRFN[Dt];
            TIME2:=Dt*SAMPLEINT;
          END;
        END
      ELSE
        BEGIN
          IF Dt > 20 THEN
            BEGIN
              IF CORRFN[Dt] > PEAK1 THEN
                BEGIN
                  PEAK1:=CORRFN[Dt];

```

```
    TIME1:=Dt*SAMPLEINT;  
    END;  
  END;  
END;  
END;
```

```
WRITELN (IPIFILE, TIME[COUNT]:10:6, TIME1:10:6, TIME2:10:6, PEAK1:10:6, PEAK2:10:6);
```

```
  COUNT:=COUNT+1;  
  CLOSEGRAPH;  
UNTIL COUNT > N;
```

```
CLOSE (WAVEFILE);  
(** CLOSE (OUTFILE); **)  
CLOSE (IPIFILE);  
CLOSE (TIMEFILE);
```

```
INDEX1:=INDEX1+1;  
INDEX:=CHR (INDEX1);  
UNTIL INDEX1 > LIMIT;
```

```
UNTIL EOF(PARFILE);  
CLOSE (PARFILE);
```

```
END.
```